Dissertation

Submitted to the
Combined Faculties for the Natural Sciences and for Mathematics
of the Ruperto-Carola University of Heidelberg, Germany
for the degree of
Doctor of Natural Sciences

Presented by

Master of Science: Krishna Das (M.Sc.)
born in: Guwahati, India

Oral-examination: 28.07.2017

Generation of a transplantable murine tumor model expressing the human breast cancer associated tumor antigen NY-BR-1 in HLA-DRB1*0401-transgenic mice

First examiner:	PD Dr. Karin Müller-Decker
Second examiner:	Prof. Dr. Stefan Eichmüller

Declarations according to § 8 (3) b) and c) of the doctoral degree regulations:

a) I hereby declare that I have written the submitted dissertation myself and in this process have used no other sources or materials than those expressly indicated,
b) I hereby declare that I have not applied to be examined at any other institution, nor have I used the dissertation in this or any other form at any other institution as an examination paper, nor submitted it to any other faculty as a dissertation.

Heidelberg, 30.05.2017 Krishna Das

1 Abstract

Prevalence of mutations and deregulated gene expression has resulted in a wide variety of tumor antigens which can be targeted for immunotherapy. NY-BR-1 is a breast cancer associated differentiation antigen which is overexpressed in more than 60% of breast cancers. In this study we established the first NY-BR-1 expressing transplantable tumor model using the murine mammary adenocarcinoma cell line EO771 as parental cells for the generation of NY-BR-1-expressing transfectants (EONY cells) which are compatible for transplantation into HLA-DRB1*0401tg mice. Since NY-BR-1 is not endogenously expressed in these mice, transplantation of NY-BR-1 expressing tumors led to the induction of $CD4^+$ and $CD8^+$ T cells specific for HLA-DR*0401- and H2-D^b-restcried NY-BR-1 epitopes, respectively, previously identified in our lab. We also generated MHC I knockout cell lines with the aim of using them to study NK cell responses or as parental lines for transection of human MHC I molecules. Since several HLA-restricted NY-BR-1-specific T cell epitopes have been described, these cells could serve as an important tool to study the efficacy of using the epitopes as peptide vaccines and studying the synergistic effect of induced $CD8^+$ and $CD4^+$ T cells in HLA-transgenic mice co-expressing human MHC I and MHC II molecules. Additionally, we also confirmed that previously identified H2-D^b-restrcited epitope was indeed naturally processed based on detection of $CD8^+$ T cells which specifically recognized this epitope in mice following transplantation of NY-BR-1 expressing tumors or upon immunization with global NY-BR-1 antigen. We also observed that immunization with Ad.NY-BR-1 was more suitable for generating a NY-BR-1 specific $CD8^+$ T cell line compared to immunization with nonameric peptide. We also obtained evidence suggesting that the H2-D^b-restricted CTL epitope might actually be identical to the core sequence of one of the previously identified HLA-DRB1*0301-restricted $CD4^+$ T cell epitopes. Thus binding of the CTL epitope to HLA-DRB1*0301 molecules on feeder cells might have resulted in predominant restimulation of HLA-DR3B1*0401-restricted $CD4^+$ T cells *in vitro*. Cancer immunotherapy involving T cells have focused primarily on cytotoxic $CD8^+$ T cells. However, a body of evidence has emerged in the recent past that argues for including $CD4^+$ T cells because they not only eliminate tumor cells directly but also greatly enhance the outcome of cancer immunotherapy by various ways. One of the mechanisms by which $CD4^+$ T cells can contribute to successful immunotherapy is by repolarizing tumor associated macrophages (TAMs) into a less immunosuppressive phenotype in an antigen dependent fashion. In this study we could demonstrate that NY-BR-1 specific $CD4^+$ T cells could repolarize M2-like macrophages towards an M1-like phenotype upon antigen specific interaction. However, the majority of the $CD4^+$ T cells infiltrating the EONY tumors appeared to have tumor promoting functions as depletion of $CD4^+$ T cells resulted in delayed tumor growth and was accompanied by switch in the polarization status of TAMs towards an M-1like phenotype. Though Ad.NY-BR-1 immunization resulted in induction of NY-BR-1 specific $CD4^+$ T cells and slight changes in polarization of intra-tumoral macrophages; it did not seem to drastically change the proportion of tumor-promoting $CD4^+$ T cells in the tumor since the protective effect and switch in TAM phenotype was observed in both control virus and Ad.NY-BR-1 immunized mice. Therefore, antigen-specific instruction of TAMs by NY-BR-1-specific $CD4^+$ T cells could not be demonstrated *in vivo*, possibly due to the prevalence of tumor infiltrating $CD4^+$ T cells with a tumor promoting phenotype occurring in the EO771/NY-BR-1 model established within this thesis.

2 Zusammenfassung

Häufig auftretende Mutationen sowie eine deregulierte Genexpression haben zur Entstehung einer Vielzahl von Tumorantigenen geführt, die als Zielstrukturen in der Immuntherapie eingesetzt werden können. NY-BR-1 stellt ein Brustkrebs-assoziiertes Differenzierungsantigen dar, das in über 60% aller Brusttumoren über-exprimiert wird. Unter Verwendung der murinen Mammakarzinomlinie EO771 als parentale Zelllinie für die Herstellung NY-BR-1-exprmierender Transfektanten (EONY) sowie des HLA-DRB1*0401 transgenen Mausstammes, konnte in der vorliegenden Arbeit erstmals ein transplantierbares NY-BR-1exprimierendes Tumormodell etabliert werden. Da NY-BR-1 in diesen Tieren nicht endogen exprimiert wird, führte die Transplantation von NY-BR-1-exprimierenden Tumorzellen zur Induktion von $CD8^+$ und $CD4^+$ T Zellantworten gegen HLA-DR4- bzw. $H2\text{-}D^b$ restringierte T-Zellepitope, die bereits in früheren Studien unseres Labors identifiziert worden waren. Darüber hinaus wurden MHC I knock out Zelllinien hergestellt, die für die Untersuchung von NK- Zellantworten oder als parentale Ausgangslinien für die Etablierung von HLA-exprimierenden Transfektanten verwendet werden können. Nachdem mehrere HLA-restringierte, NY-BR-1-spezifische T Zellepitope beschrieben worden sind, könnten diese MHC I knock out Zelllinien als wichtiges Werkzeug dienen, um die Effizienz dieser Epitope als Peptid basierte Vakzine zu prüfen und dabei den synergistischen Effekt der $CD8^+$ und $CD4^+$ T Zellen in HLA-transgenen Mäusen zu untersuchen. Darüber hinaus konnte bestätigt werden, dass es sich bei dem bereits früher identifizierten $H2\text{-}D^b$-restringierten CTL Epitop tatsächlich um ein natürliches Prozessierungsprodukt handelt, da $CD8^+$ T Zellen mit einer spezifischen Reaktivität gegen dieses Epitop nur in Mäusen detektiert wurden, die mit NY-BR-1 exprimierenden Tumoren transplantiert oder mit globalem NY-BR-1 Antigen immunisiert worden waren. Wir konnten außerdem zeigen, dass sich die Immunisierung mit Ad.NY-BR-1, im Vergleich zur Immunisierung mit dem nonameren Peptid, besser für die Generierung einer NY-BR-1-spezifischen $CD8^+$ T Zelllinie eignet. Darüber hinaus deuten unsere Ergebnisse darauf hin, dass das $H2\text{-}D^b$-restringierte CTL Epitop identisch mit der Kernsequenz eines bereits zuvor identifizierten HLA-DRB1*0301- restringierten $CD4^+$ T Zellepitops ist, und die Bindung des CTL Epitopes an HLA-DRB1*0301 Moleküle auf den Feederzellen zu einer bevorzugten Restimulierung von HLA-DRB1*0301-restringierten $CD4^+$ T-Zellen *in vitro* führen kann. Immuntherapeutische Verfahren zur Krebsbehandlung, die T Zellen beinhalten, fokussierten sich bisher in erster Linie auf $CD8^+$ T Zellen. Inzwischen häufen sich jedoch Hinweise, die für eine Miteinbeziehung von $CD4^+$ Zellen sprechen, da diese Zellen nicht nur in der Lage sind, Tumorzellen direkt zu eliminieren, sondern den Erfolg einer Tumortherapie auf verschiedene Art und Weise verbessern können. Ein Mechanismus über den $CD4^+$ T Zellen zu einer erfolgreichen Immuntherapie beitragen können, besteht in einer Antigen-abhängigen Re-Polarisierung von Tumor-assoziierten Makrophagen (TAMs) in Richtung eines weniger immunsuppressiven Phänotyps. In der vorliegenden Arbeit konnten wir zeigen, dass NY-BR-1-spezifische $CD4^+$ T Zellen mittels Antigen-spezifischer Stimulierung in der Lage sind, M2-artige Makrophagen in Richtung eines M1-Phänotyps zu re-polarisieren. Allerdings schien die Mehrzahl der EONY-Tumor infiltrierenden $CD4^+$ T Zellen einen Tumor-fördernden Effekt aufzuweisen, da die Depletion der $CD4^+$ T Zellen zu einer Verzögerung des Tumorwachstums führte und von einem Wechsel des Polarisierungsstatus der TAMs in Richtung eines M1-artigen Phänotyps begleitet wurde. Obwohl die Immunisierung mit Ad.NY-BR-1 zu einer Induktion NY-BR-1-spezifischer $CD4^+$ T-Zellen führte und leichte Veränderungen in der Polarisierung intratumoraler Makrophagen auslöste, schien sie sich auf den Anteil Tumor-fördernder $CD4^+$ T-Zellen im Tumor kaum

auszuwirken, da der protektive Effekt und der Wechsel des TAM Phänotyps sowohl in den Kontrolltieren als auch in Mäusen, die mit Ad.NY-BR-1 immunisiert worden waren beobachtet wurde. Somit konnte die Antigen-spezifische Instruktion von TAMs durch NY-BR-1-spezifische $CD4^+$ T Zellen *in vivo* nicht gezeigt werden - möglicherweise aufgrund des hohen intratumoralen Anteils von Tumor fördernden $CD4^+$ T Zellen, der sich in dem NY-BR-1 exprimierenden Tumormodell, das im Rahmen dieser Arbeit etabliert wurde, bildet.

List of Figures

List of Tables

Abbreviations

Abbreviation	Full name
ACK	Ammonium-Chlorid-Kalium
ACT	Adoptive Cell Therapy
ADCC	Antibody-Dependent Cellular Cytotoxicity
AJCC	American Joint Committee on Cancer
APC	Allophycocyanin
APCs	Antigen Presenting Cells
APS	Ammonium Persulfate
Arg1	*Arginase 1*
ATCC	American Type Culture Collection
ATP	Adenosine triphosphate
BCIP	5-bromo-4-chloro-3-indolyl-phosphate
BRCA1	breast cancer 1
BRCA2	breast cancer 2
BSA	Bovine Serum Albumin
CAGE	cancer-associated antigen gene
CARs	Chimeric Antigen Receptors
CCD	Charge-Coupled Device
CCL	chemokine ligand
CCR	chemokine ligand
CD	chemokine receptors
CDKs	cyclin-dependent kinases
CEA	Carcinoembryonic antigen
CLL	chronic lymphocytic leukemia
CMV	cytomegalovirus
Con A	Concavalin A
CSF-1R	Colony Stimulating Factor 1 Receptor
CTG	CellTiter-Glo®
CTLA-4	cytotoxic T lymphocyte antigen-4
CTLs	cytotoxic T lymphocytes
CXCL	Chemokine (C-X-C motif) ligand
DCIS	ductal carcinoma *in situ*
DCs	dendritic cells
DKFZ	Deutsches Krebsforschungszentrum
DMEM	Dulbecco's Modified Eagle Medium
DNA	Deoxyribonucleic acid
DPBS	Dulbecco's phosphate-buffered saline
ECL	enhanced chemiluminescence
EDTA	Ethylenediaminetetraacetic acid
EGFR	Epidermal Growth Factor Receptor
ELISA	enzyme-linked immunosorbent assay
ELISPOT	Enzyme-Linked ImmunoSpot
EpCAM1	Epithelial cell adhesion molecule 1
ER	estrogen receptor
ER	endoplasmic reticulum
EREs	estrogen response elements
FACS	Fluorescence-Activated Cell Sorting

FDA	Food and Drug administration
FITC	Fluorescein isothiocyanate
GM-CSF	Granulocyte Macrophage Colony-Stimulating Factor
HCV	hepatitis C virus
HLA	human leukocyte antigen
HPV	human papillomavirus
HRG	histidine-rich glycoprotein
ICAM-1	Intercellular Adhesion Molecule 1
IDO	Indoleamine 2,3-dioxygenase
IFA	Incomplete Freund's adjuvant
IFNγ	interferon gamma
IL	interleukin
LAG-3	lymphocyte activation gene 3
LCIS	lobular carcinoma *in situ*
LPS	lipopolysaccharide
MACS	Magnetic-Activated Cell Sorting
MAGE	Melanoma-associated antigen gene
MAPKs	Mitogen-activated protein kinases
MART-1	Melanoma-associated antigen recognized by T cells
MDSCs	myeloid-derived suppressor cells
MHC	major histocompatibility complex
MIIC	MHC class II compartment
MMTV	Mouse mammary tumor virus
MPVs	Human metapneumovirus
mTOR	mechanistic target of rapamycin
MUC1	Mucin 1
NBT	nitro blue tetrazolium
NSCLC	non-small cell lung cancer
OVA	ovalbumin
PAM 50	Prediction Analysis of Microarray
PAMPs	pathogen associated molecular patterns
PARP	Poly ADP ribose polymerase
PBMC	peripheral blood mononuclear cell
PBS	Phosphate-buffered saline
PCR	Polymerase chain reaction
PD-1	programmed cell death protein 1
PE	Phycoerythrin
PECs	peritoneal exudate cells
PI3K	Phosphoinositide 3-kinase
PMSF	Phenylmethylsulfonyl fluoride
PR	progesterone receptor
PRRs	pattern recognition receptors
PSA	prostate-specific antigen
PyMT	Polyoma middle T antigen
qRT-PCR	quantitative reverse transcription-polymerase chain reaction
RNA	Ribonucleic acid

RNI	reactive nitrogen intermediates
ROI	reactive oxygen intermediates
RPMI	Roswell Park Memorial Institute
SDS	Sodium dodecyl sulfate
SEM	standard error of mean
SEREX	serological analysis of recombinant tumor cDNA expression libraries
SV40	Simian virus 40
TAAs	tumor-associated antigens
TAMs	tumor-associated macrophages
TAP	transporters associated with antigen processing
TBS	Tris-buffered saline
TCRs	T cell receptors
TEMED	Tetramethylethylenediamine
Tfh	follicular helper T
Th cells	T helper cells
TILs	tumor-infiltrating lymphocytes
TKI	Tyrosine kinase inhibitors
TLCK	Tosyl-L-lysyl-chloromethane hydrochloride
TLR	Toll-like receptor
TME	tumor microenvironment
TNBC	triple negative breast cancer
Tregs	regulatory T cells
TSS	transcription start site
UV	ultraviolet
VEGF	Vascular endothelial growth factor
αMM	Methyl α-D-mannopyranoside

3 Introduction

3.1 Cancer

Cancer is defined as a collection of many diseases that are characterized by uncontrolled proliferation of aberrant cells. Cancer cells arise due to alterations at the genetic level (i.e. mutations, translocations etc.) or at the epigenetic level both of which result in deregulated cell growth. These abnormal cells compete for nutrients and outgrow healthy cells causing fatal organ failures. Cancer cells can arise from any tissue and based on the tissue of origin they are classified into four main categories viz. carcinomas, sarcomas, hematopoietic cancers and neuroectodermal tumors. Carcinomas arise from cells of epithelial origin present in the skin, the gastrointestinal tract, mammary gland, pancreas, liver etc. Sarcomas on the other hand are cancers affecting mesenchymal cells like fibroblasts and connective tissues like bone, cartilage, fat, muscle and blood vessels. Hematopoietic cancers include leukemia, lymphomas and myelomas. Leukemia is characterized by rapidly proliferating immature white blood cells that are in the circulation whereas lymphoma results in solid tumors derived from cells of lymphoid origins like T and B lymphocytes. Conversely, myeloma is the cancer of plasma cells, another type of white blood cell which produces antibodies. Cancers arising in the brain, spinal cord and the peripheral nervous system are classified as neuroectodermal cancers and they include gliomas, glioblastomas, neuroblastomas etc. Irrespective of the tissue of origin all cancer cells are characterized by genetic instabilities and mutations(1).

Mutations in cancer cells can be caused by a wide variety of mutagens which can be mainly categorized as physical, chemical or biological agents. Physical noxae like radiation (UV rays, X-rays, γ-rays etc.) and chemical agents like 3-methylcholanthrene, benzo[a]pyrene, dibenz[a,h]anthracene etc. can result in mutations in the DNA either by inducing DNA damage which cannot be effectively repaired or by intercalating into DNA. Biological agents like viruses can also result in the introduction of oncogenes that drive uncontrolled cell proliferation (1). Genetic instability can be caused due to errors at various steps of DNA replication or faulty DNA damage response (2). Besides mutations, other genetic alterations like gross chromosomal rearrangements including gene amplifications and translocations can result in either activation of oncogenes or inactivation of tumor suppressor genes(2).

The cumulative effect of these mutations or gene alterations is that the growth of cancer cells is no longer regulated like that of normal cells. These cells have acquired increased proliferative capacity and show reduced cell death. This can be due to various reasons. The cancer cells can become independent of mitogenic signals either by producing their own growth factors or by stimulating their neighboring stromal cells to produce growth factors. They can also survive with low amounts of growth factors by upregulating their cognate receptors. Various signaling pathways rely on conformational changes of the signaling molecule to switch between active and inactive state. Some mutations in cancer cells give rise to an altered protein which cannot switch back to the inactive state thus resulting in the constitutive activation of the signaling pathway. Additionally, mutations of the receptors can lead to their activation independent of ligand binding. Cancer cells do not undergo apoptosis like normal cells in response to various stress factors. They can evade apoptosis by deregulating the balance between the pro-apoptotic and anti-apoptotic factors. Moreover, they can acquire endless replicative potential by upregulating telomerase which enables them to avoid telomere shortening that accompanies normal cell division.

The cancer cells not only proliferate endlessly but they can also alter the tumor microenvironment for their own benefit. As a tumor grows in size the available nutrients and oxygen become limiting. In order to circumvent this they can promote neo-angiogenesis by secreting factors like vascular endothelial growth factor (VEGF) or by recruiting macrophages which can do so as well. It is known that the immune system can eradicate aberrant cancer cells, however a growing tumor manages to escape being killed by the host immune system by various ways (discussed in more detail in Section 3.4). Several of the features described above and some others that enable cancer cells to proliferate in an unregulated way and develop into a tumor are summarized in Figure 1.

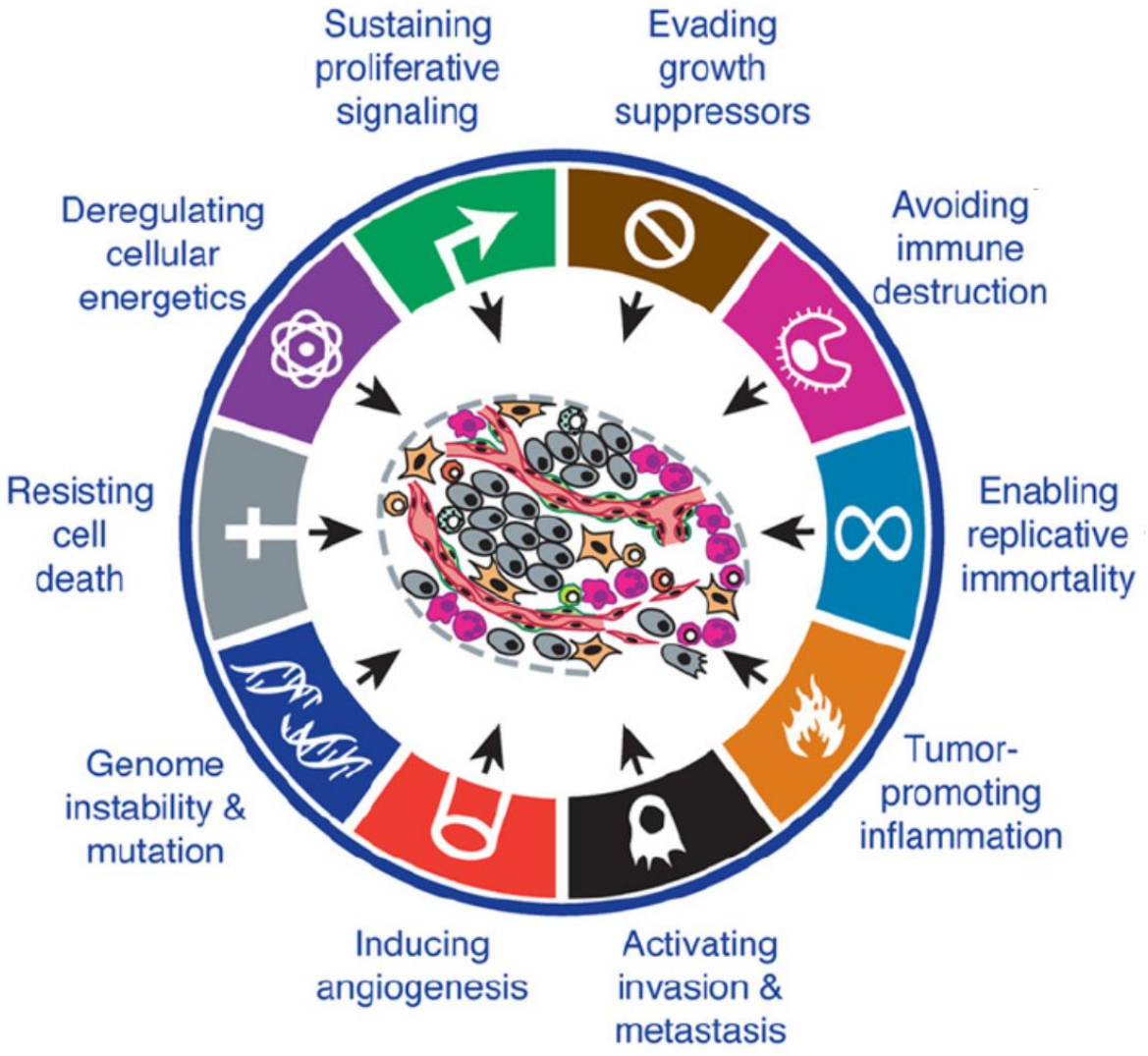

Figure 1. Hallmarks of cancer

Properties acquired by cancer cells which render them resistant to mechanisms that regulate normal cell growth thereby allowing them to proliferate indefinitely (Adapted from Hanahan and Weinberg, 2011).

3.2 Breast cancer

3.2.1 Incidence and mortality

Out of 14.1 million new cancer cases reported in 2012 worldwide, 1.7 million cases of breast cancer were reported which constituted 11.9% of all diagnosed cancers for both sexes combined and 25.2% of diagnosed cancers in females alone. In 2012, 8.2 million lives were claimed by cancer among which breast cancer alone resulted in 522,000 (6.4%) deaths and was the leading cause of cancer related death in women (3).

Figure 2 demonstrates that the incidence of breast cancer did not vary too much between more developed regions and less developed regions (794,000 vs 883,000), but mortality was markedly higher in less developed regions (198,000 vs 324,000) (3). This was due to the fact that patients in less developed regions were diagnosed at advanced stages of breast cancer owing to lack of effective screening programs and did not have access to advanced therapeutic options (4). This was also reflected in the five year net survival rates of 80% or higher in regions with high development like Europe and North America compared to 60% in India and 53% in South Africa (5).

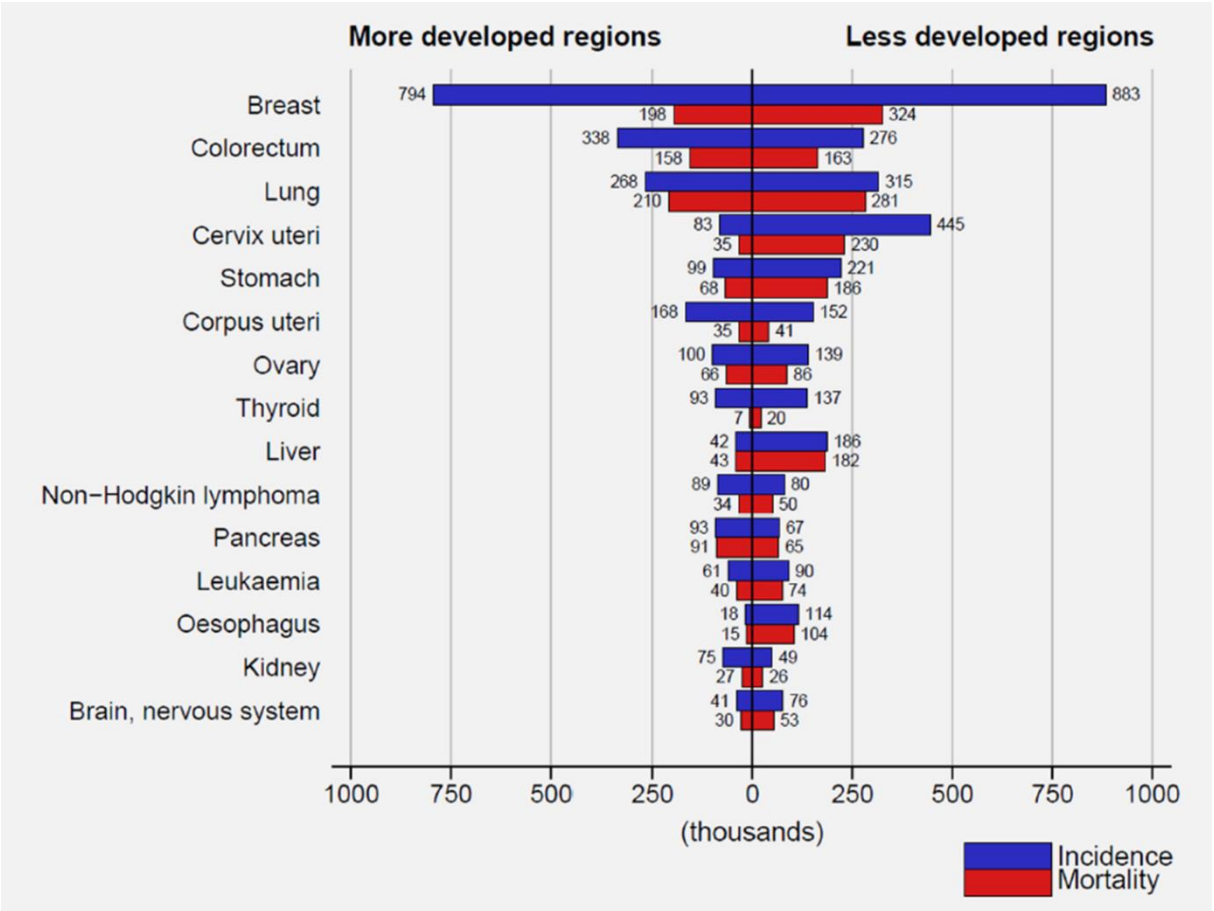

Figure 2. Incidence and mortality estimates in 2012

The numbers (in thousands) of estimated new cases and deaths due to various types of cancer in women in more developed and less developed regions of the world (Figure from GLOBOCAN 2012, Global Cancer Facts & Figures 3rd Edition).

Unlike cancers caused by viruses like cervical cancer and liver cancer which are caused by human papillomavirus (HPV) and hepatitis C virus (HCV) respectively, breast cancer cannot be prevented by vaccinations. However, there are some known risk factors which can be addressed. For example, women with mutations in *BRCA1* (breast cancer 1) and *BRCA2* (breast cancer 2) genes are genetically predisposed to develop breast cancer. It has been reported that for women carrying BRCA1 and BRCA2 mutations, prophylactic mastectomy can reduce the risk of developing cancer drastically (by 90% or more) (5). Prolonged exposure to estrogen due to early menarche and late menopause and external source of estrogen like oral contraceptives and hormone replacement therapy are also known to be associated with higher risk of developing breast cancer while tamoxifen and raloxifene was shown to lower breast cancer incidence in breast cancer prevention trials (6, 7). Other risk factors like obesity (8), lack of physical activity (9) and excessive alcohol consumption (10) can be managed by lifestyle changes.

3.2.2 Development and characterization of breast cancer

Staging of breast cancer helps clinicians to determine tumor burden and metastatic spread. Breast cancer is usually staged using the TNM system according to the American Joint Committee on Cancer (AJCC). T stands for tumor and its category (TX, T0, Tis, T1, T2, T3 and T4) is decided based on the size of the primary breast tumor and whether it has grown into the chest wall or skin. TX signifies primary tumor that cannot be assessed, whereas T0 indicates no evidence of primary tumor. Tis represents carcinoma *in situ,* whereas T1 to T4 denotes invasive tumor of increasing size, T1 representing tumors smaller than 2 cm and T4 is used to report tumors of any size that are growing into the chest wall or skin. Similarly different scores are assigned to the N category which is used to denote whether cancer cells have spread to lymph nodes and how many lymph nodes have been affected. NX stands for regional lymph nodes cannot be assessed whereas N0 means that no cancer cells were detected in regional lymph nodes. N1 indicates presence of metastases in axillary lymph nodes, N2 signifies that cancer cells have spread to internal mammary lymph nodes or have caused axillary lymph nodes to become matted and N3 indicates that cancer has been detected in the internal mammary lymph nodes or infraclavicular lymph nodes along with the axillary lymph nodes or in the supraclavicular lymph nodes. The presence of distant metastasis is indicated by the M category in which MX represents that distant metastasis cannot be assessed, M0 means lack of distant metastasis and M1 indicates that metastasis has been detected in distant organs like brain, bones or lungs. The information from T, N and M scores are then combined to obtain the stage of the cancer which varies between Stage 0 to Stage IV, Stage 0 being the earliest form of breast cancer with the best prognosis, whereas Stage IV indicating advanced metastatic disease with the worst prognosis (11, 12).

Histological classification of breast cancer is mainly based on the origin of the cancer cells and the extent of invasion into surrounding tissue. It can be classified as carcinoma *in situ* or as invasive carcinoma depending on whether or not it has invaded the surrounding tissue. If the cancer cells originated in the ducts of the mammary gland then it is called ductal carcinoma *in situ* (DCIS), whereas if the origin of the tumor cells was in the milk-producing glands (lobules) then it is known as lobular carcinoma *in situ* (LCIS). Additionally, breast cancer can be classified based on the expression of hormone receptors like estrogen receptor (ER) and progesterone receptor (PR) or growth receptors like Her2/neu/ERBB2. The receptor status of the breast cancer has a high prognostic value as it predicts susceptibility of the tumor to hormone therapy. Breast cancers which do not express any of

the receptors mentioned above are classified as triple negative breast cancer (TNBC) and are associated with poor prognosis as they are not eligible for hormone therapy.

In the year 2000, there was an important breakthrough in the classification of breast cancer when microarray derived gene expression data was used to define intrinsic molecular subtypes of breast cancer (13). The analysis of gene expression patterns of 1,753 genes in 84 cDNA microarrays from 42 individuals and 17 cultured cell lines showed that each tumor had a distinct molecular signature and samples could be clustered according to similarities in the expression of various genes. This study, besides others that followed (13-17) resulted in the definition of the following molecular or intrinsic subtypes of breast cancer. The Luminal A subtype is characterized by high expression of Estrogen receptor (ER), whereas Luminal B tumors have low expression of ER and high expression of proliferation markers like Ki-67 (13, 16, 17). Basal like- or triple negative tumors are characterized by lack of ER, PR, Her2 expression and were positive for keratins like keratin 5/6, 5/14 and 17 (16, 17). Her2 enriched tumors over-express Her2 but are negative for ER whereas normal breast like tumors were defined by the genes typically expressed by basal epithelial cells and adipose cells (16, 17). Another subtype called Claudin low was identified later (14, 15). The different molecular subtypes are summarized in figure 3, originally published by Malhotra *et al*, 2010 (18).

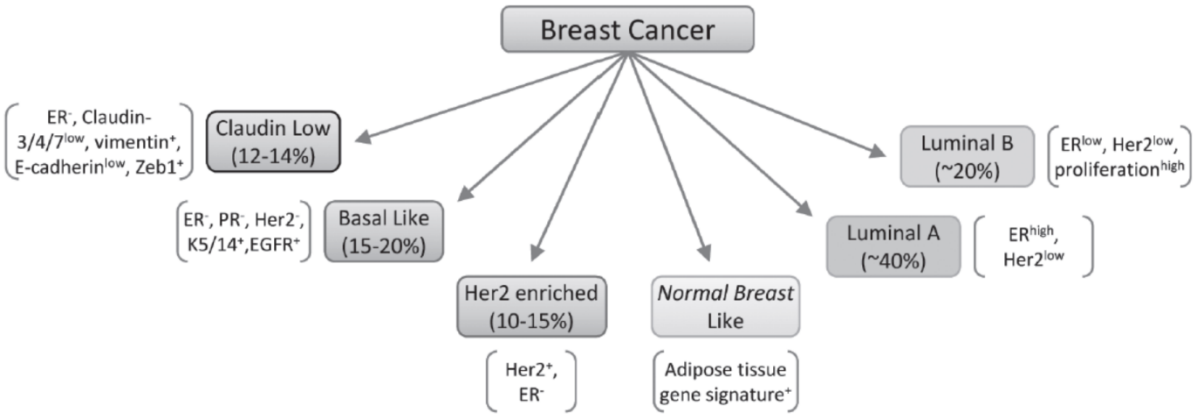

Figure 3. Molecular classification of breast cancer

Molecular subtypes of breast cancer are classified based on the clustering analysis of microarray gene expression data obtained from patient tumors. This led to identification of associated genes which effectively define the different subtypes. (Adapted from Malhotra *et al*, 2010).

The most significant advantage of this classification is that each molecular subtype had distinct clinical outcomes in terms of survival of patients with Luminal A subtype having the most favorable prognosis and Luminal B and normal breast like- having intermediate prognosis followed by Her2 enriched and basal like- which have the worst outcome for patient survival (14, 16, 17, 19). Additionally, the molecular subtypes could explain previously observed differences in the varied clinical outcomes for ER^+ subtypes which could not be explained based on ER^+ status alone (18). However, using microarray analysis routinely in the clinics is not economic, thus Parker *et al* defined a group of 50 genes termed PAM 50 (Prediction Analysis of Microarray) which could be tested by qPCR and could effectively classify tumors into the relevant intrinsic molecular subtype (19). Another method that can be used in clinics easily and reliably is to use immunohistochemistry of ER, PR and HER2 and combine it with Ki-67 index to distinguish Luminal A and Luminal B subtypes (20) and ER,

HER1, HER2 and cytokeratin 5/6 to identify basal-like tumors (21). The stage and the molecular subtype of the breast cancer are very important in determining the treatment options which are discussed in the following section.

3.2.3 Current therapies

The treatment options for breast cancer include surgery, radiation, hormone therapy, chemotherapy, targeted therapies and immunotherapy or a combination of two or more of the aforementioned therapies. The decision is based on how advanced the breast cancer is, the size of the tumor and on whether it has metastasized into neighboring lymph nodes or to distant organs. Additional information that helps in the decision making process is whether the breast cancer is positive for estrogen receptor and the status of Her2 expression. The indications for various treatments according to the stage of the breast cancer are discussed below.

Surgery is included in the treatment options for most women and in DCIS patients, effective surgical intervention results in survival of nearly 100% of patients (22). For tumors that have a pathologically clear margin, breast conserving surgery is an option which is becoming increasingly popular among women with advancement in surgical techniques including the use of laser assisted surgery or robot assisted surgery. On the other hand, for locally advanced large or diffuse tumors without a clear margin, radical mastectomy is used which involves the removal of the entire breast, pectoralis fascia and axillary lymph nodes (22). Some women may opt for prophylactic mastectomy of the other breast (known as contralateral mastectomy) as well, especially if BRCA mutations are detected. Additionally, radiation therapy is prescribed to patients when patients opt for breast conserving surgery in order to minimize the chance of recurrence or when cancer was found to have spread to sentinel lymph nodes. The chest wall is targeted for radiation after a mastectomy when no lymph nodes were detected to be positive. In case lymph nodes were positive for cancer cells, then areas where axillary and supraclavicular lymph nodes are located can be targeted as well (23). Neoadjuvant chemotherapy can also be used to reduce tumor burden before surgery in order to increase the prospects of better surgical outcome or to enable breast conserving surgery instead of mastectomy. For metastatic breast cancer, the treatment options are decided according to the scheme in Figure 4.

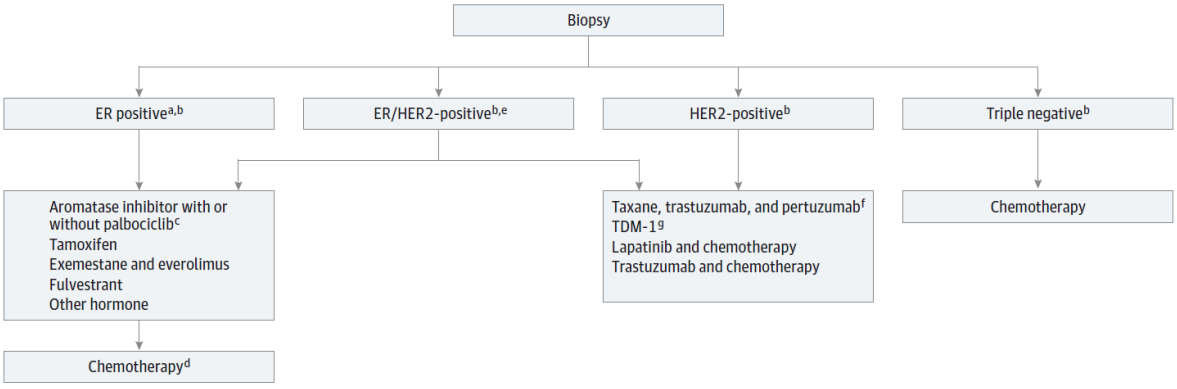

Figure 4. Schematic for deciding treatment of metastatic breast cancer

The therapeutic options for patients with metastatic breast cancer are based on expression of ER and Her2. For ER+ tumors, menopausal status of the patients is also taken under consideration. $Her2^{+}$ patients receive Her2 targeting agents and chemotherapy is prescribed to triple negative breast cancer patients (Adapted from Santa-Maria and Gradishar, 2015).

For hormone receptor positive tumors, endocrine therapy is the first option. Luminal A subtype is best treated with tamoxifen. However, Luminal B tumors have a better response to tamoxifen in combination with chemotherapeutic agents like doxorubicin and cyclophosphamide as Luminal B subtype is characterized by low ER expression and high expression of proliferation genes like Ki-67 (24, 25). For premenopausal women, ovarian suppression may be required in addition to tamoxifen administration as ovaries are an important source of estrogen. In case tamoxifen is not tolerated, then ovarian function suppression alone or with aromatase inhibitor can be used. Aromatase inhibitors work by inhibiting the enzyme aromatase which is required for the conversion of androgens into estrogen, however it does not work on premenopausal women as it cannot suppress estrogen production by ovaries (26). A new study in 2015 showed that aromatase inhibitors like exemestane in combination with ovarian suppression had slightly improved disease outcome for pre-menopausal women who were at sufficient risk for recurrence (27). On the other hand, post-menopausal women benefit from tamoxifen alone or combined with aromatase inhibitors if too many lymph node metastases have been detected (25). Aromatase inhibitors like anastrozole, letrozole and exemestane have been shown to be superior to tamoxifen (28) and letrozole and anastrozole are increasingly used as first-line treatment in postmenopausal women (26). Fulvestrant was better than anastrolzole as a single agent as first line treatment of advanced breast cancer (29). Combining fulvestrant and anastrozole prolonged progression free survival compared to anastrozole alone in a study conducted in 2012 (30).

However, ER^+ and PR^+ tumors can become resistant to endocrine therapies as they can develop mutations that allow them to proliferate independently of ER signaling. For example, aberrations in PI3K-Akt-mTOR signaling pathway can result in resistance to endocrine therapy (31). A phase 3 clinical trial reported that mTOR inhibitor everolimus combined with aromatase inhibitor exemestane increased the progression free survival in postmenopausal patients with advanced breast cancer which was hormone receptor positive (32). However combining pictilisib which is a PI3K inhibitor with fulvestrant (ER antagonist) was not better that fulvestrant alone (33). Combination of Palbociclib which is a small molecule inhibitor of cyclin-dependent kinases (CDKs) 4 and 6 with letrozole was found to be effective in comparison to letrozole alone (34).

HER2 overexpression is correlated to aggressive breast cancer (35-37) with one of the worst prognosis which is only better than triple negative breast cancer (TNBC). Trastuzumab, which is a recombinant humanized monoclonal antibody binding the extracellular domain of HER2 is now standard of care treatment for $HER2^+$ tumors. The most notable mechanism of action of trastuzumab is the inhibition of the MAPK and PI3K-Akt-mTOR signaling pathways which are downstream of HER2 by blocking HER2 dimerization (38). Trastuzumab can also work by causing HER2 to be internalized followed by its degradation (38). It can also mediate antibody-dependent cellular cytotoxicity (ADCC) by attracting immune cells like natural killer (NK) cells to the tumor site (38). The combination of trastuzumab with standard chemotherapeutic agents like anthracyclines and cyclophosphamide or paclitaxel has been shown to work better than chemotherapy (39) or trastuzumab alone (40). Following the success of trastuzumab, other targeted therapies for $HER2^+$ breast cancer that have been developed are lapatinib (which is a tyrosine kinase inhibitor), pertuzumab (Anti-HER2 monoclonal antibody) and trastuzumab-emtansine (trastuzumab conjugated to emtansine). Addition of pertuzumab improved the median overall survival of $Her2^+$ patients by 15 months compared to trastuzumab and decotaxel alone (41). However, not all $HER2^+$ patients

respond to these therapies and the majority of responders relapse quickly due to a variety of resistance mechanisms like loss of the antibody binding extracellular domain, overexpression of Mucin-4 which masks the antibody binding site, aberrant expression of HER3 which cannot be inhibited by trastuzumab, loss of PTEN resulting in constitutively active PI3K/Akt signaling to name a few (38). To overcome this, various combination therapies are being tested in clinical trials. Combining everolimus, trastuzumab and paclitaxel showed improved clinical outcome in patients with $HER2^+$ advanced breast cancer resistant to trastuzumab and taxane treatment in phase 2 studies (42). Also, novel tyrosine kinase inhibitors that target additional isoforms of HER2 like afatinib (which targets HER1 and HER2) and neratinib (which is a pan HER-TKI) are being tested in clinical trials (43).

TNBC is the most aggressive form of breast cancer and has the worst prognosis. The therapy most widely applied to TNBC patients is based on anthracyclines and taxanes in combination with an alkylating agent like cyclophosphamide (25). However, a phase 2 study in 2014 showed that for TNBC patients with non-metastatic disease, addition of carboplatin to the combination of paclitaxel and doxorubicin improved the likelihood of achieving pathological complete response (44). A lot of women with TNBC also carry germline BRCA mutations (45) which results in defective homologous recombination DNA repair which in turn drives carcinogenesis due to high mutational load. However, this makes cells susceptible to PARP inhibition as double strand breaks in the DNA cannot be repaired effectively leading to a halt in DNA replication (46). PARP inhibitor olaparib has been shown to have benefits for BRCA positive patients with different tumor types including breast cancer (46, 47). Another PARP inhibitor iniparib was tested in combination with gemcitabine and cisplatin for treatment of TNBC patients and was found to improve overall survival when used as second-/third-line therapy (48). Combination of angiogenesis inhibitor bevacizumab with paclitaxel was found to increase progression free survival compared to paclitaxel alone in advanced metastatic breast cancer and subgroup analysis showed that this was true for TNBC as well (49).

In summary, hormone receptor positive early stage breast cancer has the best prognosis, however, once it has metastasized; it is treated with a combination of endocrine therapy and chemotherapy. Also $HER2^+$ tumors and TNBC are more aggressive and although chemotherapy is used as standard of care, survival rates still need to be improved. Thus, other treatment approaches like immune therapy are promising and should be investigated. Immunotherapy for breast cancer is described in section 3.4, following a brief description of the immune system and the role of anti-tumor immune response.

3.3 Immune system and cancer

3.3.1 Role of immune system

The immune system has evolved as a way to defend us against foreign particles including pathogenic microorganisms and allergens. Thus, it is capable of discriminating between self- and nonself-antigens (e.g. derived from invading pathogens) including altered self-antigens (e.g. tumor cells carrying mutated antigens). It is comprised of innate and adaptive immune response. The innate immune response acts as the first line of defense against invading pathogens and is composed of the complement system and cells like neutrophils, macrophages and NK cells. The complement system consists of a family of plasma proteins which upon activation can opsonize bacteria for phagocytosis or result in the formation of transmembrane pores causing them to lyse. Neutrophils and macrophages can phagocytose

pathogens, whereas NK cells can kill antibody coated cells. Components of the innate immune system can recognize pathogens based on glycoproteins selectively expressed by the pathogen. For example, the complement system is activated by carbohydrate containing mannose residues. Innate immune cells, on the other hand, are activated when their pattern recognition receptors (PRRs) recognize pathogen associated molecular patterns (PAMPs) like lipopolysaccharide (LPS) or double stranded RNA (50, 51).

Conversely, the adaptive immune system is comprised of precursor cells with certain specificities which are activated upon encountering their cognate antigen. Upon activation they undergo clonal expansion to develop into effector cells, some of which persist as memory cells. The memory cells form the basis of immunological memory and provide long-lasting immunity against pathogens. Since the specific effector cells require approximately a week to develop after the first exposure to a particular antigen, adaptive immune response takes longer than innate immune response to clear the pathogen. However, in the case of subsequent exposure to the same antigen, there is a rapid activation and proliferation of memory cells resulting in an accelerated pathogen clearance. The adaptive immune system is comprised of B and T cells both of which have antigen receptors which confer specificity for different pathogenic antigens. For example, T cell receptors (TCRs) are heterodimers composed of either combination of α/β chains or of γ/δ chains. There are multiple genes for each segment of the chain designated as follows: variable (V), diversity (D), joining (J) and constant (C). For instance, the α chain locus of the TCR has 70-80 V_α and 61 J_α genes followed by the constant gene, whereas the β chain locus is comprised of 52 V_β, 2 D_β, 13 J_β and 2 constant genes (50). The genes undergo somatic rearrangement to give rise to numerous α and β chains which dimerize to yield a wide range of TCRs, each with a different specificity. For instance, in humans 25 α chains and 10^6 β chains have been identified which can pair to give rise to $25x10^6$ clonotypes (52). Antigen receptors of B cells and γ/δ T cells are generated by a similar rearrangement process.

B cells can secrete antibodies specific against foreign antigens which can opsonize pathogens and facilitate their phagocytosis or mediate antibody-dependent cell-mediated cytotoxicity (ADCC). T cells are classified into 2 major types: $CD8^+$ cytotoxic T lymphocytes (CTLs) and $CD4^+$ T helper (Th) cells. CTLs can kill target cells infected with intracellular pathogens by secreting perforins or granzyme B resulting in apoptosis of the recognized cell (53). Additionally, CD95L expressing CTLs can trigger apoptosis of CD95 positive target cells or kill target cells via secretion of cytokines like IFNγ and TNFα (53). There are different subtypes of $CD4^+$ T helper (Th) cells. Th1 cells provide immunological help for activation of $CD8^+$ cytotoxic T cells and macrophages, thus playing an important role in the elimination of intracellular pathogens (54). Th2 cells activate IgE production by B cells, thereby helping in the elimination of extracellular parasites including helminthes (54). Th17 cells secrete IL-17 crucial for defense against extracellular pathogens (54). There is another class of $CD4^+$ T cells, called regulatory T cells (Tregs) which can dampen $CD8^+$ and $CD4^+$ T cell proliferation and responses in order to prevent auto immunity (54).

T cells can recognize their cognate antigen only when the relevant antigenic peptide is presented on the major histocompatibility complex (MHC) molecule. TCRs on $CD8^+$ T cells can interact with MHC I-peptide complex, whereas TCRs on $CD4^+$ T cells can recognize peptides presented on MHC II molecule. Both, CD8 and CD4 molecule act as a co-receptors as depicted in Figure 5. The peptides that are displayed on MHC I are derived from self-proteins or from intracellular pathogens like viruses, but MHC II molecules can present

peptides originating from extracellular proteins that have been taken up by endocytosis or pinocytosis. This is due to the fact that antigen processing machinery is different for MHC I and MHC II restricted T cell epitopes. Endogenous cytosolic proteins synthesized within the host cell including viral proteins are enzymatically cleaved by the proteasome into smaller peptides which are transported in the endoplasmic reticulum (ER) by transporters associated with antigen processing (TAP) proteins 1 and 2 (55). Inside the ER, the peptides can bind the MHC I molecule and then the loaded MHC molecule is trafficked to the cell surface (55). Peptides originating from endocytosed extracellular pathogens are loaded onto the MHC II in endocytic vesicles called MHC class II compartment (MIIC) (55). However, certain subsets of DCs and macrophages can present exogenous antigens on MHC I context, the phenomenon is known as cross-presentation (56). Additionally autophagosomes can supply cytoplasmic antigens to the MHC II antigen loading pathway resulting in presentation of endogenous antigens on the MHC II molecule of both professional and non-professional APCs which can present cytosolic antigens on MHC II (57, 58). MHC I is expressed on all nucleated cells whereas MHC II is expressed mostly on professional antigen presenting cells (APCs) like dendritic cells (DCs) and macrophages. However, IFNγ can stimulate other cell types like endothelial cells, fibroblasts, epithelial cells and tumor cells to upregulate MHC II and they can act as non-professional APCs (58).

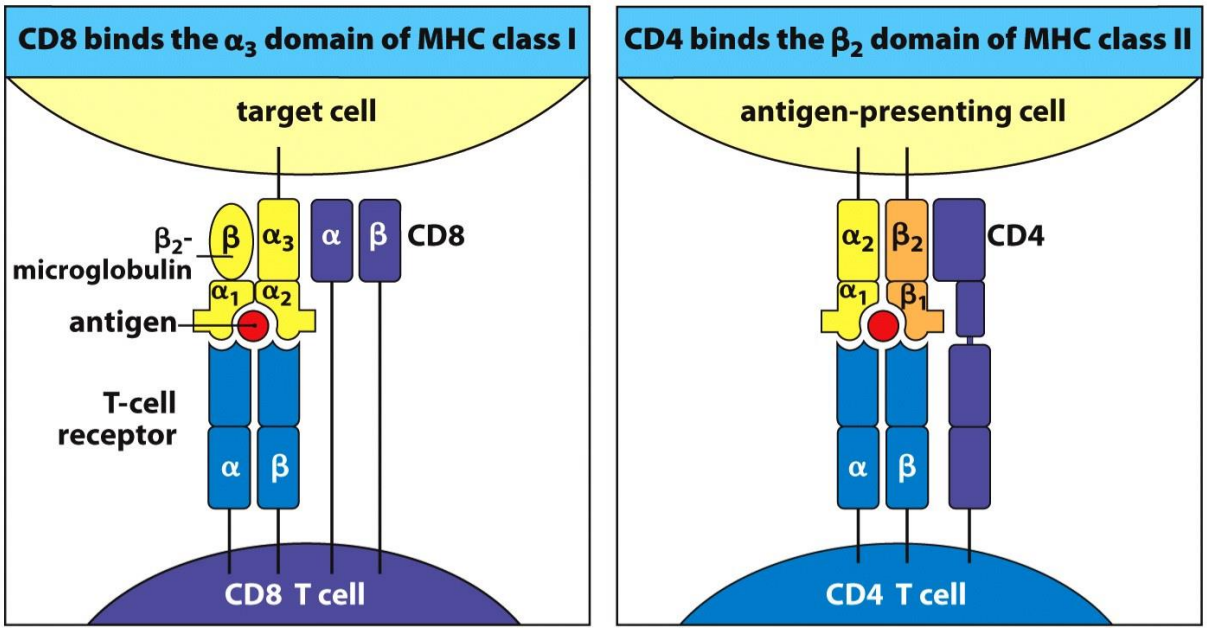

Figure 5. Interaction of TCR with respective MHC-peptide complex

The TCR on $CD8^+$ T cells can recognize peptides presented on MHC class I molecules whereas the $CD4^+$ T cells interact with antigen presenting cells via their TCRs which bind peptide-MHC class II complex (Figure from Immunobiology, 5th Edition 2001).

MHC molecules are encoded by the MHC complex and they are highly polymorphic. The MHC I molecule is composed of an α chain and a β_2-microglobulin (β_2m) whereas the MHC II molecule is a heterodimer of an α and a β chain (figure 5) (50). In humans, the MHC I α chain is encoded by the human leukocyte antigen (HLA) -A, -B and –C genes and the loci within the HLA complex encoding the α and the β chains of the MHC II molecules are designated as HLA-DR, -DP and DQ (50).

Due to its high degree of polymorphism, huge numbers of MHC I and MHC II allotypes are expressed within a population where each allotype displays an allele-specific peptide binding groove. Thus, only peptides with a given allele-specific binding pattern can bind to a given allotype and are therefore presented as an HLA-restricted epitope to T cells expressing a cognate TCR. Additionally, the size of the peptide that can bind the peptide binding grooves varies between MHC I and MHC II due to their structural differences. For example, the peptide cleft of MHC II is open and can hold peptides of 12-25 amino acids (59), however the peptide binding groove of MHC I is fixed and can accommodate shorter peptides of 8-11 amino acids (59, 60). The information about the presence of anchor residues within the epitope sequence required for stable binding and the length of peptide that can fit into the peptide binding groove enables the *in silico* prediction of possible epitopes derived from a particular protein (60-62). Once the predicted epitopes are validated *in vitro*, synthetic peptides can be used for developing peptide vaccines.

3.3.2 Immune surveillance of cancer

The concept of immunosurveillance of cancer is well accepted. The idea was initially postulated by Paul Ehrlich and further propagated by Burnet and Thomas (63). Various studies have demonstrated that immunodeficient mice are more prone to tumor development (both spontaneous and carcinogen induced) (64). The role of various types of immune cells in controlling tumor growth has been shown using genetically engineered mouse models which lack particular cell types (64).

Since the immune system can not only control tumor growth but also modify the tumor, the idea of cancer immunosurveillance has evolved into that of cancer immunoediting which has three stages denoted by “3 Es”: elimination, equilibrium and escape. The first stage is called *elimination,* where transformed cells which can potentially give rise to tumors are eliminated by the immune system. The next stage is called *equilibrium* where tumor cells are maintained in a steady state where they are present but cannot grow. It has been demonstrated that MCA transformed tumor cells are held in check by components of adaptive immunity and their ablation results in tumor outgrowth (65). The third stage is called *escape* and is characterized by the spontaneous escape of immune edited and less immunogenic tumor cells from the state of equilibrium leading to progressive tumor growth (65). Tumors evolve in order to escape immune mediated destruction by reducing antigen presentation or developing resistance to apoptosis (63). Besides, developed tumors are distinguished by an immunosuppressive microenvironment and are infiltrated by immune suppressive cells like myeloid derived suppressor cells (MDSCs), Tregs and tumor-associated macrophages (TAMs), which makes it difficult to sustain an effective anti-tumor immune response. In addition to being suppressed by the aforementioned cells, infiltrating T cells are rendered anergic due to persistent exposure to the tumor antigen (66, 67) or display an exhausted phenotype characterized by the expression of inhibitory receptors like programmed cell death protein 1 (PD-1), cytotoxic T lymphocyte antigen-4 (CTLA-4), lymphocyte activation gene 3 protein (LAG-3) etc. (68). The presence of active anti-tumor immunity in humans has been substantiated by various studies which have shown strong correlation between immune cell infiltration and prognosis (69). This has led to the development of ‘Immunoscore’ that takes into account number, type and location of immune cells infiltrating the tumor and it has proven to be a more robust prognostic factor than other clinical classifications like cancer staging or TNM staging (70, 71). The effect of the infiltrating immune cells is achieved by the net effect of opposing forces of anti-tumor T cells and immune suppressive cells. Anti-tumor

T cell responses and the types of antigens they recognize are described in more detail in the next section.

3.3.3 Anti-tumor T cell responses

The types of T cells infiltrating the tumor are crucial in determining whether they are beneficial to the patient or not. In general, infiltrating cytotoxic $CD8^+$ T cells and Th1 cells are associated with improved survival and Tregs are associated with poor prognosis with some exceptions (69). Various studies have investigated the relation between high immune cell infiltration and patient outcome in breast cancer (72). High density of $CD8^+$ tumor-infiltrating lymphocytes (TILs) positively correlates to better survival (73-75) and is indicative of an effective response to chemotherapy (76, 77) and Trastuzumab therapy (78). Different $CD4^+$ T cell subsets have different roles in predicting patient outcome. $CD4^+$ Th1 cells (79, 80) and follicular helper T (Tfh) cells (81) are good prognostic markers whereas, $CD4^+$ Th2 (80) and Th17 (82) cells are associated with bad prognosis. The role of $CD4^+Foxp3^+$ Tregs is not clear in breast cancer as they are associated with high risk of relapse (83) but also with good prognosis (84) and response to therapy (77) especially in presence of $CD8^+$ T cells. Cytotoxic $CD8^+$ T cells can directly kill tumor cells through various mechanisms including secretion of granzyme B and perforin (85) whereas $CD4^+$ Th1 cells are essential to prime and sustain an effective CTL response. $CD4^+$ T cells are capable of killing tumor cells directly in response to antigen presented on MHC II of tumor cells (86) in addition to MHC II deficient tumor cells (87).

The prognostic value of TILs confirms the fact that they play an active role in anti-tumor immunity, but the antigens recognized by these T cells had not been identified for a long time. Studies with TILs in melanoma have shown that they are reactive against various tumor-associated antigens (TAAs) (88, 89) and against neo-antigens generated by mutations (90). Tumor associated antigens include a wide range of antigens which arise from mutations, viral infection or due to deregulated expression in tumor cells. They are broadly classified as follows (91, 92) :

a. Oncofetal: expressed during embryonic development and in cancer cells. *E.g.* carcinoembryonic antigen (CEA)
b. Oncoviral: virus-derived proteins that drive oncogenesis. *E.g.* human papilomavirus (HPV) encoded E6 and E7
c. Non-mutated overexpressed: expressed by normal tissues but overexpressed by malignant cells. *E.g.* Her2/neu and EpCAM1
d. Cancer-testis: expressed in testis/placenta in healthy individuals but overexpressed in neoplastic tissue. *E.g.* MAGE and CAGE
e. Neoantigens: antigens only expressed by cancer cells that arise from mutations. *E.g.* Ras and p53
f. Differentiation antigens: expressed on differentiated cells and malignant tissue arising from them. *E.g.* Tyrosinase and MelanA
g. Post-translationally altered: posttranslational modifications are altered in tumor tissue. *E.g.* MUC1 is hypoglycosylated in tumors

Since T cells recognize epitopes presented on MHC molecules, various studies were carried out to identify epitopes derived from TAAs which are presented by tumor cells or by antigen presenting cells (APCs) themselves (93). Identifying TAAs can not only provide us with deeper insight into the process of tumorigenesis but also assist in the development of novel

diagnostic tools, prognostic markers or therapeutic targets. Another advantage of identifying tumor antigens/epitopes is that they can be used for strengthening anti-tumor immunity either by vaccination or by adoptive transfer of genetically engineered antigen specific T cells (details in section 3.4). The tumor associated antigen NY-BR-1 which is the focus of this project is described in the next section.

3.3.4 NY-BR-1

NY-BR-1 was first identified and cloned using SEREX (serological analysis of recombinant tumor cDNA expression libraries) technology (94). SEREX is based on screening of a cDNA expression library derived from tumor tissue with autologous patient sera which should contain high titer immunoglobulins against immunogenic tumor antigens. In healthy individuals, NY-BR-1 mRNA has been detected only in the mammary gland, testis and prostate, and at very low levels in the placenta (94, 95). However, 70-84% of breast tumor samples tested positive for NY-BR-1 mRNA (94, 95), whereas 60% expressed the NY-BR-1 protein (96). The fact that NY-BR-1 is overexpressed in breast cancer was confirmed in another study using subtracted cDNA libraries and cDNA microarrays (97). Since NY-BR-1 is overexpressed by the majority of breast tumors, but not in healthy tissues with the exception of the ductal epithelium of breast, it appears as a suitable target for immune therapy of breast cancer. The function of NY-BR-1 is not yet known, however based on the presence of a nuclear localization signal and the bZIP motif, it was presumed to be a transcription factor (94). The detection of NY-BR-1 in the nucleus in breast tumor sections by confocal microscopy strengthens this hypothesis (96). However, subsequent studies showed that ectopically expressed NY-BR-1 localized to cytoplasm and the cell membrane in living cells and was only detected in the membrane fraction of metastatic lesions (98) which could be due to NY-BR-1 degradation products which have lost the hydrophobic membrane targeting domain. NY-BR-1 expression was found to positively correlate to ERα expression suggesting transcriptional control of NY-BR-1 by estrogen (99). The presence of 4 estrogen response elements (EREs) around the transcription start site (TSS) of NY-BR-1 suggests that estrogen might control NY-BR-1 expression. However, this is only partial as NY-BR-1 expression can occur independently of ERα expression, as some $ERα^-$ tumors express NY-BR-1 (99) and there was no significant difference in NY-BR-1 expression between pre-menopausal and post-menopausal women (100). Interestingly, it was found that in patients treated with Tamoxifen, NY-BR-1 expression was reduced in recurrent disease compared to primary tumor obtained from the same patient independent of ERα expression (99). Although some studies showed that NY-BR-1 expression was less frequent in higher grade tumors compared to lower grade tumors (96), comparison of a primary tumor with distant metastases and recurrent disease from the same patient showed that it does not seem to get lost while disease progresses (100). Importantly, NY-BR-1 expression was confirmed in metastatic samples (98), which is important if NY-BR-1 is to be targeted for immunotherapy. NY-BR-1 expressed on the membrane could be recognized by a monoclonal antibody, which makes it a potential target for antibody therapy (98). It is also an attractive target for T cell based therapies, as HLA-A2 restricted epitopes have been identified and CTL clones against these epitopes could be generated from PBMCs derived from healthy individuals and breast cancer patients (95, 101). Co-expression analysis of NY-BR-1 and HLA class I revealed that approximately 6% of the patients could be eligible for vaccination with recognized epitopes (100). Additionally, HLA-DRB1*0301and HLA-DRB1*0401-restricted $CD4^+$ T cell epitopes have been identified (102). Since $CD4^+$ Th1 cells are very important for sustained anti-tumor CTL response (103), this can augment immunotherapy directed against NY-BR-1. NY-BR-1

expression was found to be beneficial for patient outcome (100) which could be due to intrinsic anti-NY-BR-1 immunity. Thus, NY-BR-1 is an ideal target for cancer immunotherapy due to its selective expression pattern as well as the presence of detectable anti-NY-BR-1 immune response in breast cancer patients.

3.4 Immunotherapy of cancer

3.4.1 Cancer immunotherapy

Any therapeutic intervention in order to kill cancer cells or inhibit their proliferation, that includes the activation (or reactivation) of the host immune system or involves the administration of components derived from the immune system, can be classified as cancer immunotherapy. The various strategies developed for cancer immunotherapy have been described below according to the type of agent used:

Cell based therapies

DC vaccines

Dendritic cell (DC) therapy is based on mostly autologous DCs that are matured or activated *ex vivo,* loaded or transfected with tumor antigen, and re-infused into patients in order to prime and activate T cells directed against tumor antigens. Mature DCs can be generated from peripheral blood mononuclear cell (PBMC) derived monocytes, which are loaded with synthetic peptides representing TAA derived epitopes (104), transfected (105) or electroporated (106) with mRNA encoding tumor antigen, or transduced with adenovirus expressing TAA (107). One of the first cellular vaccines to be approved by the Food and Drug administration (FDA) in 2010 was sipuleucel-T (APC 8015, trade name Provenge) based on its success in clinical trials (108).

TILS

Tumor infiltrating lymphocytes (TILs) can be isolated from pieces of resected tumor and can be expanded *ex vivo* with IL-2, monoclonal anti-CD3 antibody OKT3 and irradiated feeder cells (109), and can be adoptively transferred to the patients. In one of the pioneering studies, these T cells were shown to mediate effective anti-tumor responses in melanoma in 60% of patients who had not received any IL-2 prior to treatment and 40% of patients who had received IL-2 previously (110). Successive studies that included lymphodepleting regimens (chemotherapy and/or irradiation) prior to adoptive cell therapy (ACT), achieved better outcomes in terms of prolonged cell persistence (111, 112). The most successful aspect of the therapy was that the majority of patients who had complete regressions, had durable responses which lasted during follow-up period of 5 years or longer (112).

CAR T cells

Alternatively, T cells can be engineered to express chimeric antigen receptors (CARs) that consist of an extracellular antigen binding domain derived from a single chain variable fragment (scFv) directed against a tumor antigen and an intracellular signaling domain derived from the CD3 ζ chain of the TCR. This allows the T cells to target tumor cells independently of MHC expression on the tumor cells. Second and third generation CAR T cells express one or more co-stimulatory molecules respectively. Inclusion of domains from co-stimulatory molecules like CD27, CD28, OX40, 4-1BB etc. improves the quality of T cells in terms of prolonged persistence *in vivo* and better functional capacity (113). Different CAR

transduced T cells targeting CD19 which is expressed in B cell malignancies, have been successfully used in various clinical studies (114).

TCR transduced T cells

Another approach for adoptive transfer of T cells for cancer immunotherapy involves the use of T cells genetically engineered to express TCRs directed against tumor antigens. One advantage of this strategy over the use of TILs is that the generation of TILs depends on the presence of resectable metastatic lesions which are infiltrated by tumor-reactive T cells. The proportion of actual tumor reactive T cells can be highly variable in the TIL product, but the use of TCR transduced T cells allows the transfer of high number of specific T cells. A first study was performed with MART-1 TCR transduced T cells in metastatic melanoma patients (115), which was followed by others targeting carcinoembryonic antigen (CEA) for colorectal cancer (116).

Peptide, recombinant protein, DNA and RNA vaccines

Peptide, recombinant protein, DNA or RNA vaccines can act as a source of antigen *in vivo* resulting in their uptake by APCs which can prime or reactivate T cells specific for TAA. There has been some clinical success in the treatment of premalignant lesions caused by HPV 16 infection using synthetic long peptides (117) or a recombinant fusion protein (118) by targeting the HPV 16 derived E6 and E7 oncoproteins. The outcome of peptide vaccination can be enhanced by the use of synthetic long peptides or polyvalent vaccines or by combining them with anti-CD40 antibody or TLR ligands plus adjuvant (119). Vaccination using naked DNA has also been effective in generation of HPV 16 and HPV18 specific immune response (120, 121) and also in clearance of premalignant lesions and virus (121). Use of RNA encoding multiple TAAs as vaccine had limited clinical success (122, 123), probably due to limitations of the RNA delivery platform. However, recently the use of RNA encoding neo-epitopes (124) and RNA-lipoplexes (125) for efficient targeting of RNA to DCs has shown very promising results in pre-clinical models and could revive the use of RNA vaccines if ongoing clinical trials can recapitulate the success of the pre-clinical research.

Viruses

Viruses can be used for cancer immunotherapy either as a vector to deliver DNA for vaccination or as oncolytic agents (126, 127). Sometimes genes encoding immunomodulating agents like costimulatory molecules (e.g. CD80, ICAM-1), cytokines (IL-2) or chemokines (GM-CSF) are added in order to generate a strong immune response (127). The efficacy can be further enhanced by a heterologous prime-boost regimen to prevent the premature clearance of the virus when the same virus is used for boosting vaccine induced immunity. For example, PROSTVAC which is directed against prostate-specific antigen (PSA) utilizes a vaccinia virus vector followed by fowlpox virus vector for boosting. A phase II trial with PROSTVAC and GM-CSF was shown to have benefits for patients in terms of prolonged overall survival (128). Some oncolytic viruses have intrinsic tropism for cancer cells whereas others can be engineered in order to target them to malignant tissue which overexpresses their respective entry receptors. Of various oncolytic viruses tested in clinical trials, Herpes Simplex Virus-1 (T-VEC) (129) and Adenovirus (H101) (130) which had been genetically engineered to enhance tumor cell tropism and reduce pathogenicity to normal cells have advanced to Phase III and Phase II trials, respectively, where they have shown clinical benefit. The additional benefit of using oncolytic viruses is

that the lysed tumor cells release TAAs which can be taken up by APCs which can prime tumor-specific T cell response. Oncolytic viruses have danger signals (DAMPs) which further boost the anti-tumor immune response.

Immunostimulatory cytokines, chemokines or PRR agonists

Immunostimulatory cytokines, chemokines or PRR agonists augment the effect of immunotherapy. Interleukin-2 (IL-2) is one of the most widely used immunostimulatory cytokines which is essential for T cell proliferation and activation (131). It is used as a standalone therapy (132) or as an adjuvant in vaccination trials (133) or adoptive T cell transfer (111, 112, 134). Interferon-α2a and Interferon-α2b have also been demonstrated to have clinical benefit in some trials in melanoma patients (135). Granulocyte-macrophage colony-stimulating factor (GM-CSF) is a chemokine that is known to recruit antigen presenting cells like macrophages into the tumor and can support the generation of an effective anti-tumor immune response. GM-CSF is added to different vaccination modules including peptide vaccines (136), viral vaccines (129) where the virus encodes for GM-CSF to have a locally concentrated dose of GM-CSF or to engineer allogeneic tumor cells to express GM-CSF and use irradiated tumor cells (137) to prime anti-tumor T cell response. PRR agonists like poly-ICLC which is a toll-like receptor (TLR) agonist (138), CpG (139) and Imiquimod (118) can be used as adjuvants with vaccines to generate potent T cells responses.

Monoclonal antibodies

mAbs directed against tumor associated antigens

Monoclonal antibodies can act against cancer in various ways. Tumor targeting monoclonal antibodies Trastuzumab (anti-Her2/neu) (39) and Cetuximab (anti-EGFR) (140) can either block or inhibit signaling pathways required by tumor cells for rapid proliferation. Additionally, such antibodies can be conjugated to a drug (*e.g.* Trastuzmab emtansine) (141) or to a radioisotope (yttrium-90 ibriturnomab tiuxetan) (142) for targeted killing of the tumor cells. Some antibodies like Rituximab (anti-CD20) can opsonize the tumor cells and can trigger complement dependent cytotoxicity (CDC) and antibody dependent cell mediated cytotoxicity (ADCC) by recruiting effector cells (143). Bispecific T cell engagers like blinatumomab which is directed against CD19 can cross-link the tumor cell to T cells to facilitate T cell mediated tumor cell killing (144).

Immunomodulatory antibodies

Immunomodulatory antibodies can act either by activating the immune system or by abrogating immune suppressive mechanisms. The agonistic CD40 antibody has been demonstrated to mediate clinical responses by promoting tumoricidal function of macrophages (145). Anti-tumor immune responses can be dampened by the same mechanisms that help prevent tissue damage following pathogen clearance in the normal anti-pathogen immune response. Antibodies designed to block the function of these inhibitory ligands and receptors can reactivate the anti-tumor immune response. This is known as immune checkpoint blockade and anti-CTLA-4 antibody, Ipilimumab was the first antibody which showed clinical activity in advanced melanoma patients (146). Other antibodies targeting PD-1 that followed, like Nivolumab (147) and Pembrolizumab (148) have been successful and showed fewer toxicities compared to Ipilimumab. The unprecedented

success of this approach highlights the fact that successful immunotherapy relies on counteracting immunosuppressive mechanisms.

Thus, the immune system can be harnessed in various ways to generate anti-cancer responses. Combination of different types of immunotherapy as an adjuvant therapy after the bulk of tumor has been resected might be more effective as the suppressive tumor microenvironment has been removed. It has been shown that low dose chemotherapy (149) and radiotherapy (150) have immunostimulatory properties and could be combined with other immunotherapies. Targeted therapies can also be combined with immunotherapy for better outcomes as they can modulate immune responses as well (151). The immunotherapeutic strategies employed to treat breast cancer are described in the next section.

3.4.2 Immunotherapy of breast cancer

Breast cancer suffered a lack of focus with respect to immunotherapy due to the initial belief that they are not immunogenic. However, it is now catching up and there are a lot of clinical trials ongoing that are testing various immunotherapies for breast cancer (sometimes in combination with other agents). Anti-Her2 antibody, trastuzumab is the most successful immunotherapy available for breast cancer as it improved the survival of $Her2^+$ patients drastically, especially since it used to have one of the worst prognosis (39). Initially, it was believed that it only inhibits Her2 signaling but it turned out that it can also have immune mediated effects like ADCC (38). Trastuzumab-emtansine has shown promising results in clinical trials and is approved for Her2 positive metastatic breast cancer (141, 152). Bispecific antibody against Her2 (153) which links the tumor cells to T cells have been designed as well and has shown efficacy in preclinical models but clinical data is missing. On the other hand Ertumaxomab; a tri-functional Her2 directed antibody which can crosslink tumor cells to T cells and innate cells like macrophages and NK cells has been tested in Phase I trial which had acceptable toxicity profile (154). Antibodies targeting other breast cancer associated antigens have been used in clinical trials as well with limited success.

Her2/neu has also been targeted for vaccination approaches of breast cancer. In a phase I/II trial breast cancer patients were vaccinated with HLA-A2/A3 restricted Her2 derived peptides in combination with GM-CSF to prevent disease recurrence. Even though the vaccine was found to be safe and successfully induced Her2/specific immunity (155), it improved 5 year disease free survival only in patients who were optimally dosed and not for the entire vaccinated group (156). A phase III trial is ongoing to determine efficacy of the vaccine. Other studies have tried to induce Her2/neu specific $CD4^+$ T cell response using peptide pulsed DCs (157) or modified MHC II restricted Her2 epitope in order to generate long lasting immunity. PANVAC which is a virus based vaccine targeting MUC1 and CEA along with providing co-stimulatory signals also showed some promise in Phase II trials (158). However, most immunotherapeutic approaches for breast cancer have resulted in modest outcomes. This could be due to suboptimal vaccine formulation, lack of appropriate adjuvants or to a highly immune suppressive tumor microenvironment. Nevertheless, recent success of immune checkpoint blockade in a wide variety of tumor entities have led investigators to evaluate the possibility of this approach in breast cancer as well and several early phase trials with Tremelilumab (159), Pembrozilumab (160) and MPDL3280A (161) have shown feasibility and promising results. Until recently, most success stories of immunotherapy involve melanoma as it is highly immunogenic and has a high mutational load resulting in numerous neo-antigens which are targeted by TILs and make them susceptible to checkpoint blockade (90, 162). Even though breast cancer is considered less immunogenic, recent

studies have indicated that the presence of active anti-tumor immunity as T cell infiltration positively correlate with improved survival in $Her2^+$ subtypes (163) and TNBC (78). However, the frequency of TILs is quite low in $Her2^+$ breast tumors and TNBC (78) and thus checkpoint blockade might not function alone as there are not enough TILs that can be reactivated. Thus, a vaccine or TLR agonist can be used to elicit an anti-tumor immune response followed by checkpoint blockade to maintain it (164). Another approach is to use cryoablation (165), low dose chemotherapy or radiation to release tumor antigens to initiate an immune response followed by immune checkpoint blockade.

3.4.3 Immunosuppressive tumor microenvironment (TME)

As mentioned earlier, nascent tumors are constantly eradicated by the immune system, but the tumor adopts various mechanisms to escape immune surveillance. The recent success of immune checkpoint blockade therapy underscores the fact that the tumor microenvironment is very immunosuppressive and even if immune cells with potential to eradicate the tumor manage to infiltrate the tumor, they are quickly neutralized by the immunosuppressive micro-milieu. Evading immune destruction has been identified as one of the hallmarks of cancer (166) and is mediated either by avoiding recognition or by rendering the infiltrating immune cells non-functional. Tumors avoid T cell mediated killing by downregulation of surface expression of MHC molecules which can result from genetic alterations at the MHC locus or defective antigen processing machinery leading to empty MHC molecules which are rapidly internalized (167). Immunoediting by antigen specific T cells also selects for antigen loss variants (168, 169) which give rise to resistant tumors. Moreover, tumor cells express PD-L1 which is a ligand for PD-1, a receptor expressed on T cells that negatively regulates T cell function (170). Additionally, tumors are known to secrete cytokines like TGF-β, IL-4 and IL-10 and enzymes like IDO which have an immune suppressive effect. TGF-β (171) and IL-10 (172) induce Tregs whereas IL-4 (173) promote polarization of TAMs towards an M2-like phenotype both of which lead to suppression of T cell function. For example, Sousa *et al* showed that breast cancer cells secreted M-CSF which induces an M2-like phenotype in macrophages (174). Besides recruiting immune suppressive cells, IL-10 can directly impair cytokine release and cytotoxicity of T cells and priming by APCs (175). Tumor derived IDO contributes to the suppressive microenvironment by recruiting myeloid-derived suppressor cells (MDSCs) (176) while simultaneously impairing T cell activation by tryptophan depletion. Chemokines secreted by the tumor like CCL22 facilitate the trafficking of CCR4 expressing Tregs into the tumor via CCL22-CCR4 interaction (177). Thus, the immune suppressive tumor microenvironment is the result of tumor derived factors and recruitment of suppressor cells like Tregs, MDSCs and TAMs. The role of TAMs is described in more detail in the following section.

3.4.4 Tumor associated macrophages

Macrophages are part of the innate immune system and in case of an infection by pathogenic bacteria; macrophages are activated by TLR ligands like LPS and Th1 cytokines like IFNγ which results in the classical activation of macrophages (178). These classically activated macrophages are characterized by expression of pro-inflammatory cytokines like TNFα, IL-1, IL-12 etc. (178) and they initiate an adaptive immune response by attracting/activating effector cells. They can also produce reactive oxygen species or the enzyme nitric oxide synthase which generates nitrogen molecules both of which can directly kill infected cells. Thus, these cells mediate the clearance of pathogens following an infection. However in case of chronic infection or infection by a parasite, macrophages are

alternatively activated in response to Th2 cytokines like IL-4 or IL-13 (178, 179). They are characterized by secretion of immune-suppressive cytokines like IL-10 and TGF-β which are required to dampen the immune response. They express high levels of scavenging receptors like CD204 which allow them to take up dying tissue and secrete angiogenic factors like VEGF to promote neo-angiogenesis in order to facilitate tissue repair and wound healing (178, 179). Thus M1 and M2 polarized macrophages not only require different stimuli but also are characterized by different expression markers and functions (summarized in Figure 6).

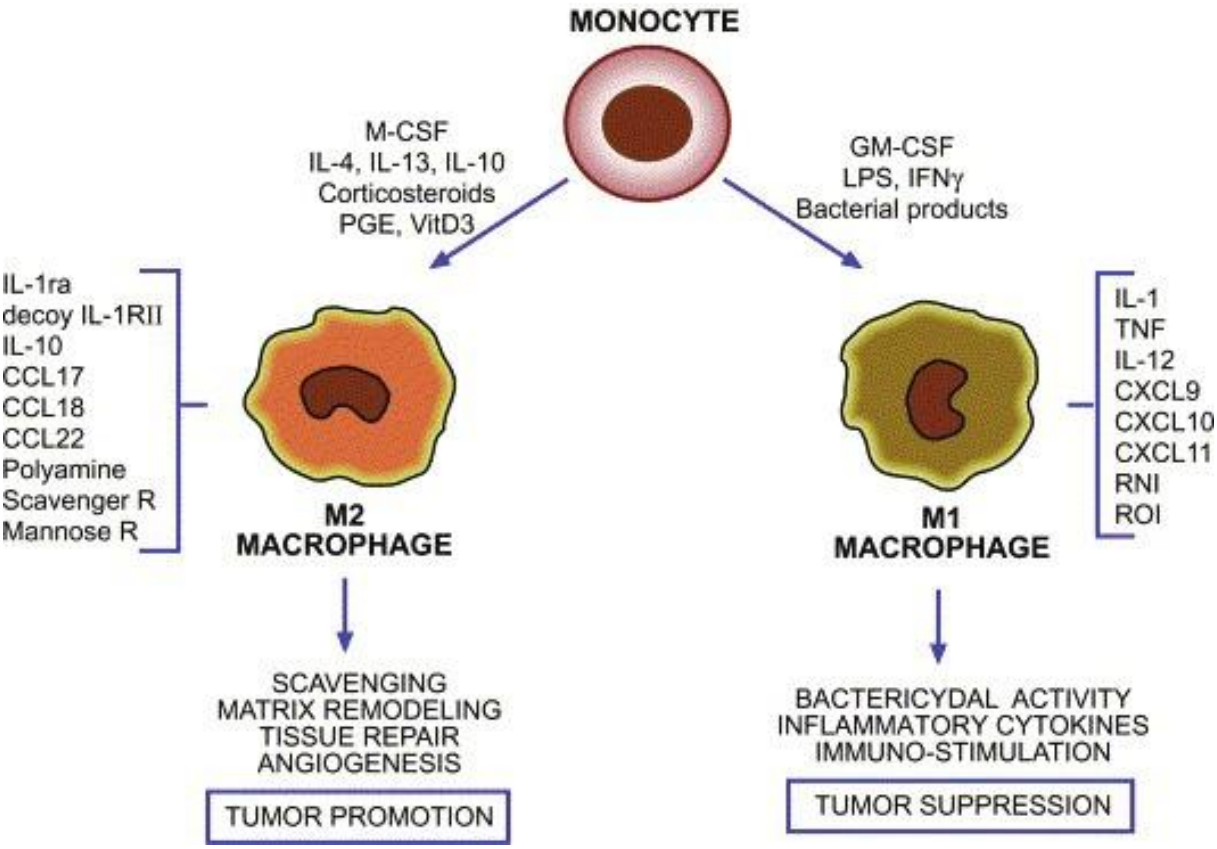

Figure 6. Differential polarization of macrophages

Differentiation and polarization of macrophages depend on the stimuli received. Differentiated macrophages can be distinguished based on expression of different surface markers and cytokines which also define their distinct functions (Figure from Quatromoni and Eruslanov, 2012).

It has been demonstrated in mouse models that tumor-associated macrophages (TAMs) switch from classically activated M1-like phenotype to an alternatively activated M2-like phenotype as the tumor progresses (180, 181) and various studies have demonstrated that late stage tumors are dominated by immunosuppressive TAMs (182). This is mediated by the tumor which secretes various factors to skew the TME towards an immunosuppressive milieu as a mechanism to escape immune-mediated destruction (183). However, not all TAMs are tumor-promoting. It has been described that TAMs with different phenotypes can be found within the same tumor but distributed in different regions of the tumor (180). IFNγ activated macrophages have been shown to phagocytose chronic lymphocytic leukemia (CLL) cells by ADCC in presence of Rituximab (anti-CD20 antibody) (184). Additionally, macrophages activated by exposure to bacterial components have been shown to generate ROI (reactive oxygen intermediates) or RNI (reactive nitrogen intermediates) which have tumoricidal

properties (185). However, these intermediates can also promote tumor formation due to their mutagenic properties. On the other hand, M2-like TAMs have been shown to have pro tumorigenic function due to their ability to promote angiogenesis, extravasation and metastasis (183). This could explain why high macrophage infiltration can either be good or bad for patient survival depending on the functional phenotype and the location of TAMs present.

For example, in case of colorectal cancer high infiltration of $CD68^+$ macrophages along the tumor front correlated with good prognosis (186). Another tumor type where high density of infiltrating macrophages had beneficial effect on patient survival is non-small cell lung cancer (NSCLC) (187). However, for most tumors types like bladder, glioma and cervical cancer high density of infiltrating TAMs correlates with poor prognosis (188). Various studies have reported that high TAM infiltration is predictive of poor prognosis in breast cancer patients (189-196), even though there is some debate if CD68 which is the most commonly used marker for TAM infiltration has a prognostic value on its own and whether there are other markers like CD163 which could be more predictive. Also, the localization of the infiltrating TAMs could be a crucial factor as it was found that TAMs from the tumor stroma but not the tumor nest are an independent prognostic marker (193) which could be due to the fact that sessile and migratory TAMs which have different functional phenotype are differentially located (197). Additionally, high TAM infiltration was also found to correlate with other bad prognosticators like high tumor grade, ER and PR negativity and Her2 positivity (192, 193, 195). The negative effects of TAM infiltration were partially mediated by their angiogenic properties as indicated by the high VEGF expression and microvessel density in these heavily infiltrated tumors (194) or by their ability to enhance migration and stem cell like properties of tumor cells (192).

Since in breast cancer TAMs are associated with poor prognosis, they are an obvious target for therapeutic intervention. Various approaches have been applied for targeting TAMs for anti-cancer therapy (Figure 7). The first approach is to reduce the numbers of TAMs infiltrating the tumor either by depleting them or by inhibiting their recruitment into the tumor. The depletion of TAMs by the use of Clodronate loaded Liposomes (198) or Trabectedin (105) resulted in inhibition of tumor growth and reduction in tumor vascularization in mouse tumor models. Additionally, anti-CSF-1R antibody can also deplete TAMs resulting in delayed tumor growth which was accompanied by increase in the ratio of tumor infiltrating $CD8^+/CD4^+$ T cells (199). This antibody also showed effective TAM depletion and clinical benefit in patients (199). Blocking of recruitment of TAMs into the tumor can be achieved by blocking of one of the following: CCL2/CCR2 signaling, CSF-1 or VEGF signaling. Disruption of CCL2/CCR2 interaction by anti-CCL2 antibody resulted in reduced metastasis and prolonged survival in murine breast cancer model (200). In patients it was found to be safe, however did not have any clinical benefit as a monotherapy (201). Additionally, blocking of CSF-1 signaling by anti-CSF-1R antibody could control tumor growth (202) and this effect could have been mediated by the fact that anti-CSF-1R antibody can reduce the extravasation of monocyte precursors resulting in reduced MHC II^{lo} (M2-like) macrophages into the tumor (203). Inhibition of VEGF can also affect macrophage recruitment into tumors and blocking of VEGF resulted in delayed tumor growth in mouse tumor models (204). Another approach is to reprogram the TAMs from an immunosuppressive M2-like phenotype to an M1-like phenotype. Various studies in mouse models have demonstrated that TLR9 ligands like CpG (205), bacterial products (206) or agonist CD40 antibody (145, 207) or histidine-rich glycoprotein (HRG) (208) which have shown anti-tumor activity do so by

repolarization of TAMs into a M1-like phenotype. Also low dose irradiation can shift the macrophages towards a more M1-like phenotype (150). Additionally, antigen specific $CD4^+$ T cells can repolarize TAMs toward a MHC II^{hi} M1-like phenotype in an IFNγ dependent way which corresponds to successful immunosurveillance (209). This demonstrates that repolarization of TAMs is an attractive approach for anti-tumor therapy which needs to be investigated further in a clinical setting.

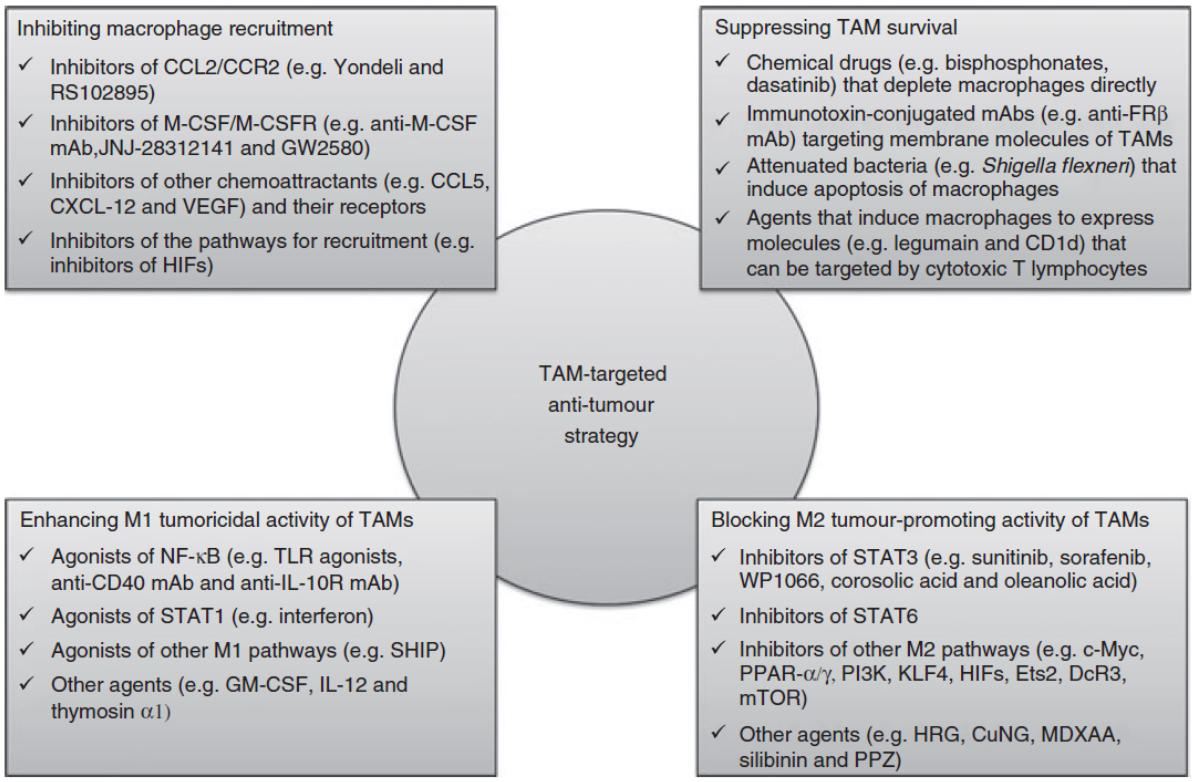

Figure 7. Strategies for therapeutic targeting of TAMs

Targeting of TAMs for anti-tumor therapy is based on either abrogation of the immunosuppressive macrophages in the tumor microenvironment or inducing an M1-like phenotype (Figure from Tang *et al*, 2013).

3.5 Aim of the study

In the recent years immunotherapy of cancer has shown promising results in a variety of settings; however, there are major issues that need to be addressed for successful immunotherapy. Two major factors to consider include combining different treatments to activate different compartments of the immune system and overcoming the immune suppressive tumor microenvironment. The antigen specific $CD4^+$ T cells can augment the therapeutic effect of tumoricidal $CD8^+$ T cells by helping to break tolerance against self-derived non-mutated tumor antigens (210, 211) or by activating memory $CD8^+$ T cells (103, 212). Additionally, antigen specific $CD4^+$ T cells can re-polarize immunosuppressive M2-like TAMs pulsed with their cognate epitope to an M1-like phenotype (213). This is mediated by IFNγ secreted by the activated $CD4^+$ T cells. It has been demonstrated in a myeloma model that TAMs can take up secreted tumor antigen and present it to the antigen specific $CD4^+$ T cells thereby activating them (209, 214, 215) which results in successful immunosurveillance. We wanted to establish an NY-BR-1 expressing tumor model which would allow us to investigate if TAMs could take up and process the breast cancer associated differentiation antigen NY-BR-1 and present it to NY-BR-1 specific $CD4^+$ T cells thereby activating them. This model could also be used to answer whether IFNγ secreted by the activated $CD4^+$ T cells would re-polarize the TAMs to an M1-like phenotype allowing $CD8^+$ T cells to eradicate the tumor. Since HLA-DR4 restricted NY-BR-1 specific $CD4^+$ T cell epitopes and corresponding $CD4^+$ T cell lines had been previously established our lab, the aim of the current thesis was to set up a transplantable NY-BR-1 expressing tumor model compatible with HLA-DR4tg mice. Another goal was to generate an NY-BR-1 specific CTL line which could be adoptively transferred into tumor bearing mice to study their anti-tumor activity following the re-polarization of TAMs by NY-BR-1 specific $CD4^+$ T cells.

4 Materials and methods

4.1 Materials

4.1.1 General instrumentation

Table 1. General instrumentation

Machine	Manufacturer
ABI 7300 Real-time PCR System	Applied Biosystems, Foster City, USA
Biofuge Fresco Centrifuge	Heraeus, Hanau, Germany
Biological Safety Cabinet	Heraeus, Hanau, Germany
BioPhotometer	Eppendorf, Hamburg, Germany
BioRad Mini-gel apparatus	Bio-Rad, Richmond, USA
CASY1 Cell counter	Schaerfe System, Reutlingen, Germany
CO2 incubator	Binder, Tuttlingen, Germany
ELISPOT Reader System	AID Diagnostika, Straßberg, Germany
ELISPOT Reader System	Cellular Technology Limited, Shaker Heights, USA
FACS Calibur1 Flow Cytometer	Becton Dickinson, Heidelberg, Germany
FACSAria I Cell Sorter	Becton Dickinson, Heidelberg, Germany
FACSAria II Cell Sorter	Becton Dickinson, Heidelberg, Germany
FACSCanto II Flow Cytometer	Becton Dickinson, Heidelberg, Germany
Fluoroskan Ascent Microplate Fluorometer	Thermo Scientific, Dreieich, Germany
Gammacell 1000 Elite	MDS Nordion, Ottawa, Canada
Gel Documentation System	INTAS Science Imaging Instruments, Göttingen, Germany
Gene Mate Gel Electrophoresis System	Star Lab, Hamburg, Germany
Innova 4230 Incubator Shaker	New Brunswick Scientific, Edison, USA
Innova 4230 Refrigerated Incubator Shaker	New Brunswick Scientific, Edison, USA
Leica DM1L Microscope	Leica, Wetzlar, Germany
LSR II Flow Cytometer	Becton Dickinson, Heidelberg, Germany
Magnet Stirrer	Heidolph Instruments, Schwabach, Germany
Megafuge 2.0 R	Heraeus Instruments, Hanau, Germany
Microbiological Incubator	Heraeus, Hanau, Germany
Microwave intellowave	LG, Seoul, South Korea
Mini-PROTEAN Tetra Handcast Systems	Bio-Rad, Richmond, Germany
MP220 pH Meter	Mettler Toledo, Columbus, OH
Multichannel Pipette	Eppendorf, Hamburg, Germany
Multifuge X1R	Thermo Scientific, Karlsruhe, Germany
Multifuge x3 FR centrifuge	Heraeus, Hanau, Germany
Neubauer counting chamber	Brand, Wertheim, Germany
peqstar 2x Gradient	peqlab, Erlangen, Germany
pH-meter 766 Calimatic	Knick, Berlin, Germany
Pipetboy	Brand, Wertheim, Germany
Pipette (P2, P10, P100, P200, P1000)	Gilson, Bad Camberg, Germany
Power PAC 300 power supplier	Bio-Rad, Richmond, Germany
Refrigerator	Liebherr, Ochsenhausen, Germany
Sorvall RT7 Centrifuge	Sorvall, Newton, CT

Spectrophotometer NanoDrop 2000	Thermo Scientific, Karlsruhe, Germany
Tecan Infinite 200 PRO	Tecan, Männedorf, Switzerland
Thermomixer	Eppendorf, Hamburg, Germany
UV light N90 LW, 366 nm	Konrad Benda, Wiesloch, Germany
Veriti 96 Well Plate Thermocycler	Applied Biosystems, Foster City, USA
Vortex Genie2	Scientific Industries, New York, USA
Waterbath SW20	Julabo Labortechnik, Seelbach, Germany
Wet Blotting System Mini Trans-Blot Cell	Bio-Rad, Richmond, Germany

4.1.2 General consumables

Table 2. General consumables

Material	Manufacturer
Falcon tubes 15ml, 50ml	Greiner, Frickenhausen, Germany
Pipette filter tips (10, 20, 100, 200, 1000µl)	Starlab, Milton Keynes, United Kingdom
Pipette tips (10, 20, 100, 200, 1000µl)	Greiner, Frickenhausen, Germany
Combitips (2.5, 5ml)	Eppendorf, Hamburg, Germany
Sterile serological pipettes (5, 10, 25ml)	Greiner, Frickenhausen, Germany
Safe-Lock tubes (0.5, 1.5, 2ml)	Eppendorf, Hamburg, Germany
Tissue culture flasks (25, 75, 150 cm^2)	TPP, Trasadingen, Switzerland
Cell culture test plates, flat bottom (6, 12, 24, 96 wells)	TPP, Trasadingen, Switzerland
Round bottom 96-well plates TPP, Trasadingen, Switzerland	TPP, Trasadingen, Switzerland
Nunc™ MaxiSorp™ ELISA Plates, Uncoated	BioLegend, San Diego, U.S.
96 well black/clear flat bottom plates (for CellTiter-Glo® Assay)	Corning, Big Flats, NY, USA
UVette™ Cuvets	Eppendorf, Hamburg, Germany
PCR strip tube	Greiner, Frickenhausen, Germany
MicroAmp Optical 96-well pate	Applied Biosytems, Foster City, U.S.
MicroAmp Optical adhesive film	Applied Biosytems, Foster City, U.S.
Petri Dishes	Greiner, Frickenhausen, Germany
Cryotubes	Greiner, Frickenhausen, Germany
Nitrocellulose membrane	Whatmann, Dassel, Germany
Needles (18G, 27G)	Becton Dickinson, Heidelberg, Germany
Inject-F, Syringes	Braun, Melsungen, Germany
Liquid reservoirs	Carl Roth GmbH, Karlsruhe, Germany
FACS tubes	Becton Dickinson, Heidelberg, Germany
Terumo Syringe (5, 10 ml)	Terumo, Leuven, Belgium
Cell strainers (40, 70 µm)	Becton Dickinson, Heidelberg, Germany
ELISpot plates	Merck Milipore, Darmstadt, Germany

4.1.3 Chemicals and Reagents

4.1.3.1 General chemicals

Table 3. General chemicals

Material	Manufacturer
Acetic Acid	Avantor, Center Valley, USA
Agarose	Sigma-Aldrich, Saint Louis, USA
Ammonium Persulfate (APS)	Sigma-Aldrich, Saint Louis, USA
Bovine Serum Albumin (BSA)	Sigma-Aldrich, Saint Louis, USA
Bromphenol Blue	Sigma-Aldrich, Saint Louis, USA
Concanavalin A	Sigma-Aldrich, Saint Louis, USA
Dimethyl sulfoxide	AppliChem, Darmstadt, Germany
Ethanol	Sigma-Aldrich, Saint Louis, USA
Ethidium Bromide solution 0.025%	Carl Roth, Karlsruhe, Germany
Ethylenediaminetetraacetic acid (EDTA)	Acros Organics, Geel, Belgium
Glycerol	Sigma-Aldrich, Saint Louis, USA
Glycine	Gerbu Biotechnik, Geiberg, Germany
Methanol	Sigma-Aldrich, Saint Louis, USA
Non-fat milk powder	Carl Roth GmbH, Karlsruhe, Germany
Paraformaldehyde	Sigma-Aldrich, Saint Louis, USA
Phenylmethylsulfonyl fluoride (PMSF)	Sigma-Aldrich, Saint Louis, USA
Sodium dodecyl sulfate (SDS)	Sigma-Aldrich, Saint Louis, USA
Tetramethylethylenediamine (TEMED)	Bio-Rad, Munich, Germany
Tris Base	Sigma-Aldrich, Saint Louis, USA
Trypan Blue	Biochem, Berlin, Germany
Tryptone	Sigma-Aldrich, Saint Louis, USA
Trypsin/EDTA 1x	Life technologies, Carlsbad, U.S.
Tween 20	Gerbu Biotechnik, Geiberg, Germany
Water	Sigma-Aldrich, Saint Louis, USA
β-Mercaptoethanol	Sigma-Aldrich, Saint Louis, USA
Lipopolysaccharide (LPS)	Sigma-Aldrich, Saint Louis, USA
Methyl α-D-mannopyranoside (αMM)	Sigma-Aldrich, Saint Louis, USA
Thioglycolate Medi m	AppliChem, Darms adt, Germany

4.1.3.2 General reagents

Table 4. General reagents

Material	Manufacturer
BD Matrigel Basement Membrane Matrix	BD Biosciences, Bedford, MA, USA
6x Orange Loading Dye	Fermentas, St. Leon-Rot, Germany
dNTP Mix 10 mM	Thermo Scientific, Karlsruhe, Germany
Gene Ruler 100bp DNA Ladder	Fermantas, St. Leon-Rot, Germany
O´Gene Ruler 1kb DNA Ladder	Fermantas, St. Leon-Rot, Germany
Power SYBR® Green PCR Master Mix	Life technologies, Carlsbad, U.S.
Effectene® Transfection Reagent	Qiagen, Hilden, Germany
PolyFect® Transfection Reagent	Qiagen, Hilden, Germany
X-tremeGENE HP DNA Transfection reagent	Roche Diagnostics, Mannheim, Germany

Cell Lysis Buffer	Cell Signaling Technology, Beverly, USA
ECL Prime Western Blot Detection Reagent	GE Healthcare, Munich, Germany
Precision Plus Protein Dual Color Standard	Bio-Rad, Munich, Germany
Bio-Rad Protein Assay Reagent	Bio-Rad, Richmond, USA
Qiazol	Qiagen, Hilden, Germany
BCIP/NBT Liquid Substrate System	Sigma, Saint Louis, MO
TaqMan® Universal PCR Master Mix	Applied Biosytems, Foster City, U.S.
Pvu I restriction enzyme (#ER0621)	Life technologies, Carlsbad, U.S.

4.1.3.3 Cell culture

Table 5. Cell culture

Material	Manufacturer
Accutase (#SCR005)	Merck Millipore, Schwalbach, Germany
Dulbecco's phosphate-buffered saline (DPBS)	Life technologies, Carlsbad, U.S.
DMEM, high glucose, GlutaMAX™	Gibco-Invitrogen, Karlsruhe, Germany
Fetal Bovine Serum	Biochrom, Berlin, Germany
HEPES buffer solution	Sigma-Aldrich, Saint Louis, USA
L-Glutamine	Sigma-Aldrich, Saint Louis, USA
Penicillin/Streptomycin (Pen/Strep)	Life technologies, Carlsbad, U.S.
RPMI Medium 1640 (1x) + GlutaMAX	Life technologies, Carlsbad, U.S.
X-VIVO 20	Lonza, Basel, Switzerland
Zeocin Selection Reagent	Life Technologies, Darmstadt, Germany
αMinimum Essential Medium Eagle (MEM)	Sigma-Aldr ch, Saint Louis, USA
ACK lysis Buffer	Gibco-Invitrogen, Karlsruhe, Germany
Hanks' Balanced Salt Solution (HBSS)	Sigma-Aldrich, Saint Louis, USA
Zeocin	Invitrogen, Carlsbad, CA
G418(Neomycin)	Gibco-Invitrogen, Karlsruhe, Germany

4.1.3.4 Cytokines

Table 6. Cytokines

Material	Manufacturer
Human IL-2 IS, premium grade (#130-097-745)	Miltenyi Biotec GmbH, Gladbach, Germany
Mouse IFN gamma Recombinant Protein Carrier-Free (#34-8311-82)	eBioscience, San Diego, U.S.
Recombinant Mouse IL-4 (carrier-free) (#574302)	BioLegend, San Diego, U.S.

4.1.3.5 Bacteria

Table 7. Bacteria

Material	Manufacturer
One Shot® TOP10 Chemically Competent E. coli (#C4040-06)	Life technologies, Carlsbad, U.S.

4.1.3.6 Reagents for flow cytometry

Table 8. Reagents for flow cytometry

Material	Manufacturer
LIVE/DEAD® Fixable Yellow Dead Cell Stain (#L-34959)	Life technologies, Carlsbad, U.S.
LIVE/DEAD® Fixable Blue Dead Cell Stain Kit (#L-23105)	Life technologies, Carlsbad, U.S.
7-AAD Viability Staining Solution (#420403)	BioLegend, San Diego, U.S.
Propidium Iodide (#P3566)	Life technologies, Carlsbad, U.S.
CountBright™ Absolute Counting Beads (#C36950)	Life technologies, Carlsbad, U.S.
CD16/CD32 (mouse BD Fc block) (#553142)	BD Pharmingen, San Diego, U.S.
OneComp eBeads (#01-1111-42)	eBioscience, San Diego, U.S.
Rat serum (#GTX73216)	GeneTex, Irvine, USA
Normal Syrian Hamster Serum (#007-000-120)	Jackson Immunoresearch, West Grove, USA
Protein Transport Inhibitor (Containing Monensin) (#554724)	BD Biosciences, San Jose, U.S.
BD Cytofix/Cytoperm™ Fixation/Permeabilization Kit (#554714)	BD Biosciences, San Jose, U.S.
Lympholyte®-M cell separation medium (#CL5035)	Cedarlane Labs, Burlington, Canada

4.1.4 Primers for qRT-PCR using SYBR Green

Table 9. Primers for qRT-PCR using SYBR Green

Primer	Sequence 5' to 3'	Source
Ym1_qPCR_FP1	CACCATGGCCAAGCTCATTCTTGT	Tatano *et al*, 2014 (216)
Ym1_qPCR_RP2	TATTGGCCTGTCCTTAGCCCAACT	
Fizz1_qPCR_FP3	ACTGCCTGTGCTTACTCGTTGACT	
Fizz1_qPCR_RP4	AAAGCTGGGTTCTCCACCTCTTCA	
IL-6_qPCR_FP5	GTCTTCTGGAGTACCATAGC	Movahedi *et al*, 2010 (180)
IL-6_qPCR_RP6	GTCAGATACCTGACAACAGG	
CXCL10_qPCR_FP7	TCTGAGTCCTCGCTCAAGTG	
CXCL10_qPCR_RP8	CCTTGGGAAGATGGTGGTTA	
CXCL9_qPCR_FP9	TCAACAAAAGAGCTGCCAAA	
CXCL9_qPCR_RP10	GCAGAGGCCAGAAGAGAGAA	
IL12b_qPCR_FP11	GAAAGACCCTGACCATCACT	
IL12b_qPCR_RP12	CCTTCTCTGCAGACAGAGAC	
NOS2_qPCR_FP15	GCTTCTGGTCGATGTCATGAG	
NOS2_qPCR_RP16	TCCACCAGGAGATGTTGAAC	
VEGFA_qPCR_FP17	CAGGCTGCTGTAACGATGAA	
VEGFA_qPCR_RP18	AATGCTTTCTCCGCTCTGAA	
ARG1_qPCR_FP19	TCACCTGAGCTTTGATGTCG	
ARG1_qPCR_RP20	TTATGGTTACCCTCCCGTTG	

Mrc1_qPCR_FP21	GCAAATGGAGCCGTCTGTGC	
Mrc1_qPCR_RP22	CTCGTGGATCTCCGTGACAC	
CD206_qPCR_FP23	TTGGACGGATAGATGGAGGG	Zhu et al, 2014 (217)
CD206_qPCR_RP24	CCAGGCAGTTGAGGAGGTTC	
HPRT_qPCR_FP25	AGTACAGCCCCAAAATGGTTAAG	
HPRT_qPCR_RP26	CTTAGGCTTTGTATTTGGCTTTTC	
bACTIN_qPCR_FP27	TGGAATCCTGTGGCATCCATGAAAC	Davis *et al*, 2013 (218)
bACTIN_qPCR_RP28	TAAAACGCAGCTCAGTAACAGTCCG	
IL10_fw31	GCTCTTACTGACTGGCATGAG	Shaul et al, 2010 (219)
IL10_rev32	CGCAGCTCTAGGAGCATGTG	
CD163_fw35	TCCACACGTCCAGAACAGTC	Tatano *et al*, 2014 (216)
CD163_rev36	CCTTGGAAACAGAGACAGGC	
STAT6_fw37	CTGGGGTGGTTTCCTCTTG	Shaul *et al*, 2010 (219)
STAT6_rev38	TGCCCGGTCTCACCTAACTA	
IL1β_fw39	CTGGTGTGTGACGTTCCCATTA	
IL1β_rev40	CCGACAGCACGAGGCTTT	
STAT1_fw41	CTGAATATTTCCCTCCTGGG	
STAT1_rev42	TCCCGTACAGATGTCCATGAT	
VEGF_fw43	CCTTCGTCCTCTCCTTACCC	
VEGF_rev44	AAGCCACTCACACACACAGC	
CD86_fw45	TCTCCACGGAAACAGCATCT	
CD86_rev46	CTTACGGAAGCACCCATGAT	
CD80_fw47	GGCAAGGCAGCAATACCTTA	
CD80_rev48	CTCTTTGTGCTGCTGATTCG	
TGFβ1_fw49	AAGTTGGCATGGTAGCCCTT	
TGFβ1_rev50	GCCCTGGATACCAACTATTGC	
PPARg_qPCR_FP51	CGAGTCTGTGGGGATAAAGC	Ralph Schulz, DKFZ
PPARg_qPCR_RP52	CAAACCTGATGGCATTGTGA	

4.1.5 Plasmids

Table 10. Plasmids

Material	Source
pcDNA3.1(-)zeo	Invitrogen, Carlsbad, CA
pcDNA3.1(-)zeocin-NY-BR-1	Dr. Adriane Gardyan

4.1.6 Peptides

All peptides were synthesized and HPLC-purified at the peptide synthesis core facility of the German Cancer Research Center, Heidelberg.

Table 11. List of peptides

MHC RESTRICTION	DESIGNATION IN THESIS	SEQUENCE
H2-D^b	peptide # 3	VYTSNDSYI
H2-D^b	peptide # 6	STIYNNEVL
H2-D^b	peptide # 57	KASANDQRF

H2-D^b	peptide # 136	HTHENENYL
HLA-DRB1*0301	peptide #8797	VVTFLVDRKCQLDVL
HLA-DRB1*0301	peptide #9017	DVSSTIYNNEVLHQP
HLA-DRB1*0301	peptide #8756	KSKITIDIHFLERKM
HLA-DRB1*0401	peptide #8862	AFELKNEQTLRADPM
HLA-DRB1*0401	peptide #9251	TIYNNEVLHQPLSEA

4.1.7 Antibodies and hybridoma supernatants

4.1.7.1 Antibodies used for ELISPOT assay

Table 12. ELISPOT antibodies

Material	Manufacturer
Purified Rat Anti-Mouse IFN-γ (#551216)	BD Pharmingen, San Diego, U.S.
Biotin Rat Anti-Mouse IFN-γ (#554410)	BD Pharmingen, San Diego, U.S.
Alkaline phosphatase streptavidin (#554065)	BD Pharmingen, San Diego, U.S.

4.1.7.2 Antibodies and hybridoma supernatants used for Western blot analysis

Table 13. Western blot antibodies

Material	Manufacturer
mouse anti-NY-BR-1 monoclonal antibody clone#2	group of Prof. Jäger, NCT, Heidelberg
Mouse anti-Actin monoconal antibody (#691001)	MP Biomedical, Solon, USA
Goat-anti-mouse IgG-HRP (#sc2005)	Santa Cruz Biotechnology, Santa Cruz, USA

4.1.7.3 Antibodies used for flow cytometry

Table 14. FACS antibodies

Material	Manufacturer
Alexa Fluor® 488 anti-mouse CD107a (LAMP-1) Antibody (#121608)	BioLegend, San Diego, U.S.
PerCP/Cy5.5 anti-mouse/human CD11b Antibody (#101228)	BioLegend, San Diego, U.S.
V450 Hamster Anti-Mouse CD11c (#560521)	BD Biosciences, San Jose, U.S.
FITC anti-mouse CD14 Antibody (#123307)	BioLegend, San Diego, U.S.
Brilliant Violet 605™ anti-mouse CD206 (MMR) Antibody (#141721)	BioLegend, San Diego, U.S.
PerCP/Cy5.5 anti-mouse CD3 Antibody (#100217)	BioLegend, San Diego, U.S.
Brilliant Violet 510™ anti-mouse CD3 Antibody (#100233)	BioLegend, San Diego, U.S.
APC Anti-Mouse CD4 (#17-0041-81)	eBioscience, San Diego, U.S.
APC/Cy7 anti-mouse CD4 Antibody (#100414)	BioLegend, San Diego, U.S.

PerCP/Cy5.5 anti-mouse CD4 Antibody (#100540)	BioLegend, San Diego, U.S.
V450 Rat anti-Mouse CD4 (#560470)	BD Biosciences, San Jose, U.S.
Alexa Fluor® 488 anti-mouse CD45.2 Antibody (#109816)	BioLegend, San Diego, U.S.
APC Rat Anti-Mouse CD8a (#553035)	BD Pharmingen, San Diego, U.S.
PE/Cy7 anti-mouse CD8a Antibody (#100722)	BioLegend, San Diego, U.S.
Anti-Mouse CD8a FITC (#11-0081-81)	eBioscience, San Diego, U.S.
Alexa Fluor® 647 anti-mouse F4/80 Antibody (#123122)	BioLegend, San Diego, U.S.
Alexa Fluor® 700 anti-mouse Ly-6G/Ly-6C (Gr-1) Antibody (#108422)	BioLegend, San Diego, U.S.
APC/Cy7 anti-human HLA-DR Antibody (#307618)	BioLegend, San Diego, U.S.
PE Mouse Anti-Mouse I-A[b] (#553552)	BD Pharmingen, San Diego, U.S.
Purified Mouse Anti-Mouse I-A[b] (#553603)	BD Pharmingen, San Diego, U.S.
Brilliant Violet 421™ anti-mouse IFN-γ Antibody (#505830)	BioLegend, San Diego, U.S.
Anti-Mouse NOS2 PE-Cyanine7 (#25-5920-82)	eBioscience, San Diego, U.S.
APC mouse anti-mouse NK1.1 (#561117)	BD Pharmingen, San Diego, U.S.

4.1.7.4 Isotype controls for flow cytometry antibodies

Table 15. Isotypes for FACS antibodies

Material	Manufacturer
Alexa Fluor® 488 Rat IgG2a, κ Isotype Ctrl Antibody (#400525)	BioLegend, San Diego, U.S.
PerCP/Cy5.5 Rat IgG2b, κ Isotype Ctrl (#400632)	BioLegend, San Diego, U.S.
V450 Hamster IgG1, λ1 Isotype Control (#560552)	BD Biosciences, San Jose, U.S.
PerCP/Cy5.5 Rat IgG2b, κ Isotype Ctrl (# 400631)	BioLegend, San Diego, U.S.
APC/Cy7 Rat IgG2b, κ Isotype Ctrl (#400624)	BioLegend, San Diego, U.S.
Alexa Fluor® 488 Mouse IgG2a, κ Isotype Ctrl (#400233)	BioLegend, San Diego, U.S.
Alexa Fluor® 647 Rat IgM, κ Isotype Ctrl (#400813)	BioLegend, San Diego, U.S.
APC Rat IgG2a κ Isotype Control (#553932)	BD Pharmingen, San Diego, U.S.
PE/Cy7 Rat IgG2a, κ Isotype Ctrl (#400522)	BioLegend, San Diego U.S.
Brilliant Violet 605™ Rat IgG2a, κ Isotype Ctrl Antibody (#400539)	BioLegend, San Diego, U.S.
Alexa Fluor® 647 Rat IgG2a, κ Isotype Ctrl (#400526)	BioLegend, San Diego, U.S.
Alexa Fluor® 700 Rat IgG2b, κ Isotype Ctrl (#400628)	BioLegend, San Dieg , U.S.

APC/Cy7 Mouse IgG2a, κ Isotype Ctrl (#400229)	BioLegend, San Diego, U.S.
PE Mouse IgG2a, κ Isotype Control (#553457)	BD Pharmingen, San Diego, U.S.
PE/Cy7 Rat IgG2a, κ Isotype Ctrl (#400522)	BioLegend, San Diego, U.S.
Brilliant Violet 421™ Rat IgG1, κ Isotype Ctrl Antibody (#400429)	BioLegend, San Diego, U.S.
Brilliant Violet 510™ Rat IgG2b, κ Isotype Ctrl Antibody (#400645)	BioLegend, San Diego, U.S.
FITC Rat IgG2a, κ Isotype Ctrl Antibody (#400505)	BioLegend, San Diego, U.S.

4.1.7.5 Hybridoma supernatant for flow cytometry

Table 16. Hybridoma supernatant for flow cytometry

Name	Specificity	Species	Isotype	Reference
E3-25	mouse H2-K^b	mouse	IgG2a	Evan *et al*, 1983
B22.249	mouse H2-D^b	mouse	IgG2a	Lemke *et al*, 1979

4.1.7.6 Secondary antibodies for flow cytometry

Table 17. Secondary FACS antibodies

Material	Manufacturer
APC Goat Anti-Mouse Ig (#550826)	BD Pharmingen, San Diego, U.S.
FITC conjugated AffiniPure $F(ab')_2$ Fragment Goat Anti-Mouse IgG (H+L)	Jackson Immunoresearch, West Grove, USA

4.1.7.7 Antibodies for depletion of cells *in vivo*

Table 18. *In vivo* antibodies

Material	Manufacturer
*InVivo*MAb anti NK1.1 (#BE0036)	BioXCell, West Lebanon, NH
*InVivo*MAb Mouse IgG_{2a} (#BE0085)	BioXCell, West Lebanon, NH
*InVivo*MAb anti-mouse CD4 (#BE003-1)	BioXCell, West Lebanon, NH
*InVivo*MAb Rat IgG_{2b} Isotype control; anti KLH (#BE0090)	BioXCell, West Lebanon, NH

4.1.8 MHC multimers

4.1.8.1 HLA-DR tetramers from NIH

Table 19. HLA-DR tetramers

MHC Allele	Peptide sequence	peptide designation
HLA-DR*0301	VVTFLVDRKCQLDVL	peptide #8797
HLA-DR*0301	KSKITIDIHFLERKM	peptide #8756
HLA-DR*0301	PVSKMRMATPLLMQA	CLIP
HLA-DR*0401	AFELKNEQTLRADPM	peptide #8862
HLA-DR*0401	TIYNNEVLHQPLSEA	peptide #9251
HLA-DR*0401	PVSKMRMATPLLMQA	CLIP

4.1.8.2 H2-D^b dextramers from Immudex

Table 20. H2-D^b dextramers

MHC Allele	Peptide sequence	peptide designation	product code
H2-D^b	STIYNNEVL	peptide #6	JA4335-APC
H2-D^b	RAHYNIVTF	HPV 16 E7$_{49-57}$	JA2195-APC

4.1.9 Kits

Table 21. Kits

Material	Manufacturer
CD11b MicroBeads, mouse/human (#130-049-601)	Miltenyi Biotec GmbH, Gladbach, Germany
CD4 Microbeads, mouse (#130-052-301)	Miltenyi Biotec GmbH, Gladbach, Germany
CD8a (Ly-2) MicroBeads, mouse (#130-049-401)	Miltenyi Biotec GmbH, Gladbach, Germany
CellTiter-Glo® Luminescent Cell Viability Assay (#G7572)	Promega Corporation, Madison, U.S.
Dynabeads® Mouse T-Activator CD3/CD28 (#11456D)	Life technologies, Carlsbad, U.S.
iScript cDNA Synthesis Kit (#170-8891)	Bio-Rad, Richmond, USA
Mouse IFN gamma ELISA Ready-SET-Go (#88-7314)	eBioscience, San Diego, U.S.
Mouse IFN-γ Secretion Assay (#130-090-516)	Miltenyi Biotec GmbH, Gladbach, Germany
NK Cell Isolation Kit II, mouse (#130-096-892)	Miltenyi Biotec GmbH, Gladbach, Germany
Pierce™ BCA Protein Assay Kit (#23225)	Thermo Fisher Scientific, Waltham, U.S.
QIAamp® DNA ini and Blood Mini Handbook (#51104)	Qiagen, Hilden, Germany
QIAGEN Plasmid Maxi Kit (#12162)	Qiagen, Hilden, Germany
QIAGEN Plasmid Midi Kit (#12143)	Qiagen, Hilden, Germany
QIAGEN Plasmid Mini Kit (#12123)	Qiagen, Hilden, Germany
QIAquick Gel Extraction Kit (#28704)	Qiagen, Hilden, Germany
QIAquick PCR Purification Kit (#28104)	Qiagen, Hilden, Germany
QIAshredder spin columns (#79654)	Qiagen, Hilden, Germany
QuikChange Lightning Site-Directed Mutagenesis Kit (#210518)	Agilent Technologies, La Jolla, U.S.
Rapid DNA Ligation Kit (#11 635 379 001)	Roche Diagnostics, Mannheim, Germany
RNeasy Plus Micro Kit (#74034)	Qiagen, Hilden, Germany
RNeasy Plus Mini Kit (#74134)	Qiagen, Hilden, Germany
Transcriptor First Strand cDNA Synthesis Kit (#04 379 012 001)	Roche Diagnostics, Mannheim, Germany

4.1.10 Cells lines

Table 22. Cell lines

Cell line	Species	Source	Cell line type
EL4	*Mus musculus*	German Cancer Research Center, Heidelberg (DKFZ), Germany	T lymphoma (220)
D8P3	*Mus musculus*	German Cancer Research Center, Heidelberg (DKFZ), Germany	EL4/NY-BR-1 clone (generated by Dr. Adriane Gardyan)
A5P1	*Mus musculus*	German Cancer Research Center, Heidelberg (DKFZ), Germany	EL4/NY-BR-1 clone (generated by Dr. Adriane Gardyan)
EO771	*Mus musculus*	TEBU-Bio (Offenbach, Germany)	mammary adenocarcinoma (221)
EONY #9	*Mus musculus*	generated in this thesis	EO771/NY-BR-1 clone
EONY #17	*Mus musculus*	generated in this thesis	EO771/NY-BR-1 clone
EONY #19	*Mus musculus*	generated in this thesis	EO771/NY-BR-1 clone
EONY/PX458	*Mus musculus*	German Cancer Research Center, Heidelberg (DKFZ), Germany	control EONY #19 transfectant (222)
EONY/M1KO	*Mus musculus*	German Cancer Research Center, Heidelberg (DKFZ), Germany	EONY #19 derived MHC I knockout (222)
B16F10	*Mus musculus*	German Cancer Research Center, Heidelberg (DKFZ), Germany	melanoma
B16F10/PX458	*Mus musculus*	German Cancer Research Center,Heidelberg (DKFZ), Germany	control B16F10 transfectant (222)
B16F10/M1KO	*Mus musculus*	German Cancer Research Center, Heidelberg (DKFZ), Germany	B16F10 derived MHC I knockout (222)
HEK293T	*Homo sapiens*	ATCC, Rockville, MD	human embryonic kideny
T2	*Homo sapiens*	T2 (ATCC®CRL-1992TM)	174xCEM.Z2; fusion of B-LCL 721 and T lymphoma (223)

T2/DR3	*Homo sapiens*	German Cancer Research Center, Heidelberg	T2 transfectant expressing HLA-DRB1*0301
T2/DR4	*Homo sapiens*	German Cancer Research Center, Heidelberg	T2 transfectant expressing HLA-DRB1*0401

4.1.11 Software

Table 23. Software

Software	Source
Microsoft Office 2010	Microsoft, Redmont, USA
GraphPad Prism 5	GraphPad Software, Inc., San Diego, USA
Cell Quest	BD Biosciences, San Jose, U.S.
Ascent Software	Thermo Scientic, Dreieich, Germany
FlowJo	BD Biosciences, San Jose, U.S.

4.2 Methods

4.2.1 Preparation of buffers and medium

4.2.1.1 Molecular Biology

Table 24. Buffers for molecular biology

Name	Composition
50x Tris-acetate-EDTA (TAE) Buffer	242 g Tris base 57.1 ml Acetic acid 100 ml 500 mM EDTA solution Adjust to a final volume of 1 L with ddH2O pH 8.0

4.2.1.2 Microbiology

Table 25. Buffers for microbiology

Name	Composition
LB Medium	10 g Tryptone 5 g Yeast extract 10 g NaCl Adjust to a final volume of 1 L with ddH2O pH 7.5
LB-amp Medium	LB medium p u 150 µg/ml Ampicilin
LB-amp Plates	7.5 g Agar in 500 ml LB-amp edium

4.2.1.3 Cell Biology and Cell Culture

Table 26. Composition of various cell culture media

Name	Composition
Complete CTL Medium	500 ml αMinimum Essential Medium Ea 10% FCS

	100 U/ml penicillin 100 µg/ml streptomycin 2 mM L-glutamine 50 µM β-mercaptoethanol 5% (v/v) culture supernatant fr m concavalin A stimulated rat spleen cells 5% (v/v) Methyl α-D-mannopyranoside (αMM)
Freezing Medium	90% (v/v) FC 10% (v/v) Dimethyl sulfoxide (DMSO)
RPMI Complete Medium	RPMI Medium 1640 (1x) + GlutaMAX 10% FCS 100 U/ml penicillin 100 µg/ml strep omycin
RPMI Complete Medium with HEPES	RPMI Medium 1640 (1x) + GlutaMAX 10% FCS 100 U/ml penic ll n 100 µ /ml streptomycin 5mM HEPES
DMEM Complete medium for PECs	DMEM, high glucose, GlutaMAX™ 10% FCS 100 U/ml penicillin
DMEM Complete medium for NK cells	DMEM, high glucose, GlutaMAX™ 10% FCS 100 U/ml penicillin 50 µM β-ME 2 mM L-gl tamine 1x MEM non-essential amino acids 1 mM sodium pyruvate 1700 U/ml human IL-2

4.2.1.4 Immunobiology

Table 27. Buffers for immunobiology

Name	Composition
FACS Buffer	3% FCS v/v) 5ml 2% Sodium Azide (NaN3) Adjust to a final volume of 500 ml with PBS
MACS Buffer	4 ml 0.5M EDTA 5g BSA Adjust to a final volume of 1 L with 1x PBS

4.2.1.5 Protein Biochemistry

Table 28. Buffers for protein biochemistry

Name	Composition
10% Separation Gel	4 ml H2O 2.6 ml Lower Buffer, pH 8.8 3.3 ml 30% Acrylamide 100 µl 10% APS

	4 µl TEMED
10x Running Buffer	7.5 g Trisma Base 25 ml 10% SDS fill up to 250 ml with ddH2O
10x Transfer Buffer	15 g Trisma Base 72.5 g Glycine 20 ml 10% SDS fill up to 250 ml with d 2O
1x TBS	2.24g Tris Base 57.1 ml acetic acid 100 ml 0.5 M EDTA solution fill up to 1 L with ddH2O
1x TBS-T	1x TBS 0.1% Tween20
1x Transfer Buffer	100 ml 10x transfer buffer 200 ml methanol fill up to 1 L with ddH2O
5% Stacking Gel	2.7 ml H2O 540 µl Upper Buffer, pH 6.8 680 µl 30% Acrylamid 40 µl 10% APS 4 µl TEMED
5x Protein Loading Dye	0.02% Bromophenol Blue 30% Glycerol 10% SDS 250 mM Tris-Cl pH 6.8 add 10% β-Mercaptoethanol before use
Lower Buffer	90.85 g 1.5M Trisma Base 20 ml 10% SDS fill up to 250 L with ddH2O pH 8.8
Upper Buffer	15.15 g 0.5M Trisma Base 10 ml 10% SDS fill up to 250 ml with ddH2O pH 6.8

4.2.1.6 ELISPOT washing buffer

Table 29. washing buffer for ELISPOT

Name	Composition
1x PBS-T	PBS 0.5% Tween20

4.2.2 Cell culture

EL4, B16F10, B16F10/PX458 and B16F10/M1KO cells were cultured in complete RPMI 1640 medium. D8P3 and A5P1 cells were cultured in complete RPMI 1640 medium supplemented with 40 µg/ml Zeocin. EO771, EONY #9, EONY #17, EONY #19, EONY/PX458 and EONY/M1KO cells were cultured in complete RPMI 1640 medium

containing 1mM HEPES buffer and 40 µg/ml Zeocin was used for all EONY cells. All cell lines were maintained at 37°C in a humidified 5% CO2 incubator.

4.2.3 IFNγ treatment of tumor cells

EO771 or EONY#17 cells were seeded at a density of $1x10^5$ cells per well in a 6 well plate with 2 ml of culture medium. Mouse IFNγ (eBioscience, #34-8311-82) was added to the culture medium to a final concentration of 20U/ml and the cells were incubated overnight.

4.2.4 Titration of Zeocin concentration on EO771 cells

EO771 cells were seeded at a density of $1x10^5$ cells per well in a 12 well plate and 24 hours later Zeocin was added at various concentrations ranging from 0 µg/ml to 1600 µg/ml with increments of 200 µg/ml. The proportion of viable cells was monitored with an optical microscope to determine the minimal concentration of Zeocin that was lethal to 100% cells within duration of 3 days.

4.2.5 Generation of stable NY-BR-1 expressing transfectant clones

EO771 cells were seeded at a density of $2.5x10^5$ cells per well in a 6 well plate and allowed to attach overnight and transfected with 1.2 µg of linearized pcDNA3.1(-)zeo-NY-BR-1 DNA on the next day using the Effectene® Transfection Reagent from Qiagen. The DNA was diluted in EC buffer to a final volume of 100 µl and 9.6 µl of enhancer was added. The mixture was vortexed briefly and incubated for 5 minutes at room temperature, following which it was centrifuged for 5 seconds. Ten microliter Effectene® reagent was added and mixed by vortexing for 10 seconds. The mixture was incubated for 10 minutes at room temperature. During the incubation period, medium from the cell culture plates containing the cells was aspirated and the cells were washed once with PBS following which 1.6 ml culture medium was added to each well. Six hundred microliter of culture medium was added to the DNA- Effectene® complexes. It was mixed by pipetting up and down twice and was added immediately to wells in drop-wise manner. The medium was replaced with fresh culture medium 48 hours after transfection and 400 µg/ml Zeocin was added to select for successfully transfected cells. Culture medium containing 400 µg/ml Zeocin was replaced every 2-3 days and the cells were expanded for 6 weeks when the bulk culture was tested for NY-BR-1 expression. Once NY-BR-1 expression confirmed, single cell clones were obtained by limiting dilution. Briefly, cells were adjusted to a concentration of 3 cells/ml in a total volume of 60 ml and 100 µl was distributed in each well of 96 well plate; with the assumption that every 3rd well will have a single cell which will give rise to clone. Single cell clones obtained as such were further characterized for NY-BR-1 expression by qRT-PCR and Western blot.

4.2.6 RNA isolation

RNA isolation was performed using the RNeasy Plus Mini Kit for cell lines and whole tumor lysates or using the RNeasy Plus Micro Kit for tumor infiltrating macrophages sorted by flow cytometry. Cells and sorted macrophages were lysed using the RLT Plus buffer included in the kit. Tumors were snap frozen in liquid nitrogen and homogenized using the Retsch Mixer Mill following which they were lysed with RLT Plus buffer. The lysates were further homogenized by passing through QIAshredder spin columns and RNA isolation was carried out according to manufacturer's instructions.

4.2.7 Reverse transcription and qPCR

RNA isolated from cell lines and whole tumor lysates was quantified with a Nanodrop Spectrophotometer and reverse transcribed using the Transcriptor First Strand cDNA Synthesis Kit (Roche) according to the protocol below.

Step 1	Components	Volume per reaction
	RNA template (500 ng)	x µl
	nuclease free water	(12-x) µl
	Anchored-oligo($dT)_{18}$ primer (50 pmol/µl)	1 µl
	Total volume	13 µl

The reaction mix was incubated at 65 °C for 10 minutes and rested on ice for 5 minutes before adding the remaining components.

Step 2	Components	Volume per reaction
	Reaction mix from Step 1	13 µl
	Transcriptor Reverse Transcriptase Reaction Buffer (5x)	4 ml
	Protector RNase Inhibitor (40 U/ µl)	0.5 µl
	Deoxynucleotide Mix (10 mM each)	2 µl
	Transcriptor Reverse Transcriptase (20 U/µl)	0.5 µl
	Total volume	20 µl

Complete reaction mix was incubated in a thermal cycler at 50 °C for 60 minutes, at 85 °C for 5 minutes and cooled down to 4 °C and strored at -20 °C until further use.

RNA isolated from sorted macrophages was eluted in a volume of 17 µl in nuclease free water but was not quantified due to low RNA yield. 15 µl was used for reverse transcription using the iScript cDNA Synthesis Kit (Roche) according to the protocol below.

Components	Volume per reaction
RNA template	15 µl
5x iScript reaction mix	4 µl
iScript reverse transcriptase	1 µl
Total volume	13 µl

Complete reaction mix was incubated in a thermal cycler at 25 °C for 5 minutes, at 42 °C for 30 minutes, at 85 °C for 5 minutes and cooled down to 4 °C and strored at -20 °C until further use.

Quantitification of gene expression was performed using quantitative real-time PCR with TaqMan® Universal PCR Master Mix (Applied Biosystems) for NY-BR-1 expression or Power SYBR® Green PCR Master Mix (Life Technologies) for macrophage markers in the ABI 7300 Real-time PCR System (Applied Biosystems) according to the protocol below.

qRT-PCR using TaqMan® Universal PCR Master Mix

Components	Volume per reaction
cDNA (diluted 1:5 in nuclase free water)	2 µl
TaqMan® Universal PCR Master Mix (2X)	10 µl
TaqMan® primer + probe (20X)	1 µl
water	7 µl
total	20 µl

Pre-incubation (1 cycle)	50 °C	2 minutes
	95 °C	10 minutes
Amplification (45 cycles)	95 °C	15 seconds
	60 °C	1 minute

qRT-PCR using Power SYBR® Green PCR Master Mix

Components	Volume per reaction
cDNA (diluted 1: 4.3 in nuclease free water)	2 µl
Power SYBR® Green PCR Master Mix (2X)	10 µl
Forward primer (10 µM)	0.4 µl
Reverse primer (10 µM)	0.4 µl
water	7.2 µl
total	20 µl

Pre-incubation (1 cycle)	50 °C	2 minutes
	95 °C	10 minutes
Amplification (45 cycles)	95 °C	15 seconds
	60 °C	1 minute
	72 °C	30 second
Melting curve (1 cycle)	98 °C	15 seconds
	60 °C	1 minute
	95 °C	15 seonds
	60 °C	15 seonds

4.2.8 Isolation and quantification of protein

Cell lysates were generated addition of appropriated amounts of the Cell Lysis Buffer (Cell Signaling) and incubated for 15 min on ice followed by 30 min centrifugation at 13,000 rpm, 4°C. Protein concentration was determined either by Bio-Rad Protein Assay or by Pierce™ BCA Protein Assay kit. For the Bio-Rad Protein Assay, the reagent was diluted 1:5 with ddH_2O and 500 µl was added to 5µl protein lysate and incubated for 5 minutes at room temperature. The Cell Lysis Buffer was used to set the Blank and protein concentration was measured using the “Bradford” program on the BioPhotometer. Protein lysates were stored at -80°C until further use.

4.2.9 Protein detection by Western blot

Heat denatured whole cell protein samples (15µg- 50µg) were mixed with 5x loading dye and separated on a 10% polyacrylamide gel, and electro-transferred onto nitrocellulose

membranes. Successful protein transfer was confirmed by Ponceau S staining of the nitrocellulose membrane. Before blocking of the membrane with 5% of non-fat milk in TBS-T, Ponceau S was washed away with TBS-T buffer. After blocking, the membranes were incubated overnight at 4°C on a shaking platform with the respective primary antibody or NY-BR-1 hybridoma supernatant diluted in 0.5% non-fat milk in TBS-T buffer. Next membranes were washed with TBS-T three times, first time after 10 minutes followed by two 5 minute intervals. Then the membrane was incubated with the respective horseradish peroxidase conjugated secondary antibody diluted in 0.5% non-fat milk in TBS-T for 1h at RT. Following another interval of washing with TBS-T buffer, protein signals were detected using the enhanced chemiluminescence (ECL) system either by exposing blots to an X-ray film or by a charge-coupled device (CCD)-camera .

4.2.10 Estimation of cell viability (CellTiter-Glo® Assay)

Cell viability was assessed by CellTiter-Glo® (CTG) assay and it relies on measuring the ATP content which is directly proportional to the amount of cells present. Briefly, a known number of viable cells were seeded in a flat bottomed 96 well plate in 100µl culture medium (RPMI medium with 10% FCS and 1% Pen/Strep). 100 µl of CellTiter-Glo® reagent was added to each well of 96 well plate. The contents were mixed for 2 minutes by gentle shaking on an orbital shaker and incubated for 10 minutes at room temperature. A luminescent signal is generated which is directly proportional to the amount of ATP released from the lysed. The luminescence signal was with the Fluoroskan Ascent-Microplate Fluorometer according to the manufacturer´s recommendation.

4.2.11 Immunization of mice with peptide

For immunization of mice with peptides, peptide #6 (H2-Db-restricted NY-BR-1 specific CTL epitope) was adjusted to a concentration of 4 mg/ml and the H2-IAb-restrcited epitope HBV core 128-140 was adjusted to a concentration of 5.6 mg/ml. 250µl of each peptide prepared above was mixed with 500µl IFA and taken up in an 1 ml syringe and passed through a special adapter to another 1 ml syringe. This process was repeated 10-20 times to obtain a homogenized emulsion and this was stored once ice until injection. Each mouse was immunized with 50 µl peptide emulsion injected *s.c.* on the left and right breast. The immunized mice were sacrificed and spleens were harvested 14 days post immunization unless mentioned otherwise.

4.2.12 Immunization of mice with recombinant adenovirus (Ad.NY-BR-1 or Ad.Control)

Recombinant adenovirus encoding NY-BR-1 (Ad.NY-BR-1) and the empty virus (Ad.Control) were purchased from GeneCust (Dudelange, Luxembourg). The gene encoding the E1 viral protein was deleted by the supplier thus rendering the virus replication deficient. The virus was provided at a concentration of 10^{12} VP/ml which corresponds to $1x10^{10}$ pfu/ml and it was diluted 1:1 to obtain a working solution of $5x10^{9}$ pfu/ml. For immunization, each mouse was injected with $5x10^{8}$ pfu (100µl of the working solution) intraperitoneally. Splenocytes were harvested 14 days post immunization unless indicated otherwise.

4.2.13 Establishment and *in vitro* propagation of antigen specific $CD8^+$ T cells

Immunized mice were sacrificed 14 days post immunization and spleens were harvested. Single cell suspension of splenocytes was prepared by passing the spleens through a 70 µm

cell strainer using a plunger. The cells were centrifuged at 1400 rpm for 10 minutes and the cell pellet was resuspended in 1 ml of ACK lysis buffer and incubated for 1 minute at room temperature. The ACK lysis buffer was neutralized by adding 49 ml PBS and the cells were again centrifuged at 1400 rpm for 10 minutes. The cells were then resuspended in incomplete CTL medium (complete CTL without ConA supernatant) and $2x10^7$ spleen cells were restimulated in a total volume of 10 ml in upright standing T25 flasks by co-cultivating them with different stimulator cells as described below. On day 5, cells were harvested from T25 flasks and centrifuged at 1400 rpm for 10 minutes. The cells were then resuspended in 1 ml of complete CTL medium and distributed in one row of a 24 well plate in roughly titrated aliquots with the highest number of cells being seeded in the first well receiving and the lowest number of cells in the last well. For *in vitro* propagation of the T cells, the cells were restimulated with the same stimulator cells as the first round every 7 days. The cells were used for assays on day 5 after the last restimulation and half of the culture medium was replaced with fresh complete CTL medium on the same day.

4.2.13.1 Restimulation with irradiated NY-BR-1 transfectant cells

Restimulation with NY-BR-1 transfectant cells as stimulator cells were carried out with EL/NYBR-1 transfectant clone D8P3 or with EO771/NY-BR-1 transfectant clone #19 (EONY#19). The first restimulation *ex vivo* was carried out by adding $2x10^6$ stimulator cells which had been irradiated at 200 Gy to the splenocytes. For subsequent *in vitro* propagation of NY-BR-1 specific $CD8^+$ T cells, $2x10^5$ stimulator cells irradiated at 200 Gy and $5x10^6$ syngeneic feeder cells irradiated at 33 Gy were added to each well of the 24 well plate. In case of $CD8^+$ T cells sorted for dextramer-labeled cells, the first restimulation step was skipped.

4.2.13.2 Restimulation with peptide loaded feeder cells

Ex vivo restimulation was performed by adding the antigenic peptide (peptide #6 or peptide #136) to the splenocytes at the final concentration of 100 ng/ml. For subsequent restimulation rounds, syngeneic splenocytes were harvested and adjusted $5x10^6$ cells/ml in XVIVO-20 medium and incubated with 1µg/ml peptide #6 or peptide #136 at 37°C for 1 hour. The cells were then washed 3 times with PBS to wash away the unbound peptide and resuspended in complete CTL medium at a concentration of $5x10^7$ cells/ml. The cells were then irradiated at 33 Gy and 100 µl containing $5x10^6$ cells/ were added to each well of the 24 well plate.

4.2.13.3 Restimulation with Dynabeads® Mouse T-Activator CD3/CD28

Dynabeads® Mouse T-Activator CD3/CD28 were used to stimulate single $CD8^+$ T cells sorted for dextramer-labeled cells in 96 well plate. One milliliter MACS buffer was added to 5µl beads and vortexed for 5 seconds and placed on the magnet for 3 minutes and the supernatant was discarded. The beads were resuspended in 40 ml complete CTL medium and 100 µl was added to each well of 96 well plate.

4.2.14 *In vitro* propagation of antigen specific $CD4^+$ T cells

HLA-DRB1*0401-restricted NY-BR-1 specific CD4+ T cell lines #8862 and #9251 were thawed and the cells were seeded in 24 well plates in 2 ml complete CTL medium (with ConA supernatant), and restimulated with 2µg/ml respective peptide. Additionally, $5x10^6$ syngeneic splenocytes were irradiated at 33 Gy and added as feeder cells to each well. Every 5-7 days, half of the supernatant was exchanged with fresh complete CTL medium.

Restimulation was repeated every 4 weeks by addition of $5x10^6$ irradiated syngeneic feeder cells and 2 µg/ml antigenic peptide.

4.2.15 Peptide binding assay

For the peptide binding assay, $2x10^5$ cells were incubated overnight with varying concentrations of the peptide and the stabilization of the H2-D^b and H2-K^b molecule on the cell surface was quantified by flow cytometry as an indirect measure of peptide binding. RMA-S cells were harvested and adjusted to a concentration of $2x10^6$ cells/ml in X-VIVO 20 medium. Peptide working solution with concentration of 200 µg/ml was prepared. In round bottom-96 well plate, the wells highlighted in pink were filled with 100 µl X-VIVO 20 medium and the 110 µl of the peptide working solution was added to the wells A1-A3. Ten microliter of peptide working solution was transferred from the wells A1-A3 to wells in the second row and mixed by pipetting. The process was repeated by transferring 10 µl from the wells in the second row to those in the third row and so on. The final 10 ml from the 7^{th} row (row G) was discarded and the 8^{th} row did not contain any peptide (see scheme below). Finally, 100 µl of RMA-S cell suspension containing $2x10^5$ cells were added to each well and incubated at 37 °C overnight. This was followed by measurement of MHC I molecule on the cell surface using the H2-D^b-specific monoclonal antibody B22.249 or H2-K^b-specific monoclonal antibody E3-25.

4.2.16 IFNγ ELISPOT

Splenocytes from immunized mice or established T cell lines were isolated and IFNγ secretion was analyzed in an IFNγ ELSIPOT assay. Briefly the PVDF membrane of MultiScreen$_{HTS}$-IP (Merck Milipore, Darmstadt, Germany) was activated by addition of 15 µl of 80% Ethanol and then washed twice with 200 µl PBS. The membrane was then coated with 5 µg/ml anti-mouse IFNγ capture antibody (BD Pharmingen, San Diego, U.S.) for 1 hour at 37 °C or overnight at 4°C. The unbound antibody was washed twice with 200 µl PBS and the membrane was blocked with 200 ml of culture medium (RPMI with 10% FCS and 1%Pen/Strep) for 1 hour at 37°C. Unless otherwise indicated, $1x10^5$ effector cells were incubated overnight at 37°C and 5% CO_2 with $5x10^4$ target cells or 100 ng/ml peptide. The cells were discarded and plates were washed 4 times with 1x PBS-T followed by one wash with PBS. 100 µl of 1µg/ml biotinylated anti-mouse IFNγ was added to each well and incubated at 4°C for 1 hour. The antibody was washed 4 times with PBS and 100 µl of avidin-conjugated alkaline phosphatase antibody (diluted 1:500) was added to each well and incubated for 30 minutes at room temperature. The wells were washed 4 times with PBS IFN γ secretion was detected by adding 100 µl BCIP/NBT (Sigma, Saint Louis, U.S.) per well and incubation at room temperature for 5 minutes. The reaction was stopped by washing the wells with distilled water. ELISPOT results were analyzed using the AID ELISPOT reader or CTL ELISPOT reader. Statistical anaylsis performed using Mann Whitney test.

4.2.17 IFNγ catch assay

To analyze NY-BR-1 specific $CD8^+$ or $CD4^+$ T cell responses, splenocytes obtained from immunized mice were stained for $CD8^+IFN\gamma^+$ or $CD4^+IFN\gamma^+$ T cells by Mouse IFN-γ Secretion Assay – Detection Kit (Miltenyi Biotec GmbH, Gladbach, Germany) according to the optimized manufacturer´s protocol. Briefly, $2x10^6$-$2.5x10^6$ murine spleen cells were seeded in 12 well plates in 2 ml culture medium (RPMI plus 10% FCS and 1% Pen/Strep) and stimulated overnight with 5 µg/ml of the respective peptide. On the following day, cells were harvested and transferred to a round bottomed 96 well plate and washed twice with MACS

buffer before addition of the IFNγ catch reagent. The cells were then incubated at 37 °C for 2-3 hours for the secretion period. Subsequently, cells were washed twice with PBS and dead cells were stained using the LIVE/DEAD® Fixable Yellow Dead Cell Stain or LIVE/DEAD® Fixable Blue Dead Cell Stain Kit. The cells were then washed twice with FACS buffer and following which they were stained with fluorochrome labelled anti-mouse CD4 antibody, anti-mouse CD8 antibody and anti-IFN-γ PE (Miltenyi Biotec GmbH, Gladbach, Germany). Data was acquired on a FACS Calibur1, FACS Canto II or LSR II and analyzed with FlowJo software. Statistical anaylsis performed using Mann Whitney test.

4.2.18 IFNγ ELISA

Secreted mouse IFNγ was quantified using the Mouse IFN gamma ELISA Ready-SET-Go (BioLegend, San Diego, U.S.) according to manufacturer's instructions. Briefly, Nunc™ MaxiSorp™ ELISA Plates, Uncoated (BioLegend, San Diego, U.S.) were coated with the capture antibody by incubating overnight at 4°C. The unbound antibody was washed twice by adding 250 µl wash buffer per well and the wells were blocked with 100 µl of 1x ELISA/ELISPOT Diluent for 1 hour at room temperature. Two fold serial dilution of the provided IFNγ was performed to obtain standards with concentrations ranging from 2000 pg/ml to 15.625 pg/ml. The wells were washed once with 250 µl wash buffer per well before addition of the IFNγ standards and the samples which were incubated overnight at 4°C. On the following day, the wells were washed 5 times with 250µl wash buffer per well and the diluted 1x detection antibody was added (100ml/well) and incubated for 1 hour at room temperature. The wells were washed again 7 times with 250 µl wash buffer per well and the diluted 1x avidin-HRP antibody was added (100µl/well) and incubated for 30 minutes at room temperature. 100µl substrate was added per well and incubated for 5-10 minutes at room temperature followed by addition of 50 µl stop solution per well. The absorbance was measured on Tecan reader at 450 nm. The IFNγ concentration of the samples was determined by using the standard curve generated using GraphPad Prism.

4.2.19 CD107a degranulation assay

Fifty thousand NK cells were incubated with RMA, RMA-S, EONY#19, EONY/PX458, EONY/M1KO, B16F10, B16F10/PX458 or B16F10/M1KO cells at an effector to target ratio of 1:10 or with 50 ng/ml PMA and 250 ng/ml Ionomycin for unspecific stimulation. The incubation was carried out at 37°C for 4 hours in the presence of anti-CD107a antibody (diluted 1:100) or the corresponding isotype control (diluted 1:100) in a total volume of 200 µl. The protein transport inhibitor containing Monensin was added at a final dilution of 1:1500 during the last 3 hours of the incubation period. The cells were washed and the Fc receptors were blocked by incubating the cells with FCR block (diluted 1:10) and rat serum and hamster serum (diluted 1:100) for 30 minutes at 4°C. The cells were washed and stained with antibody cocktail containing LIVE/DEAD® Fixable Blue stain (diluted 1:1000) and anti-CD3 and anti-NK1.1 antibody (both diluted 1.100) in FACS buffer for 1 hour at 4 °C. The cells were washed and analyzed by flow cytometry.

4.2.20 Isolation of peritoneal exudate cells (PECs) and *in vitro* polarization

Mice were injected with 1 ml of 3% Thioglycollate broth (AppliChem, Darmstadt, Germany) intraperitoneally and 4 days later mice were sacrificed. The abdomen was sterilized with 70% ethanol and a small part of the skin was removed without breaking the peritoneum. 1 ml cold PBS was injected into the peritoneum and the abdomen was massaged gently. The peritoneal exudate was collected using an 18G needle and a Pasteur pipette. The cells were

counted and $1.8x10^6$ cells were seeded in each well of 6 well plate in PECs culture medium (DMEM with 10% FCS and 1% Pen/Strep). The macrophages were allowed to attach for 2 hours at 37°C and the remaining unattached cells were washed away with warm PBS. M1-like macrophages were obtained by culturing them with PECs culture medium with 100 ng/ml LPS and 50 ng/ml IFNγ whereas M2-like macrophages were obtained by polarizing them by addition of 10 ng/ml IL-4 to PECs culture medium.

4.2.21 *In vivo* tumor growth

Tumor cells were harvested by trypsinization and the trypsin was neutralized by addition of culture medium containing FCS. The harvested cells were washed three time with PBS and resuspended in PBS. Viable cells were counted and cell count was adjusted as required and 100 µl was injected onto the right flank of mice. In case of tumor cell injections with Matrigel (BD Pharmingen, San Diego, U.S.), cells were prepared in Matrigel diluted 1:1 with PBS. For injection into mammary fat pad, cells were prepared similarly but 50µl cell suspension was injected onto 4^{th} right mammary fat pad.

4.2.22 Isolation of tumor infiltrating leukocytes

Tumors were harvested and cut into small pieces using a scalpel. This was digested using a mix of Collagenase D (0.5 mg/ml), DNAse I (10 µg/ml), TLCK inhibitor (0.1 µg/ml) and HEPES buffer (10mM) in HBSS by shaking at 200 rpm for 1 hour at 37 °C. The tumor pieces were then passed through a 70 µm cell strainer using a plunger and the cell strainer was flushed with PBS. The cell suspension was centrifuged at 1400 rpm for 10 minutes. The cell pellet was resuspended in 5 ml RPMI medium and layered on the top of 5 ml Lympholyte M in a 15 ml Falcon tube. The cells were centrifuged at 1500g without brake at room temperature. The leukocytes from the interphase were collected and washed with PBS and used for further experiments like flow cytometry or MACS. The tumor cell pellet at the bottom of the tube was washed with PBS and used for RNA and protein isolation as required.

4.2.23 Isolation and activation of murine NK cells for *in vitro* assays

Spleens were isolated from C57/BL6 mice and single cell suspensions prepared by passing them through 70 µM cell strainer using a plunger and the cell strainer was flushed with PBS. The cell suspension was centrifuged at 1400 rpm for 10 minutes. Erythrocyte lysis was performed by resuspending the cells in 2ml ACK lysis buffer followed by 1 minute incubation at room temperature. The cells were washed with 49 ml PBS and resuspended in MACS buffer to obtain a single cell suspension. NK cells were isolated using the mouse NK Cell Isolation Kit II (Miltenyi) according to the manufacturer's instructions. In order to activate the NK cells, $1x10^6$ NK cells were seeded in a 6 well plate with 5ml NK cell medium containing 1700 U/ml IL-2 and cultured for 7 days for use in ELISPOT assay or 6 days for CD107a degranulation assay.

4.2.24 Magnetic activated cell sorting (MACS) for positive selection

Cytotoxic T cells among *in vitro* cultured T cells were enriched by using the CD8a microbeads. The cells were harvested and counted using Neubauer chamber. The cells were resuspended in MACS buffer and 10 µl CD8a microbeads were added for every $1x10^7$ cells at a final dilution of 1:10 and incubated for 30 minutes at 4 °C. The cells were then washed twice with MACs buffer and resuspended in 500 µl MACS buffer. An MS column was placed on the OctoMACS magnet and washed with 500 µl MACS buffer. The cells were then applied

to the column and allowed to pass through the column and the column was washed thrice with 500 µl MACS buffer during which the unlabeled cell fraction was collected. The column was then removed from the magnet and 1 ml MACS buffer was added to the column. The cells were immediately flushed out by firmly applying the plunger. Tumor-infiltrating myeloid cells were enriched using CD11b microbeads. Tumor-infiltrating leukocytes were isolated as described above and counted using a Neubauer chamber. For every $1x10^7$ cells, 80 µL MACS buffer and 20 µl CD11b microbeads were added to the cells and mixed. The cells were incubated for 30 minutes at 4 °C. The cells were washed twice with MACS buffer and resuspended in 3 ml MACS buffer. An LS column was placed on the QuadroMACS magnet and washed with 3 ml MACS buffer. The cells were then applied to the column and allowed to pass through the column and the column was washed thrice with 3 ml MACS buffer during which the unlabeled cell fraction was collected. The column was then removed from the magnet and 1 ml MACS buffer was added to the column. The cells were immediately flushed out by firmly applying the plunger.

4.2.25 Dextramer staining

Spleens were harvested from mice immunized with Ad.NY-BR-1 or Ad.Control and single cell suspensions were prepared followed by erythrocyte lysis and cells were counted using a Neubauer Chamber. The cells were washed with PBS and $1x10^6$ cells were incubated with LIVE/DEAD® Fixable Yellow Dead Cell Stain diluted 1:1000 in PBS for 30 minutes at 4 °C. The cells were washed again with PBS and incubated with dextramers diluted as indicated in 60 µl FACS buffer for 30 minutes at room temeperature in dark. Fluorescently labeled FACS antibodies for CD3, CD8, CD4 and CD14 or the respective isotype control were diluted 1:50 in 60 µl FACS buffer and added to the cells without washing of the dextramers so that the final diltuon of the antibodies was 100 fold. They cells were incubated with the antibody mix at 4°C for 30 minutes. The cells were then washed and analyzed by flow cytometry or sorted for live $CD3^+CD14^-CD8^+dextramer^+$ cells.

4.2.26 Tetramer staining

$CD4^+$ T cells were harvested and counted in a Neubauer chamber. The HLA-DRB1*0401 and HLA-DRB1*0301 tetramers were diluted in FACS as indicated and $1x10^6$ $CD4^+$ T cells were incubated with the tetramer at 37°C or at 4 °C, as indicated for the duration indicated. The cells were then washed with FACS buffer and counterstained with anti-CD4 and anti-CD8 antibody diluted 1:100 in FACS buffer by incubating them at 4 °C for 1 hour or 45 minutes. In some cases, the tetramer staining was carried out in FACS buffer containg 5 nM dasatinib.

4.2.27 Flow cytometry for analysis and cell sorting

For flow cytometry analysis, $1x10^6$ cells were used for each sample unless otherwise mentioned. Cells were harvested and washed with twice with 200 µl FACS buffer. A mix of 0.05mg/ml Purified Rat Anti-Mouse CD16/CD32 (BD Pharmingen, San Diego, U.S.), rat serum (GeneTex, Irvine, USA) and hamster serum (Jackson Immunoresearch, West Grove, USA) was used for blocking the FC receptors on tumor infiltrating leukocytes and PECs by incubating them at 4° for 20 minutes. For tumor cell lines and splenocytes this step was not done. The cells were then washed twice with 200 µl PBS. LIVE/DEAD® Fixable Yellow Dead Cell Stain or LIVE/DEAD® Fixable Blue Dead Cell Stain Kit, for UV excitation (Life technologies, Carlsbad, U.S.) was diluted 1:1000 in PBS and 100 µl was added to each sample. The cells were incubated for 30 minutes at 4°C and washed twice with 200 µl FACS buffer. The cells were stained for surface markers with respective antibodies (or isotype

controls) diluted 1:100 in 100µl FACS buffer per sample and incubation was carried out for 1 hour at 4°C. The cells were then washed twice with 200 µl FACS buffer and resuspended in 200-400 µl FACS buffer and analyzed or sorted on a flow cytometer. In case intracellular proteins needed to be stained, the cells were fixed and permeabilized using the BD Cytofix/Cytoperm Fixation/Permeabilization Kit (BD Biosciences, San Jose, U.S.). Briefly, the cells were resuspended in 100µl fixation permeabilization solution and incubated at 4°C for 20 minutes and then washed twice with 200 µl 1x BD Perm/Wash buffer. The antibodies for intracellular staining (or isotype controls) were diluted 1:100 in 100 µl 1x BD Perm/Wash buffer per sample and the cells were incubated for 1 hour at 4°C. The cells were washed twice with 200 µl 1x BD Perm/Wash buffer and resuspended in 200-400 µl FACS buffer for analysis.

4.2.28 *In vivo* depletion of NK cells and $CD4^+$ T cells

For NK cell depletion, 100 µg NK1.1 specific monoclonal antibody clone PK136, or isotype control clone C1.18.4 (both BioXcell, West Lebanon, NH) were administered intraperitoneally 2 days prior to the day of tumor injection. To maintain NK cell depletion, antibody injection was repeated on the day of tumor injection and on days 7 and 13 after tumor inoculation. For $CD4^+$ T cell depletion, 100 µg CD4 specific monoclonal antibody clone GK1.5, or isotype control clone LTF-2 (both BioXcell, West Lebanon, NH) were administered intraperitoneally daily for 3 days prior to tumor inoculation and repeated on days 1, 4, 7, 10, 13 and 16 after tumor inoculation.

5 Results

5.1 Establishment of a heterologous transplantable NY-BR-1 expressing tumor model

The lymphoma cell line EL4 is derived from C57BL/6 mice (220) and expresses the MHC I molecules namely the H2-D^b and H2-K^b. EL4 cells are negative for MHC II expression on the surface and fail to upregulate it even after IFNγ treatment. This makes them suitable for being used as a stimulator cell for the *in vitro* expansion of NY-BR-1-specific $H2^b$-restricted CTLs and for transplantation in HLA-DR4tg mice since HLA-DR4tg mice have H2-D^b and H2-K^b for MHC I and chimeric HLA-DR4 molecule for MHC II. This cell line had been transfected previously in our lab with linearized plasmid pcDNA3.1(-)zeo-NY-BR-1, giving rise to single cell clones expressing NY-BR-1 (Gardyan et al). EL4/NY-BR-1 clone D8P3 and clone A5P1, referred to as D8P3 and A5P1 from now on were found to express high levels of NY-BR-1 RNA and protein and thus were selected for *in vivo* experiments.

5.1.1 Characterization of EL4/NY-BR-1 transplantable model

5.1.1.1 Determination of optimal number of transplanted tumor cells *in vivo*

In order to characterize the growth kinetics of EL4/NY-BR-1 transfectants *in vivo*, single cell clones D8P3 and A5P1 were injected subcutaneously into HLA-DR4tg mice in varying numbers and growth rate was monitored. Tumors developed in all mice latest by day 13 after tumor cell injection, even with the lowest cell number of $5x10^4$ cells per mouse. Palpable tumors could be detected in the mice receiving $5x10^5$ cells or $1x10^5$ cells already 7 days after tumor inoculation (Figure 8). On day 13 after tumor injection, tumors derived from $5x10^5$ A5P1 cells showed signs of necrosis and hence were excluded from further group analysis. Thus, the dose dependent effect of the tumor cell number on the tumor growth curve is not apparent in this group (Figure 8B). The tumor growth rate in the remaining mice was monitored (Figure 8B, right panel). The growth rate of D8P3 clearly showed a dose dependent effect with the highest cell number of $5x10^5$ cells giving rise to tumors of average size of 285 mm^2 by day 18 (Figure 8A) when they were sacrificed owing to large tumors. The other tumors were monitored until they attained the maximum allowed size or until day 24 when the experiment was terminated. Due to the fact that different numbers of D8P3 cells gave rise to tumors with corresponding growth kinetics without developing necrosis, they were selected for further experiments.

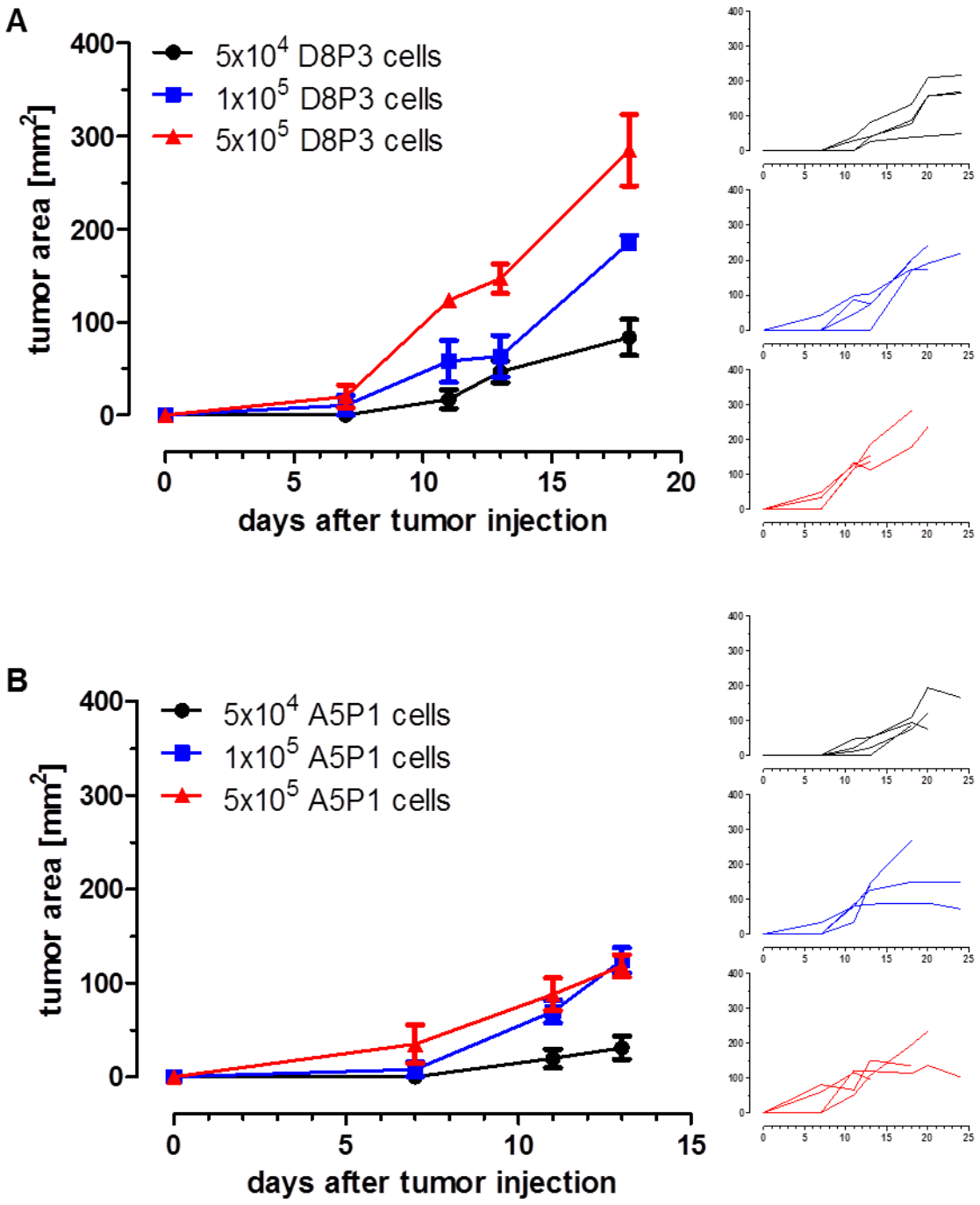

Figure 8. Comparison of tumor growth curves of EL4 derived, NY-BR-1-expressing clones D8P3 and clone A5P1

(A) $5x10^4$, $1x10^5$ or $5x10^5$ D8P3 or (B) A5P1 cells were injected *s.c.* into the right flank of HLA-DRB1*0401tg mice (n=4) and tumor growth was monitored for 24 days after injection. Tumor dimensions were measured by calipers and tumor size was calculated by the following formula (area= length x breadth). Error bars represent SEM. Mice were sacrificed when tumor size reached 225 mm^2 and mean tumor size is depicted until the first mouse dropped out. The tumor growth curve of individual mice is depicted on the right.

5.1.1.2 NY-BR-1 expression is retained in tumors *in vivo*

In order to test whether NY-BR-1 expression alters the growth rate of the parental EL4 cell line *in vivo*, the growth rate of EL4 and D8P3 derived tumors was initially compared applying

$1x10^6$ tumor cells. Both tumor cell lines injected subcutaneously into the flank of HLA-DR4tg mice grew at a comparable rate (Mann Whitney test, p=0.6857) (Figure 9A). The NY-BR-1 transfectants were always cultured under Zeocin selection pressure *in vitro*, however once inoculated into mice the tumor cells can lose NY-BR-1 expression. To address this issue, the tumors were harvested on day 14 after tumor inoculation and the expression of NY-BR-1 protein and RNA was analyzed in the excised tumors. The highest level of NY-BR-1 RNA was detected in mouse 1 followed by mouse 3 (Figure 9B) which corresponds to the level of NY-BR-1 protein detected by Western blot (Figure 9C, lane 1 and 3). NY-BR-1 was not detected in the tumors derived from the parental cell line EL4 either at the RNA level (Figure 9B, grey bars) or at the protein level (Figure 9C). It is important to note that NY-BR-1 protein is known to have a molecular weight of 159kDa which is the uppermost band detected (as indicated by the arrow) but additional unspecific bands of lower sizes were detected in all tumor lysates.

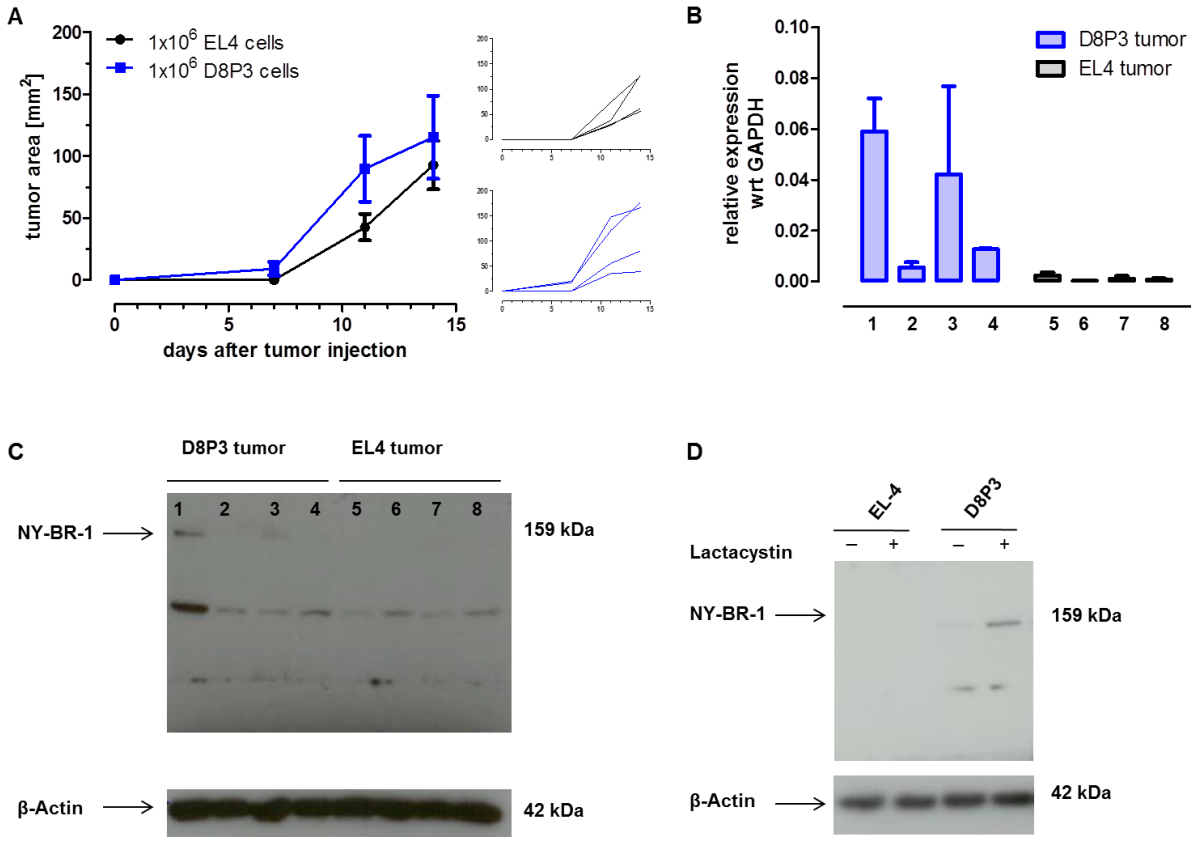

Figure 9. NY-BR-1 expression in EL4 cells did not alter its growth *in vivo*

(A) HLA-DRB1*0401tg mice were injected *s.c.* on the right flank with $1x10^6$ EL4 cells or D8P3 cells and tumor growth was monitored for 14 days after injection. Tumor dimensions were measured as described earlier. Error bars represent SEM (n=4). The tumor growth curve of individual mice is depicted on the right. **(B)** Tumors were resected 14 days post injection and expression of NY-BR-1 mRNA was analyzed by qRT-PCR. Bars represent individual mice and error bars depict SEM of triplicates in qRT-PCR. **(C)** NY-BR-1 expression at protein level could also be detected in at least 2 mice that were injected with D8P3 cells (Exposure time: NY-BR-1, 20 minutes and β-Actin, 5 seconds). (D) EL4 cells and D8P3 cells were treated with lactacystin as described earlier and NY-BR-1 expression was analyzed by Western blot (Exposure time: NY-BR-1, 15 minutes and β-Actin, 10 seconds). More NY-BR-1 protein was detected in D8P3 cells after lactacystin treatment as a result of impaired protein degradation.

5.1.1.3 NY-BR-1 protein has a high turnover rate in EL4/NY-BR-1 transfectant clone D8P3

The continuous expression of NY-BR-1 protein by the tumor cells *in vivo* is indispensable for their recognition by T cells. However, T cells recognize the antigenic peptides derived from degradation products when displayed on MHC molecules. Thus, absence of high levels of intracellular NY-BR-1 protein could be due to the fact that it is degraded very rapidly by the proteasome. Therefore, inhibiting the proteasome activity should allow the detection of native NY-BR-1 protein. In order to test whether the low level of NY-BR-1 expression by D8P3 cells was due to high turnover of NY-BR-1 in these cells, they were treated with 5 µM lactacystin for 18 hours and NY-BR-1 expression was analyzed by Western blot. The inhibition of proteasome increased the detectable amount of NY-BR-1 protein in D8P3 cells (Figure 9D) compared to untreated D8P3 cells. EL4 cells on the other hand, remained negative for NY-BR-1 even after lactacystin treatment.

5.1.2 Establishment of EO771/NY-BR-1 tumor model

Since EL4 tumors are lymphoma derived and NY-BR-1 is a breast cancer associated differentiation antigen, a mammary carcinoma cell line would allow the establishment of an orthotopic model. Thus, a murine mammary adenocarcinoma cell line derived from C57BL/6 mice called EO771 was selected to generate NY-BR-1 expressing mammary carcinoma cell line.

5.1.2.1 Generation and characterization of EO771/NY-BR-1 transfectant clones

EO771 cells were seeded at a density of $1x10^5$ cells per well in a 6 well plate and one day later Zeocin was added at varying concentrations to determine the minimal lethal concentration. The number of viable cells was monitored optically under a microscope and the concentration 400 µg/ml was found to be lethal to 100% cells within 3 days. Thus, this concentration was used for selection of EO771 cells successfully transfected with the linearized plasmid pcDNA3.1(-)zeo-NY-BR-1.

Transfected EO771 cells were cultured with 400 µg/ml Zeocin in order to select for successfully transfected cells. Seven days after selection with Zeocin, colonies of successfully transfected cells were observed under the microscope as the untransfected cells failed to grow. The cells were then expanded and harvested for analyzing NY-BR-1 RNA and protein expression. The NY-BR-1 was protein corresponding to a molecular weight of 160 kDa was detected by Western blot in the EO771/NY-BR-1 transfectants (Figure 10A, lane 4) but not in the parental EO771 cells (Figure 10A, lane 3). Protein lysates from MaMel21 cells infected with control adenovirus Ad5.Control were used as a negative control whereas MaMel21 cells infected with NY-BR-1 expressing Ad.NY-BR-1 were used as a positive control. NY-BR-1 RNA was quantified using qRT-PCR and was absent in the EO771 cells as expected whereas EO77/NY-BR-1 transfectant cells tested positive for NY-BR-1 RNA (Figure 10B).

Single cell clones of EO771/NY-BR-1 transfectant cells were obtained by limiting dilution and in total 19 clones tested for NY-BR-1 expression levels by Western blot and qRT-PCR. All EO771/NY-BR-1 clones are henceforth designated as EONY followed by the clone number. All the 19 clones tested positive for NY-BR-1 protein and clones #9, #20 and #22 were found to possess the highest levels of NY-BR-1 protein (Figure 10D). This correlated well with NY-

BR-1 RNA expression results obtained by qRT-PCR (Figure 10C). Additionally, the clone EONY #19 was also found to express high levels of NY-BR-1 RNA.

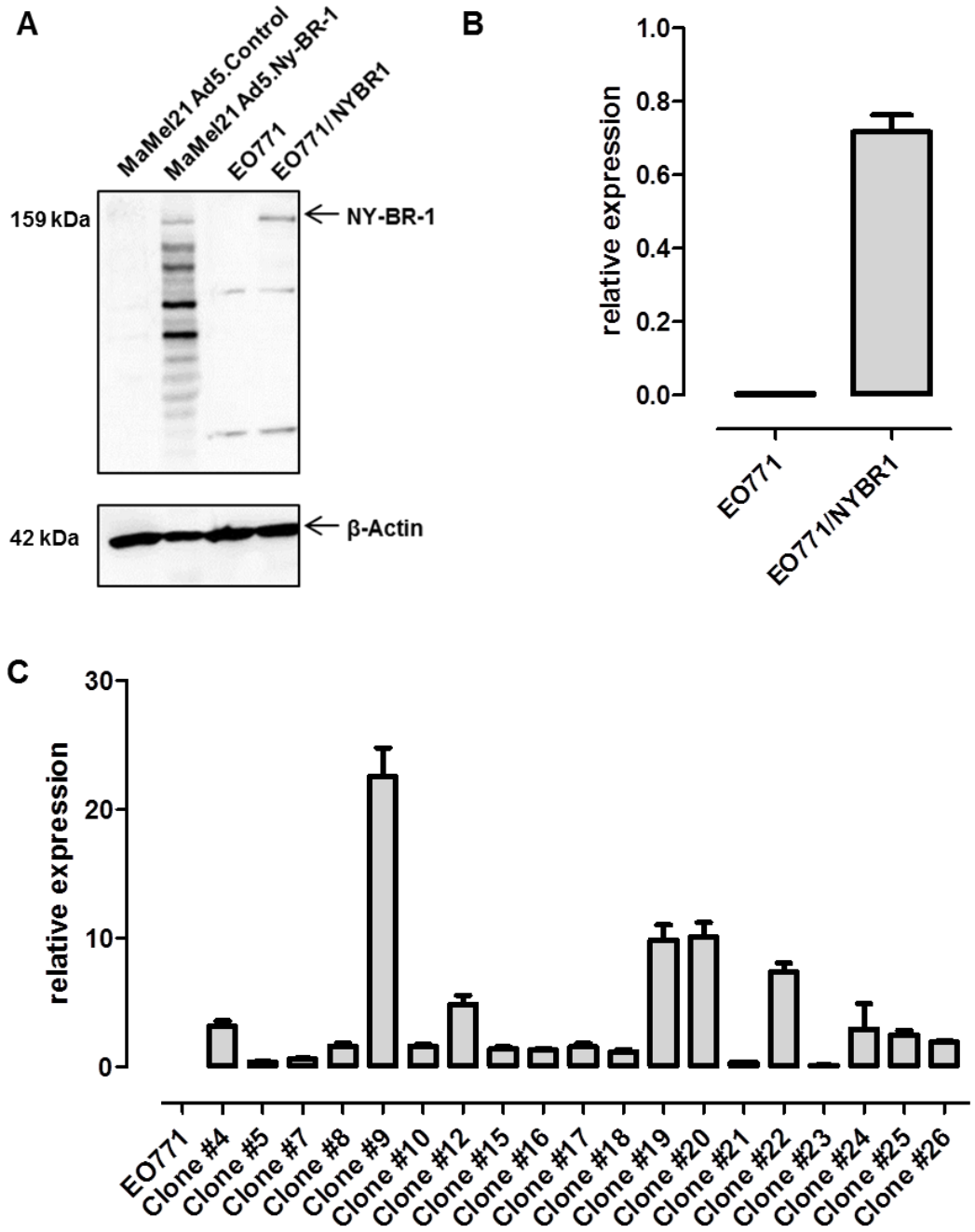

Figure 10. Generation of EO771/NY-BR-1 transfectant clones

EO771 cells were transfected with a linearized plasmid pcDNA3.1-NY-BR-1 and stably transfected cells were selected by culturing them under Zeocin selection pressure. **(A)** The bulk culture was tested for NY-BR-1 expression by Western blot to confirm successful transfection. The molecular mass (in kDa) of NY-BR-1 and β-actin is indicated on the right hand side. **(B)** The expression of NY-BR-1 in the bulk culture of EO771/NY-BR-1 was confirmed at the mRNA level by qRT-PCR. Several single cell clones of EO771/NY-BR-1 cells were obtained by limiting dilution and they were tested for the level of NY-BR-1 expression by **(C)** qRT-PCR and **(D)** Western blot. NY-BR-1 expression relative HMBS is shown and error bars depict SEM of triplicates in qRT-PCR.

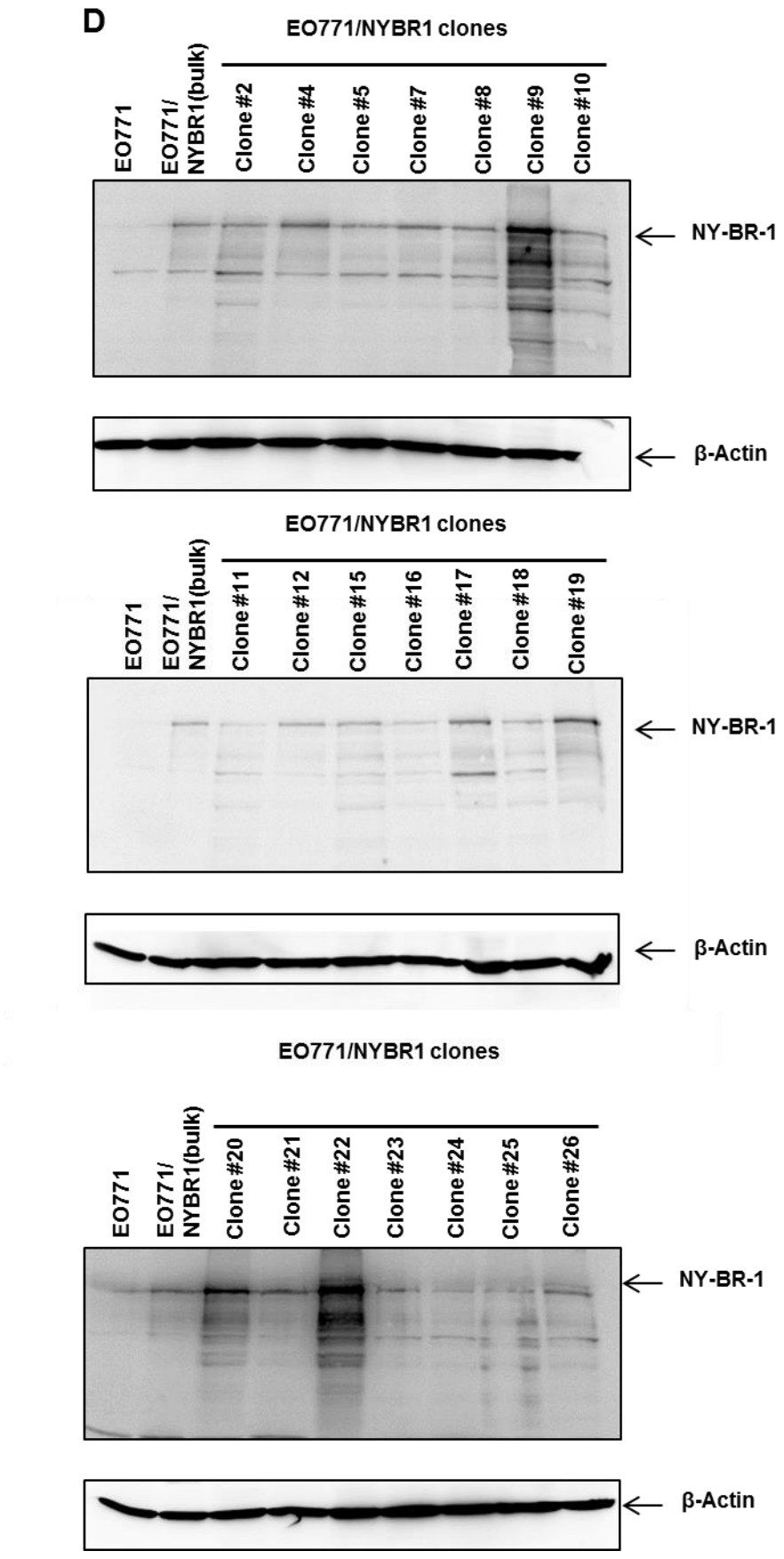

Figure 10 (contd). Generation of EO771/NY-BR-1 transfectant clones

(D) Expression of NY-BR-1 protein in the various single cell clones was tested by Western blot.

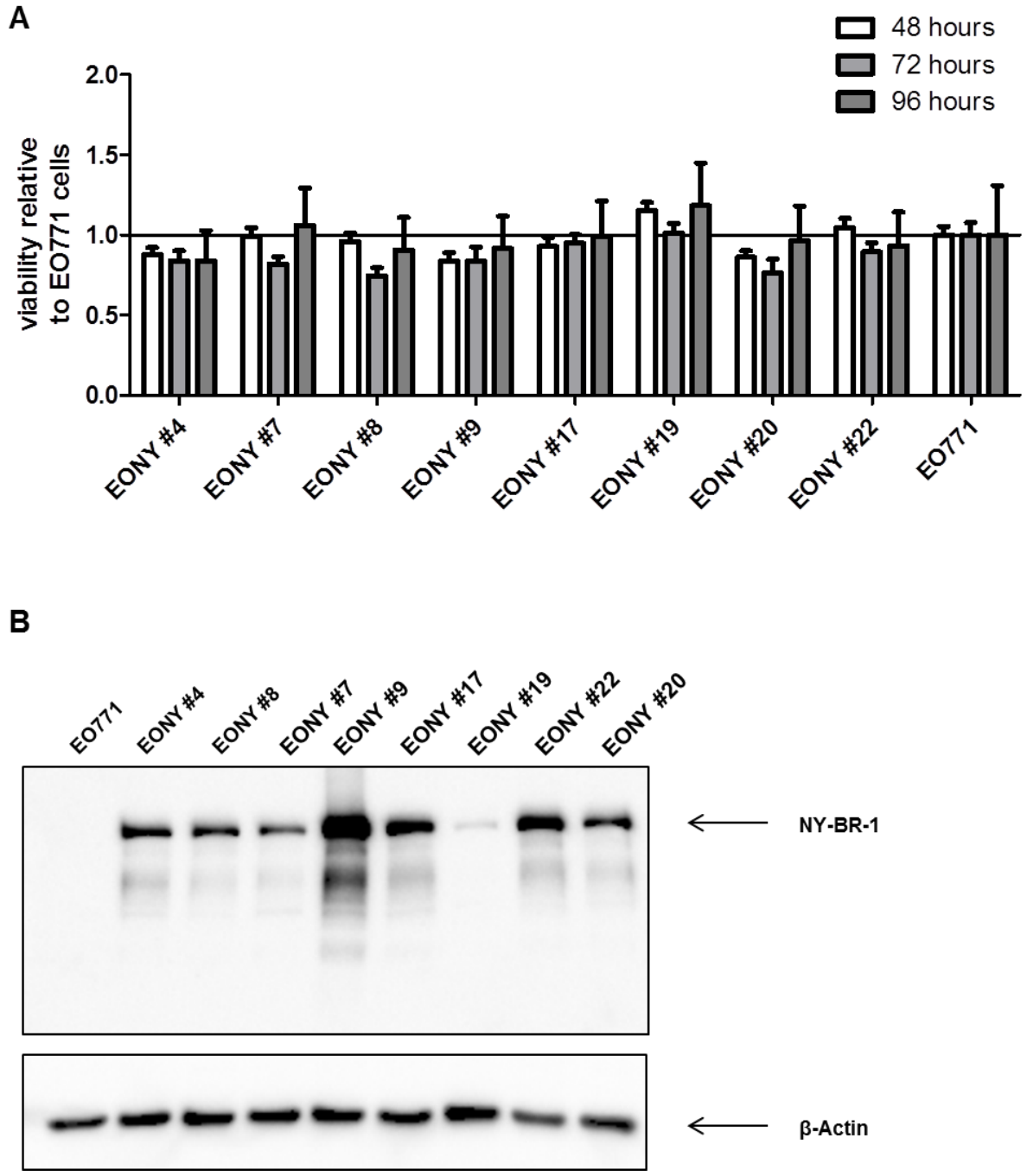

Figure 11. Characterization of EO771/NY-BR-1 transfectant clones

(A) $2x10^4$ cells of different EONY clones were seeded and the amount of viable cells was measured after 48, 72 and 96 hours later using the CellTiter-Glo® Assay. The relative luminescence units (RLU) obtained is proportional to the number of viable cells. The viability of each clone normalized to parental EO771 cells is depicted for the different time points. **(B)** NY-BR-1 protein expression in the selected clones after 6 weeks *in vitro* culture was analyzed by Western blot.

Using linearized plasmid instead of circular plasmids for transfection allows the plasmid to be integrated into the genomic DNA resulting in stable transfectants. However, the genomic DNA locus where it integrates is random and could potentially affect cell viability if for example it disrupts an important gene or promoter. Thus, 8 clones with different levels of NY-BR-1 expression were selected for assessing cell viability. Equal numbers of cells were

seeded and the amount of viable cells was measured after 48, 72 and 96 hours later using the CellTiter-Glo® Assay. There was no substantial effect on the viability of the EO771/NY-BR-1 clones compared to the EO771 cells (Figure 11A). In order to confirm that NY-BR-1 expression was retained *in vitro* after prolonged culture of the clones, cell lysates were prepared from EONY clones cultured for 6 weeks and NY-BR-1 protein expression was tested by Western blot. It was observed that EONY#9 consistently expressed the highest amount of NY-BR-1 protein, whereas EONY#19 lost its high expression of NY-BR-1 over time (Figure 11B). Still, EONY #19 was chosen for the initial *in vivo* experiments since the NY-BR-1 protein was clearly detected in clone #19 without a lot of unspecific products as in the case of clones #9, #20 and #22 (Figure 10D). Besides, it expressed NY-BR-1 RNA at high levels and displayed no reduction in cell viability. However, after it was discovered that NY-BR-1 expression is not stable in EONY#19, EONY#9 and EONY#17 were selected for later experiments.

5.1.2.2 EO771 cells lack surface expression of I-A^b molecules

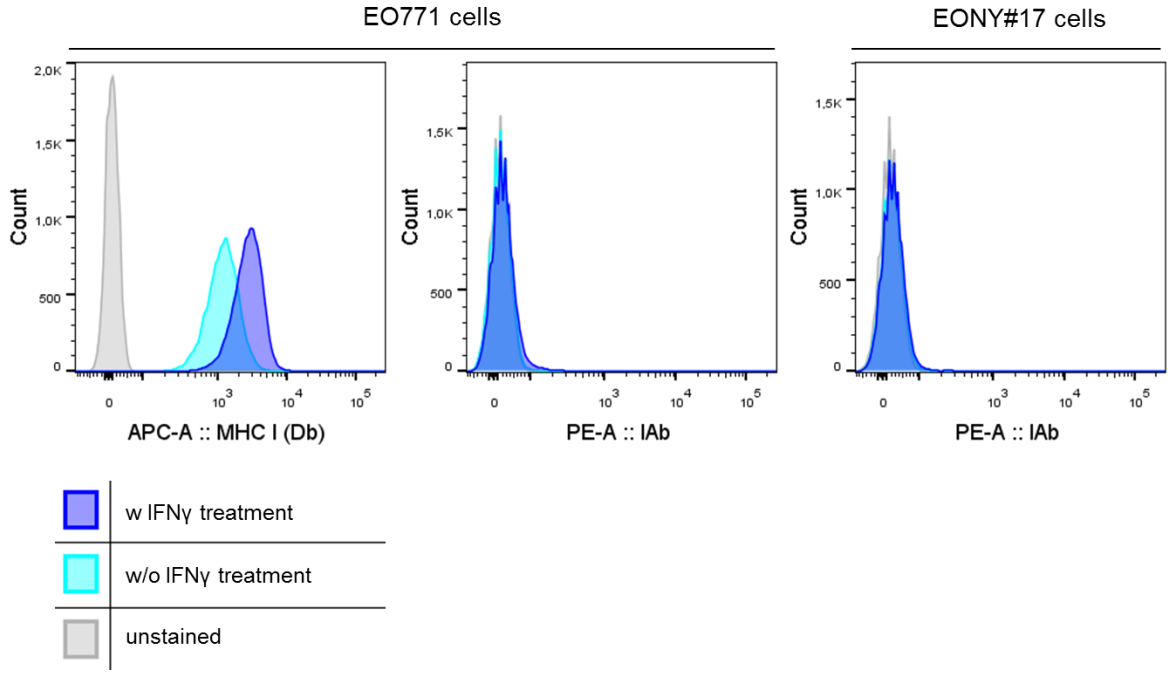

Figure 12. EO771 and EONY#17 cells lack surface expression of I-A^b molecules

Untreated EO771 or EONY#17 cells or those stimulated overnight with 20 U/ml IFNγ were stained for MHC I molecule using hybridoma supernatant which specifically binds H2-D^b and for MHC II molecule using a monoclonal antibody directed against I-A^b. The staining results are displayed as histograms for unstained sample (grey curve), without IFNγ treatment (light blue curve) and with overnight IFNγ treatment (dark blue curve). The level of MHC I expression on EO771 cells (left panel), MHC II on EO771 cells (middle panel) and MHC II on EONY#17 cells (right panel) is depicted.

EO771 cells are derived from C57BL/6 mice and therefore are syngeneic to HLA-DR4tg mice with respect to MHC I molecule and express H2-K^b and H2-D^b but differ in terms of their MHC II expression. Since C57BL/6 mice express I-A^b molecules, tumor cells derived from C57BL/6 mice might generate an immune response when transplanted into HLA-DR4tg mice which are knocked out for I-A^b molecule and therefore would recognize it as a xeno-antigen. Thus, EO771 cells were tested for the expression of I-A^b molecules on their surface by flow cytometry. No I-A^b molecules were detected on EO771 cells (Figure 12, middle panel) and on EONY#17 cells (Figure 12, right panel). *In vivo*, IFNγ might be present in high amounts in the

tumor microenvironment resulting in the upregulation of both MHC I and MHC II molecules (224). The level of MHC I expression on EO771 cells was increased when exposed to 20 U/ml IFNγ overnight (Figure 12, left panel), however EO771 cells (Figure 12, middle panel) and EONY #17 (Figure 12, right panel) failed to upregulate I-A^b on their cell surface following stimulation with IFNγ. Thus, EO771 and EONY#17 appear suitable for transplantation into HLA-DR4tg mice without the risk of inducing xenoreactive immune responses.

5.1.2.3 Characterization of EO771/NY-BR-1 clones *in vivo*

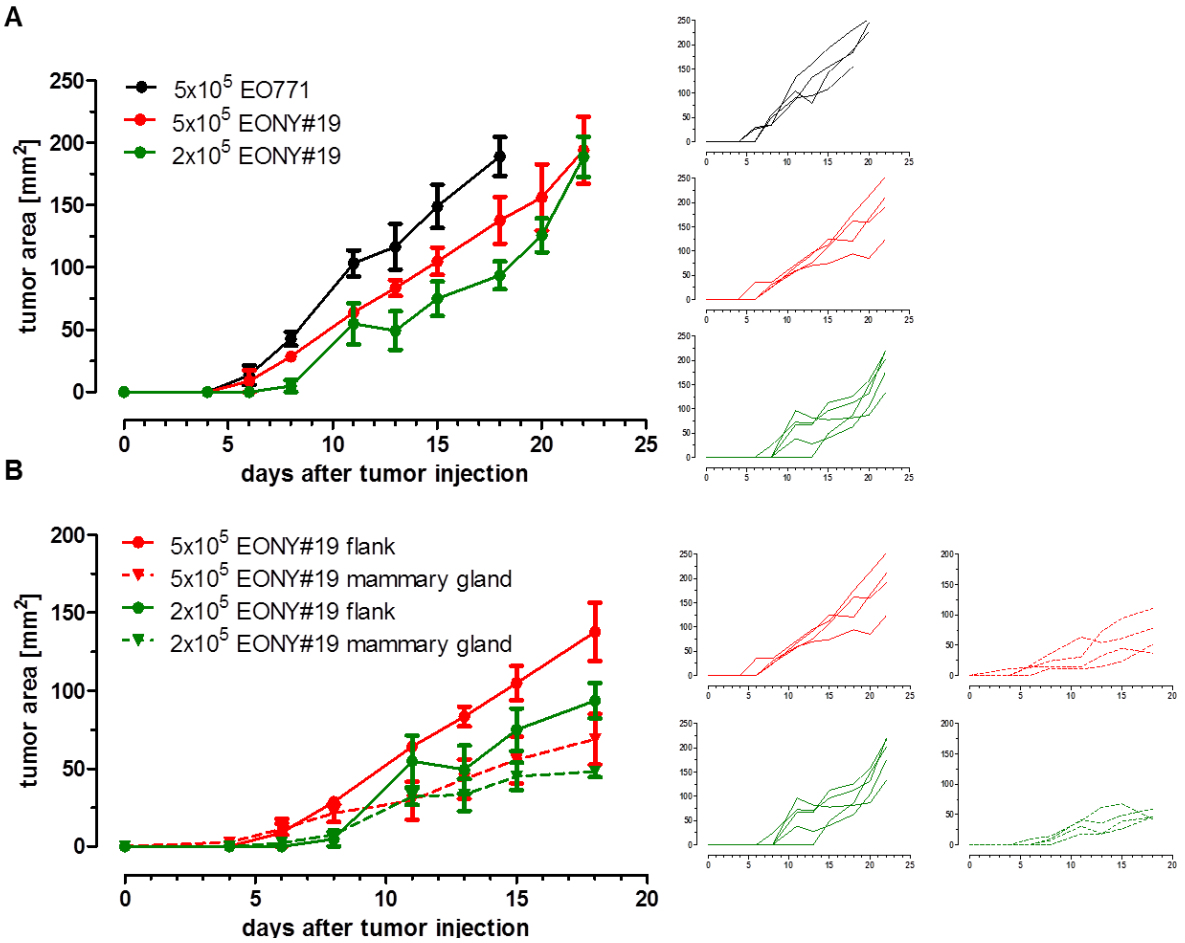

Figure 13. Optimization of transplantation of EO771 and EO771/NY-BR-1 clone #19 in the flank and in the mammary fat pad

EO771 or EONY #19 cells ($5x10^5$ or $2x10^5$) were injected *s.c.* into the right flank or the fourth mammary fat pad on the right side of HLA-DRB1*0401tg mice (n=4) and tumor growth was monitored for 22 days post injection. **(A)** Average size of tumors derived from $5x10^5$ EO771 cells (black), $5x10^5$ EONY#19 cells (red) and $2x10^5$ EONY#19 cells injected *s.c.* into the flank is depicted (left panel) and the corresponding tumor growth curves of individual mice are shown (right panel). **(B)** Comparison of tumor growth kinetics of $5x10^5$ or $2x10^5$ EONY#19 cells injected *s.c.* into the right flank or the fourth mammary fat pad is shown (left panel) along with the individual growth curves of each mouse.

NY-BR-1 is a breast cancer associated antigen and EO771 is a murine mammary adenocarcinoma cell line, thereby making EONY#19 cells an ideal candidate for establishing an orthotopic model. Thus, $5x10^5$ or $2x10^5$ EONY#19 cells were injected into the right flank or the fourth mammary fat pad of HLA-DR4tg mice and the growth rate was monitored. When EONY#19 cells were injected into the flank, the first tumors were apparent by day 6 for $5x10^5$ cells and by day 11 for $2x10^5$ cells (Figure 13A). Thus, the growth rate of the tumors

corresponded to the number of tumor cells injected. On the other hand, injection of cells in the mammary fat pad was not as successful in giving rise to tumors. There was no difference in the growth rate between the groups receiving different numbers of tumor cells. Even though the tumors began to develop after day 6, they failed to develop in size over time (Figure 13B). Notably, the tumors transplanted into the mammary fat pad turned necrotic and this could also be the reason why they did not grow in size.

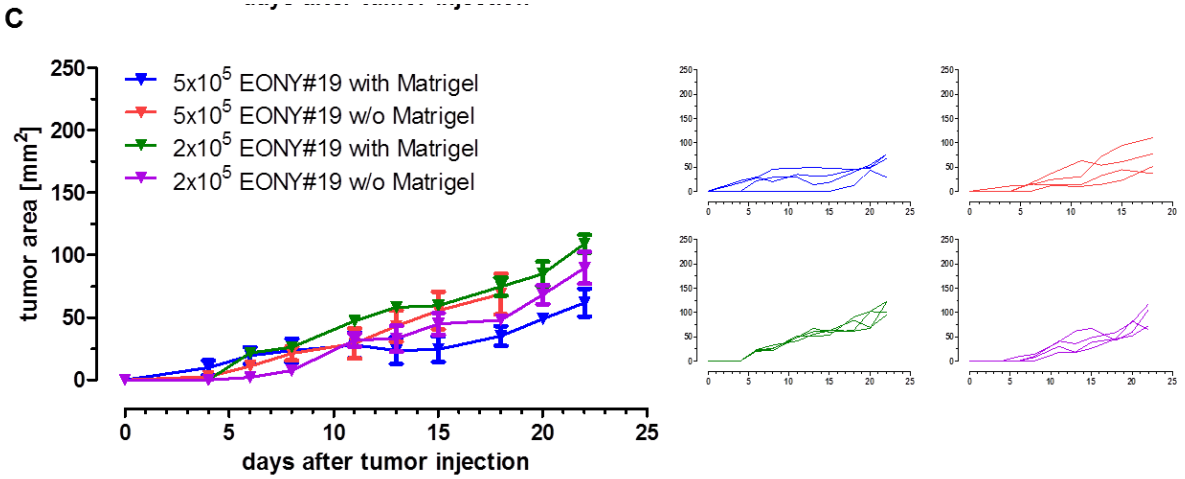

Figure 13 (contd). Optimization of transplantation of EO771 and EO771/NY-BR-1 clone #19 in the flank and in the mammary fat pad

(C) The growth rate 5x105 or 2x105 EONY#19 tumor cells transplanted orthotopically into the mammary fat pad with Matrigel (diluted 1:1) or without it is presented (left panel) in addition to the growth rate of individual tumors.

Matrigel is solubilized basement membrane matrix that is derived from Engelbreth-Holm-Swarm cells (mouse sarcoma) and is known to be a liquid at 4°C but solidifies at room temperature. It is used in tumor models especially for hematologic tumors to facilitate formation of a solid tumor. Additionally, it can act as a short term reservoir for growth factors enhancing the growth rate of tumor cells *in vivo*. Thus EONY#19 cells were injected in the mammary fat pad in Matrigel diluted 1:1 and the effect on tumor growth was measured. Addition of Matrigel did not improve the formation of mammary tumors by orthotopically transplanted EONY#19 cells as there was no difference in the tumor growth curves when $5x10^5$ or $2x10^5$ EONY#19 cells were injected in Matrigel (Figure 13C).

Thus, it was decided to use the heterotopic transplantation model where the breast cancer derived tumor cells are injected *s.c.* into the flank of the recipient mice. As described in the previous section, EONY#19 lost its NY-BR-1 expression over time and thus EONY#9 and EONY#17 cells were selected for subsequent studies. Tumor growth rates of EONY#9, EONY#17 and EO771 cells subcutaneously transplanted into HLA-DR4tg mice were measured. The different tumor cell lines grew at significantly different rates. Among mice injected with $2x10^5$ EO771 cells the first palpable tumors could be detected by day 7 and all mice developed tumor by day 10 (Figure 14A, black curve). In spite of slight variations in the growth rate among the individual mice all the tumors progressively grew in size and reached an average size of 102.57 mm^2 by day 18 (Figure 14A, black curve). Even though tumor growth was monitored until day 20 and individual growth curves are depicted (Figure 14A, right panel, black curves), comparison of tumor sizes was terminated on day 18 as some of the EO771 derived tumors developed necrosis and shrank in size. The same number of

EONY #9 cells failed to grow *in vivo* in all mice and only 7 out of 10 mice developed detectable tumors 20 days after tumor inoculation (Figure 14A, right panel, red curves). EONY#17 cells grew at intermediate rate giving rise to tumors in all mice 18 days after injection (Figure 14A, blue curve). Twenty days after tumor injection, the tumors were harvested and snap frozen in liquid nitrogen and NY-BR-1 expression in the tumors was analyzed by qRT-PCR and Western blot. NY-BR-1 RNA could be detected in EONY#9 and EONY#17 derived tumors but not in EO771 tumors (Figure 14B). RNA from EONY#9, EONY#17 and EO771 cells isolated on the day of injection of the tumors were included as positive and negative controls, respectively for reference. Unfortunately, NY-BR-1 protein could not be detected in the resected tumors originating from EONY#9 cells (Figure 14C, red line) or EONY#17 cells (Figure 14C, blue line). NY-BR-1 expression in EONY#9 and EONY#17 cell lysates prepared on the day of tumor injection could be confirmed (Figure 14C, green line). However, an indirect evidence of persistent NY-BR-1 protein expression *in vivo* was observed as NY-BR-1 specific T cells were detected in mice bearing NY-BR-1 expressing tumors. This is described in detail in section 5.4.1.

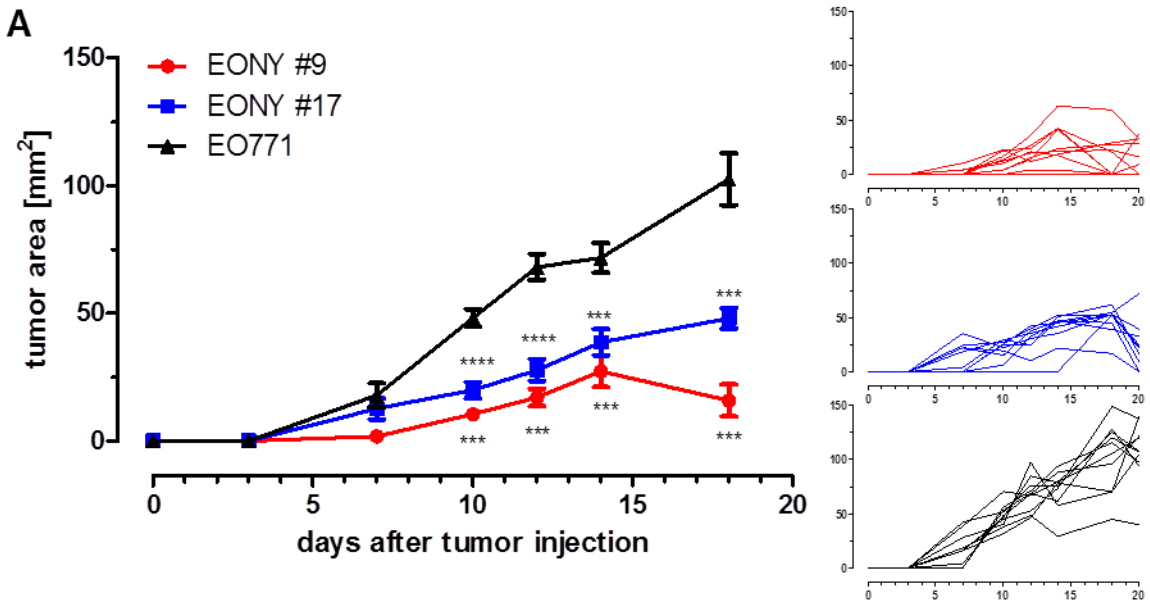

Figure 14. Comparison of tumor growth curves of parental EO771 cells and EONY #9 and EONY #17

HLA-DRB1*0401tg mice were injected *s.c.* on the right flank with 2x105 EO771, EONY #9 or EONY #17 cells and tumor growth was monitored for 20 days post injection. On day 20, tumors were resected and single cell suspensions were prepared by enzymatic digestion. Immune cells were isolated by performing gradient centrifugation using Lympholyte-M and collecting the interphase. The remaining cell pellet containing tumor cells was used for RNA isolation and NY-BR-1 expression was analyzed by qRT-PCR and Western blot. **(A)** Tumor area was calculated from tumor dimensions measured as described earlier. Error bars represent SEM (n=10) and statistical analysis was performed for tumor size of EONY#9 and EONY#17 tumors compared to EO771 tumors. ***, $p<0.001$; ****, $p<0.0001$ (Mann Whitney test). The tumor growth curve of individual mice is depicted on the right.

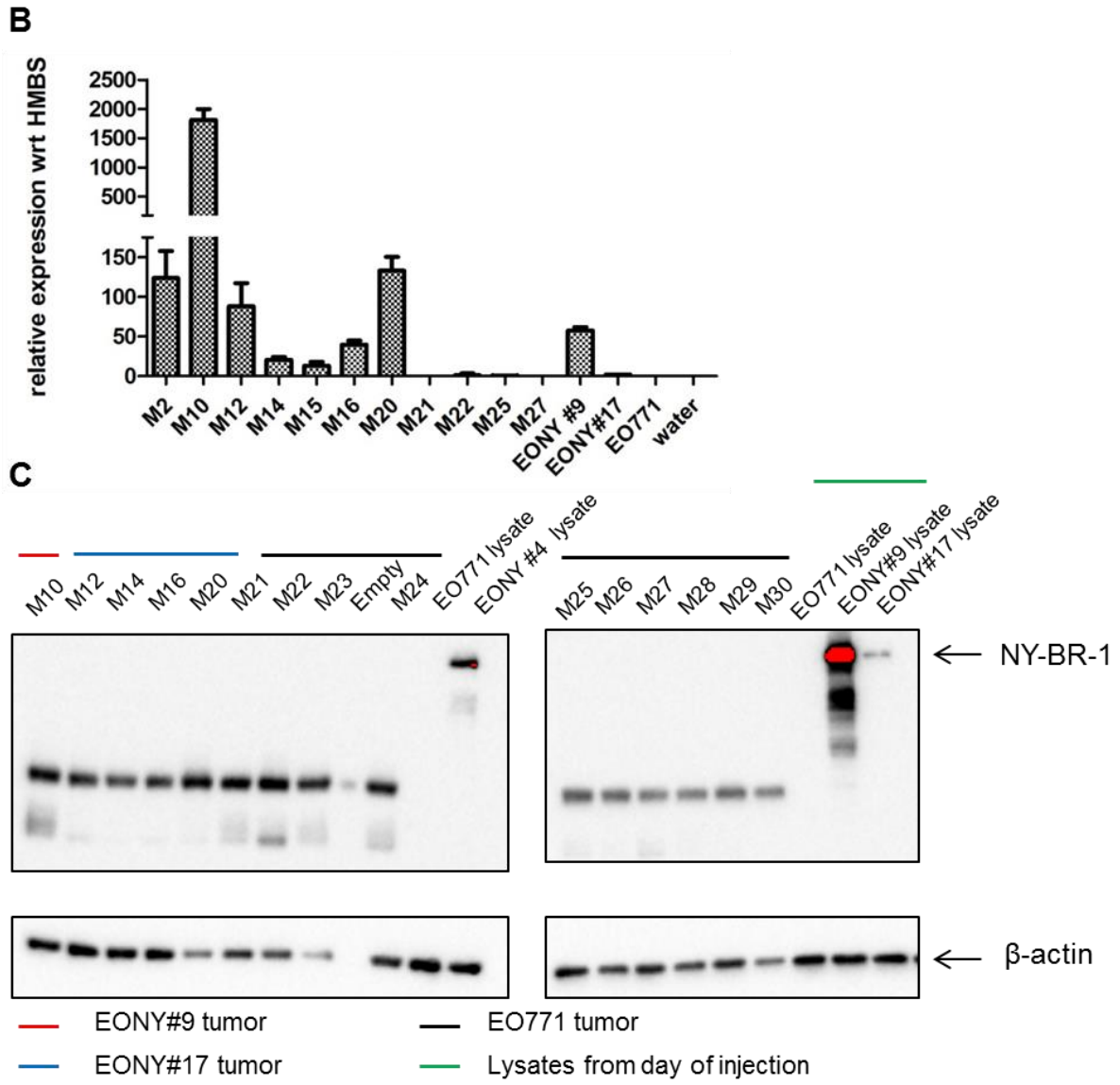

Figure 14 (contd) Comparison of tumor growth curves of parental EO771 cells and EONY #9 and EONY #17

(B) NY-BR-1 expression relative to HMBS is depicted here and each bar represents tumor derived from an individual mouse and error bars represent SEM of triplicates in qRT-PCR. Tumors derived from some mice have not been included here due to poor RNA yield or quality. **(C)** Western blot analyzing the NY-BR-1 expression in tumor lysates and β-actin used as a loading control. The origin of the sample is indicated with different colors (red line, EONY#9 tumors; blue line, EONY#17 tumors; black line, EO771 tumors and green line, cell lysates from the day of injection.

5.1.2.4 Characterization of MHC I knockout cells

Cytotoxic T cells and NK cells are known as major effector populations of the cellular immune system, able to directly kill tumor cells. Whereas CTL mediated target cell recognition depends on cell surface expression of MHC I molecules, NK cells on the contrary attack tumor cells lacking expression of MHC I molecules on the cell surface. Thus, in order to have a tool available enabling investigation of NK cell and CTL responses in our NY-BR-1-expressing tumor model, MHC I knockout tumor cell line was created to delineate the functional contributions of $CD8^+$ T cells and NK cells in the scenario of immunological tumor eradication.

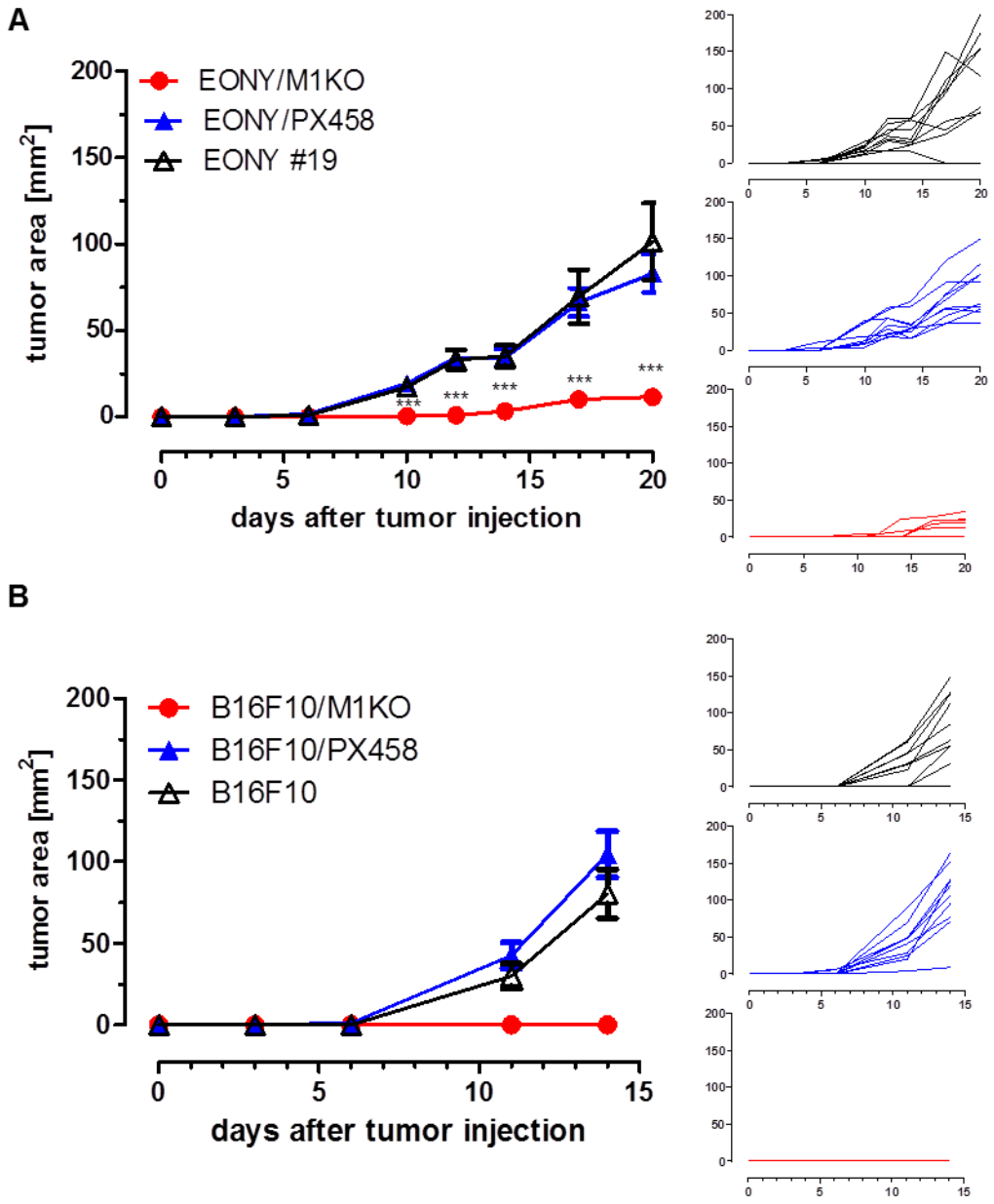

Figure 15. MHC I knockout tumor cell lines fail to grow out *in vivo*

C57BL/6 mice (n=10) were injected *s.c.* on the right flank with $2x10^5$ tumor cells and tumor growth was monitored. Tumor dimensions were measured and tumor area was calculated as described earlier. Mean tumor area of transplanted **(A)** EONY #19, EONY/PX458 or EONY/M1KO tumors or **(B)** B16F10, B16F10/PX458 or B16F10/M1KO tumors is depicted. Error bars represent SEM (n=10) and statistical analysis was performed for tumor size of EONY/M1KO tumors compared to EONY/PX458 tumors. ***, p<0.001; (Mann Whitney test). The tumor growth curve of individual mice is depicted on the right.

MHC I complex is comprised of an α chain and a β_2-microglobulin (β_2m) molecule (Figure 5). The β_2m molecule is critical for the stability of the MHC I complex on the cell surface and defective β_2m expression results in lack of surface expression of MHC I (225). Hence we deleted the β_2m molecule using the CRISPR/Cas9 technology for gene editing, resulting in β_2m deficient clone EONY/M1KO and MHCI expressing control clone EONY/PX458 (222).

In order to characterize the tumor growth kinetics *in vivo*, the growth rate of subcutaneously transplanted EONY-M1KO and B16F10-M1KO tumors (the latter described in Das *et al*. 2017) was compared to those obtained from their respective parental cell lines and EONY/PX458 and B16F10/PX458 tumors. The growth of EONY-M1KO tumors was delayed and the first palpable tumors developed 12 days after inoculation compared to 7 days in the case of EONY/PX458 and EONY #19 derived tumors (Figure 15A, left panel). Notably, only 50% mice injected with EONY-M1KO cells developed tumors which were significantly smaller and the mean tumor area on day 20 was 4 times smaller compared to EONY/PX458 and EONY#19 tumors which had comparable growth kinetics (Figure 15A). Remarkably, B16F10/M1KO cells on the other hand completely failed to give rise to tumors compared to B16F0/PSX458 and B16F10 cells (Figure 15B).Since NK cells can sense the lack of MHC I expression on the cell surface and can reject tumor cells lacking MHC I (226), we tested if the EONY/M1KO and B16F10/M1KO cells were susceptible to NK cell mediated killing. NK cells isolated from splenocytes of C57BL/6 mice were activated with IL-2 and co-cultured with the MHC I knockout cell lines and their corresponding parental cells. NK cell activation was measured in the form of secreted IFNγ in an ELISPOT assay and by ELISA. RMA-S cell which are known NK cell targets (226) were included as a positive control along with the parental RMA cells. The activated NK cells secreted high amount of IFNγ which resulted in partially saturated wells in the ELISPOT assay especially when RMA-S, B16F10/PX458 and B16F10/M1KO were used as targets, which made the quantification of spot number difficult (Figure 16A). Therefore, we attempted to quantify the secreted IFNγ by ELISA. NK cells secreted 140% more IFNγ when stimulated with the MHC I knockout cells compared to the parental cell lines or those transfected with PX458 (Figure 16B). As expected, the MHC I deficient mutant cell line RMA-S was recognized by NK cells resulting in a strong IFNγ response which was 4 fold higher compared to IFNγ secreted in response to wildtype RMA cells (Figure 16B). This confirmed that MHC I knockout cells generated by CRISPR/Cas9 system become NK cell targets and stimulated them to secrete IFNγ. In order to prove that lack of MHC I surface expression also renders these cells more susceptible to NK cell mediate killing we performed CD107a degranulation assay (227). Activated NK cells were incubated with target cells and the extent of degranulation was measured by surface staining for CD107a. Fifty percent more NK cells upregulated CD107a on their cell surface in response to EONY/M1KO cells compared to EONY/PX458 cells (Figure 16C). B16F10/M1KO cells induced degranulation in 1.9 times more NK cells compared to B16F10/PX458 (Figure 16C). Parental B16F10 cells which have been demonstrated to express activating NK cell receptors NKp46 and DNAM-1 (228) were also targets for NK cell mediated cytoxicity as indicated by degranulation of NK cells (Figure 16C). RMA-S cells which were used as positive controls were two times more susceptible to NK cell cytolysis compared to RMA cells (Figure 16C). Since MHC I knockout clones were susceptible to NK cell mediated cytotoxicity; we wanted to investigate if NK cells were the effector population that mediate the rejection of MHC I knockout cell lines *in vivo* after transplantation into C57BL/6 mice. In order to do so we depleted the NK cells in the recipient mice prior to tumor inoculation by using a NK cell depleting antibody (PK136). Figure 17A depicts the scheme of administration of depleting antibody or the corresponding isotype control and of tumor inoculation. Indeed B16F10/M1KO cells could give to tumors in mice which received the NK cell depleting antibody (Figure 17B, closed red circles) as compared to the isotype control (Figure 17B, open red circles). B16F10/PX458 derived tumors also grew at a faster rate in the absence of NK cells (Figure 17B, closed blue triangles) but the difference was not statistically significant when compared to those in mice treated with the isotype control

(Figure 17B, open blue triangles). Thus, we could show that CRISPR/Cas9 system could be successfully utilized to generate MHC I knockout cells which are susceptible to NK cell recognition and killing both *in vitro* and *in vivo*.

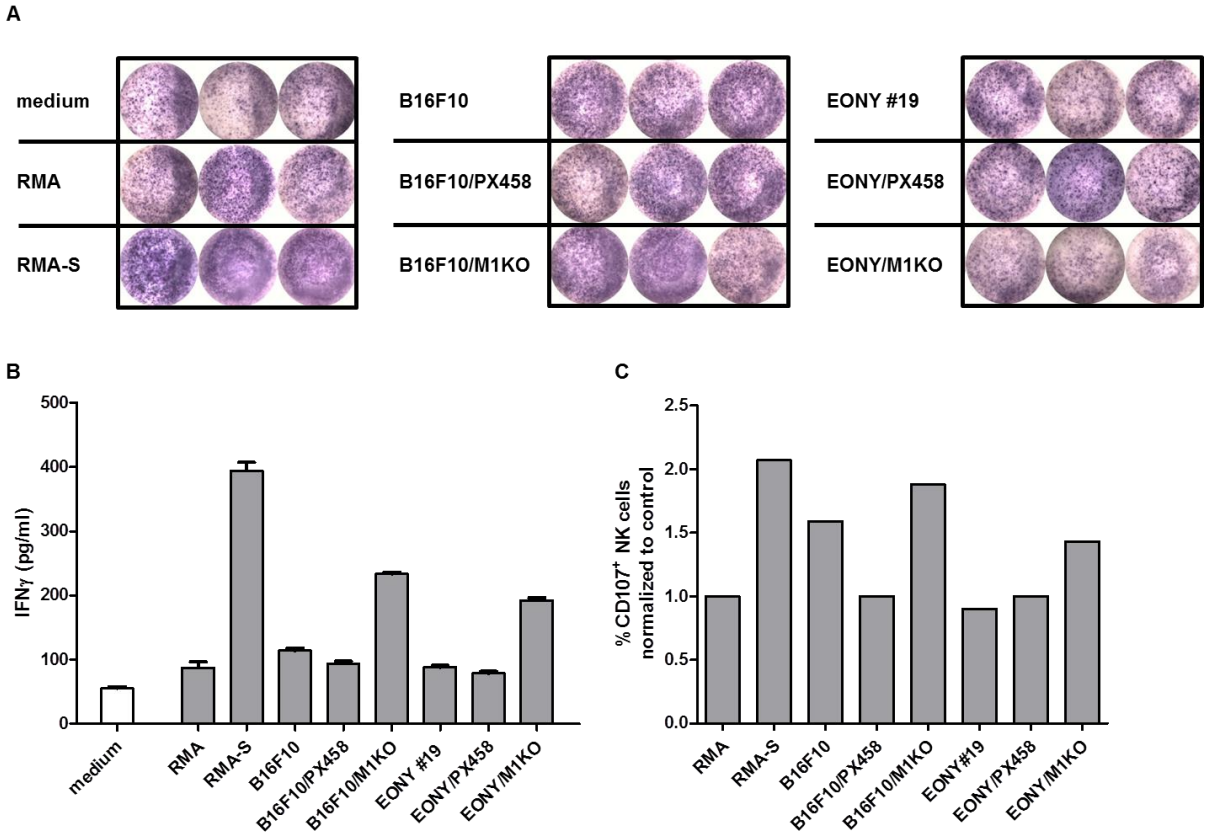

Figure 16. Knockout of MHC I surface expression on tumor cell lines by CRISPR/Cas9 makes them NK cell targets

NK cells were isolated from splenocytes of C57BL/6 mice by negative selection and activated for 7 days with 1700 U/ml IL-2. The activated NK cells were co-cultured with RMA, RMA-S, B16F10, B16F10/PX458, B16F10/M1KO, EONY #19, EONY/PX458 and EONY/M1KO cells and their susceptibility to NK cell recognition and NK cell mediated killing was analyzed. **(A)** $5x10^4$ activated NK cells were co-cultured for 8 hours with $2.5x10^5$ target cells and the IFNγ response was measured by an ELISPOT assay. The representative wells of the ELISPOT plate are depicted but spot number could not be quantified to due to partially or fully saturated wells. **(B)** The secreted IFNγ present in the supernatant of the co-culture was quantified using an IFNγ ELISA and is depicted in pg/ml. Error bars show SEM of duplicates measured by ELISA. **(C)** $5x10^4$ activated NK cells were incubated with target cells at an effector to target ratio of 1:10 for 4 hours in the presence of anti-CD107a antibody and protein transport inhibitor monensin followed by surface staining for CD3 and NK1.1. The percentage of $CD107a^+$ cells among $CD3^-NK1.1^+$ cells normalized to the respective controls is depicted (RMA-S was normalized RMA, B16F10 and B16F10/M1KO were normalized to B16F10/PX458 and EONY #19 and EONY/M1KO were normalized to EONY/PX458).

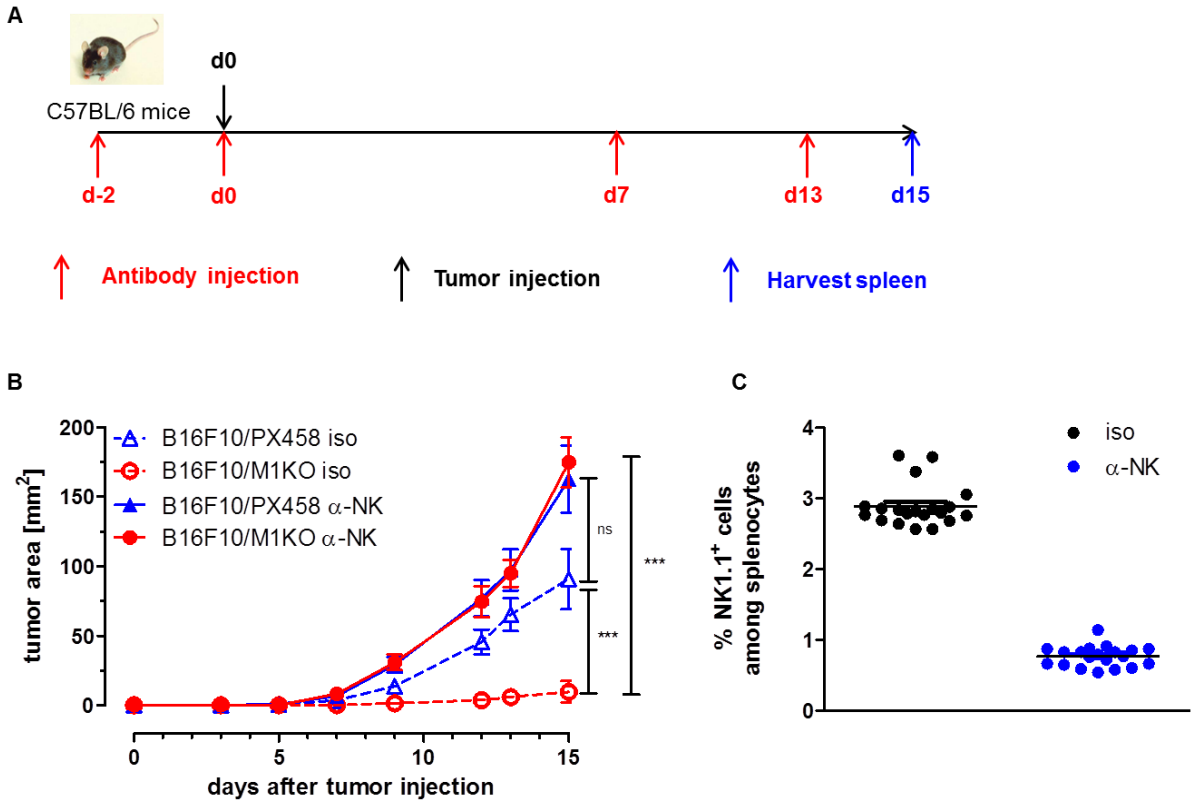

Figure 17. NK cells inhibit the outgrowth of MHC I knockout cells *in vivo*

C57BL/6 mice (n=10) received 100 µg of PK136 antibody (α-NK) or the C1.18.4 isotype control (iso) intraperitoneally and $2x10^5$ B16F10/PX458 or B16F10/M1KO cells were injected *s.c.* on the right flank and tumor growth was monitored. On day 15 after tumor inoculation spleens were harvested and the single cell suspensions were prepared. The depletion of NK cells in the splenocytes was analyzed by flow cytometry after surface staining for NK cell marker NK1.1. **(A)** The time points of administration of depleting antibody (PK136) or the isotype control (C1.18.4) and of tumor transplantation is depicted. **(B)** Tumor area was calculated as described earlier and mean tumor area of the different groups is depicted. Error bars represent SEM (n=10) and statistical analysis was performed using the Mann Whitney test (ns, not significant; ***, p<0.001). **(C)** The frequency of $NK1.1^+$ NK cells among splenocytes of mice which received the isotype control (iso) or the NK cell depleting antibody (α-NK) is depicted.

5.2 Generation of NY-BR-1 specific $CD8^+$ T cells

Among the two HLA-DR3-restricted, NY-BR-1 specific $CD4^+$ T cell epitopes previously identified in our lab (102), immunization of HLA-DR3tg mice with one of the epitopes namely #9017 (Table 11) resulted in the NY-BR-1 specific $CD8^+$ T cell response which suggested that a H2-K^b- or H2-D^b-restricted NY-BR-1 specific $CD8^+$ T cell epitope is contained within this $CD4^+$ T cell epitope. A combination of *in silico* prediction by SYFPEITHI and *in vivo* experiments previously performed in our lab had resulted in the identification of an H2-D^b-restricted NY-BR-1 specific $CD8^+$ T cell epitope (M. Vormehr, unpublished). This epitope is referred to as peptide #6 from now on. The amino acid sequence of the all the epitopes used in this study including the published epitopes are depicted in Table 11.

In order to generate a NY-BR-1 specific $CD8^+$ T cell line specific for this epitope, HLA-DRB1*0301tg or C57BL/6 mice both of which express the murine MHC class I molecules, H2-D^b and H2-K^b were immunized by various methods as described in section 4.2. Spleen

cells were isolated from immunized mice and restimulated by different protocols as reported in the methods section to allow the expansion of NY-BR-1 specific $CD8^+$ T cells.

5.2.1 Peptide immunization results in NY-BR-1 specific T cell response

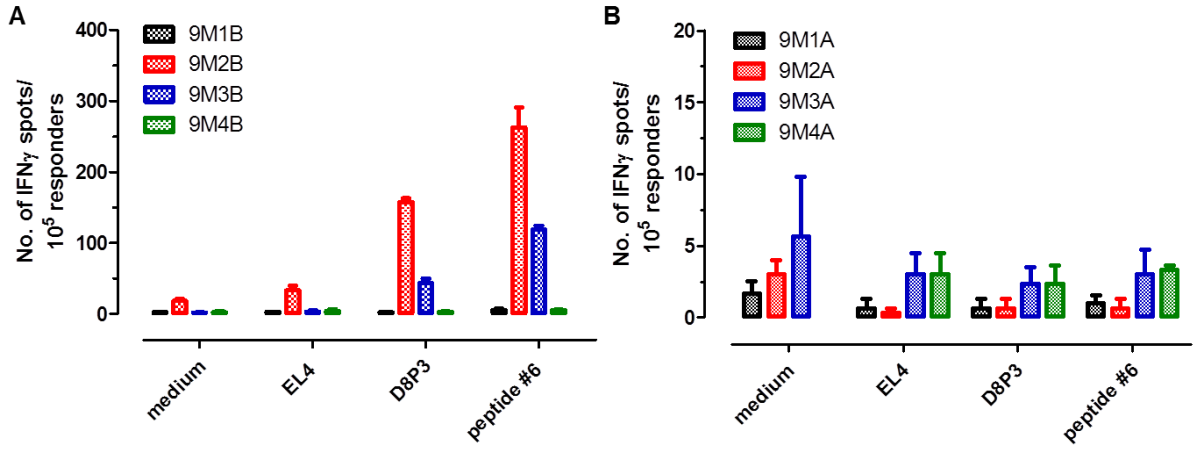

Figure 18. NY-BR-1 specific T cell response generated in HLA-DRB1*0301tg mice by peptide immunization

HLA-DRB1*0301tg mice (n=4) were immunized with 100 µg synthetic peptide #6 and 140 µg helper epitope HBV core #128-140 in IFA, and splenocytes were harvested 14 days post immunization. Harvested splenocytes were restimulated with **(A)** irradiated EL4/NY-BR-1-transfectant clone D8P3 together with syngeneic feeder cells (9M1B, 9M2B, 9M3B and 9M4B) or **(B)** with irradiated syngeneic feeder cells loaded with 100 ng/ml peptide #6 (9M1A, 9M2A, 9M3A and 9M4A). After six rounds of restimulation, the different T cell lines were tested in an ELISPOT assay with $1x10^5$ responder cells, $5x10^4$ target cells per well and peptide concentration of 500 ng/ml. Each bar represents T cell line derived from an individual mouse. Error bars represent SEM of triplicates in IFNγ ELISPOT assay.

Four T cell lines obtained by immunization of 4 HLA-DR3tg mice with synthetic peptide #6 followed by 6 rounds of *in vitro* restimulation with irradiated D8P3 cells and irradiated feeder cells from syngeneic mice were tested for specificity in an ELISPOT assay. Each line was generated from an individual mouse. Lines 9M2B and 9M3B specifically recognized NY-BR-1 expressing D8P3 cells but not the parental EL4 cells (Figure 18A, red and blue bars) as measured by IFNγ spots. The soluble peptide #6 elicited the IFNγ response in the two T cell lines indicating that they were specific for this epitope. The T cell lines 9M1B and 9M4B on the other hand did not show any reactivity against NY-BR-1 expressing transfectants D8P3 or the soluble peptide (Figure 18A, black and green bars). The baseline IFNγ secretion by T cells in the assay medium was negligible in all cell lines except 9M2B. However, the number of IFNγ spots obtained with 9M2B cells co-cultured with the NY-BR-1 positive targets viz. D8P3 cells and the soluble peptide was 8.6 times and 14.35 times, respectively compared to medium alone (Figure 18A). T cells restimulated with peptide #6 pulsed syngeneic feeder cells could not be stimulated by D8P3 cells or soluble peptide#6 to stimulate IFNγ (Figure 18B). The T cell line 9M2B and 9M3B which had a NY-BR-1 specific IFNγ response were further characterized by flow cytometry to quantify the frequency of $CD4^+$ and $CD8^+$ T cells. Unexpectedly, the T cell line 9M2B consisted of 88.8% $CD4^+$ T cells and 2.64% $CD8^+$ T cells whereas in the line 9M3B the proportion of $CD4^+$ and $CD8^+$ T cells was 83.7% and 0.16%, respectively (Figure 18C, left column). Thus, enrichment of the $CD8^+$ T cell was attempted by MACS using magnetic microbeads coupled to anti-CD8 antibody. However, the percentage of $CD8^+$ T cells changed to 2.78% from 2.64% after MACS for line 9M2B (Figure 18C, middle column). The frequency of $CD8^+$ T cells in line 9M3B increased 38 fold from 0.16% to 6.10%

(Figure 18C, middle column) even though it is clear that the enrichment was not effective as the high proportion of $CD4^+$ T cells was still present. The unlabeled fraction (flow through) on the other hand did not have many $CD8^+$ T cells remaining (Fig7C, right column).

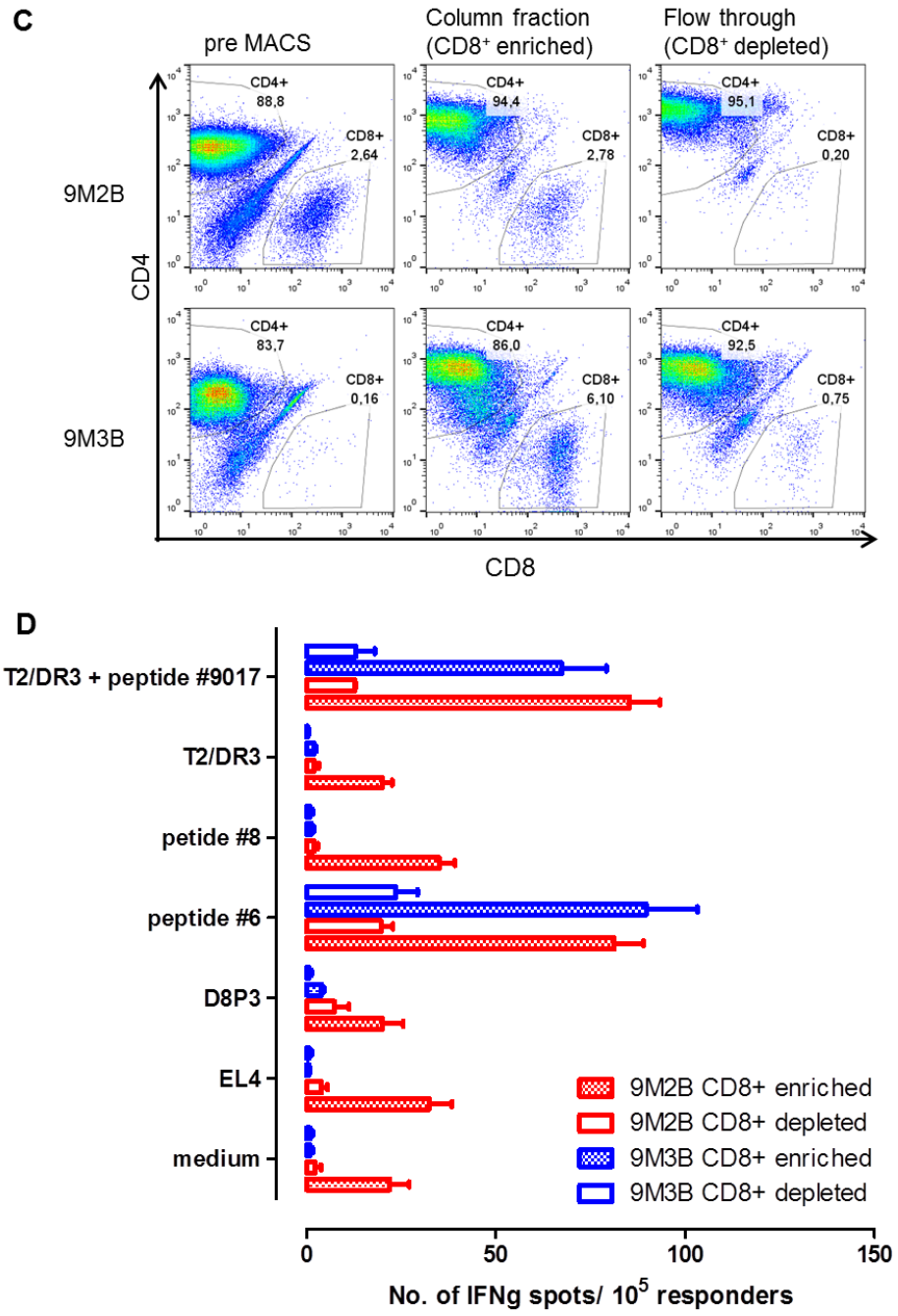

Figure 18 (contd). NY-BR-1 specific T cell response generated by peptide immunization

(C) The proportion of $CD4^+$ and $CD8^+$ T cells in the T cell lines 9M2B and 9M3B before MACs purification, in the column fraction and in the flow through as determined by flow cytometry is depicted as dot plots. The cells were pre-gated on single cells based on forward and side scatter characteristics. **(D)** The $CD8^+$ enriched and $CD8^+$ depleted fractions of the T cell lines 9M2B and 9M3B were separately expanded by restimulation with irradiated D8P3 cells and syngeneic feeder cells. They were tested for their reactivity against NY-BR-1 by using either soluble peptide #6 or D8P3 cells or T2/DR3 cells with soluble peptide #9017 as targets in an ELISPOT assay. Soluble peptide #8, parental EL4 cells or T2/DR3 cells alone were used as controls. $1x10^5$ responder cells and $5x10^4$ target cells per well were used for the ELISPOT assay and the peptide concentration used was 500 ng/ml. Error bars represent SEM of triplicates in IFNγ ELISPOT assay.

The different fractions were separately maintained in culture and restimulated for another two rounds and the cells were tested again in an IFNγ ELISPOT assay. Since the 9 mer peptide #6 sequence is contained within a HLA-DR3 restricted $CD4^+$ T cell epitope designated peptide #9017, it was speculated that the $CD4^+$ T cells present in the T cell lines 9M2B and 9M3B could be specific for this epitope. Thus, T2/DR3 cells pulsed with the synthetic peptide #9017 were used as targets in addition to previously used targets. The $CD8^+$ T cell enriched fraction derived from both cell lines could be activated by soluble peptide #6 and peptide #9017 presented on the HLA-DR3 molecule on the surface of T2/DR3 cells to secreted IFNγ which was measured by ELISPOT assay (Figure 18D). The 9M3B line after enrichment for $CD8^+$ T cells seemed more specific as there was not much baseline IFNγ secretion in the medium control, T2/DR3 cells alone or when an irrelevant H2-D^b restricted epitope namely peptide#8 was added as a soluble peptide (Figure 18D). On the other hand, the $CD8^+$ enriched fraction of line 9M2B had a high IFNγ secretion on its own (medium control), with T2/DR3 cells alone and with peptide #8 which meant the signal to noise ratio was low (Figure 18D). Importantly, D8P3 cells were not recognized by either of the cell lines specifically when compared to the parental EL4 cell line (Figure 18D). The $CD8^+$ depleted fractions had weak positive response to peptide pulsed T2/DR3 cells and soluble peptide #6 and the few number of IFNγ spots meant that they were not functionally active even though they might possess specificity. Further restimulation of these cells was not successful as the cells did not expand and died. Thus it was decided to adopt another immunization approach which is described in the next section.

5.2.2 Adenovirus immunization results in strong NY-BR-1 specific T cell response in C57BL/6 mice

Since C57BL/6 mice express H2-D^b molecule, they should be capable of developing H2-D^b restricted $CD8^+$ T cell response following a successful immunization. Since the peptide immunization resulted in a T cell line predominantly composed of $CD4^+$ T cells, we decided to test the Ad5.NY-BR-1 vector encoding the whole NY-BR-1 protein for immunization and generation of NY-BR-1 specific $CD8^+$ T cell line. Ad5.NY-BR-1 vector is a recombinant adenovirus vector derived from adenovirus serotype 5. The deletion of its E1 genes resulted in a replication deficient vector which can be used for immunization by inserting the antigen of interest into the viral genome (229). It is known to be highly immunogenic and induces strong antigen specific immune responses (229).

Four C57BL/6 mice were immunized with $5x10^8$ pfu Ad.NY-BR-1 and 14 days later the immunized mice were sacrificed and spleens were harvested. Splenocytes isolated from individual mice were cultured separately and restimulated with irradiated D8P3 cells and syngeneic feeder cells as described earlier. After one round of restimulation, the T cell lines obtained were tested for specific recognition of NY-BR-1 expressing D8P3 cells and peptide #6 as targets. T cell line AdNyM1B was strongly reactive to peptide #6 and resulted in saturated ELISPOT wells making it impossible to obtain a spot count and thus this is represented by open bars (Figure 19A). It is noteworthy that this line displayed reactivity to D8P3 cells and resulted in two times more spots compared to medium alone or NY-BR-1 deficient EL4 cells. The absolute spot number was quite low (40 spots for $1x10^5$ cells) even though it appears that recognition of D8P3 was NY-BR-1 specific. Unlike the response to transfectant clone D8P3, the response to soluble peptide #6 resulted in saturated wells (Figure 16A). On the other hand, T cell lines AdNyM2B and AdNyM3B showed a weak IFNγ response against peptide #6 and resulted in an average spot number of 40-50 for $1x10^5$

effector cells (Figure 16A). The line AdNyM4B had barely detectible IFNγ response against peptide #6 (mean spot number = 10). Concavalin A (Con A) which is known to be a mitogen and acts as a strong T cell stimulus resulting in their activation and IFNγ production was used a positive control to assess the potential of the T cell lines to produce IFNγ following activation. The mean spot number obtained after activation with ConA for the cell lines AdNyM2B, AdNyM3B and AdNyM4B was quite low and ranged between 30 and 66. Since the T cell lines were generated from whole splenocytes without any enrichment, it is probable that the frequency of activated antigen specific T cells is too low to result in a strong NY-BR-1-specific IFNγ response.

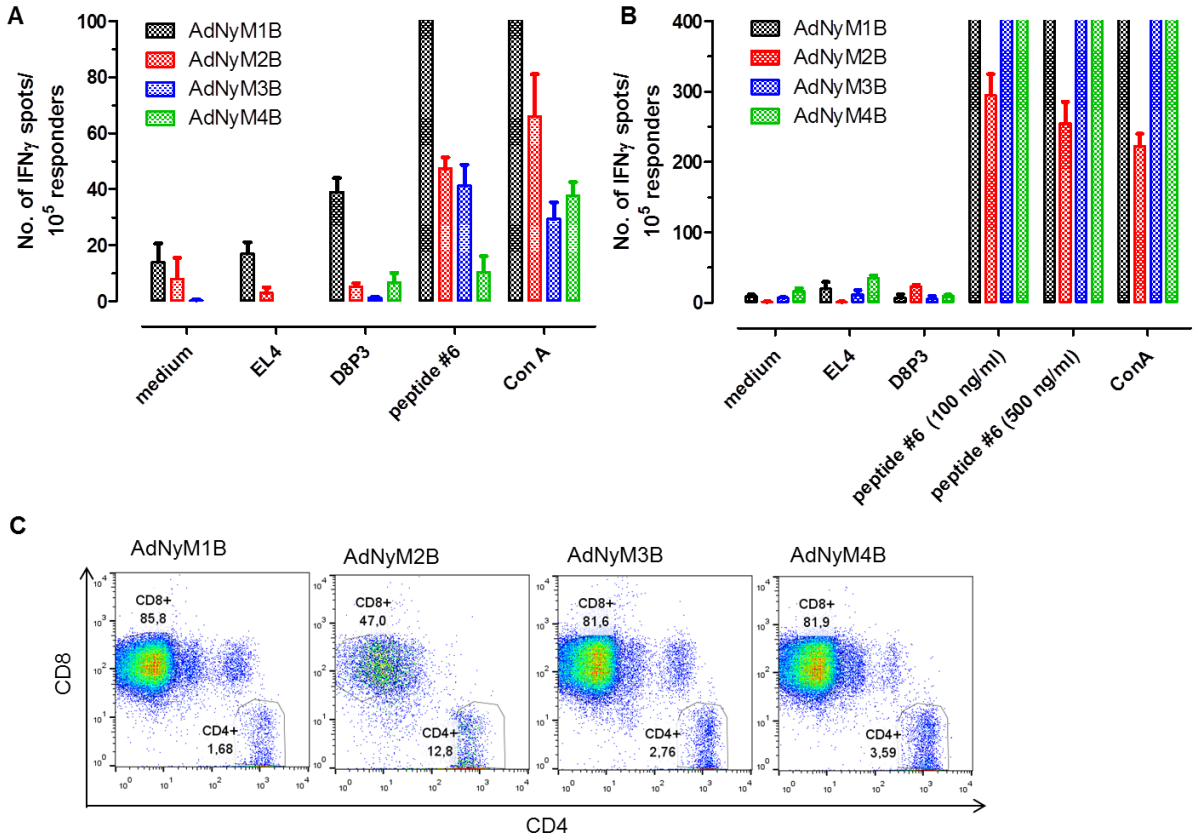

Figure 19. NY-BR-1 specific T cell response generated by immunization with recombinant adenovirus

C57BL/6 mice (n=4) were immunized with 5x10^8 pfu Ad.NY-BR-1 *i.p.* and splenocytes were harvested 14 days post immunization. Harvested splenocytes from individual mice were restimulated with irradiated EL4/NY-BR-1-transfectant clone D8P3 together with syngeneic feeder cells to obtain four T cell lines. These T cell lines were tested for their NY-BR-1 specific response in an IFNγ ELISPOT assay using either peptide #6 in a soluble form or EL4 cells or D8P3 cells as target cells. Concavalin A was used as positive control. The ELISPOT assay was performed after **(A)** 3 or **(B)** 5 rounds of restimulation. 1x10^5 responder cells and 5x10^4 target cells per well were used for the ELISPOT assay and the peptide concentration used was 500 ng/ml in the first ELISPOT **(A)** and either 100 ng/ml or 500 ng/ml in the second ELISPOT **(B)**. Error bars represent SEM of triplicates in IFNγ ELISPOT assay. Oversaturated wells are depicted by out of range bars. **(C)** The dot plots depict the distribution of CD4$^+$ and CD8$^+$ T cells in the different T cell lines. All T cell lines except AdNyM2B have a majority of CD8$^+$ T cells.

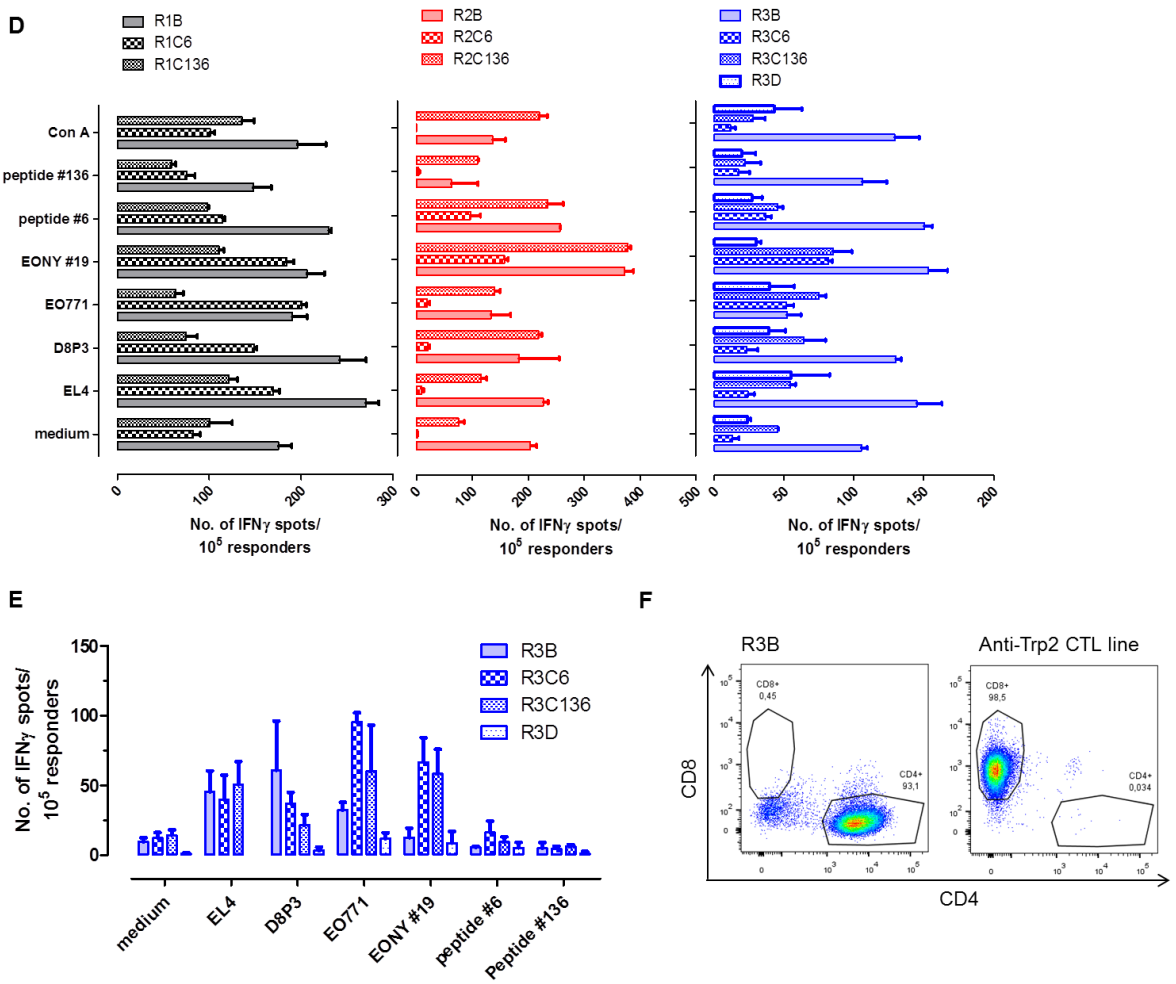

Figure 19 (contd). NY-BR-1 specific T cell response generated by immunization with recombinant adenovirus

C57BL/6 mice (n=3) were immunized with $5x10^8$ pfu Ad.NY-BR-1 *i.p.* and splenocytes were harvested 14 days post immunization. Harvested splenocytes from individual mice were restimulated in various ways to obtain different T cell lines. They were restimulated with either irradiated EL4/NY-BR-1-transfectant clone D8P3 together with syngeneic feeder cells (R1B, R2B and R3B) or with irradiated syngeneic feeder cells loaded with either peptide #6 (R1C6, R2C6 and R3C6) or with peptide #136 (R1C136, R2C136 and R3C136). The splenocytes from one of the mice were also restimulated with irradiated EO771/NY-BR-1-transfectant clone EONY #19 together with syngeneic feeder cells (R3D). **(D)** The various T cell lines thus obtained were tested for their NY-BR-1 specific response in an IFNγ ELISPOT assay using either peptide #6 or peptide #136 in a soluble form. Additionally EL4 cells, D8P3 cells, EO771 cells or EONY #19 cells were used as target cells. Concavalin A was used as positive control. The ELISPOT assay was performed after 3 rounds of restimulation. $1x10^5$ responder cells and $5x10^4$ target cells per well were used for the ELISPOT assay and the peptide concentration used was 100 ng/ml. Error bars represent SEM of triplicates in IFNγ ELISPOT assay. **(E)** Only the T cell lines R3B, R3C6, R3C136 and R3D could be expanded effectively and they were tested again after 9 rounds of restimulation in an ELISPOT assay with similar conditions as described above. **(F)** The best expanding T cell line R3B was analyzed by flow cytometry to check the distribution of $CD4^+$ and $CD8^+$ T cells. The dot plots depict the distribution of $CD4^+$ and $CD8^+$ T cells among single cells. Anti-Trp2 CTL line was used as positive control.

Thus, the assay was repeated after another round of restimulation with D8P3 transfectants, expecting that an additional round of restimulation will allow the expansion of antigen specific T cells and increase their proportion in all the T cell lines. All the T cell lines demonstrated strong reactivity against peptide #6 which resulted in saturation of IFNγ signal but no

recognition of the D8P3 cells was observed (Figure 19B). In order to determine the distribution of $CD8^+$ and $CD4^+$ T cells in the T cell lines they were analyzed by flow cytometry. It was observed that lines AdNyM1B, AdNyM3B and AdNyM4B comprised of over 80% $CD8^+$ T cells among live single cells whereas AdNyM2B consisted of 47% $CD8^+$ T cells (Figure 19C). Thus, immunization with the global NY-BR-1 antigen using the Ad.NY-BR-1 followed by restimulation with irradiated D8P3 cells and feeder cells turned out to be more successful in the generation of NY-BR-1 specific CD8+ T cells. Since the majority of cells were $CD8^+$ T cells, the cells were restimulated further to expand them for subsequent experiments. Unfortunately, the cells did not proliferate further and started to die. Attempts to expand these T cell lines from vials frozen earlier as a backup also failed as the frozen cells did not grow after thawing. This led us to hypothesize that the restimulation protocol might not have been optimal for long term *in vitro* culture of these cells.

Thus, immunization was repeated in three C57BL/6 mice (designated R1, R2 and R3) with Ad.NY-BR-1 in order to evaluate other protocols for restimulation. Splenocytes isolated 14 days after immunization were divided into three fraction for mice R1 and R2 and four fractions for mouse R3 and each fraction was restimulated differently. The first fraction was restimulated with irradiated D8P3 cells in combination with irradiated syngeneic feeder cells as previously described and this is designated by the suffix B (e.g. R1B, R2B and R3B). The other two parts were restimulated with syngeneic splenocytes that were pulsed with the synthetic peptide #6 or peptide #136 followed by irradiation. Peptide #136 is another predicted H2-D^b-restricted epitope derived from NY-BR-1 which is described in more detail in section 5.3.3. These spleen cell lines are indicated with the suffix C6 and C136 respectively (e.g. R1C6 and R1C136). Additionally, some of the splenocytes from mouse R3 were restimulated with the irradiated EONY#19 cells along with irradiated feeder cells and they are called R3D. It was observed that the restimulation with peptide pulsed feeder cells and irradiated EONY#19 cells was not optimal for inducing proliferation of the T cell lines. Nonetheless, an ELISPOT assay was performed with these cells after one round of restimulation to estimate if one of the restimulation methods would result in generation of an NY-BR-1 specific CTL line. R2B cells could specifically recognize the EONY#19 cells compared to parental EO771 cells but not D8P3 cells or the soluble peptide #6 and #136 (Figure 19D). Even though the baseline IFNγ secretion by R2B T cells was quite high, a two fold increase was observed when they were stimulated by EONY#19 cells (Figure 19D). The line R3B also showed a tendency to specifically recognize the EONY#19 cells and the soluble peptide #6 when compared to the EO771 cells or medium only. R3C6 had a weak reactivity towards EONY#19 cells with respect to EO771 cells. Only the cells derived from mouse R3 could be successfully maintained for the next 8 rounds of restimulation to obtain enough cells to repeat an ELISPOT assay with these cell lines. However, none of the T cell lines secreted IFNγ in response to NY-BR-1 transfectant clones or H2-Db restricted NY-BR-1 epitope added in the form of a soluble peptide (Figure 19E). The line R3B which proliferated slightly better than the others was also tested in FACS to test whether they constituted of $CD8^+$ T cells. Surprisingly, this line was entirely composed of $CD4^+$ T cells (Figure 19F). Anti-Trp-2 CTL line was included as a positive control (Figure 19F). The fact that adenovirus immunization does induce a strong NY-BR-1 specific immune response is demonstrated in the next section. However, it seemed that during restimulation $CD4^+$ T cells expand preferentially overgrowing the antigen specific $CD8^+$ T cells. Thus, we thought that enrichment of antigen specific CTLs before *in vitro* expansion would allow us to circumvent this issue. The strategy used is described in the following section.

5.2.3 Identification of new H2-Db restricted NY-BR-1 epitopes

Peptide-MHC multimers are routinely used to identify antigen specific T cells. They were introduced as tetramers comprised of biotinylated HLA-A2 monomers loaded with the peptide and held together by a PE conjugated deglycosylated avidin molecule (230). The antigen specific T cells which express the specific TCR can bind the MHC-peptide complex. Since the MHC multimer is fluorescently labeled, they can be used to sort the specific T cells by flow cytometry. MHC I dextramers are based on a similar principle but are comprised of multiple peptide-MHC I monomers and fluorophores assembled on a dextran backbone thereby being more sensitive and stable. Thus, they could be used to enrich for NY-BR-1 specific CTLs before expansion. However, it is important to choose a strong epitope to synthesize the MHC dextramer to increase the likelihood of isolating high quality T cells. Thus it was decided to test additional H2-D^b-restricted NY-BR-1 epitopes that have been predicted by SYFPEITHI to identify a suitable candidate for generating the dextramer. The details are listed in Table 30.

Table 30. Nomenclature and sequence of predicted H2-D^b-restricted epitopes

MHC RESTRICTION	DESIGNATION IN THESIS	SEQUENCE	POSTION	SYFPEITHI score
H2-D^b	peptide # 3	VYTSNDSYI	25-33	24
H2-D^b	peptide # 6	STIYNNEVL	1241-1249	26
H2-D^b	peptide # 57	KASANDQRF	460-468	24
H2-D^b	peptide # 136	HTHENENYL	1092-1100	24

The binding affinity of the peptide to the corresponding MHC molecule is important for the generation of a high quality dextramer. Thus, the binding affinity of the candidate epitopes for H2-D^b molecule was assessed. As described in the methods section, RMA-S cells which have low MHC I expression due to defective antigen processing machinery, can be loaded externally with peptides which stabilize the MHC molecule on the cell surface. The level of MHC I expression can then serve as an indirect measure of the peptide binding affinity of the corresponding peptide. Thus, RMA-S cells were incubated with different concentrations of the candidate epitopes and the surface MHC I expression was measured by flow cytometry using hybridoma supernatant B22.249 or E3-25 specifically binding to H2-D^b or H2-K^b molecules, respectively. Peptide #6 had the highest binding affinity and could stabilize surface expression of H2-D^b molecules at concentrations as low as 10 ng/ml (Figure 20A). There is a dose dependent effect observed in the peptide binding with increasing peptide concentration (Figure 20A). Peptide #136 displayed weak binding capacity to the H2-D^b molecule whereas peptide #3 and #57 did not manage to stabilize the H2-D^b molecule at the cell surface, even at the highest concentration of 100 µg/ml (Figure 20A). A known H2-D^b-restricted epitope derived from the HPV16 oncoprotein E7 ($E7_{49-57}$) (231); was used as a positive control and interestingly, peptide #6 had a stronger binding affinity compared to it (Figure 20A). To demonstrate that the epitopes are indeed H2-D^b restricted, the surface expression of H2-K^b molecule was also measured following peptide incubation. None of the predicted epitopes bound to the H2-K^b molecule in contrast to the H2-K^b-restricted ovalbumin derived SIINFEKL peptide which served as the positive control (Figure 20B).

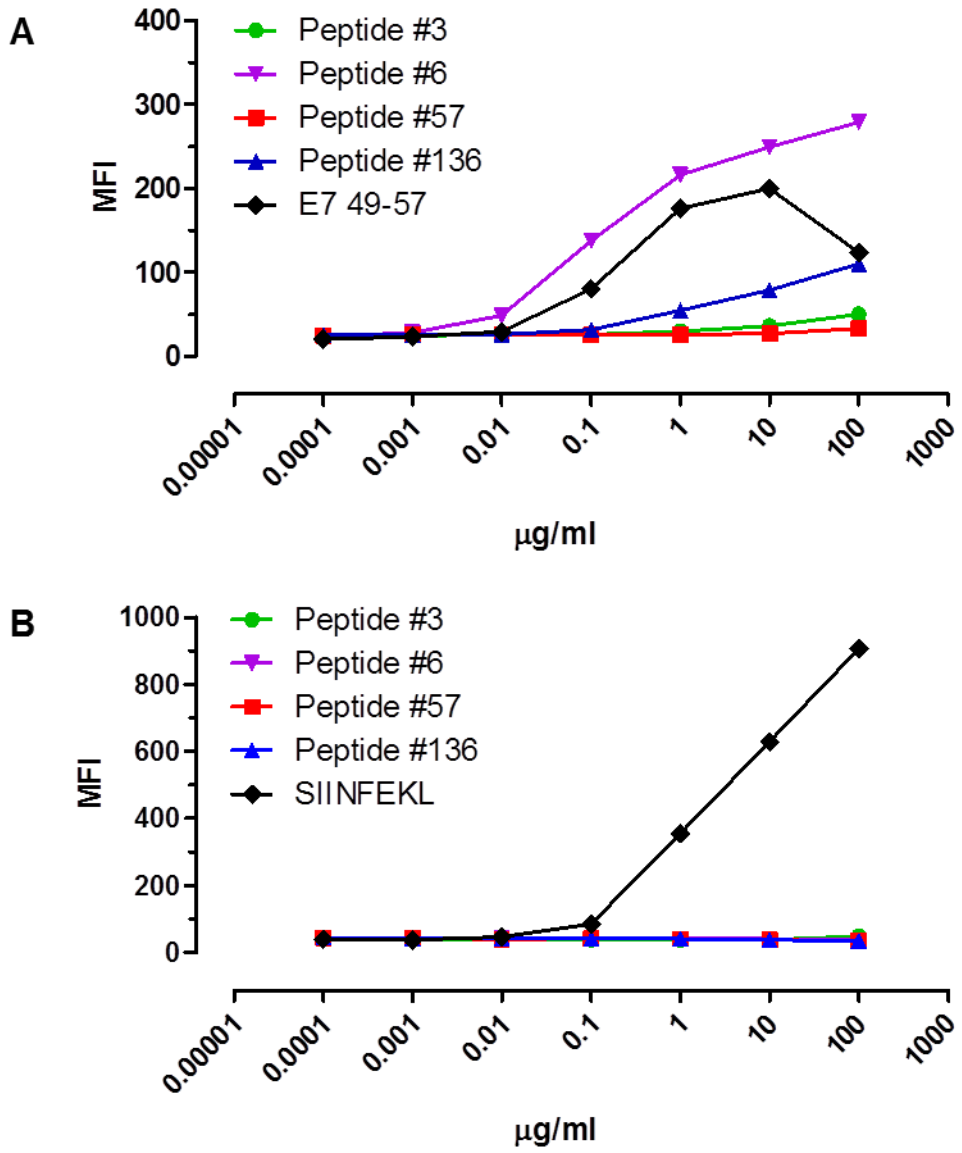

Figure 20. Identification of new H2-D^b restricted NY-BR-1 specific CTL epitopes

Peptide binding assay was performed for the predicted H2-D^b-restricted NY-BR-1 specific CTL epitopes to test their binding affinity to the H2-D^b molecule. Briefly, empty MHC I (H2-D^b/H2-K^b) molecules on the surface of TAP deficient RMA-S cells are stabilized on binding externally added predicted NY-BR-1 epitopes. Surface expression of stabilized MHC I molecules was measured by flow cytometry using **(A)** H2-D^b-specific monoclonal antibody B22.249 or **(B)** H2-K^b-specific monoclonal antibody E3-25 to provide an estimate of peptide binding. The H2-D^b restricted E7 epitope $E7_{49-57}$ and the H2-K^b-restricted OVA epitope SIINFEKL served as positive controls.

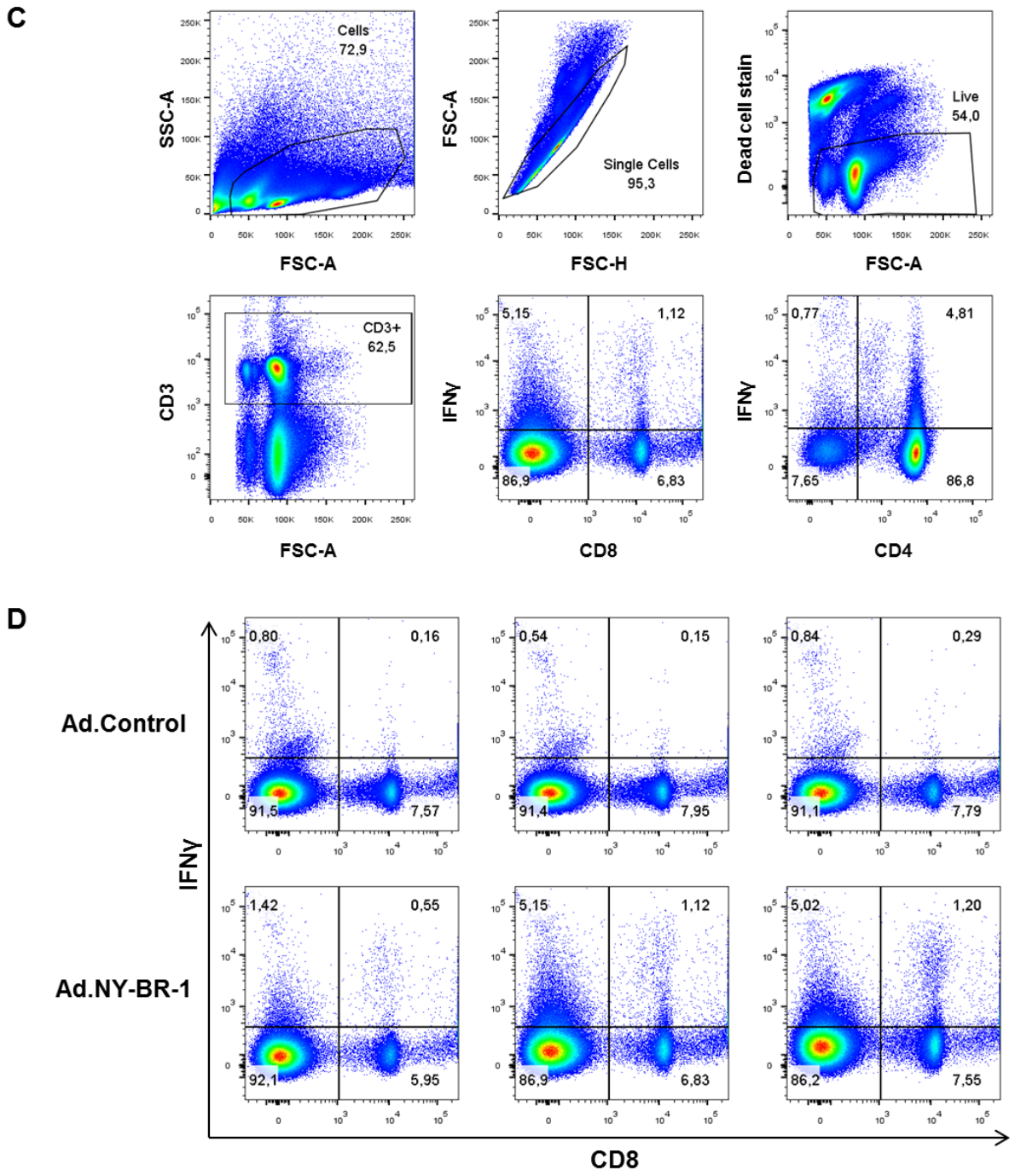

Figure 20 (contd). Identification of new H2-D^{b} restricted NY-BR-1-specific CTL epitopes

HLA-DRB1*0401tg mice were immunized *i.p.* either with 5x10^{8} pfu Ad.NY-BR-1 (n=3) or with 5x10^{8} pfu Ad.Control (n=3) and splenocytes were harvested 14 days post immunization. Harvested splenocytes from individual mice were incubated overnight with various predicted H2-D^{b} restricted NY-BR-1 epitopes (peptide #3, peptide #57 and peptide #136) in the form of synthetic peptides. Secreted IFNγ by activated T cells was measured by IFNγ catch assay and IFNγ ELISPOT assay. **(C)** Gating scheme employed for the IFNγ catch assay is depicted. **(D)** The IFNγ response by CD8^{+} T cells reactive to peptide #6 in mice immunized with Ad.Control (upper panel) or with Ad.NY-BR-1 (lower panel) is shown in a representative dot plot.

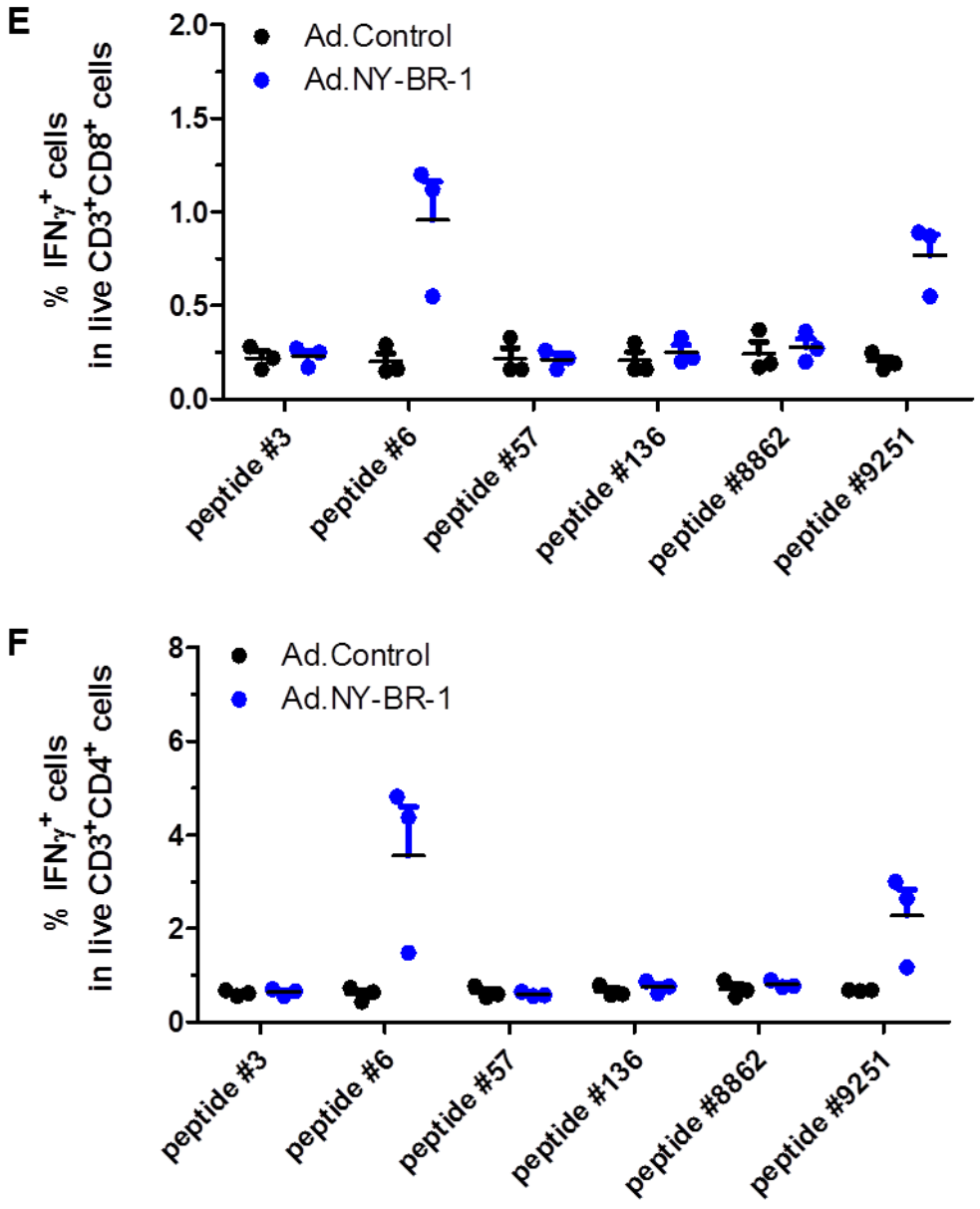

Figure 20 (contd). Identification of new H2-D^b restricted NY-BR-1-specific CTL epitopes

The percentage of IFNγ$^+$ cells among live **(E)** CD3$^+$CD8$^+$ T cells and **(F)** CD3$^+$CD4$^+$ T cells for all the peptides tested is depicted.

Since the tumor model is based on HLA-DR4tg mice it was decided to immunize HLA-DR4tg mice in order to assess if Ad.NY-BR-1 can induce an effective anti-NY-BR-1 immune response in these mice and to ensure that the epitopes that are identified are naturally processed and presented in these mice. Therefore, three HLA-DR4tg mice were immunized with Ad.NY-BR-1 or with Ad.Control and induction of NY-BR-1 specific T cells in the spleens was analyzed by IFNγ catch assay. Briefly, splenocytes from immunized mice were isolated 14 days post immunization and stimulated overnight with the synthetic peptides representing

the predicted epitopes. The activation of the specific T cells was estimated by the secreted IFNγ. In order to analyze the IFNγ secreting T cells, the cells were first gated based on their forward and side scatter characteristics, followed by singlet discrimination. Viable cells were selected by excluding the cells which stained positive for a dye that selectively binds dead cells. The $CD3^+$ T cells were then analyzed for the expression of $CD8^+$ or the $CD4^+$ co-receptor in combination with IFNγ expression. The gating scheme employed is depicted in Figure 20 C. The NY-BR-1 response is quantified by the frequency of $CD3^+CD8^+$ T cells which secrete IFNγ following stimulation by peptide #6 (Figure 20D). The percentage of $CD8^+IFN\gamma^+$ among live $CD3^+$ is clearly enhanced in mice immunized with Ad.NY-BR-1 (Figure 20D, lower row) compared to those in mice which received the control adenovirus (Figure 20D, upper row). Each dot plot represents an individual mouse. Adenovirus immunization successfully induced a strong $CD8^+$ T cell response against the peptide #6 but not against the other predicted H2-Db epitopes viz. peptide #3, #57 and #136 (Figure 20E). HLA-DR4-restricted $CD4^+$ T cell epitopes #8862 and #9251 were included as positive controls and $CD4^+$ T cells specific for peptide #9251 could be detected at a higher frequency following Ad.NY-BR-1 immunization (Figure 20F). Since, ELISPOT is more sensitive in detecting IFNγ response compared to IFNγ catch assay (232, 233); splenocytes from adenovirus immunized HLA-DR4tg mice were also tested in an IFNγ ELISPOT assay to screen for responses against the predicted epitopes. Administration of the control adenovirus did not result in NY-BR-1 specific T cells as expected (Figure 20G) but immunization with NY-BR-1 encoding adenovirus gave rise to T cells which showed strong peptide #6 reactivity in all the mice including the ones which were immunized with a lower dose of adenovirus (Figure 20G, blue bars). Additionally, peptide #57 specific T cells were detected in one mouse immunized with $5x10^8$ pfu virus and in one mouse immunized with 5 times low dose of $1x10^8$ pfu virus (Figure 20G, purple bars). Very weak responses to peptide #3 could be detected as well (Figure 20G, pink bars). The efficacy of the immunization was monitored by using previously validated HLA-DR4 restricted epitopes #9251 and #8862 which resulted in a positive IFNγ signal in the ELISPOT assay (Figure 20H). Since the strength of the responses were generally weaker and not consistent among individual mice when $1x10^8$ pfu virus was used (Figure 20G,H); it was decided to use the manufacturer recommended dose of $5x10^8$ pfu for the subsequent experiments. So far, peptide #6 reactive cells seemed to be the strongest candidate epitope.

Thus peptide #6 qualified as the best candidate for the synthesis of dextramers since adenovirus immunization resulted in T cells specific for this epitope and it had the highest binding affinity to the $H2\text{-}D^b$ molecule. The optimization of dextramer staining and its use for sorting NY-BR-1 specific T cells is described in the following section.

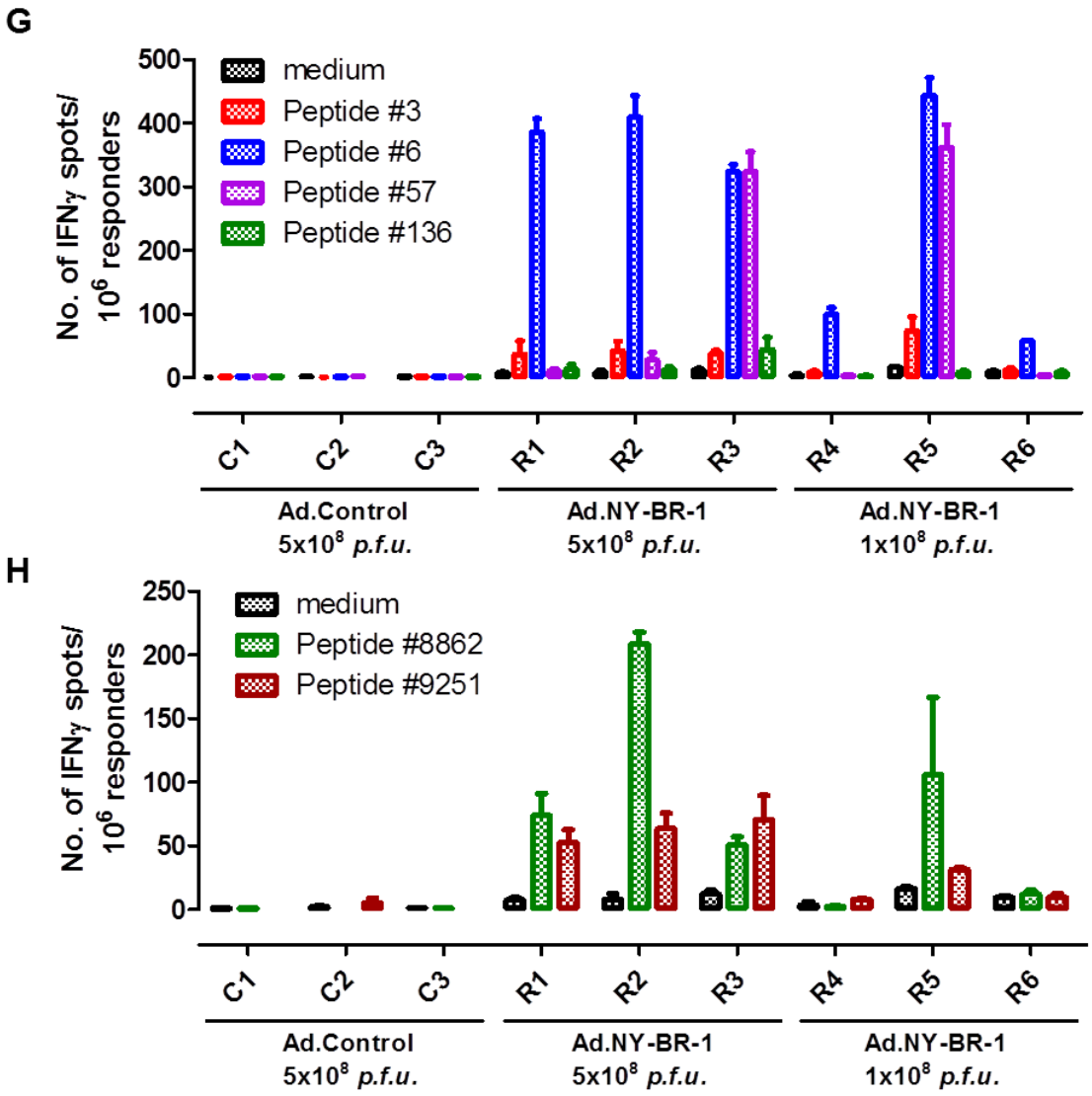

Figure 20 (contd). Identification of new H2-D^b restricted NY-BR-1 epitopes

Induction of NY-BR-1 specific T cell response in HLA-DR4tg following immunization with 5x10^8 or 1x10^8 pfu Ad.NY-BR-1 and 5x10^8 Ad.Control was measured by ELISPOT assay. 1x10^6 splenocytes from the immunized mice were incubated overnight with 2µg/ml peptide in the ELISPOT plate. **(G)** The IFNγ response to the predicted H2-D^b-restricted NY-BR-1 epitopes is depicted as number of spots. **(H)** HLA-DRB1*0401-restricted NY-BR-1 epitopes #8862 and #9251 were also included as a positive control and specific IFNγ responses could be detected against these peptides indicating that the immunization with the Ad.NY-BR-1 was successful. Each bar represents an individual mouse and error bar show SEM.

5.2.4 Optimization of dextramer staining for NY-BR-1 specific CTLs

Adenovirus immunization has resulted in a very strong NY-BR-1 specific T cell response against peptide #6. Thus, splenocytes from adenovirus immunized HLA-DR4tg mice were used to test the binding of the dextramer to peptide #6-specific CTLs. The dextramer was purchased from Immudex and as recommended by them, the cells were incubated with the dextramer diluted 1:6 times followed by surface staining with anti-CD8 and anti-CD4 antibodies. The gating strategy used is depicted (Figure 21A). Briefly, the cells were gated based on their forward and side scatter characteristics followed by exclusion of doublets and dead cells. They were then analyzed for CD8 and dextramer double positive population. In

order to ascertain the specificity of the NY-BR-1 dextramer, a control dextramer loaded with an irrelevant peptide was used at the same dilution. Splenocytes from mice immunized with the control virus (Ad5.Control) which should not contain T cells reactive against peptide #6 served as an additional negative control. As expected, $CD8^+$dextramer$^+$ cells could be detected only in mice immunized with Ad5.NY-BR-1 when the specific dextramer was used and not with the control dextramer (Figure 21B). Surprisingly, both the control and NY-BR-1 specific dextramer did bind a population which was $CD8^-$ irrespective of what virus the mouse was immunized with; indicating that this was unspecific binding (Figure 21B). The cumulative data depicting the frequency of dextramer$^+$ $CD8^+$ cells among live cells from mice immunized with control virus (n=2) and with NY-BR-1 encoding virus (n=3) shows that dextramer positive cells can be induced in all mice by immunization with the Ad5.NY-BR-1 (Figure 21C). $CD14^+$ monocytes are known to unspecifically bind MHC I multimers (234), thus it was decided to use an anti-CD14 antibody to exclude monocytes from analysis of dextramer labeled cells. In order to optimize the amount of dextramer used, dextramer diluted 1:10, 1:25 and 1:100 times was also included. Splenocytes were obtained from mice immunized with Ad.Control or Ad.NY-BR-1 and dextramer staining was performed as described in section 4.2. Following the dextramer staining, anti-CD3 and anti-CD14 antibodies were used in addition to anti-CD8 and anti-CD4 antibodies for surface staining. For quantification of dextramer$^+$ cells, cells were first gated on based on forward and side scatter followed by selection of single and live cells and then $CD3^+CD14^-$ cells were analyzed for the frequency of $CD8^+$dextramer$^+$ cells (Figure 21D). Among $CD3^+CD14^-$ lymphocytes, dextramer$^+$ cells were primarily detected among $CD8^+$ population but not among $CD4^+$ cells (Figure 21D). An exemplary dot plot shows that the percentage of dextramer labeled $CD8^+$ cells among $CD3^+CD14^-$ cells is 0.19% among splenocytes derived from control virus immunized mouse compared to average of 3.5% among splenocytes of mice receiving NY-BR-1 adenovirus when the dextramer was diluted 1:6 for the staining (Figure 21E). The specificity of the dextramer for NY-BR-1 specific T cells was demonstrated by the fact that dextramer positive cells were detected only in Ad.NY-BR-1 immunized mice but not in the Ad.Control immunized mice. Detection of peptide #6 specific T cells by the dextramer was not impaired when dilution of 1:10 was used compared to 1:6 as recommended by the manufacturer (Figure 21F). However, diluting the dextramer 50 or 100 times did reduce the number of NY-BR-1 specific $CD8^+$ T cells which could be successfully detected (Figure 21F). Thus, it was decided to use the dextramer with dilution 1:10 for further experiments.

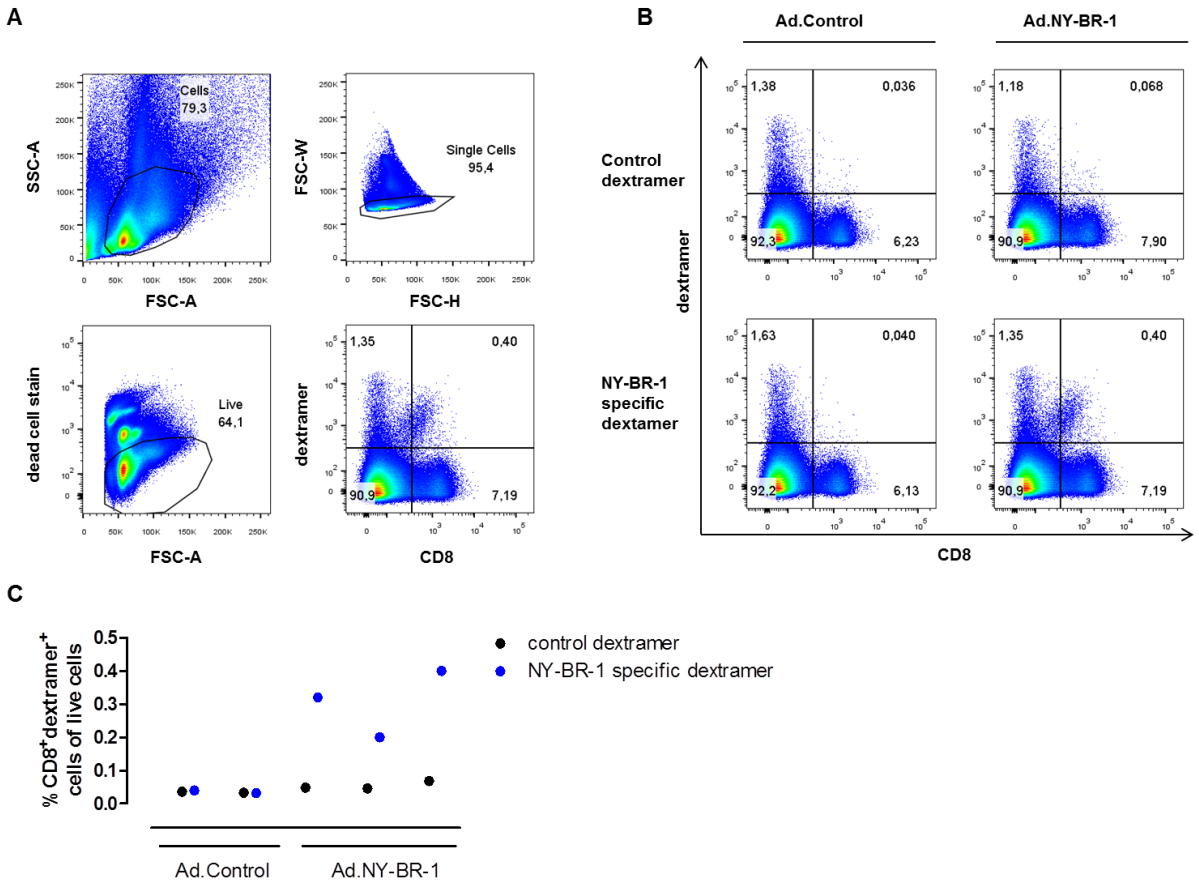

Figure 21. Dextramer staining

Splenocytes harvested from HLA-DR4tg mice received either with $5x10^8$ pfu Ad.NY-BR-1 (n=3) or with $5x10^8$ pfu Ad.Control (n=2) *i.p.* 14 days later splenocytes were isolated and stained with NY-BR-1 specific dextramer or control dextramer followed by surface staining for CD4 and CD8. **(A)** The gating scheme employed for analysis of dextramer$^+$ cells is shown for a representative sample. **(B)** Representative dot plot depicts the proportion of dextramer$^+$CD8$^+$ T cells among live splenocytes from Ad.Control immunized mice (left panel) or from Ad.NY-BR-1 immunized mice (right panel). Each column represents splenocytes from an individual mouse stained with control dextramer (top row) or NY-BR-1 specific dextramer (bottom row) both used at the dilution of 1:6. **(C)** The frequency of CD8$^+$dextramer$^+$ cells of live spleen cells for all mice is plotted.

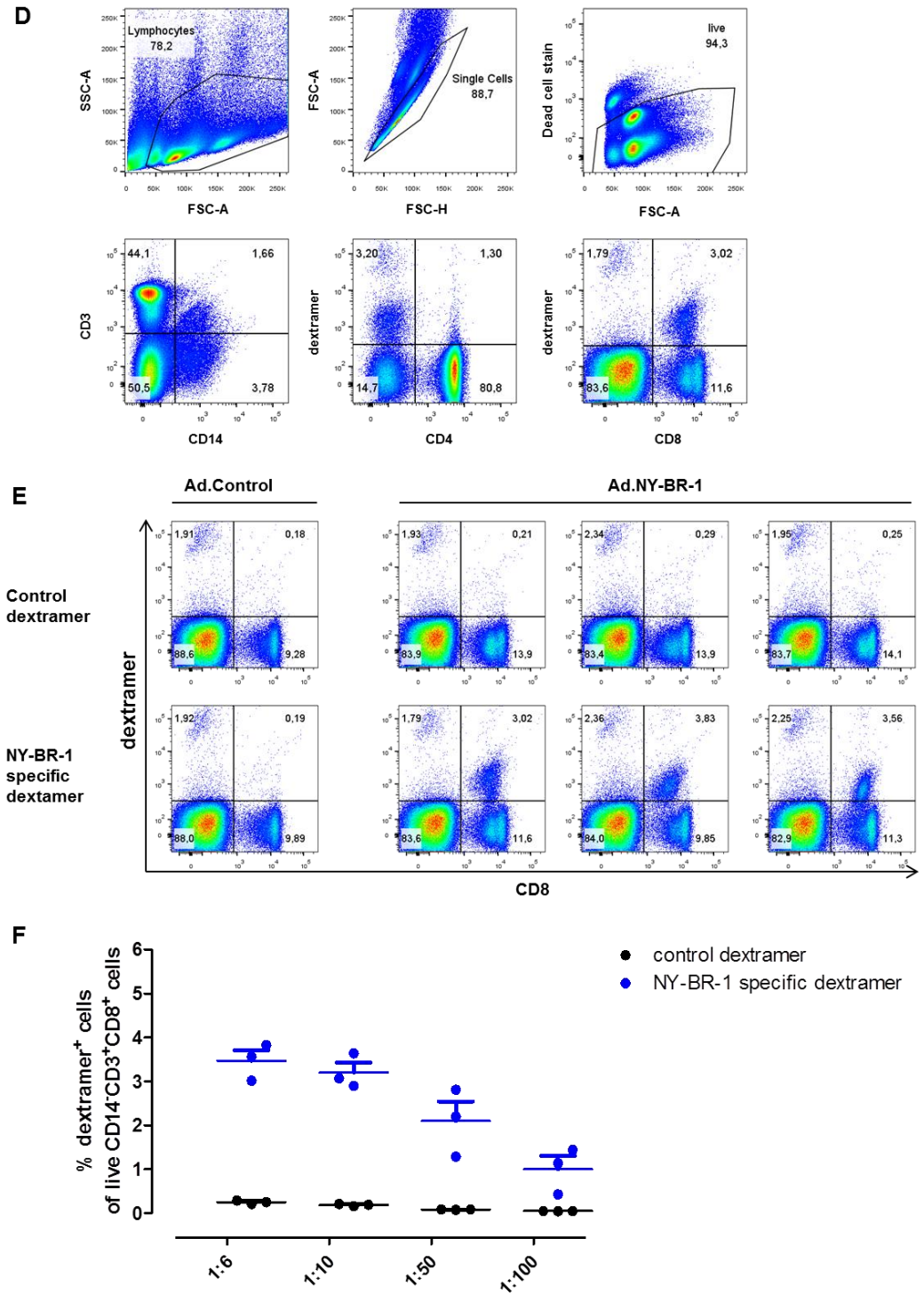

Figure 21 (contd). Dextramer staining

Splenocytes harvested from HLA-DR4tg mice immunized i.p. either with $5x10^8$ pfu Ad.NY-BR-1 (n=3) or with $5x10^8$ pfu Ad.Control (n=3) after 14 days were used for testing dextramer staining. Harvested splenocytes from individual mice were incubated with the NY-BR-1 specific dextramer or control dextramer and counterstained for CD3, CD4, CD8 and CD14. **(D)** The gating scheme of a representative sample is shown. **(E)** Representative dot plot depicts the proprtion of dextramer$^+$CD8$^+$ T cells among live CD14$^-$CD3$^+$ lymphocytes for splenocytes from Ad.Control immunized mice (left panel) or from Ad.NY-BR-1 immunized mice (right panel). Each column represents splenocytes from an individual mouse stained with control dextramer (top row) or NY-BR-1 specific dextramer (bottom row) both used at the dilution of 1:6. **(F)** The frequency of dextramer$^+$ cells of live CD14$^-$CD3$^+$CD8$^+$ cells for all mice and different dilutions of dextramer used is summarized.

5.2.5 Expansion of sorted dextramer$^+$ T cells from immunized mice

The NY-BR-1 specific CD8$^+$ T cells induced by adenovirus immunization could be successfully recognized by H2-D^b dextramer loaded with peptide #6. Previously we observed that CD4$^+$ T cells expanded preferentially over CD8$^+$ T cells when splenocytes obtained from immunized mice were restimulated with irradiated NY-BR-1 expressing target cells (Section 5.2.1). To overcome this issue, we decided to sort the NY-BR-1 specific CD8$^+$ T cells so that if CD4$^+$ T cells expand faster than CD8$^+$ T cells, they cannot overgrow the T cell culture.

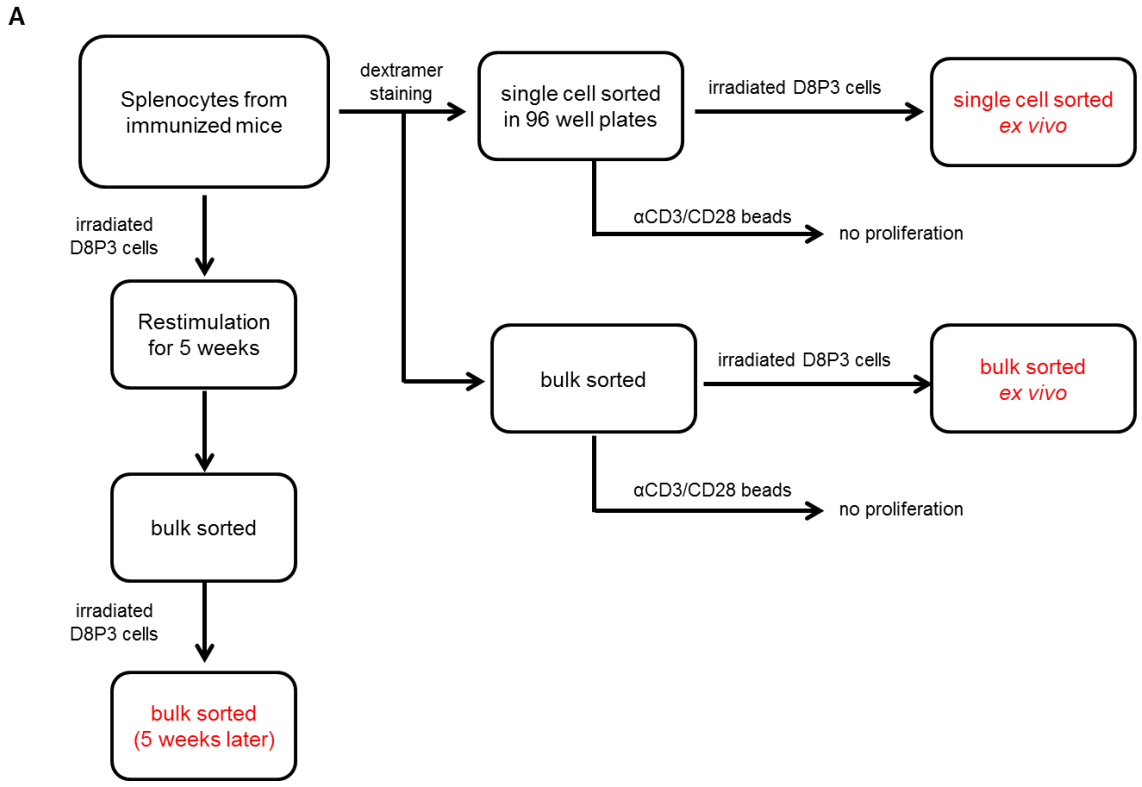

Figure 22. Establishment of NY-BR-1 specific CD8$^+$ T cell lines

(A) The schematic representation of the workflow for establishment of NY-BR-1 specific CD8+ T cell lines by sorting dextramer labeled CD8$^+$ T cells.

Thus, splenocytes from three HLA-DR4tg mice immunized with Ad.NY-BR-1 were isolated and divided into two parts; one part was cultivated *in vitro* with irradiated NY-BR-1 expressing target cells (D8P3) along with feeder cells and the other part was stained with NY-BR-1 specific H2-D^b dextramer. Single dextramer$^+$ cells were sorted into 96 well plate and the remaining dextramer$^+$ cells were sorted as a bulk culture and restimulated with anti-CD3/CD28 T activator beads or irradiated cells as mentioned above. The average frequency of dextramer$^+$ cells detected *ex vivo* was quite low (Figure 22B) compared to previous experiment (Figure 21F). The frequency of dextramer$^+$ cells among CD3$^+$CD14$^-$ splenocytes derived from mouse 1 was 0.15% when labeled with NY-BR-1 specific dextramer compared to 0.20% when labeled with the control dextramer (Figure 22B) indicating that the immunization was not effective in this mouse. Thus the cells from mouse 1 were not sorted for further culture. Adenovirus immunization resulted in the strongest induction of NY-BR-1 specific CD8$^+$ T cells in mouse 3 which had a 5 fold increase in the frequency of NY-BR-1

specific $CD8^+$ T cells (1.02%) compared to background dextramer staining (0.19%). Mouse 2 had an intermediate response resulting in the specific signal of (0.41-0.16 = 0.25%) cells. Single $dextramer^+CD8^+$ T cells from mouse 2 and mouse 3 were sorted into individual wells of 96 well plate to obtain single cell clones and the remaining cells were sorted as bulk culture to generate a T cell line. The sorted cells were then restimulated with Dynabeads® Mouse T-Activator CD3/CD28 or with irradiated target and feeder cells (as described in section 4.2). Since the frequency of dextramer positive cells was quite low, we decided to test the whole splenocytes which were restimulated for 5 rounds to check if there were dextramer positive cells that could be sorted again. Mouse 1 was still negative for dextramer positive cells and the ratio of dextramer positive cells detected by NY-BR-1 specific dextramer to those detected by control dextramer was 4.8 for mouse 2 and 11.5 for mouse 3, respectively (Figure 22C). Thus, these cells were then bulk sorted and cultured *in vitro* by restimulating with irradiated D8P3 and feeder cells. Anti CD3/CD28 beads were not used for restimulation as the T cells from the first round did not proliferate with the beads. The workflow used is detailed in Figure 22A. Only three cell lines could be finally expanded after 12 weeks and were tested for the proportion of $dextramer^+$ T cells and their reactivity to peptide #6 in an ELISPOT assay. The proliferating T cell clone and the cell line bulk sorted *ex vivo* surprisingly comprised of $CD4^+$ $CD8^-$ cells (Figure 22D, top row) whereas T cells obtained from the second bulk sort comprised of 90% $CD8^+CD4^-$ T cells. Interestingly, among T cells bulk sorted *ex vivo*, all $CD8^+$ T cells were strongly dextramer positive but among the cells sorted later, only 68.45 % of $CD8^+$ T cells were labeled by the dextramer and the intensity was in general lower (Figure 22D, bottom row). Since the single cell clone was $CD8^-$, they also did not bind the H2-D^b restricted dextramer (Figure 22D, bottom row). The T cells could be activated by the soluble peptide #6 to secrete IFNγ which was detected by ELISPOT assay. The single cell clone comprising of $CD4^+$ T cells had some unspecific response; however, cells bulk sorted later were strongly reactive with high levels of secreted IFNγ which resulted in saturated wells (Figure 22E). The cells bulk sorted *ex vivo* were also strongly reactive but corresponding to fewer $CD8^+dextramer^+$ T cells, the wells were only partially saturated (Figure 22E). The cells were further expanded and only the *ex vivo* bulk sorted cells could be maintained in culture for 23 weeks. To characterize the T cells, they were tested by FACS for presence of $CD8^+dextramer^+$ cells but unfortunately they could not be detected (Figure 22F). In a functional assay it was shown that the cells were not capable of recognizing specifically the soluble peptide #6 or the NY-BR-1 transfectant clones as no selective IFNγ production was observed (Figure 22G). Thus, immunization with Ad.NY-BR-1 results in NY-BR-1 specific CTLs which can be successfully labeled by H2-D^b dextramers loaded with peptide #6 and can be expanded *in vitro* using irradiated D8P3 cells but not with Dynabeads® Mouse T-Activator CD3/CD28. Functionally active antigen specific $CD8^+$ T cells could be maintained *in vitro* for as long as 12 weeks but prolonged restimulation for 23 weeks was not suitable.

Thus, in the first part of this thesis, a transplantable NY-BR-1 expressing tumor model in HLA-DR4tg mice was established. Additionally, natural processing of a H2-D^b-restricted T cell epitope was confirmed as peptide #6 specific $CD8^+$ T cells were induced following immunization with the global NY-BR-1 antigen. These cells could be successfully labeled by H2-D^b dextramers loaded with the cognate peptide. Unexpectedly, $CD4^+$ T cells preferentially expanded when splenocytes from peptide immunized mice were restimulated *in vitro* with inactivated NY-BR-1 expressing tumor cells in the presence of irradiated feeder cells. Immunization with the Ad.NY-BR-1 on the other hand performed better and NY-BR-1 specific

$CD8^+$ T cells could be expanded especially when they were pre-selected using the dextramers. However, these T cells were not suitable for long term culture.

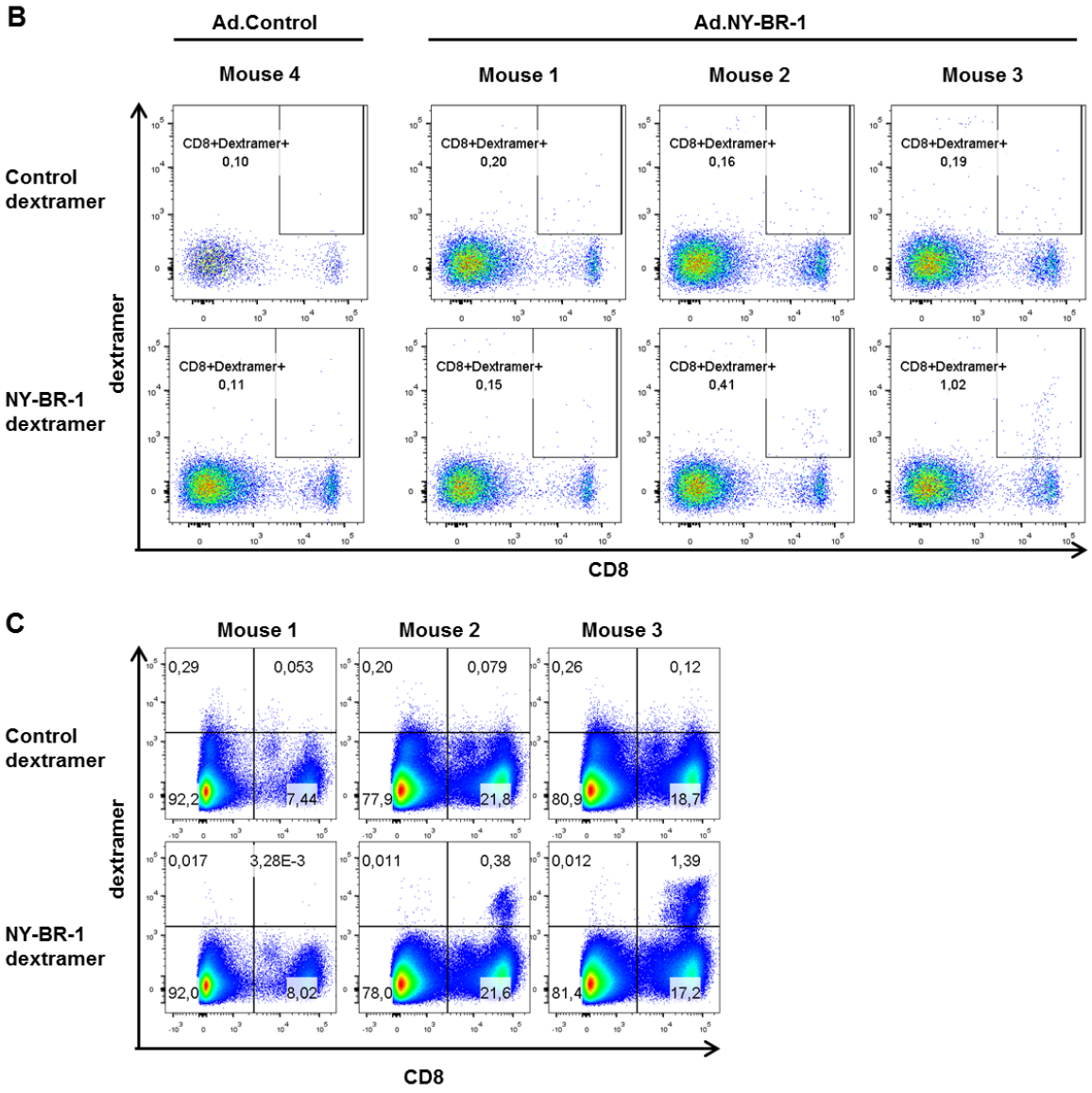

Figure 22 (contd). Establishment of NY-BR-1 specific $CD8^+$ T cell lines

(B) Splenocytes from HLA-DR4tg mice immunized with Ad.Control (n=1) or with Ad.NY-BR-1 (n=3) were stained with dextramer (diluted 1:10) and co-stained for CD14, CD3, CD4 and CD8. The frequency of sorted $CD8^+$dextramer$^+$ T cells within $CD14^-CD3^+$ cells is depicted for cells stained with the control dextramer (upper row) and with the NY-BR-1 dextramer (lower row). **(C)** Dot plots show the proportion of $CD8^+$ T cells among splenocytes restimulated with irradiated D8P3 and feeder cells for 5 weeks, which were labeled by the control dextramer (upper row) or the NY-BR-1 specific dextramer (lower row).

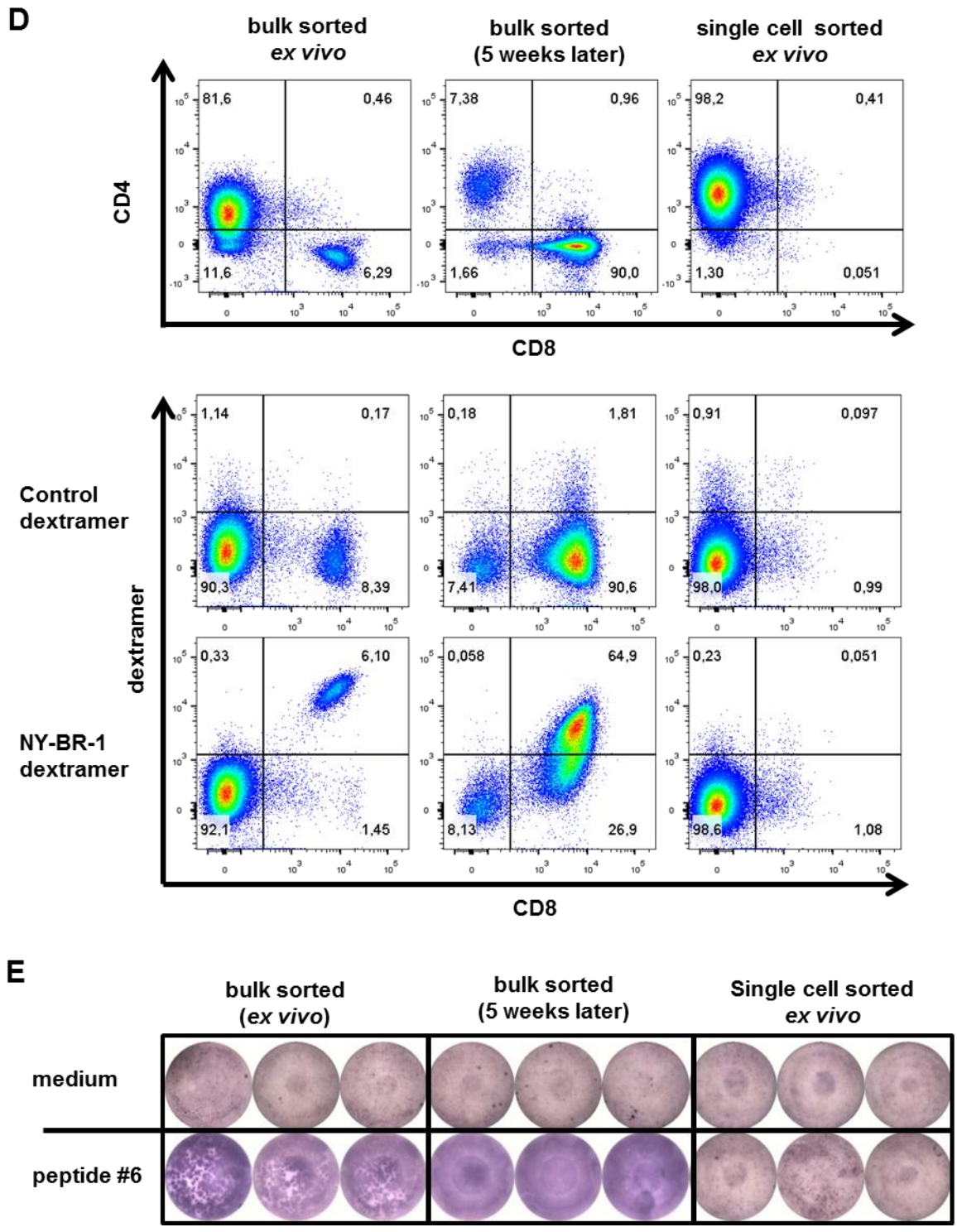

Figure 22 (contd). Establishment of NY-BR-1 specific CD8$^+$ T cell lines

Characterization of the three T cell lines obtained after 12 weeks of *in vitro* expansion of cells sorted for dextramer$^+$CD8$^+$ T cells was done by FACS staining and ELISPOT assay. **(D)** The percentage of CD4$^+$ and CD8$^+$ cells within the CD3$^+$ lymphocyte population is shown (top row). The frequency of dextramer labeled CD8$^+$ T cells among the CD3$^+$ T cells is depicted for the control dextramer (middle row) and the NY-BR-1 dextramer (bottom row). **(E)** The presence of NY-BR-1 specific T cells in the different T cell lines was tested in an IFNγ ELISPOT assay. 1x10^5 effector cells were incubated overnight with 100 ng/ml peptide #6 and the representative wells of the ELISPOT plate are depicted. Spot number not shown as it could not be quantified to due to partially or fully saturated wells.

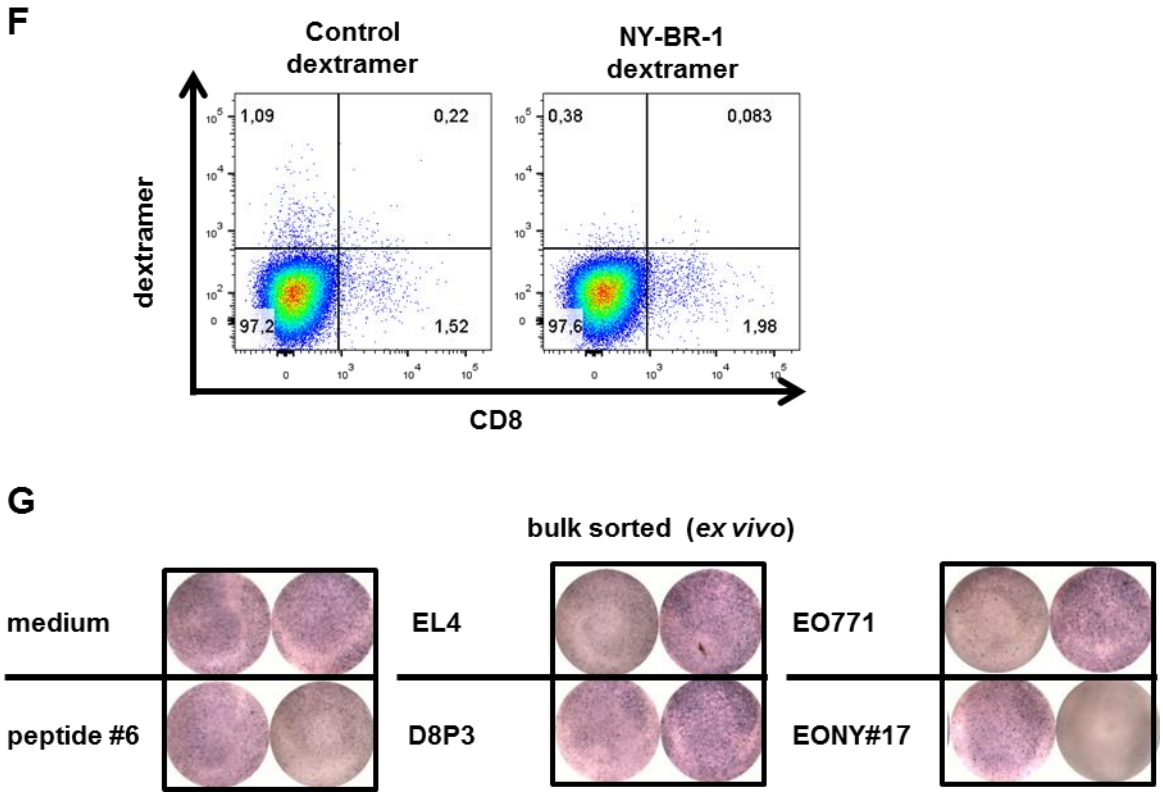

Figure 22 (contd). Establishment of NY-BR-1 specific CD8$^+$ T cell lines

Characterization of the T cell line obtained by bulk sorting of dextramer+ cells *ex vivo* after 23 rounds of restimulatuion by dextramer staining and functional assay. **(F)** The percentage of dextramer$^+$CD8$^+$ cells among all T cells is represented as dot plots. **(G)** The reactivity of the T cells against NY-BR-1 expressing D8P3 and EONY#17 cells was tested in an IFNγ ELISPOT assay. 1x10^5 effector cells were incubated overnight with 5x10^4 target cells or with 100 ng/ml of peptide #6. Parental cell lines, EL4 and EO771 which are devoid of NY-BR-1 expression were included as negative controls. Representative wells of the ELISPOT plate are depicted as spot number could not be determined.

5.3 Characterization of NY-BR-1 specific CD4$^+$ T cell lines

Successful tumor eradication mediated by cytotoxic CD8$^+$ T cells is dependent on CD4$^+$ T cell help. Tumor antigen specific CD4$^+$ T cells have been shown to be important for activation of memory CD8$^+$ T cells to effector cells (212) however there are numerous other mechanisms by which antigen specific CD4$^+$ T cells support successful immunesurveillance. One of them includes the activation of TAMs and inducing tumoricidal phenotype (214) or repolarizing them towards an M1-like phenotype (209). Thus, in the second part of this thesis we investigated whether TAMs would take up NY-BR-1 protein from dying tumor cells and present MHC II restricted T cell epitopes derived thereof to established NY-BR-1 specific CD4$^+$ T cell lines (102). Therefore, HLA-DR4 tetramers loaded with NY-BR-1 specific CD4$^+$ T cell epitopes would serve as an important tool for detection and quantification of NY-BR-1 specific CD4$^+$ T cells infiltrating the tumor. As the name suggests, they are composed of four peptide-MHC monomers and are fluorescently labeled. The class II-associated invariant peptide derived (CLIP) is known to occupy the peptide binding groove of the MHC II molecule before it gets replaced by exogenous peptides within the late endosomes. To test

the specificity of the available HLA-DR3 and HLA-DR4 restricted NY-BR-1 specific $CD4^+$ T cells, peptide-HLA-DR3 and -DR4 tetramers including CLIP loaded tetramers as negative controls were used. Additionally, specificity of $CD4^+$ T cell lines for the epitopes they were raised against was tested in an IFNγ ELISPOT assay. The sequences HLA-DRB1*0301- and HLA-DRB1*0401-restricted NY-BR-1–specific T cell epitopes identified previously (102) and their amino acid positions and the respective SYFPEITHI prediction scores are listed in Table 31. The peptide designations used in the thesis and corresponding published designations are depicted as well. The $CD4^+$ T cell lines are named accordingly. For example, the T cell line specific for peptide #8862 is designated as $CD4^+$ T cell line #8862.

Table 31. NY-BR-1 specific $CD4^+$ T cell epitopes

HLA RESTRICTION	PUBLISHED NAME (Gardyan et al)	DESIGNATION IN THESIS	SEQUENCE	POSTION	SYFPEITHI score
HLA-DRB1*0301	BR1-88	peptide #8797	VVTFLVDRKCQLDVL	88-102	34
HLA-DRB1*0301	BR1-1238	peptide #9017	DVSSTIYNNEVLHQP	1238-1252	15
HLA-DRB1*0301	BR1-1347	peptide #8756	KSKITIDIHFLERKM	1347-1361	22
HLA-DRB1*0401	BR1-537	peptide #8862	AFELKNEQTLRADPM	537-551	26
HLA-DRB1*0401	BR1-1242	peptide #9251	TIYNNEVLHQPLSEA	1242-1256	18

5.3.1 Testing of specificity and affinity of established $CD4^+$ T cell lines

The HLA-DRB1*0301- restricted $CD4^+$ T cell lines #8756 and #8797 and HLA-DRB1*001 restricted $CD4^+$ T cell lines were tested in a functional IFNγ ELISPOT assay. HLA-DR3-restricted T cell lines #8756 and #8797 had lost their specific activity (Figure 20A). HLA-DR4-restricted T cell lines #8862 and #9251 on the other hand could be specifically stimulated by the cognate peptide presented on the DR4 molecule of T2/DR4 cells and not the irrelevant CLIP peptide (Figure 23A). $1x10^5$ T cells stimulated with $5x10^4$ target cells pulsed with 1 µg/ml of the relevant peptide resulted in an average of 921 and 116 IFNγ spots for Th line #8862 and Th line #9251, respectively (Figure 23A). Importantly, the HLA-DR4 restriction was further confirmed by the fact that T2/DR3 cells pulsed with the relevant peptide did not result in IFNγ secretion (Figure 23A). Thus, HLA-DR4- restricted lines were still functional and specific for their respective epitope that they were raised against. The functional avidity of the T cell lines #9251 and 8862 was tested in an ELISPOT assay by titrating the concentration of the cognate peptide loaded on T2/DR4 cells. The highest concentration of peptide used was 1 µg/ml and this resulted in the saturated IFNγ response for both cell lines (Figure 23B). The line #8862 had a higher avidity and $1x10^5$ T cells incubated with $5x10^4$ T2/DR4 cells loaded with 500 ng/ml of relevant peptide resulted in 446 spots whereas line #9251 had only 304 spots at the same peptide concentration. Peptide concentration of 50 ng/ml or lower was not sufficient in stimulating either T cell line (Figure 23B). Additionally, varying numbers of T cells were tested on $5x10^4$ T2/DR4 cells loaded with 1 µg/ml of the cognate peptide. Th line #8862 was more sensitive than line #9251 at cell numbers lower than $2.5x10^4$ cells/well and $1.25x10^4$ #8862 cells resulted in a mean spot number of 417 compared to 316 average spots for equal number of #9251 T cells used (Figure 23B). The dose dependent dilution of secreted IFNγ was observed in both T cell lines however, $1.5x10^3$ cells of Th line #8862 resulted in an average of 150 spots whereas the same number of #9251 cells resulted in barely detectible IFNγ response.

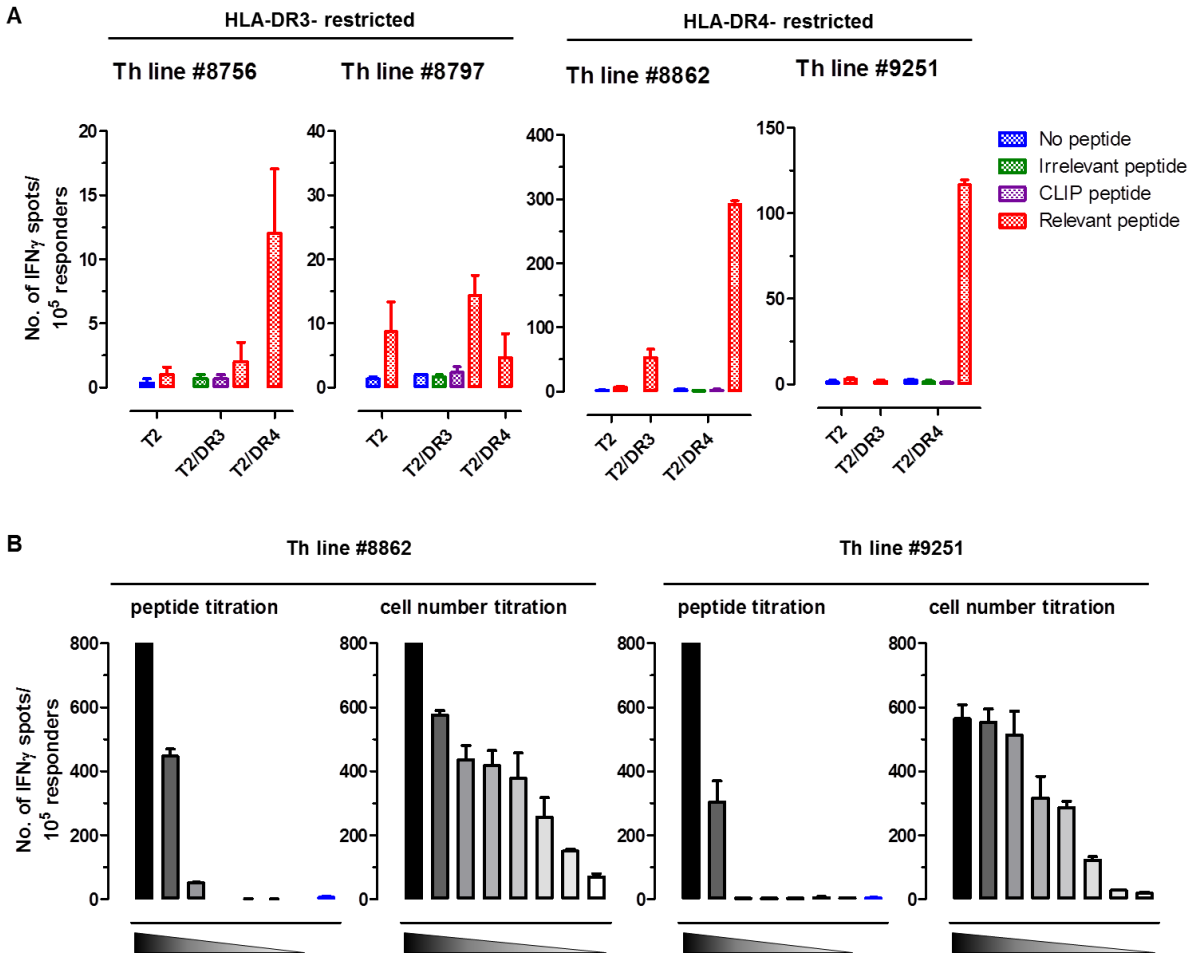

Figure 23. Characterization of NY-BR-1-specific, HLA-DR3- and -DR4-restricted murine CD4$^+$ T cell lines

HLA-DR3- restricted CD4$^+$ T cell lines #8756 and #8797 and HLA-DR4- restricted CD4$^+$ T cell lines #8862 and #9251 were tested for HLA-restriction, specificity and affinity in an ELISPOT assay. **(A)** 1x10^5 effector cells were incubated overnight with 5x10^4 target cells alone or loaded with 1 µg/ml peptide and secreted IFNγ was measured by ELISPOT assay. T2, T2/DR3 or T2/DR4 cells were used as target cells and were loaded with an unmatched 15 mer peptide (irrelevant peptide), CLIP peptide or the matched synthetic peptide (relevant peptide). Bars show mean of IFNγ spots per well and error bars show SEM of triplicates. **(B)** The HLA-DRB1*0401-restricted T cell lines #8862 and #9251 were also tested for their peptide affinity and the minimum number of T cells required for effective recognition in an ELISPOT assay. For testing the peptide affinity, 1x10^5 T cells were incubated with 5x10^4 T2/DR4 cells along with decreasing concentration of the relevant peptide. The peptide was diluted 10 fold starting from 5 µg/ml to 5 pg/ml (gray bars) and 0 pg/ml (blue bars). In order to test the minimum number of T cells required for effective recognition, the number of T cells was decreased by performing 2 fold serial dilution starting with 1x10^5 cells/well to 781 cells/well (indicated by gray). The number of target T2/DR4 cells and peptide concentration used was kept constant at 5x10^4 cells/well and 1 µg/ml, respectively. Bars show mean of IFNγ spots per well and error bars show SEM of triplicates.

5.3.2 Testing of NY-BR-1-specific HLA-DR3 and HLA-DR4 tetramers

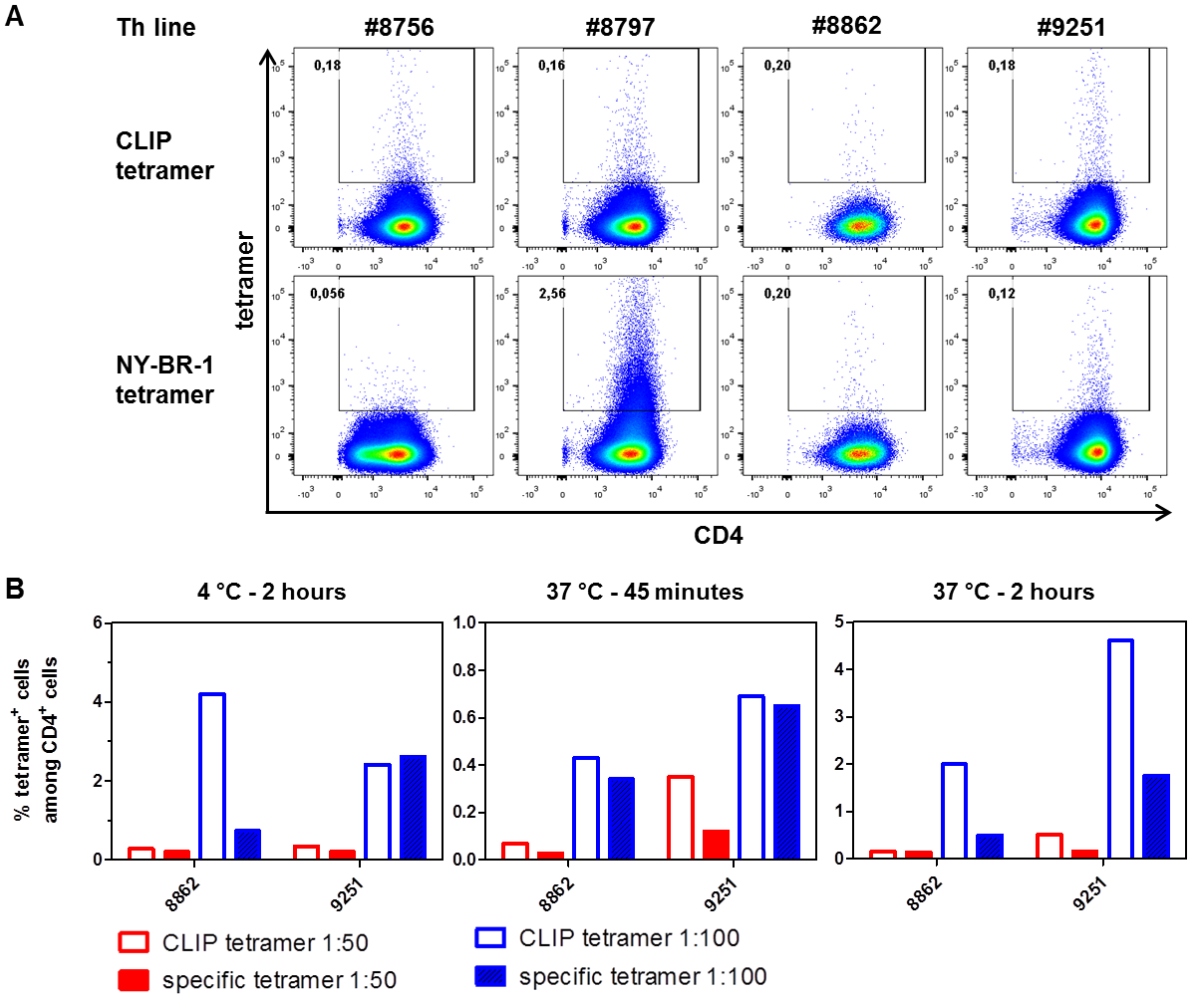

Figure 24. Testing of NY-BR-1-specific HLA-DR3 and HLA-DR4 tetramers

The NY-BR-1 specific CD4$^+$ helper T cell lines were incubated with the tetramer and counterstained with anti-CD4 antibody for FACS analysis. **(A)** T cells were incubated with tetramers (diluted 1:50) at 37°C for 2.5 hours and counterstained with anti-CD4 antibody. Representative dot plot shows the fraction of tetramer positive cells among CD4$^+$ T cells stained with the control CLIP tetramer (top row) or the corresponding NY-BR-1 specific tetramer (bottom row). **(B)** Other staining conditions for the tetramers were tested including incubation at 4°C for 2 hours, 37°C for 45 minutes or 37°C for 2 hours with tetramer dilution of 1:50 or 1:100. This was followed by surface staining with anti-CD4 antibody. Frequency of tetramer labeled cells among CD4$^+$ T cells is depicted as bar graphs.

In order to be able to detect NY-BR-1 specific CD4$^+$ T cells specific for the HLA-DR3- and HLA-DR4-restricted epitopes (described in the previous section) among tumor infiltrating lymphocytes, we wanted to use HLA-DR3 and HLA-DR4 tetramers loaded with NY-BR-1 epitopes which were obtained from NIH tetramer facility. They were tested on the various NY-BR-1 specific CD4$^+$ T cell lines available to test their specificity and binding capacity and to optimize the staining protocol. Thus, the CD4$^+$ T cells were incubated with the specific tetramer diluted 1:50 along with anti-CD4 antibody to evaluate the presence of antigen specific T cells. Only the T cell line #8797 was labeled by the specific tetramer and not by the unspecific HLA-DR3 tetramer loaded with the CLIP peptide (Figure 24A). All the remaining T cell lines did not bind the specific tetramer at a rate higher than the CLIP-loaded tetramer (Figure 24B). Since the HLA-DR3-restricted T cell lines did not contain functional CD4$^+$ T

cells which could be activated by the cognate peptide present on the context of HLA-DR3 (Figure 23A) and did not expand effectively *in vitro*, the HLA-DR4-restricted $CD4^+$ T cell lines were used for further optimization of the tetramer staining. Tetramer binding did not improve when they were incubated at 4 °C for 2 hour, or 37 °C for 45 minutes or for 2 hours (Figure 24B).

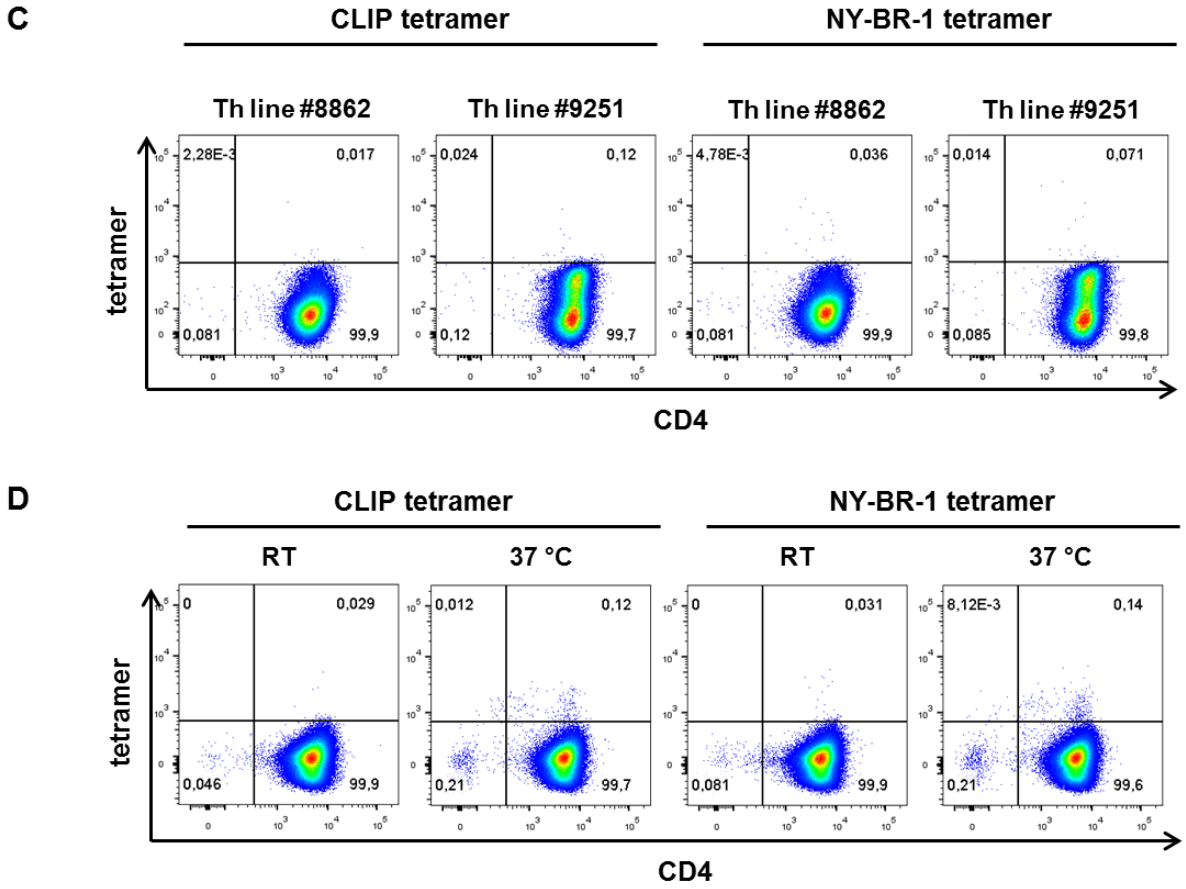

Figure 24 (contd.) Testing of NY-BR-1-specific HLA-DR3 and HLA-DR4 tetramers

HLA-DR4 tetramer loaded with the peptide #9251 (from Immunitrack) was tested for their binding to Th line #9251. **(C)** $1x10^6$ cells were incubated with the CLIP tetramer or the NY-BR-1 specific tetramer diluted 1:100 at room temperature for 1 hour followed by surface staining with anti-CD4 antibody for 45 minutes at 4 °C. Fraction of tetramer labeled $CD4^+$ T cells present in the T cell line #9251 or #8862 is depicted as dot plots. **(D)** Percentage of tetramer bound $CD4^+$ T cells in the T cell line #9251 after incubation with tetramer (diluted 1:10) in the presence of 5 nM dasatinib either at room temperature (RT) or at 37 °C for 1.5 hours is depicted.

Additionally, HLA-DR4 tetramer loaded with peptide #9251 kindly provided by Immunitrack was tested at room temperature (dilution 1:100) followed by surface staining of CD4 molecules. Th line #8862 was included as a biological negative control. There was no specific tetramer staining observed (Figure 24C). Dasatinib is a protein tyrosine kinase inhibitor which is known to stabilize the TCR on the cell surface following TCR engagement and has been demonstrated to enhance tetramer binding to TCR (235). Thus, the $CD4^+$ T cell line #9251 was incubated with the tetramer in the presence of 5 nM Dasatinib for 1.5 hours at room temperature or at 37°C, followed by surface staining. The co-incubation with Dasatinib failed to enhance binding of the tetramer to the TCR of $CD4^+$ T cell line #9251 irrespective of the temperature of incubation (Figure 24D).

5.4 Interaction between NY-BR-1 expressing tumors and the immune system

5.4.1 Analysis of NY-BR-1 specific immune response in spleens of tumor bearing mice

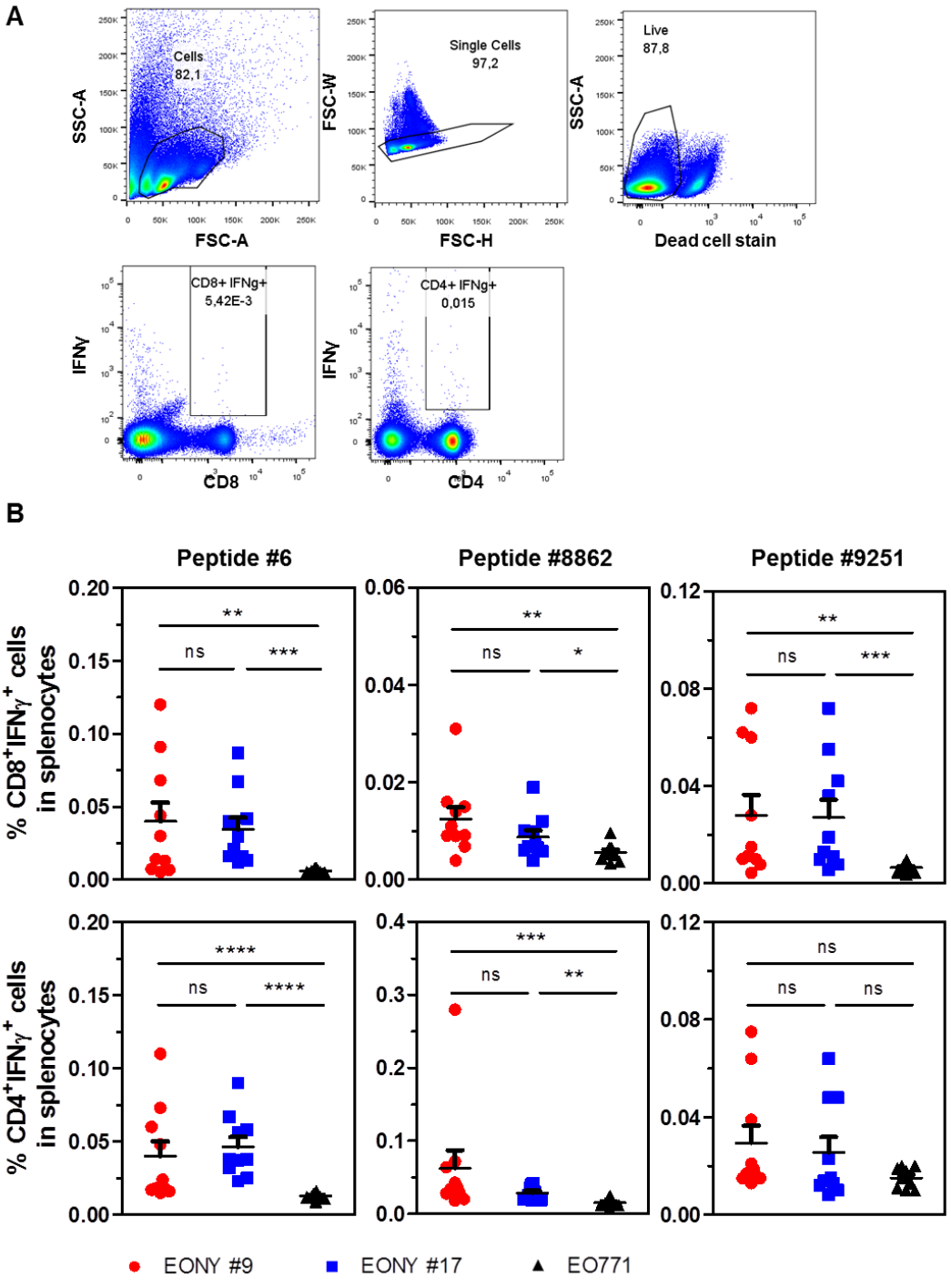

Figure 25. NY-BR-1 specific $CD8^+$ and $CD4^+$ T cells are induced after EONY tumor injection

HLA-DR4tg mice (n=10) were injected with $2x10^5$ EO771 cells, EONY#9 cells or EONY#17 cells *s.c.* and the splenocytes were isolated from the tumor bearing mice after 20 days and incubated with various NY-BR-1 epitopes. The activation of NY-BR-1 specific T cells in response to the peptides was detected by IFNγ catch assay. **(A)** Gating scheme for analysis of IFNγ secreting cells among splenocytes. **(B)** The percentage of $IFN\gamma^+CD8^+$ (upper row) and $IFN\gamma^+CD4^+$ cells (lower row) among splenocytes is shown as dot plots. (Mann Whitney test, * p≤ 0.05; ** p≤0.01; *** p≤0.001; **** p≤0.0001).

As mentioned earlier, NY-BR-1 could act as a xeno-antigen in HLA-DR4tg mice resulting in an anti-NY-BR-1 immune response. This might explain why EONY #9 and EONY#17 cells gave rise to tumors at a slower rate compared to the parental EO771 cells (Section 5.1.2.3, Figure 14A). In order to detect NY-BR-1 specific immune responses in mice transplanted with NY-BR-1 expressing tumors, splenocytes were isolated from tumor bearing mice and NY-BR-1 specific $CD4^+$ and $CD8^+$ T cells which were activated to secreted IFNγ in response to soluble peptides representing NY-BR-1 epitopes were detected using IFNγ catch assay. Exemplary gating scheme is depicted in Figure 25A. IFNγ secreting $CD4^+$ and $CD8^+$ T cells could be detected in mice bearing EONY#9 and EONY#17 tumors compared to those bearing EO771 tumor (Figure 25B) at significantly higher frequencies suggesting that NY-BR-1 expression in tumors is maintained and elicits an NY-BR-1 specific T cell response. The mean frequency of $CD8^+$ T cells specific for H2-D^b restricted NY-BR-1 epitope peptide #6 among splenocytes was 0.044% and 0.034% in mice transplanted with EONY#9 and EONY#17 cells, respectively compared to significantly lower mean frequency of 0.00625% in mice bearing EO771 tumors (Figure 25B). Besides $CD8^+$ T cells, NY-BR-1 specific $CD4^+$ T cells were also induced in mice which had NY-BR-1 expressing tumors. In mice bearing EONY#9 tumors, 0.064 % and 0.0294 % of splenocytes comprised of HLA-DR4-restricted $CD4^+$ T cells specific for peptide #8862 and peptide #9251, respectively whereas in mice transplanted with EONY#17 tumors the frequencies were 0.0287% and 0.023%, respectively. In contrast, the frequency of $CD4^+$ T cells reactive to peptide#8862 and peptide #9251 were 0.00726% and 0.015% in mice with parental EO771 tumors lacking NY-BR-1 expression (Figure 25B). Surprisingly, H2-D^b-restricted $CD8^+$ T cell epitope peptide #6 also activated $CD4^+$ T cells to secrete IFNγ and HLA-DR4- restricted $CD4^+$ T cell epitopes, peptide #8862 and #9251 induced IFNγ response from $CD8^+$ T cells when supplied as soluble peptides (Figure 25B). This cross-activation was significantly stronger in mice with EONY#9 or EONY#17 derived tumors compared to those with EO771 derived tumors (Figure 25B).

5.4.2 Characterization of tumor infiltrating leukocytes

We could detect NY-BR-1 specific $CD4^+$ and $CD8^+$ T cells in the spleens of mice transplanted with NY-BR-1 expressing tumors (Figure 25B). Therefore we wanted to investigate whether T cells and macrophages infiltrate the tumors as well. Tumors were resected 20 days after inoculation and a single cell suspension was obtained by applying a combination of mechanical disruption and enzymatic digestion. The leukocyte fraction was then enriched by using Ficoll density gradient centrifugation, followed by staining for surface markers. The gating scheme employed is shown in Figure 26A. Briefly, cells were gated based on their forward and side scatter characteristics followed by exclusion of doublets. The dead cells were then excluded based on dead cell stain followed by gating on $CD45^+$ cells to include all leukocytes. $CD45^+$ cells were then characterized as $CD4^+$ T cells, $CD8^+$ T cells and $CD11b^+F4/80^+$ macrophages. The proportion of $CD4^+$ T cells among $CD45^+$ cells infiltrating EONY#9 and EONY#17 tumors was 13% and 14%, respectively which was lower in comparison to 21% $CD4^+$ T cells in tumors arising from EO771 transplantation (Figure 26B). The other cell populations showed the reverse trend and tumors expressing NY-BR-1 were infiltrated with more $CD8^+$ T cells and $CD11b^+F4/80^+$ macrophages. However, the difference was significant for both EONY clones compared to EO771 tumors only in the case of macrophages as the fraction of TAMs in EONY#9 derived and EONY#17 derived tumors was 1.5 times and 1.46 times more than that of EO771 tumors, respectively (Figure 26B. left panel). Interestingly, macrophages comprised the most abundant cell population among the

leukocytes, with $CD11b^+F4/0^+$ comprising more than 70% of all leukocytes in some tumors (Figure 26B. left panel).

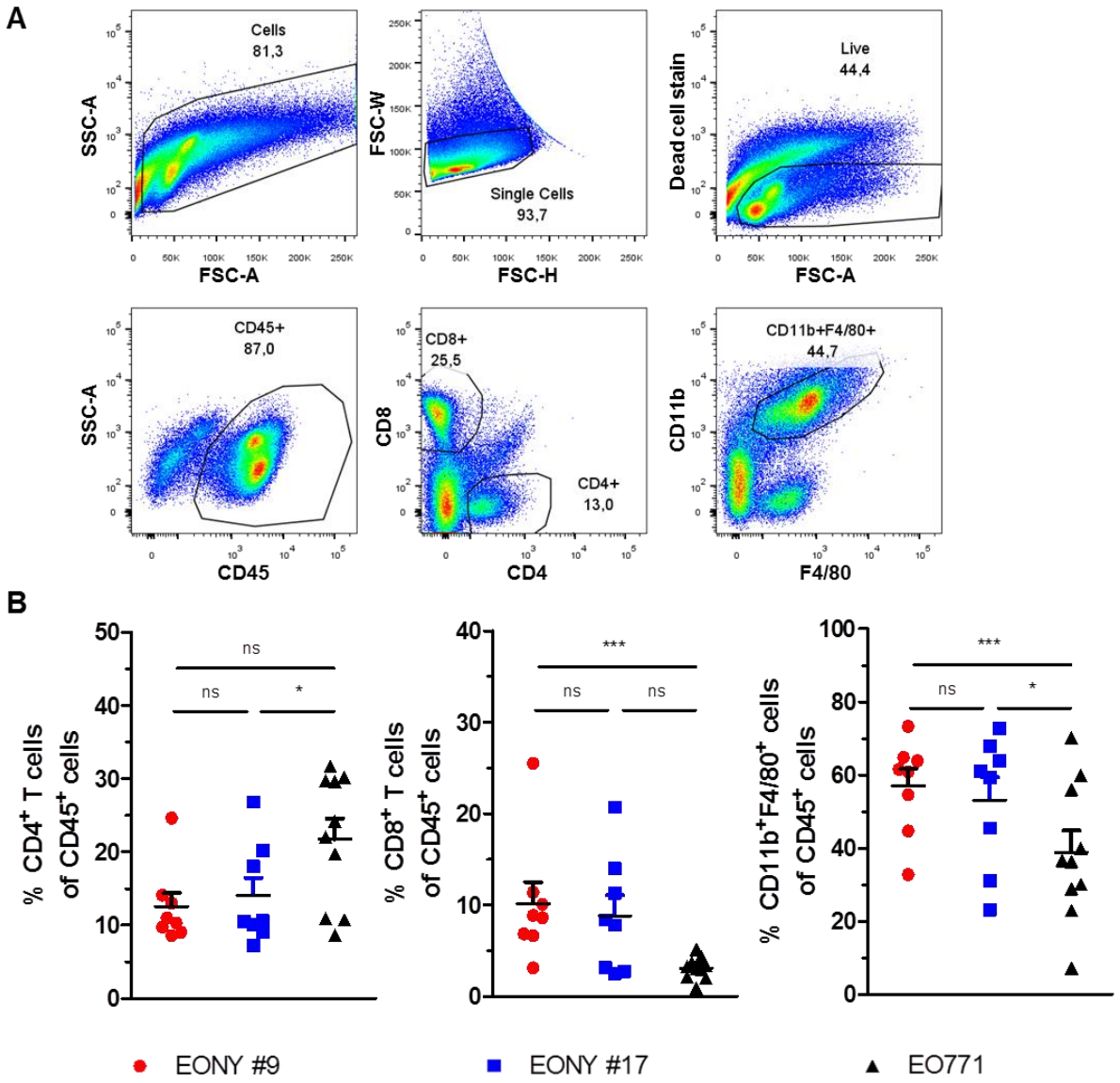

Figure 26. Characterization of tumor infiltrating leukocytes

$2x10^5$ EO771 cells, EONY#9 cells or EONY#17 cells were injected *s.c.* into the right flank of HLA-DRB1*0401tg mice (n=10). Tumors were resected and digested with Collagenase D and single cell suspension was obtained by passing them through a 70 µm mesh. Immune cells were isolated by performing gradient centrifugation using Lympholyte-M and collecting the interphase. Immune cells were then characterized by flow cytometry. **(A)** Gating scheme for analysis of tumor infiltrating $CD4^+$ T cells, $CD8^+$ T cells and $CD11b^+F4/80^+$ macrophages. **(B)** Percentage of $CD4^+$ T cells, $CD8^+$ T cells and $CD11b^+F4/80^+$ macrophages within $CD45^+$ cells is shown. (Mann Whitney test, * p≤ 0.05; ** p≤0.01; *** p≤0.001).

5.4.3 Establishment of macrophage associated markers on *in vitro* polarized peritoneal exudate cells (PECs)

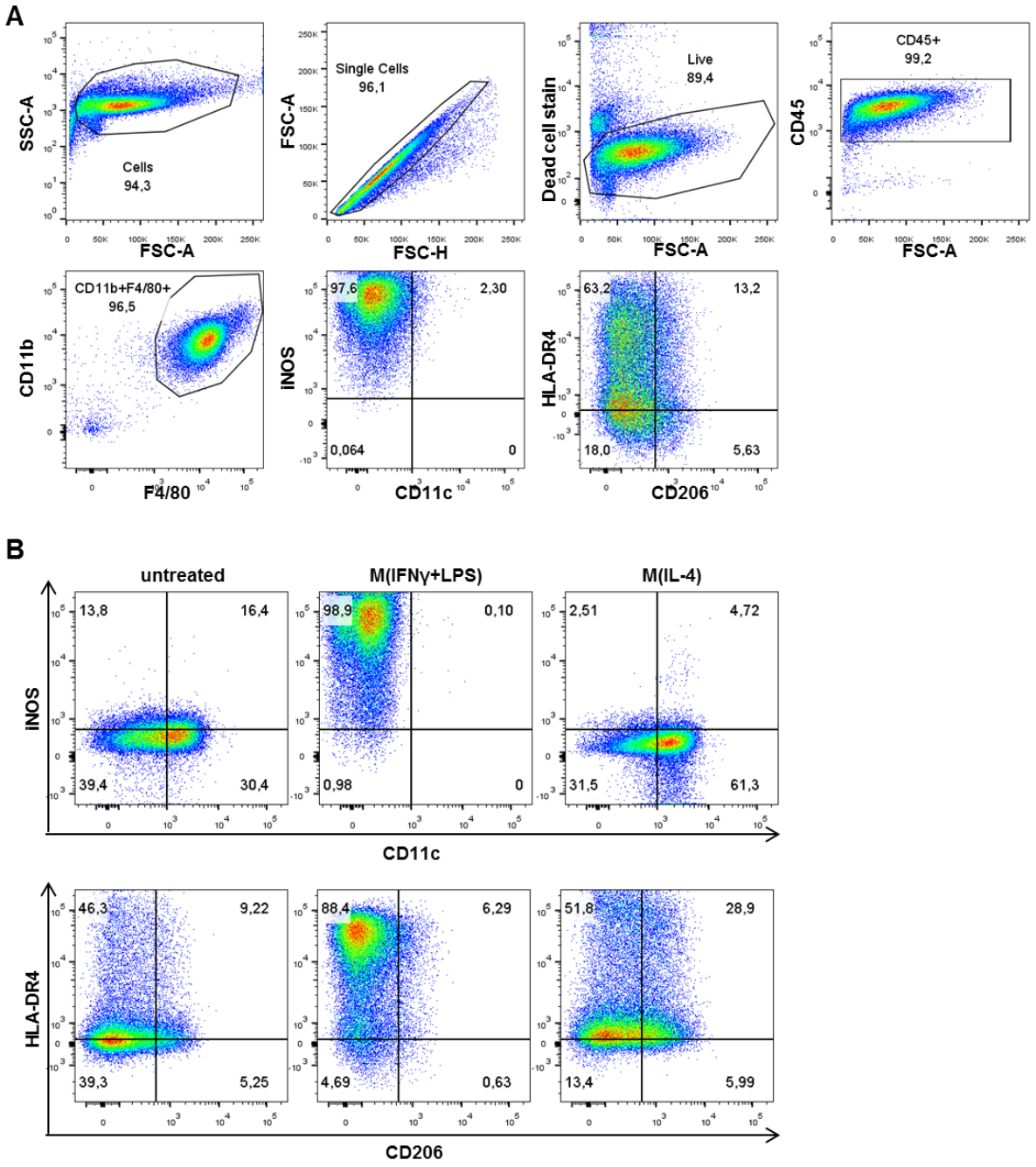

Figure 27. *In vitro* polarization of PECs

PECs isolated from HLA-DR4 mice after thioglycollate treatment for 4 days were stained for various M1- and M2- associated markers. **(A)** Gating scheme for analysis of expression of iNOS, CD11C, HLA-DR4 and CD206 on peritoneal macrophages. **(B)** Expression of various markers on untreated macrophages or those treated with IFNγ and LPS or IL-4 for 24 hours is shown in a representative dot plot.

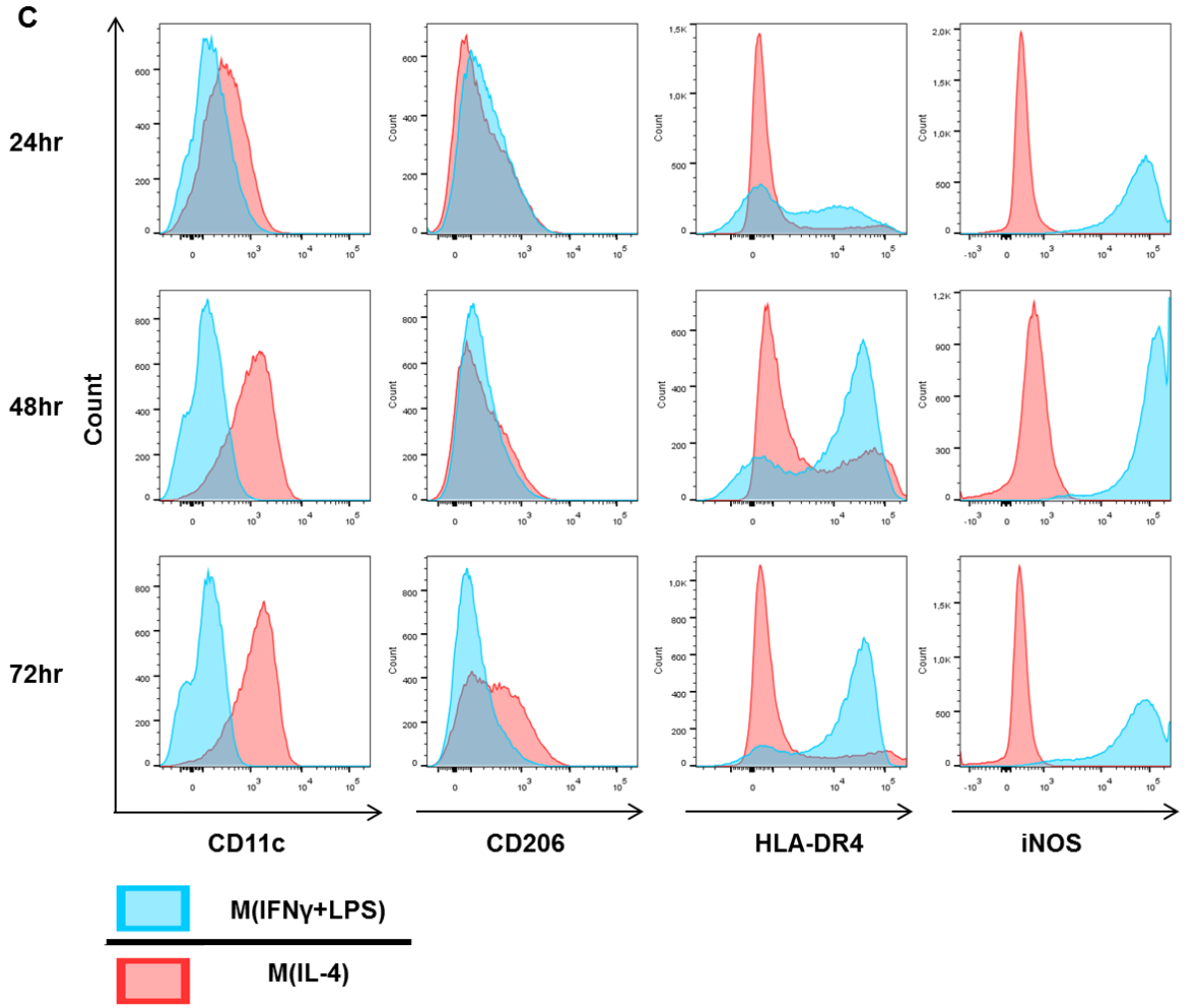

Figure 27 (contd). ***In vitro*** **polarization of PECs**

(C) Histograms depict the expression of CD11c, CD206, HLA-DR4 and iNOS on peritoneal macrophages treated with IFNγ and LPS or IL-4 for 24, 48 or 72 hours.

Having observed a significant increase in TAMs within NY-BR-1-expresssing tumors in comparison to parental EO771 tumors, we intended to analyze this myeloid infiltrate in more detail, particularly with respect to their differentiation status. In order to establish macrophage differentiation markers that would allow discrimination between M1-like and M2-like macrophages, we first made use of peritoneal exudate cells (PECs) as surrogate for tumor associated macrophages. Mouse peritoneal cavity contains quiescent macrophages which can be harvested easily, however the administration of thioglycollate broth is known to elicit macrophages (236). Since PECs from these mice are comprised of mostly macrophages, they are suitable for *in vitro* characterization of macrophages markers.

PECs were isolated on 4 days after thioglycollate administration and they were allowed to attach for 2 hours. The non-adherent cells were washed away with PBS. The attached macrophages were then polarized *in vitro* into M1-like or M2-like macrophages as described in section 4.2. The cells were then analyzed for M1- and M2-associated markers by flow cytometry. The gating scheme employed is depicted in Figure 27A. Briefly, cells were first gated based on their forward and side scatter characteristics followed by exclusion of doublets and dead cells. Then, macrophages which can be identified as $CD45^{+}CD11^{+}F4/80^{+}$ cells were analyzed for expression of the following markers: CD11c, iNOS, HLA-DR and

CD206. M1-like markers iNOS and HLA-DR are upregulated on M(IFNγ+LPS) macrophages compared to untreated and M(IL-4) macrophages by 24 hours of polarization (Figure 27B). On the other hand M(IL-4) cells upregulate CD11c in 66% cells in addition to CD206 in 34.89% cells after 24 hour stimulation (Figure 27B). However, CD11c is usually associated with M1-like macrophages, especially in adipose tissue macrophages (219). While CD11c was upregulated on M(IL-4) cells as early as 24 hours and expression increased further after 48 and 72 hours, CD206 could be detected on the surface of M(IL-4) cells only after 72 hours (Figure 27C). On the other hand, both M1-associated markers HLA-DR4 and iNOS are upregulated on IFNγ+LPS treated macrophages within 24 hours and their level of expression continue to increase with time (Figure 27C).

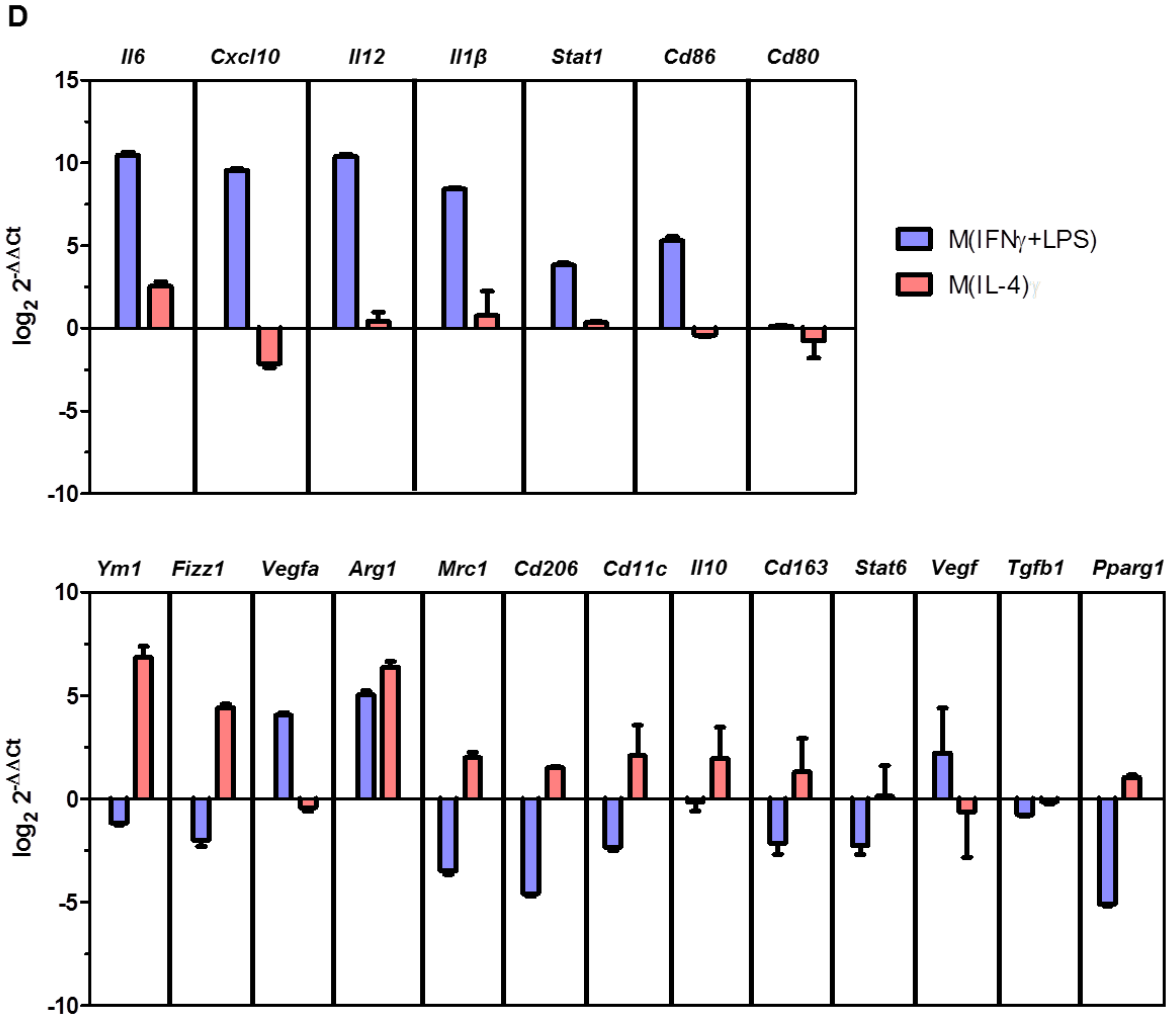

Figure 27 (contd). ***In vitro*** **polarization of PECs**

(D) RNA was isolated from PECs polarized in vitro for 24 hours with IFNγ and LPS or with IL-4 and the expression of various M1-associated genes (upper panel) or M2-associated genes (lower panel) were analyzed by qRT-PCR. The expression data has been depicted as the $\log_2$(fold change) of the gene relative to house-keeping gene normalized to untreated sample.

Additionally, RNA was isolated from PECs polarized for 24 hours and the expression of various M1- and M2- associated genes was analyzed by qRT-PCR. As expected genes known to be expressed in M1- like macrophages like *Il6*, *Cxcl10*, *Il12*, *IL1β*, *Stat1*, *Cd86* and

Cd80 were upregulated in PECs polarized with IFNγ and LPS compared to IL-4 treated PECs (Figure 27D, upper panel). Conversely, IL-4 treatment induced genes associated with M2-like macrophages, e.g. *Ym1*, *Fizz1*, *Arg1*, *Mrc1*, *Cd206*, *Cd11c*, *Il10*, *Cd163*, *Stat6*, *Pparg1* (Figure 27D, lower panel). *Vegfa* was surprisingly upregulated in PECs cultured in the presence of IFNγ and LPS, as detected by two different primer pairs (designated by *Vegfa* and *Vegf*, Figure 27D, lower panel). Thus, FACS antibodies for HLA-DR, iNOS and CD206 were shown to detect the respective M1- or M2- associated markers on *in vitro* polarized PECs. Additional genes associated with M1- or M2- like macrophages could be detected with specific primer pairs by qRT-PCR.

5.4.4 Phenotypic analysis of M1/M2-like tumor associated macrophages

Next the expression of M1- and M2- associated markers on TAMs was analyzed by flow cytometry. The proportion of HLA-DR4$^+$ macrophages was significantly lower in EONY#9 derived tumors but the level of expression of M1-associated marker HLA-DR was higher in EONY#17 TAMs compared to EO771 tumors (Figure 28A). iNOS expressing TAMs were more abundant and had higher levels of iNOS in NY-BR-1 expressing tumors (Figure 28A). CD206 showed reverse tendency in terms of frequency of positive cells and the expression levels. EONY tumors were infiltrated by more CD206$^+$ macrophages but the level of expression was more in EO771 TAMs (Figure 28A). In order to assess if the difference in the frequencies of infiltrating T cells and macrophages could be due to differences in tumor size, the frequencies of various population of infiltrating cells were plotted against tumor size (Figure 28B). The low values of coefficient of regression (R^2) suggest that the extent of infiltration by various immune cells does not correlate to tumor size. The only exception was that high iNOS expressing macrophages were more abundant in smaller tumors.

In order to evaluate the sensitivity of various primer pairs available for detection of various M1- and M2- associated markers in tumor associated macrophages, CD11b$^+$ cells were isolated from EO771 or EONY#17 derived tumors by labeling with magnetic beads and RNA was isolated from them. The expression of various genes was normalized to the respective house-keeping gene. The relative expression gives us an idea which genes could be used for later experiments based on expression levels, as low expressed gene would be difficult to detect in sorted TAMs due to low cell numbers available. Representative dot plot shows that post magnetic sorting the proportion of CD11b$^+$F4/80$^+$ cells increased from 54.4% to 83.7% (Figure 28C). Gene expression analysis on these cells for a variety of M1- and M2- like makers by qRT-PCR showed that M2-associated markers *Il-10*, *Stat6* and *Pparg1* are higher expressed on TAMs from EO771 tumors compared to EONY#17 tumors while *Fizz1*, *Arg1* and *Il-6* showed the reverse trend (Figure 28D, upper panel). On the other hand, genes described to be upregulated in M1-like macrophages such as *Il-1b*, *Stat1*, *Cxcl9* and *Nos2* were detected in lower amounts in EO771 TAMs compared to EONY#17 TAMs (Figure 28D, lower panel). This hints that macrophages infiltrating EONY tumors could resemble less immunosuppressive phenotype.

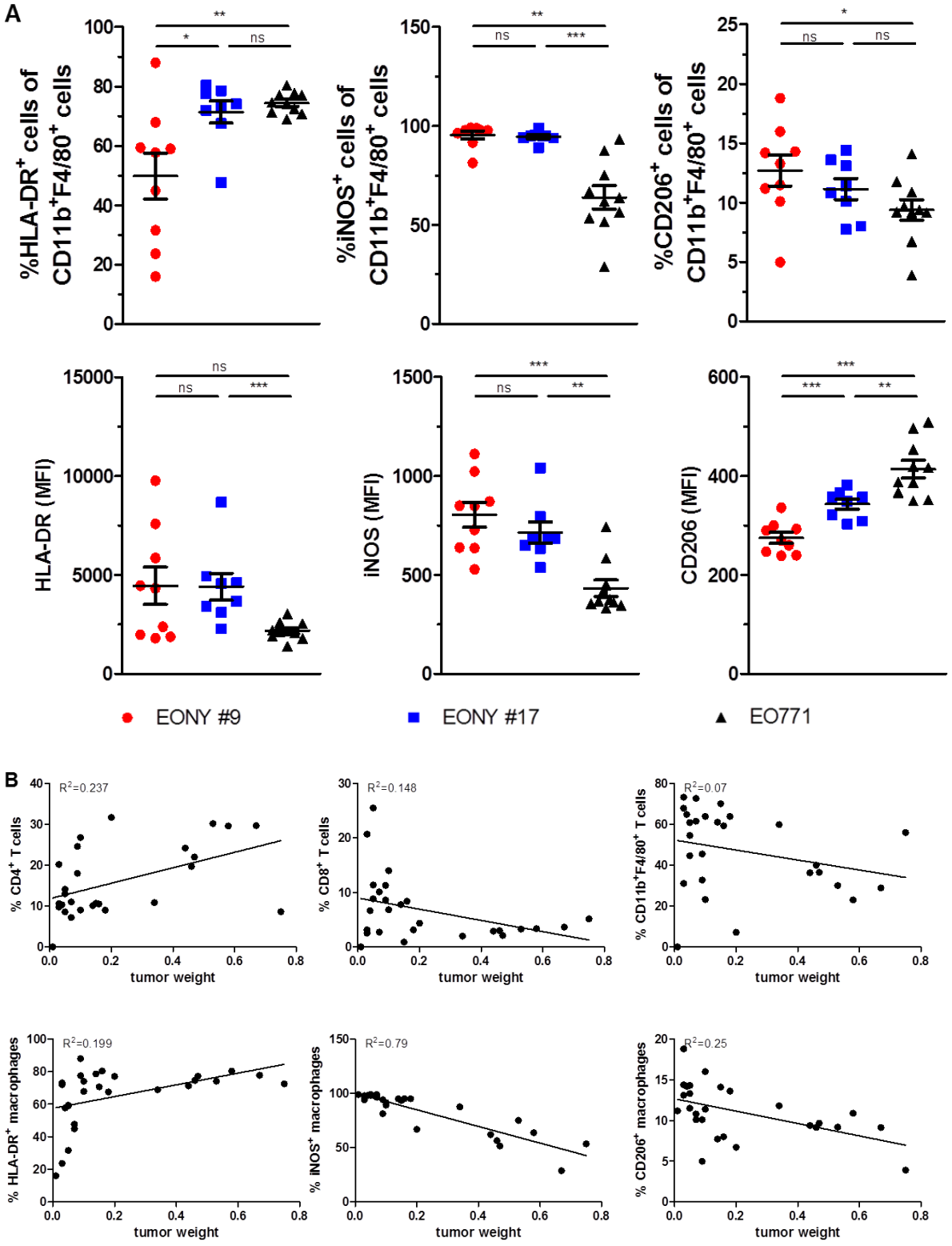

Figure 28. Characterization of tumor associated macrophages in EO771 and EONY tumors

(A) Fraction of macrophages expressing HLA-DR, iNOS and CD206 macrophages (upper panel) and the level of expression (MFI) (lower panel) for the same markers is shown. (Mann Whitney test, * p≤ 0.05; ** p≤0.01; *** p≤0.001). **(B)** Frequencies of tumor infiltrating $CD4^+$ T cells, $CD8^+$ T cells and macrophages and of different macrophage populations are plotted against corresponding tumor weight for linear regression analysis. R2 values indicate coefficient of regression.

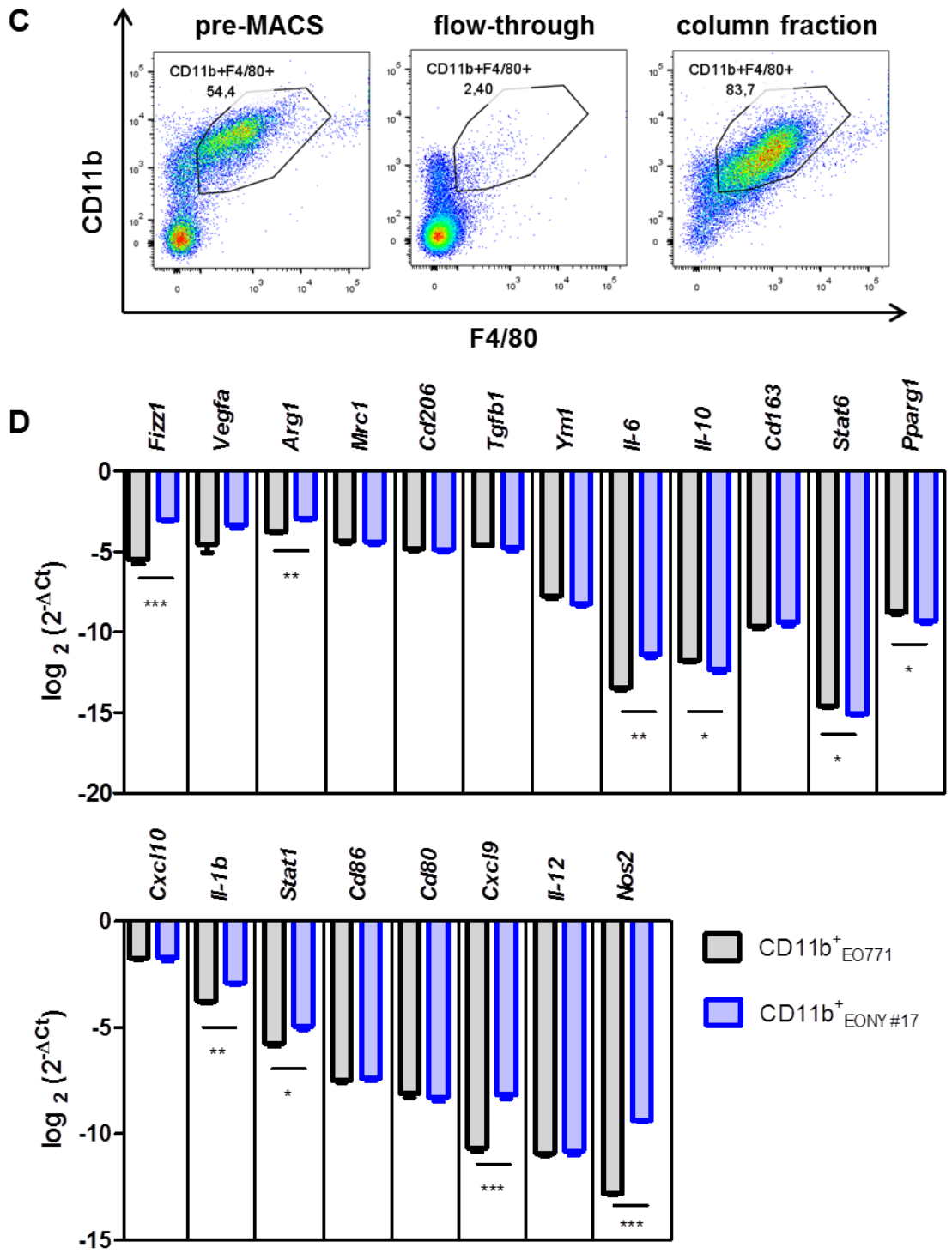

Figure 28 (contd.) Characterization of tumor associated macrophages in EO771 and EONY tumors

(C) Tumor infiltrating leukocytes isolated from EO771 and EONY#17 tumors by a combination of enzymatic and mechanical digestion followed by a density gradient centrifugation were enriched for $CD11b^+$ cells using anti-CD11b microbeads. Representative dot plot depicts the relative abundance of $CD11b^+F4/80^+$ macrophages among $CD45^+$ cells before magnetic enrichment (pre-MACS) and after positive selection in the unlabeled fraction (flow-through) and in the fraction labeled with beads (column fraction). **(D)** The expression of various genes associated with M2-like (upper panel) or M1-like (lower panel) macrophages, was analyzed in the isolated $CD11b^+$ cells by qRT-PCR. Log fold change for gene normalized to the house-keeping gene is shown. (Student's t test, * p≤ 0.05; ** p≤0.01; *** p≤0.001)

5.4.5 Impact of Ad.NY-BR-1 immunization on tumor development in HLA-DRB1*0401 transgenic mice

We could confirm the induction of NY-BR-1 specific $CD8^+$ and $CD4^+$ T cells in mice transplanted with NY-BR-1 expressing tumors. Additionally, we also observed that these tumors are infiltrated with higher frequencies of macrophages that express higher level of M1-associated markers compared to TAMs infiltrating parental tumors. We hypothesized that this could be due to NY-BR-1 specific T cells induced after tumor transplantation. Thus, immunization against NY-BR-1 to induce stronger immune responses should enhance the M1-like phenotype of the tumor infiltrating macrophages. We had already shown that immunization with the NY-BR-1 expressing Ad5.NY-BR-1 resulted in strong NY-BR-1 specific immune responses, including $CD4^+$ and $CD8^+$ T cell responses.

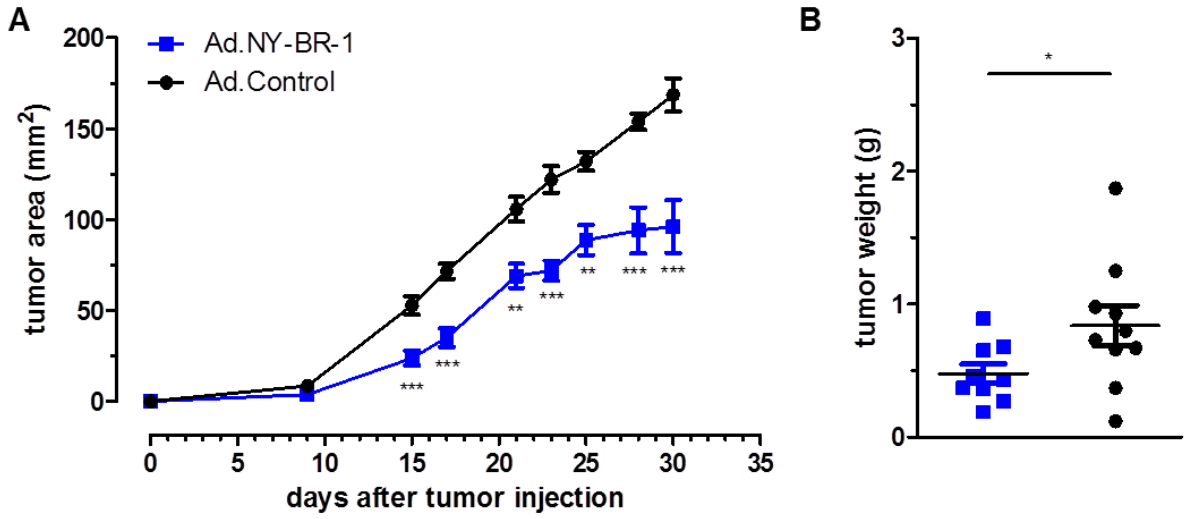

Figure 29. Immunization with NY-BR-1 encoding adenovirus delays tumor growth

HLA-DRB1*0401tg mice were immunized *i.p.* either with $5x10^8$ pfu Ad.NY-BR-1 (n=10) or with $5x10^8$ pfu Ad.Control (n=10) and $2x10^5$ EONY#17 cells were injected *s.c.* into the right flank 14 days post immunization. The tumor growth was monitored for 30 days after injection and then the tumors were harvested and tumor weight was measured. **(A)** Tumor area and **(B)** tumor weight were measured as described earlier. Error bars represent SEM (n=10) and statistical analysis was performed using Mann Whitney test (*, p<0.5; **p<0.01, ***, p<0.001; ****, p<0.0001).

HLA-DR4tg mice were immunized with the NY-BR-1 expressing Ad5.NY-BR-1 or the empty virus Ad5.Control and EONY#17 cells were injected subcutaneously 14 days post immunization and tumor growth was monitored for 30 days following tumor inoculation. The immunization induced anti-NY-BR-1 immunity translated into delayed tumor growth as well and transplanted EONY#17 cells gave rise to tumors at a slower rate in mice immunized with Ad5.NY-BR-1 compared to those immunized with Ad5.Control (Figure 29A). The first palpable tumors appeared already after 9 days of tumor inoculation in both groups of mice, but the difference in the tumor size became apparent within 15 days post tumor injection. The average size and weight of tumors in the control group was 168 mm^2 and 0.83 g, respectively compared to 96 mm^2 and 0.47 g in the group which received Ad.NY-BR-1

(Figure 29A). Thus, immunization with an adenoviral encoding NY-BR-1 had a suppressive effect on growth of EONY tumors.

5.4.6 Impact of Ad.NY-BR-1 immunization on phenotype of TAMs

We hypothesized that NY-BR-1 specific $CD4^+$ T cells could affect the phenotype of TAMs polarizing them towards an M1-like phenotype. Therefore, we investigated the phenotype of TAMs in mice immunized with Ad5.NY-BR-1 or Ad5.Control and subsequently transplanted with EONY#17 tumor cells. The fraction of macrophages among tumor infiltrating immune cells increased from an average of 36% to 61.6 % after immunization against NY-BR-1 (Figure 30A, left panel). HLA-DR expression is known to be higher on M1-like macrophages and we could demonstrate the same in *in vitro* polarized PECs isolated from HLA-DR4tg mice. Thus, the percentage of $HLA\text{-}DR4^+$ cells among TAMs was analyzed. Although there was no significant difference between the frequency of $HLA\text{-}DR4^+$ TAMs after Ad.NY-BR-1 administration (Figure 30A, middle panel), there was an increment of 1.3 times in the level of HLA-DR4 expression on the TAMs (Figure 30A, right panel) suggesting a more M1-like phenotype. However, the gene expression data obtained by qRT-PCR showed that M1-like markers, *Cxcl10* and *Stat1* was expressed to lower extent in the TAMs (Figure 30B, lower panel) whereas immunization with Ad.NY-BR-1 did not significantly alter the expression of M2-associated genes in TAMs (Figure 30B, upper panel).

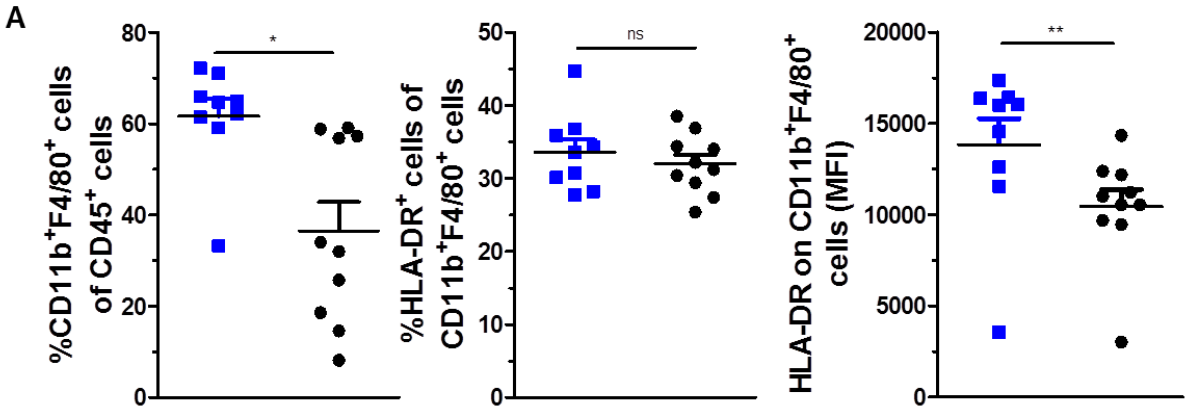

Figure 30. Characterization of TAMs following immunization with NY-BR-1 encoding adenovirus

HLA-DRB1*0401tg mice were immunized *i.p.* either with $5x10^8$ pfu Ad.NY-BR-1 (n=10) or with $5x10^8$ pfu Ad.Control (n=10) and $2x10^5$ EONY#17 cells were injected *s.c.* onto the right flank 14 days post immunization. On day 30 the tumors were harvested and tumor-infiltrating immune cells were isolated as described earlier. $CD45^+CD11b^+F4/80^+$ macrophages were FACS sorted and RNA was isolated for gene expression analysis. **(A)** The frequency of $CD11b^+F4/80^+$ macrophages among $CD45^+$ cells, $HLA\text{-}DR^+$ cells among macrophages, and the level of HLA-DR on macrophages is depicted.

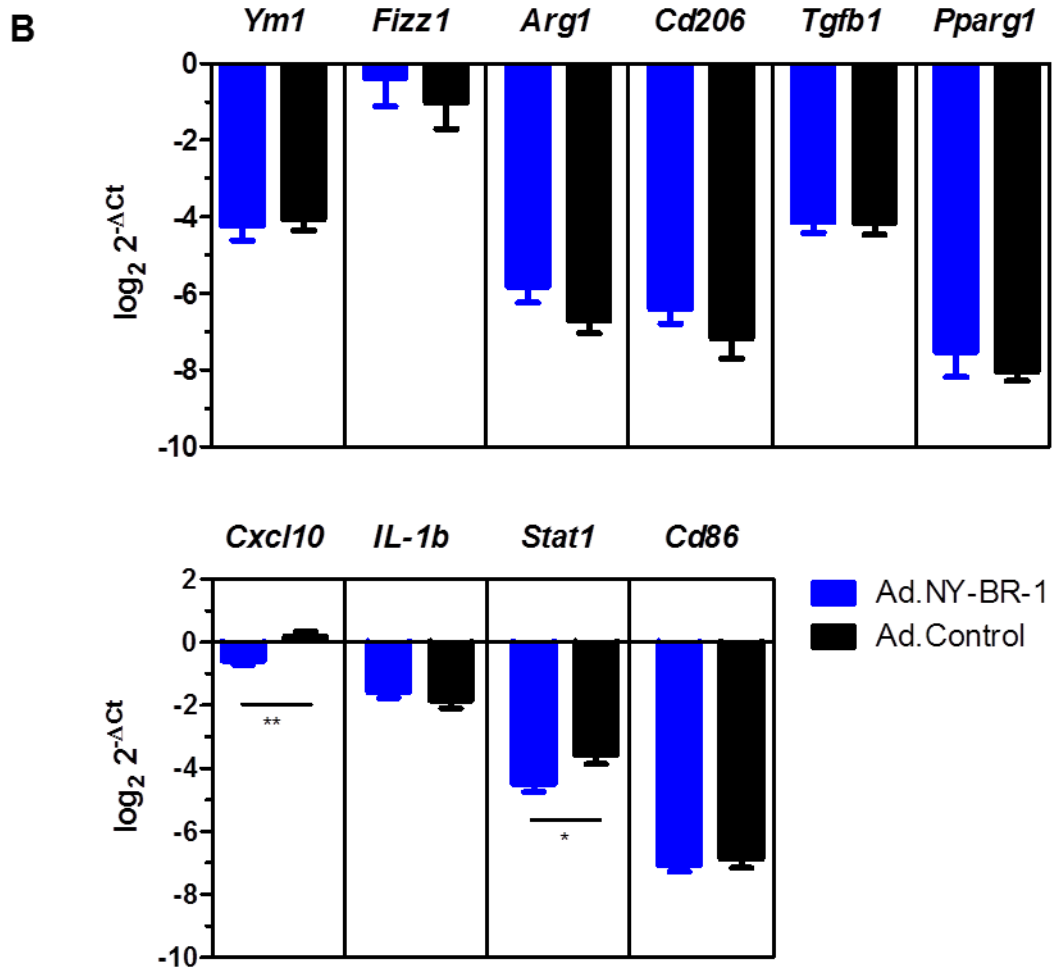

Figure 30 (contd). Characterization of TAMs following immunization with NY-BR-1 encoding adenovirus

(B) Expression of M2- (upper panel) and M1-associated genes (lower panel) in the TAMs was quantified by qRT-PCR. Log fold change for gene normalized to the house-keeping gene is shown (Student's t test, * p≤ 0.05; ** p≤0.01; *** p≤0.001).

5.5 Interaction of CD4$^+$ T cells and macrophages

It has been shown that antigen specific CD4$^+$ T cells can be stimulated by macrophages which present antigenic epitopes in the context of MHC II molecule. The macrophages in the tumor microenvironment can take up secreted tumor antigen and process it and subsequently present it on the cell surface as a peptide-MHC II complex (209). CD4$^+$ T cells specific for the epitope secrete IFNγ upon activation which can re-polarize the tumor-infiltrating macrophages into an M1-like phenotype.

5.5.1 Tumor derived peptide loaded CD11b$^+$ cells stimulate specific CD4$^+$ T cells *ex vivo*

Previous experiments demonstrated that EO771 and EONY#17 derived tumors were heavily infiltrated by macrophages and over 50% of all CD45$^+$ cells were macrophages (Figure 26B) and CD11b$^+$F4/80$^+$ macrophages comprised more than 80% of all CD45$^+$ cells (Figure 28C) after enrichment with magnetic beads coupled to anti-CD11b antibody. Thus, tumor-infiltrating CD11b$^+$ cells isolated from EO771, EONY#9 or EONY#17 derived tumors were co-

cultured overnight with HLA-DR4-restricted $CD4^+$ T cell lines specific for NY-BR-1 epitopes #8862 and #9251.

Tumor infiltrating macrophages from NY-BR-1 expressing tumors (EONY#9 and EONY#17) failed to stimulate $CD4^+$ T cells to secrete IFNγ when compared to TAMs isolated from parental EO771 tumors (Figure 31, green bars). T2/DR4 cells which express HLA-DR4 molecule were loaded with the relevant peptide and used as a positive control and could strongly activate both $CD4^+$ T cell lines. However, $CD4^+$ T cell line #8862 could recognize TAMs loaded externally with the peptide #8862 (Figure 31, red bars) indicating that the HLA-DR4 expression on the TAMs was enough for the TCR on $CD4^+$ T cells to engage with the peptide-MHC II complex. On the other hand, the $CD4^+$ T cell line specific for the NY-BR-1 epitope #9251 failed to recognize $CD11b^+$ cells loaded with the relevant peptide (Figure 31, red bars, right panel).

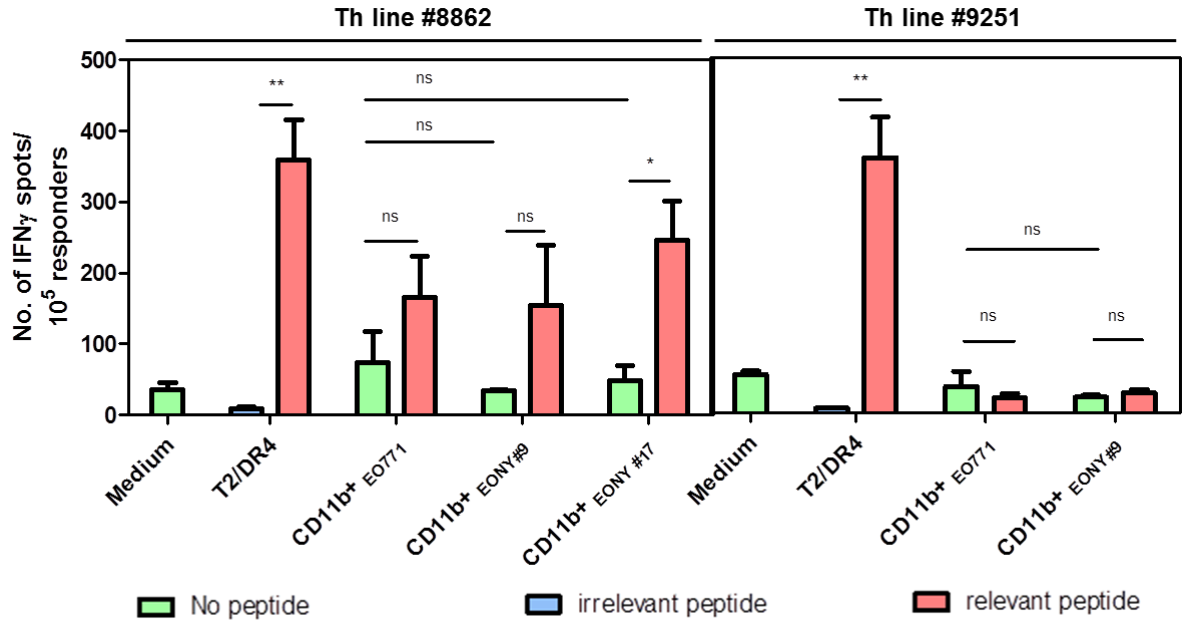

Figure 31. Peptide pulsed TAMs are recognized by NY-BR-1-specific $CD4^+$ T cell line #8862

Tumor infiltrating leukocytes isolated from EO771, EONY#9 and EONY#17 tumors by a combination of enzymatic and mechanical digestion followed by a density gradient centrifugation were enriched for $CD11b^+$ cells using anti-CD11b microbeads. The isolated cells were then used as target cells in an ELISPOT assay either alone or loaded with 1 µg/ml peptide with NY-BR-1 specific $CD4^+$ T cells. $1x10^5$ effector cells ($CD4^+$ T cells line #8862 or #9251) were incubated overnight with $5x10^4$ target cells and IFNγ secretion was measured by ELISPOT assay. Mean number of IFNγ spots is represented as bar graphs and error bars depict SEM of triplicates in ELISPOT assay (Mann Whitney test, * p≤ 0.05; ** p≤0.01; *** p≤0.001).

5.5.2 NY-BR-1 specific $CD4^+$ T cells can repolarize *in vitro* polarized M2-like macrophages towards M1-like macrophages

We demonstrated that we could successfully isolate and polarize peritoneal macrophages into M1-like and M2-like phenotype. In order to investigate if NY-BR-1 specific $CD4^+$ T cells are capable of reducing the immunosuppressive phenotype of M2-like macrophages, PECs were polarized to M2-like macrophages using IL-4 and then co-cultured with NY-BR-1 specific $CD4^+$ T cells in the presence of the relevant peptide or tumor lysates for 48 hours. The activation of the $CD4^+$ T cells in response to their cognate epitope was measured by the

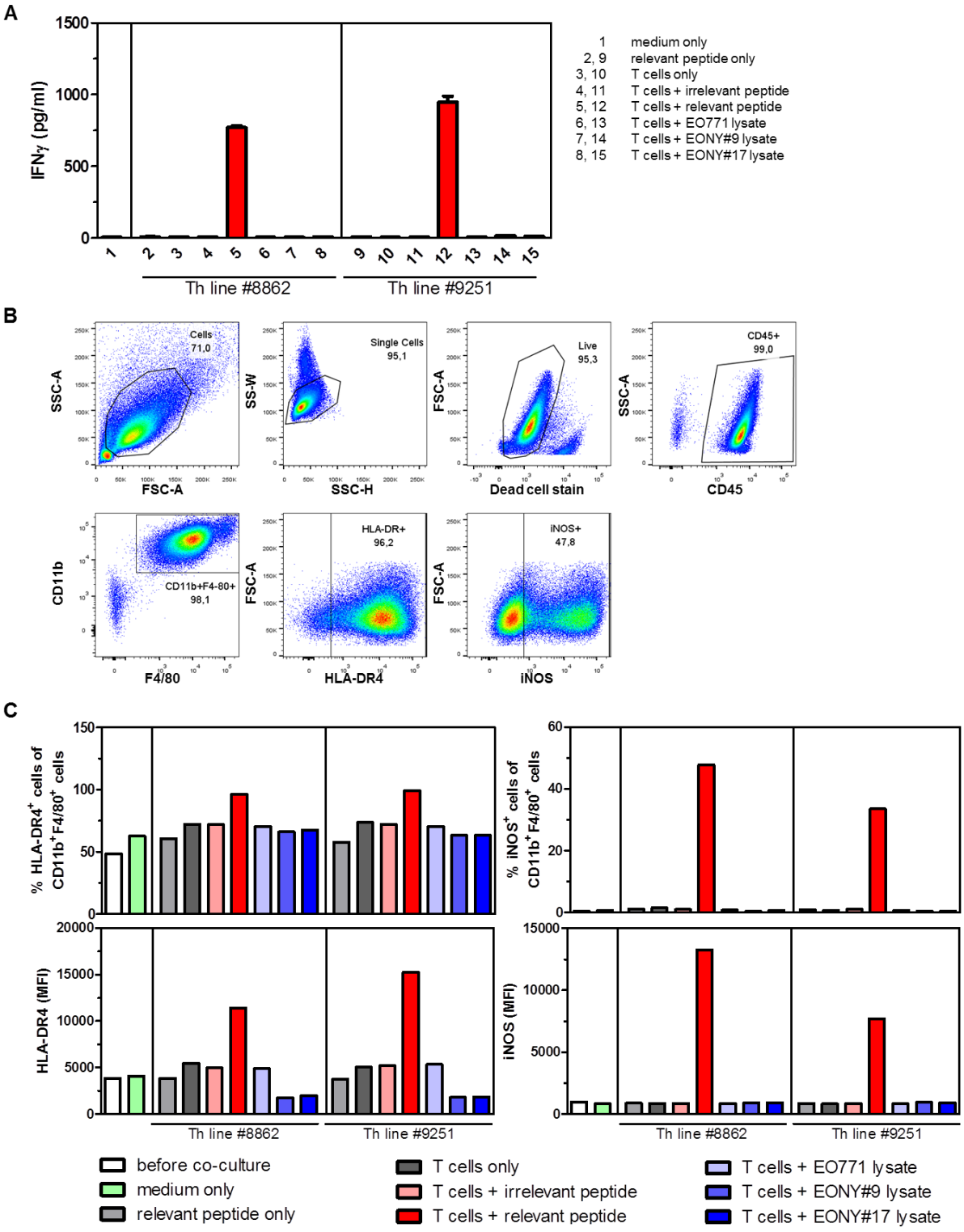

Figure 32. NY-BR-1-specific CD4$^+$ T cell lines #8862 and #9251 re-polarize M2-like macrophages

PECs isolated from HLA-DR4tg mice were polarized to M2-like macrophages for 48 hours using 10 ng/ml IL-4. 1.8 x10^6 polarized PECs were co-cultured with 1x10^6 CD4$^+$ T cells and 5 µg/ml synthetic peptide or with protein lysates from tumor cells containing 50 µg total protein. Supernatant and PECs were harvested after 48 hours for analysis. **(A)** Bar graph shows the quantity of secreted IFNγ in the supernatant as measured by ELISA and error bars depict SEM of duplicates in the ELISA. **(B)** Representative dot plots show gating scheme for the analysis of HLA-DR4 and iNOS expression on the PECs following co-culture with the CD4$^+$ T cells. **(C)** Bar graphs show the percentage of HLA-DR4$^+$ and iNOS$^+$ macrophages and the level of expression as median fluorescence intensities (MFI) after 48 hours of co-culture.

secreted IFNγ present in the supernatant. IFNγ response could only be detected when the $CD4^+$ T cell lines #8862 and #9251 were co-cultured with the PECs in the presence of the corresponding peptide in the soluble form (Figure 32A, bars 5 and 12). T cells did not secrete detectible levels of IFNγ when co-cultured with the PECs alone (Figure 32A, bars 3 and 10) or in the presence of an irrelevant peptide (Figure 32A, bars 4 and 11). PECs loaded with lysates from EO771, EONY#9 and EONY#17 tumor cells also failed to elicit an IFNγ response that could be detected in the supernatant after 48 hours of co-culture (Figure 32A, bars 6, 7, 8, 13, 14 and 15).

The harvested PECs were then characterized for the expression of various M1- and M2-associated markers by flow cytometry or qRT-PCR. The gating scheme employed is depicted in Figure 32B. Briefly, cells were gated based on their forward and side scatter characteristics, followed by exclusion of doublets and cells positive for dead cell stain. The live cells were gated on $CD45^+$ events which comprised 99% of all live cells. Within the $CD45^+$ leukocytes, 98% of the cells were determined to be macrophages based on the expression of CD11b and F4/80. These $CD11b^+F4/80^+$ cells were then analyzed for the expression of M1-associated markers, HLA-DR4 on the cell surface or intracellular iNOS. Forty eight percent of the PECS treated with IL-4 for 48 hours expressed HLA-DR4 molecule on their surface. The proportion of $HLA\text{-}DR4^+$ PECs increases slightly to 62% when IL-4 containing medium is replaced with fresh medium without IL-4 (Figure 32C, upper left panel, medium only). Soluble peptide representing HLA-DR4-restricted $CD4^+$ T cell epitopes does not result in further increase of HLA-DR4 expression levels on the surface of PECs.

Addition of $CD4^+$ T cells alone or in combination with irrelevant peptide results in the approximately 14% increase in HLA-DR4 surface expression compared to medium alone. However, the strongest increase in HLA-DR4 expression on PECs is observed when PECs are co-cultured with NY-BR-1 specific CD4+ T cell lines in the presence of the specific peptide in the soluble form (Figure 32C, upper left panel). The proportion of macrophages positive for HLA-DR4 on the cell surface increased from 71.9% to 96.2% and 72% to 99.1% when co-cultured with the CD4+ T cell lines #8862 and #9251 and their corresponding epitopes, respectively compared to $CD4^+$ T cells with irrelevant peptide. Similar tendency is observed in the level of HLA-DR4 expression measured by the median fluorescence intensity (MFI) values (Figure 32C, lower left panel). The baseline iNOS expression in M2 polarized PECs is almost negligible and is not induced by addition of T cells alone or with the irrelevant peptide (Figure 32C, upper right panel). However, interaction of the $CD4^+$ T cell lines #8862 or #9251 with PECs loaded with the relevant peptide resulted in the induction of iNOS expression in 47.8% and 33.6% of the PECs, respectively (Figure 32C, upper right panel). This increase in iNOS levels was reflected in the MFI values which showed 15.58 and 9.09 fold increase when compared to PECs loaded with irrelevant peptide and co-cultured with #8862 and #9251 T cells, respectively (Figure 32C, lower right panel). PECs loaded with lysates from NY-BR-1 expressing EO771 derived clones, EONY #9 and EONY #17 failed to upregulate of HLA-DR or iNOS post co-culture with NY-BR-1 specific $CD4^+$ T cells (Figure 32C, blue bars).

D

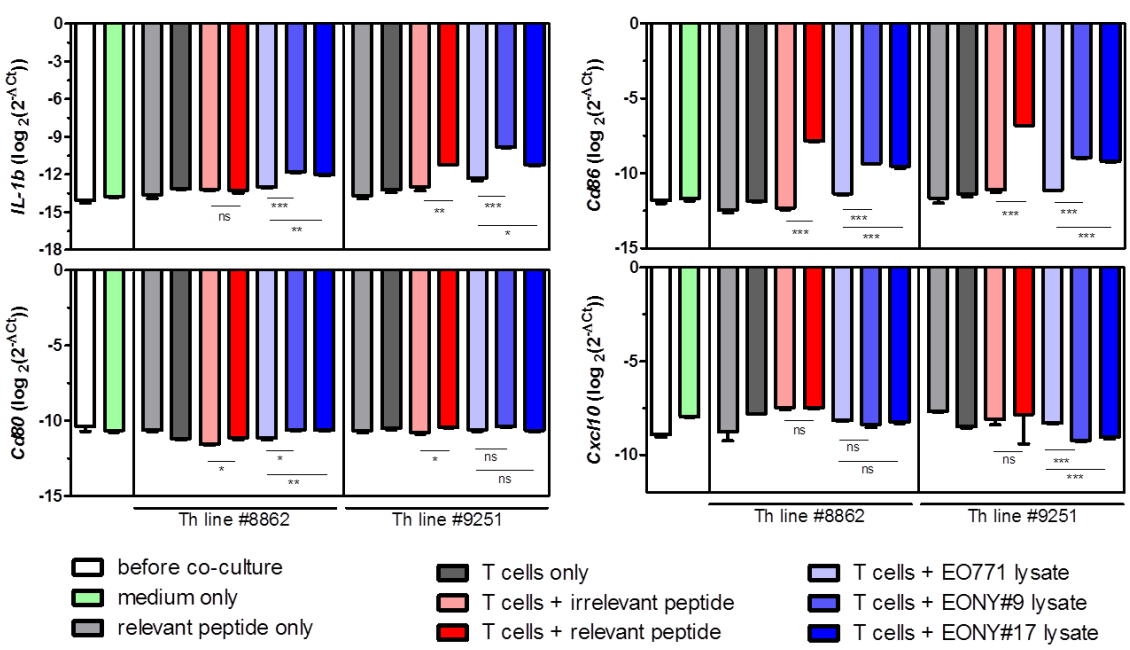

Figure 32 (contd.) NY-BR-1-specific CD4$^+$ T cell lines #8862 and #9251 re-polarize M2-like macrophages

(D) Expression of M1-assoclated genes in the PECs after co-culture was quantified by qRT-PCR. Log fold change for gene normalized to the house-keeping gene is shown. (Student's t test, * p≤ 0.05; ** p≤0.01; *** p≤0.001)

Additional M1- and M2-associated genes were analyzed by qRT-PCR to further characterize the change in the phenotype of the PECs following the co-culture. Co-incubation of the CD4$^+$ T cells with M2-polarized PECs loaded with their cognate peptide significantly enhanced the expression of M1-associated genes *Cd80, Cd86* and *IL-1b* compared to PECs loaded with an irrelevant peptide (Figure 32D, red bars). Interestingly, PECs loaded with lysates from NY-BR-1 expressing tumor cells expressed higher levels of *Il-1b*, *Cd80* and *Cd86* compared to PECs loaded with EO771 tumor cell lysates when co-cultured with NY-BR-1 specific CD4$^+$ T cells (Figure 32D, blue bars). Surprisingly, *Cxcl10* expression showed the reverse trend when Th line #9251 was used. M2-associated genes *Fizz1* and *Pparg1* were both downregulated in PECs following antigen specific interaction between both CD4$^+$ T cells and M2-polarized PECs (Figure 32E, red bars). Remarkably, other M2-associated markers *Tgfb1* and *Ym1* were also downregulated in the case of CD4$^+$ T cell line #9251 but showed the reverse trend in the group with T cell line #8862. *Fizz1*, *Pparg1 and Ym1* levels are reduced under the influence of NY-BR-1 specific CD4$^+$ T cell activity in presence of tumor cell lysate containing NY-BR-1 compared to parental cell lysate. Unexpectedly, *Arg1* expression was increased in PECs co-cultured with both CD4$^+$ T cell lines in the presence of the relevant peptide or EONY lysate. However, one important fact to keep in mind is that *Arg1* was also detected in M1-polarized macrophages (Figure 28D), albeit to lower levels compared to M2-polarized macrophages. Taken together, the FACS data and qRT-PCR data suggest that the interaction of NY-BR-1 specific CD4$^+$ T cell lines #8862 and #9251 with M2-polarized PECs which present the cognate peptide can result in the polarization of the PECs towards and M1-like phenotype.

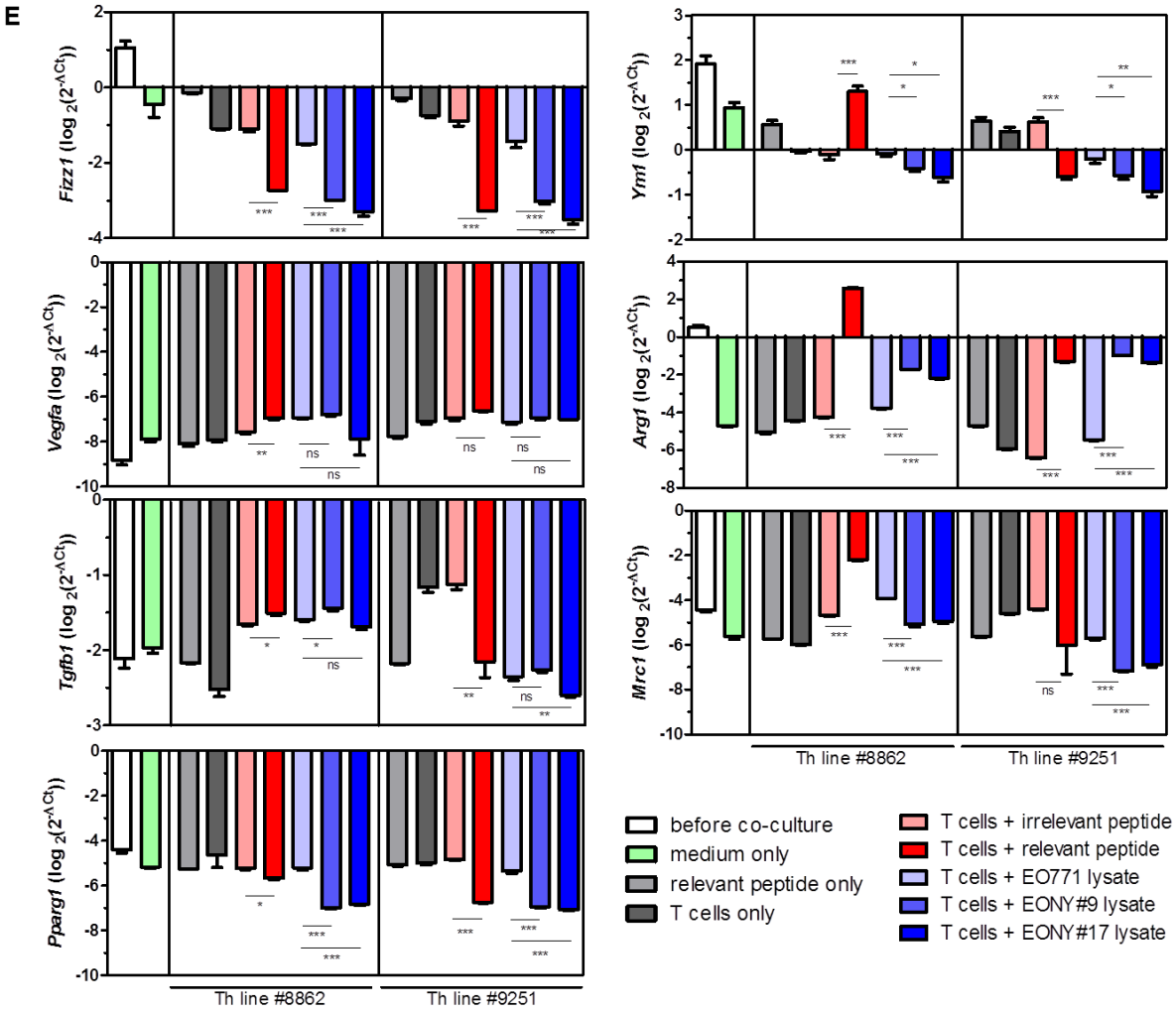

Figure 32 (contd). NY-BR-1-specific CD4$^+$ T cell lines #8862 and #9251 re-polarize M2-like macrophages

(E) Expression of M2-assoclated genes in the PECs after co-culture was quantified by qRT-PCR. Log fold change for gene normalized to the house-keeping gene is shown. (Student's t test, * p≤ 0.05; ** p≤0.01; *** p≤0.001)

5.5.3 Depletion of CD4$^+$ T cells resulted in delayed tumor growth and switch in macrophage polarization

The immunization of HLA-DR4tg mice with Ad.NY-BR-1 induced strong NY-BR-1 specific T cell response and had a suppressive effect on the growth of EONY#17 tumors. Additionally, EONY tumors induced CD8$^+$ and CD4$^+$ T cell responses against NY-BR-1 and were infiltrated with macrophages that resembled M1-like phenotype. Since Ad.NY-BR-1 immunization resulted in higher expression of HLA-DR4 molecules on tumor infiltrating macrophages and NY-BR-1 specific CD4$^+$ T cells could repolarize macrophages to M1-like phenotype *in vitro*, we hypothesized that adenovirus immunization induced NY-BR-1 CD4$^+$ T cells could also repolarize TAMs towards less immunosuppressive M1-like macrophages *in vivo*. In order to test our hypothesis, we immunized mice against NY-BR-1 using the adenovirus with the objective of inducing CD4$^+$ and CD8$^+$ T cells against NY-BR-1. This was followed by depletion of CD4$^+$ T cells using the GK1.5 antibody shortly before tumor

inoculation to investigate the role of the $CD4^+$ T cells on macrophage polarization as depicted in the scheme Figure 33A.

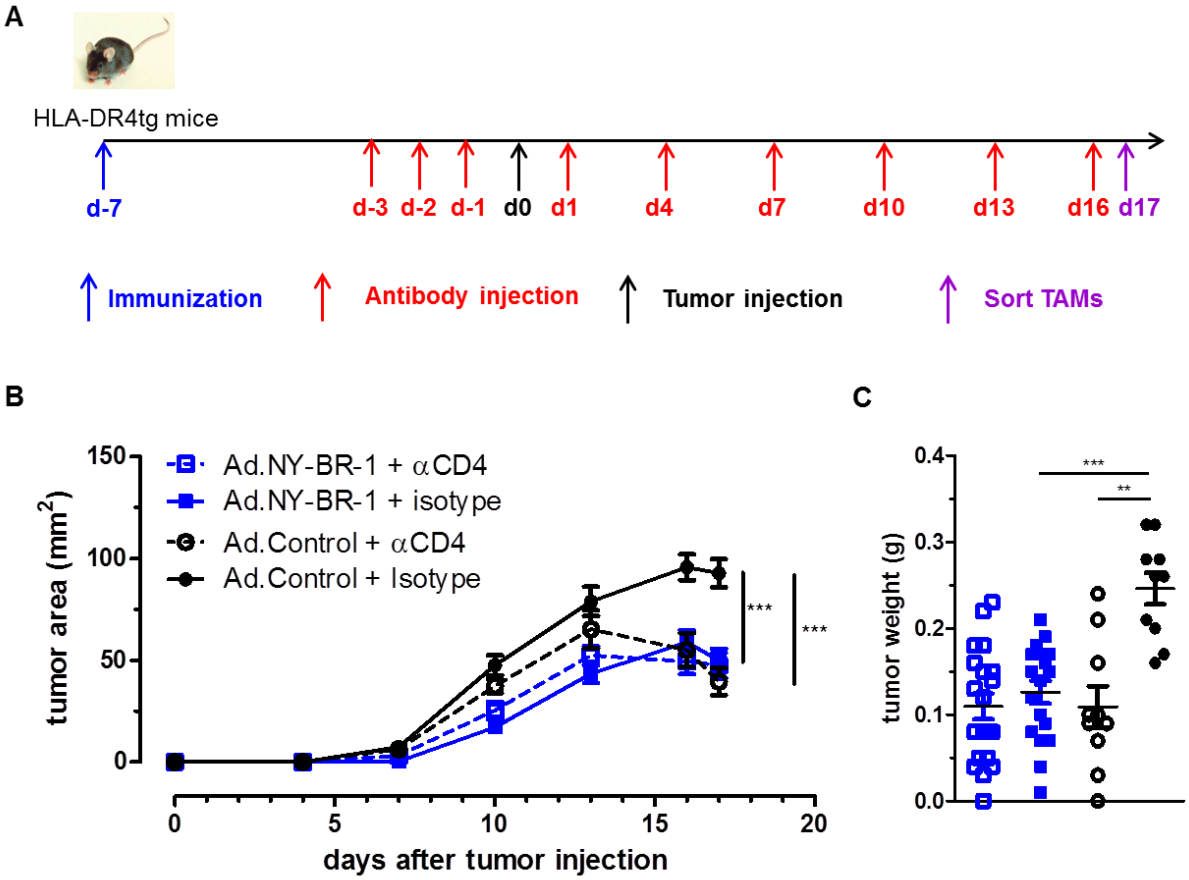

Figure 33. Depletion of endogenous $CD4^+$ T cells results in less immunosuppressive TAMs within EONY#17 tumors

HLA-DR4tg mice were immunized with $5x10^8$ pfu Ad.NY-BR-1 or Ad.control *i.p.* followed by *s.c.* injection of $2x10^5$ EONY#17 cells onto the right flank. This was combined with the depletion of $CD4^+$ T cells and 100 µg of depleting antibody, GK1.5 or the isotype control was administered *i.p.* in each dose. **(A)** Schematic representation of the experiment indicates the timeline of various treatments. **(B)** Tumor growth curve shows the tumor area measured on various days for 17 days after tumor injection. **(C)** Weight of tumors harvested after day 17 is depicted as dot plots. Error bars represent SEM and statistical analysis done by Mann Whitney test. (* p≤ 0.5; ** p≤0.01; *** p≤0.001)

Immunization of mice with Ad.NY-BR-1 resulted in delayed growth of inoculated EONY#17 tumors which reached a mean size of 49 mm^2, 17 days after tumor injection (Figure 33B, closed blue squares) compared to mice immunized with the control virus which had tumors with the average size of 92 mm^2 (Figure 33B, closed black circles). This recapitulated what was observed in previous experiments. Surprisingly, antibody mediated depletion of $CD4^+$ T cells in mice immunized with the control virus (Figure 33B, open black circles) had protective effect on the mice and inhibited tumor outgrowth with the average size of tumors being 57% smaller than in the group that received the isotype (Figure 33B, closed black circles). Interestingly, the anti-tumor effect that accompanied the depletion of $CD4^+$ T cells became apparent around day 13 after tumor transplantation. Depletion of $CD4^+$ T cells following Ad.NY-BR-1 immunzation did not further reduce the tumor growth rate (Figure 33B, open

blue squares). The tumors were excised 17 days after inoculation and the weight of the harvested tumors confirmed the results obtained by tumor measurements (Figure 33C).

The EONY#17 tumors comprised of approximately 16.8% $CD4^+$ T cells, 8.25% $CD8^+$ T cells and 54.5% $CD11b^+F4/80^+$ macrophages within $CD45^+$ leukocytes present in the tumor (Figure 33D, black closed circles). The immunization of HLA-DR4tg mice with Ad.NY-BR-1 did not significantly alter the proportion of tumor infiltrating $CD4^+$ T cells, $CD8^+$ T cells and $CD11b^+F4/80^+$ cells (Figure 33D, blue closed squares). The administration of the GK1.5 antibody successfully depleted the $CD4^+$ T cell population in the tumor (Figure 33D, open symbols). Absence of $CD4^+$ T cells changed the relative abundance of infiltrating $CD8^+$ T cells and macrophages as expected. Among the EONY#17 TAMs, 47.1% and 45% cells expressed HLA-DR4 molecules in control immunized and NY-BR-1 immunized mice, respectively (Figure 33D, lower panel). However, $CD4^+$ T cell depletion resulted in more than 1.3 fold increase in the fraction of $HLA\text{-}DR4^+$ macrophages in both groups. There was no difference in the frequency of HLA-DR4 expressing macrophages infiltrating EONY#17 tumors between the mice immunized with the control virus or the NY-BR-1 expressing virus but the level of HLA-DR4 surface expression was higher on the macrophages after immunization with the Ad.NY-BR-1, as indicated by 1.7 fold increase in the MFI value (Figure 33D, lower panel).

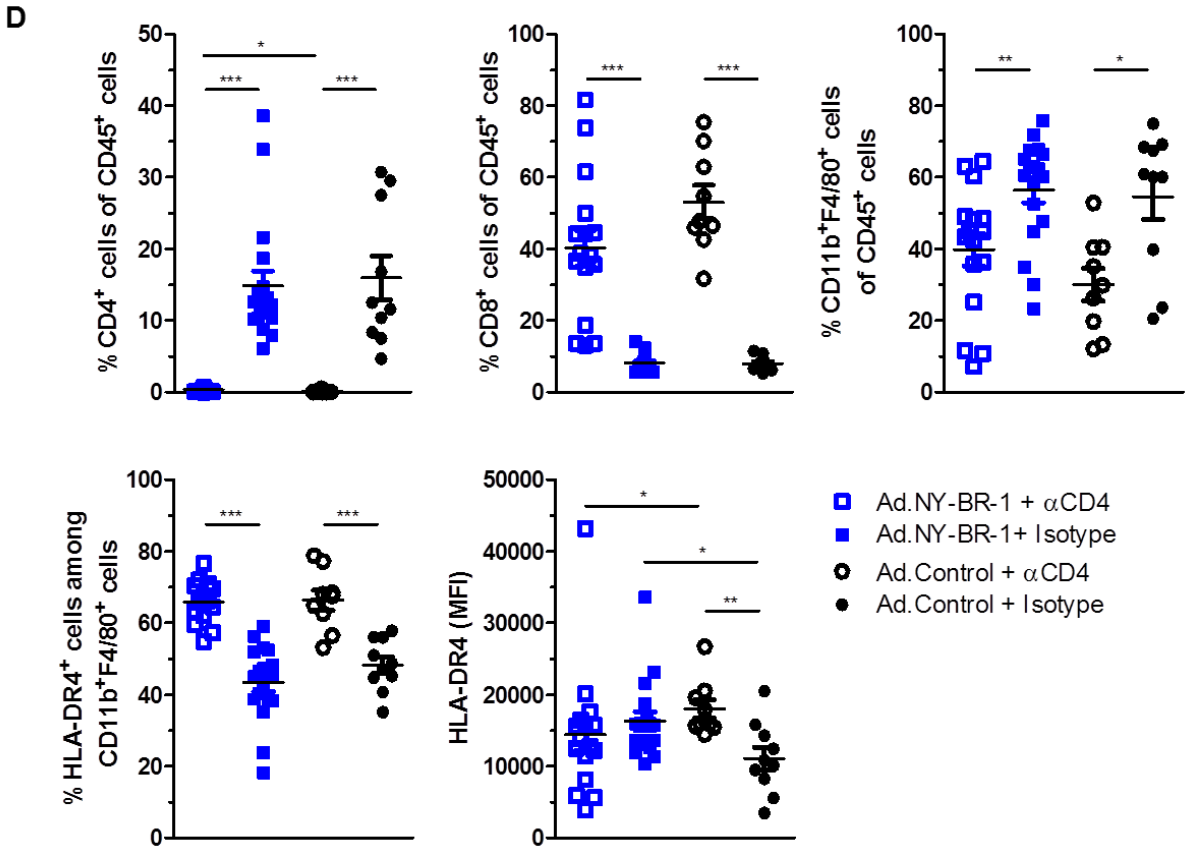

Figure 33 (contd.) Depletion of endogenous $CD4^+$ T cells results in less immunosuppressive TAMs within EONY#17 tumors

(D) The frequency of $CD4^+$ T cells, $CD8^+$ T cells and $CD11b^+F4/80^+$ macrophages among $CD45^+$ cells, $HLA\text{-}DR^+$ cells among macrophages, and the level of HLA-DR4 on macrophages is depicted.

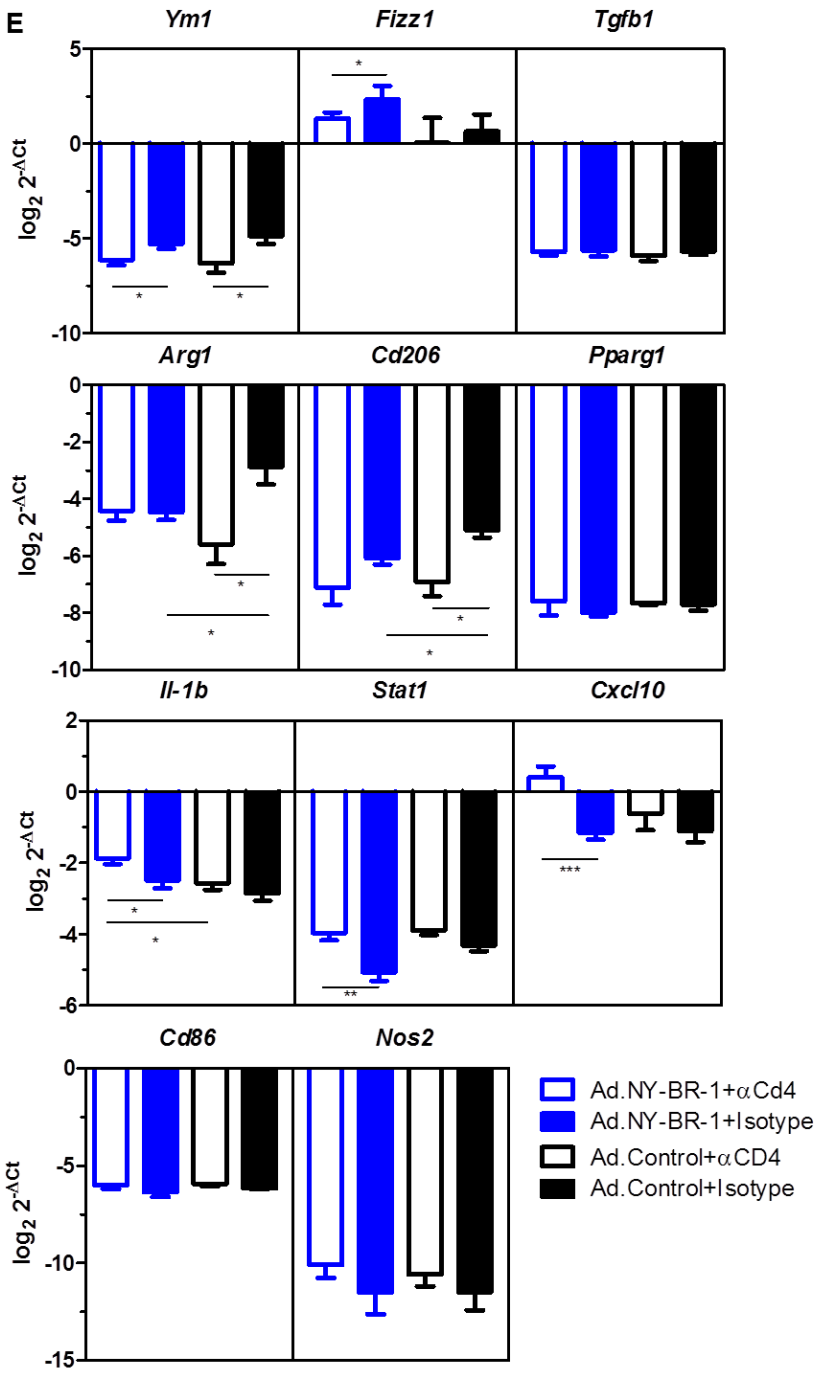

Figure 33 (contd.) Depletion of endogenous CD4$^+$ T cells results in less immunosuppressive TAMs within EONY#17 tumors

(E) Expression of M2- (upper two panels) and M1-assoclated genes (lower two panels) in sorted TAMs was quantified by qRT-PCR. Log fold change for gene normalized to the house-keeping gene is shown (Student's t test, * p≤ 0.05; ** p≤0.01; *** p≤0.001).

The macrophages were sorted and expression of M1- and M-2 associated genes was analyzed by real time PCR. Mice immunized with the Ad.NY-BR-1 had significantly lower levels of *Arg1* and *Cd206* expression in the TAMs compared to those immunized with the control virus (Figure 33E) but there was no significant difference in the expression of other genes. Remarkably, the depletion of CD4$^+$ T cells in the control group was accompanied by

repolarization of the TAMs towards an M1-like phenotype as indicated by the reduced expression of M2-associated genes like *Ym1*, *Arg1* and *Cd206* (Figure 33E, black bars). The same trend was observed in the group immunized with Ad.NY-BR-1 and *Ym1*, *Fizz1* and *Cd206* (not statistically significant for *Cd206*, p=0.1246) expression in macrophages was reduced after depletion of $CD4^+$ T cells. Additionally, tumor infiltrating macrophages upregulated genes like *Il-1b*, *Stat1* and *Cxcl10* in response to CD4+ T cell depletion in the mice immunized with Ad.NY-BR-1 suggesting a shift towards an M1-like phenotype (Figure 33E, blue bars). Thus, $CD4^+$ T cell depletion alone seems to re-polarize the TAMs towards a less immunosuppressive phenotype in EONY#17 tumors.

6 Discussion

6.1 Transplantable tumor model expressing breast cancer associated tumor antigen NY-BR-1

6.1.1 EO771/NY-BR-1 transfectants were immunogenic

NY-BR-1 is a breast cancer associated differentiation antigen which is highly overexpressed in breast cancer (94) making it an ideal target for immunotherapy. We established NY-BR-1 transfectant clones of C57BL/6 derived mammary adenocarcinoma cell line EO771. Since, NY-BR-1 is not expressed in mice and there are no known homologs; it induced an immune response when NY-BR-1 expressing EO771 transfectant clones EONY #9 and EONY #17 were inoculated into HLA-DR4tg mice. Both EONY #9 and EONY#17 gave rise tumors at a slower rate compared to parental EO771 cells (Figure 14A) even though there were no differences in their viability *in vitro* (Figure 11A). The NY-BR-1 expression was higher in EONY #9 cells than in EONY #17 cells (Figure 11B). This difference in expression levels was reflected in the growth kinetics *in vivo* and EONY #9 derived tumors had a slower growth rate than tumors arising from EONY #17 cells (Figure 14A). When splenocytes isolated from mice bearing NY-BR-1 expressing tumors were stimulated by synthetic peptides representing HLA-DR4- and H2-D^b-restricted NY-BR-1 epitopes, the NY-BR-1 specific T cells that had been induced following tumor transplantation could be stimulated to secrete IFNγ (Figure 25B). This confirms the induction of anti-NY-BR-1 immune responses against EO771/NY-BR-1 transfectants and thus, the delayed tumor growth can be attributed to anti-NY-BR-1 immune responses. Since the EONY tumors are not rejected, the model can still be used to answer the questions that we had raised.

Various tumor models that have been established rely on exogenous antigens which are not expressed by the recipient mice. An example being the chicken ovalbumin protein (OVA) which is extensively used as a model antigen in diverse murine tumor models of melanoma (237), lymphoma (238) and breast carcinoma (239) to name a few . Both $CD8^+$ (240) and $CD4^+$ T cell epitopes (241) of OVA have been identified facilitating the generation of TCR transgenic mice for both $CD8^+$ (242) and $CD4^+$ (243) T cells which makes it an attractive model antigen to study anti-tumor immune responses (244), the role of the tumor microenvironment (239, 245) and mechanisms of action of immune checkpoint blockade (245, 246) in detail. However, it has also shown immunogenicity like NY-BR-1 in our model and OVA expressing transfectants had delayed tumor growth compared to the parental tumor cell line *in vivo* (247, 248). We observed that high NY-BR-1 expressing clone EONY#9 led to slower developing tumors compared to EONY#17 which had intermediate expression (Figure14A). Interestingly, similar results have been reported for OVA expressing colon carcinoma cell line MC38 and transplantation of high OVA expressing transfectants resulted in tumor rejection (David Esiel, 249) whereas MC38-OVA transfectants with lower OVA expression gave rise to progressively growing tumors *in vivo* (248). On the other hand, other tumor models where the growth rate of cells expressing OVA was not affected significantly compared to parental cell lines have also been described (250). Irrespective of these differences in the growth behavior of OVA expressing tumor cell lines, tumor models expressing OVA have been valuable for investigating mechanisms involved in anti-tumor immunity. Thus, clone EONY #17 with intermediate NY-BR-1 expression which could give rise to tumors and was not highly suppressed as the EONY#9 clone was suitable for transplantation experiments.

6.1.2 Loss of NY-BR-1 expression *in vivo* and *in vitro*

NY-BR-1 expression could be detected in lysates from only 50% of resected D8P3 tumors by Western blot and qRT-PCR (Figure 9B, C). Inhibition of the proteasome revealed that D8P3 cells have a high turnover of NY-BR-1 which results in low amounts of detectable protein (Figure 9D). It has been demonstrated that tumor antigen can be processed and CTL epitopes derived thereof are presented despite lack of detectable protein (251). Therefore, even though NY-BR-1 protein could not be detected in EL4/NY-BR-1 transfectant clone D8P3 derived tumors due to rapid turnover as demonstrated by enhanced NY-BR-1 detection following proteasome inhibition (Figure 9D); it does not necessarily mean that NY-BR-1 expression is lost.

Besides, tumors are known to be infiltrated with various immune cells (70) and stromal cells (252, 253) and can form a significant proportion of the tumor. For example, T cell and myeloid cell infiltration in EL4 tumors have been studied (254). Thus, lysates from resected tumors which contain many other cell types might have had low amount of NY-BR-1 among the total protein which made its detection challenging. However, it is possible that NY-BR-1 expression was lost *in vivo* as it is well known that antigen loss variants can arise due to mutations in tumors (255) or due to the selection pressure exerted by the immune system (256, 257). Antigen negative tumor cells can outgrow antigen positive cells as they are not susceptible to T cell mediated killing which relies on antigenic epitopes being presented in the context of MHC molecules. Immune cells like tumoricidal macrophages which cannot distinguish between antigen positive and antigen negative tumors *in vitro* fail to control the outgrowth of antigen loss variants *in vivo* (258). Additionally, inflammatory factors like TNFα present in the tumor microenvironment can induce dedifferentiation of melanoma cells resulting in transient loss of tumor antigens (259). Since NY-BR-1 is also a differentiation antigen, it might be similarly regulated in patients. However, it is unlikely that NY-BR-1 expression was lost *in vivo* as a result of similar mechanisms as it was expressed under the control of a constitutive promoter in our model.

EONY#19 lost its expression after prolonged *in vitro* culture. The loss of gene expression in transfectant clones is not uncommon and has been attributed to a variety of factors including epigenetic downregulation of genes encoded by exogenous transcription units (260). For example, neomycin resistance gene can silence transgenes under the specific viral promoters like SV40 and MPVS promoters (261). We used linearized pcDNA3.1(-) plasmid in which CMV promoter drives the expression of NY-BR-1 and Zeocin resistance gene. Thus, similar mechanisms might be responsible in the silencing of NY-BR-1 expression in EONY#19 clone. Since, the site of integration might play a role as well and transfected DNA can integrate at any genetic locus (262), other clones might not have been affected.

6.1.3 Dominance of NY-BR-1-specific $CD4^+$ T cells *in vitro*

Upon peptide immunization of HLA-DR3tg mice with the 15 mer HLA-DR3-restricted epitope #9017, both NY-BR-1 specific $CD8^+$ T and $CD4^+$ T cell responses could be detected (Gardyan, unpublished). This led us to hypothesis that a H2-D^b- or H2-K^b-restricted epitope was contained within the HLA-DR3 restricted epitope. Using the SYFPEITHI data base for *in silico* predictions, we could predict a 9 mer H2-D^b- restricted epitope (peptide#6) contained within the 15 mer. It was later confirmed as H2-D^b-restricted epitope by *in vitro* experiments. In order to generate a CTL line for this epitope, splenocytes from HLA-DR3 mice immunized with the synthetic peptide were restimulated with irradiated EL4/NY-BR-1 transfectant clone

D8P3 along with irradiated syngeneic feeder cells. EL4/NY-BR-1 transfectant clone D8P3 should have been ideal for restimulation of $CD8^+$ T cells as they do not express MHC II (even under IFNγ stimulation). Still, this restimulation protocol resulted in selective expansion of $CD4^+$ T cells (Figure 18C) which was unexpected. A possible explanation could be that irradiated D8P3 which were added as stimulator cells released NY-BR-1 specific processed $CD4^+$ T cell epitopes while they died and this was binding to the HLA-DR3 molecules of the feeder cells. Since peptide #6 is contained within an HLA-DR3 epitope (peptide #9017); peptide #6 might represent the core sequence of #9017 and could bind to HLA-DR3 on remaining feeder cells and stimulate the $CD4^+$ T cells to secrete IFNγ (Figure 18C, D). The MHC II molecules binds peptides with a length of approx. 15 amino acids that associate through a core sequence of about nine residues with the allele specific peptide binding groove (59, 62). Surprisingly, $CD8^+$ T cells labeled with the NY- NR-1specifc H2-D^b-dextramer that were sorted still developed into a mixed culture of $CD8^+$ and $CD4^+$ T cells. These cell lines were obtained from C57BL/6 mice immunized with Ad.NY-BR-1 and stimulated with feeder cells from C57BL/6 mice and irradiated D8P3 cells and it was not expected that $CD4^+$ T cells could be stimulated by the 9 mer core sequence presented on I-A^b molecule. Therefore, it can be assumed that peptide #6 binds not only the HLA-DR3 molecule, but also to the I-A^b molecule. T cell epitopes that are restricted by various MHC molecules and are thus called promiscuous T cell epitopes have been described previously for both MHC I (263) and MHC II (264, 265) molecules. Promiscuous T cell epitopes can also bind different MHC molecules from different species as demonstrated by the identification of a Trp2 epitope which is restricted by both, the human HLA-A*0201 and the murine H2-K^b molecule (263). Similar cross-species MHC II binding epitopes have been identified for malarial parasite derived protein (266). Promiscuous $CD4^+$ T cell epitopes (267) are frequent among HLA-DR restricted epitopes because the allele specific binding motifs of MHC II molecules are more degenerated compared to that of the MHC I system (59, 62). Thus, passively released epitopes from irradiated D8P3 cells might have been presented in the context of I-A^b by irradiated feeder cells, thereby predominantly stimulating $CD4^+$ T cells among the responding splenocytes. Regarding the CTL responses against peptide #6, binding affinity of this peptide had been determined in peptide binding assays to be quite high (Figure 20A) meaning that even small amounts of passively released epitopes could have been mutually presented by H2D^b- molecules expressed on CTLs and feeder cells possibly resulting in overstimulation of the antigen specific $CD8^+$ T cells and finally in their activation induced cell death (AICD) (268, 269).

6.1.4 First NY-BR-1 expressing tumor model

We successfully established what is to our best knowledge, the first NY-BR-1 expressing tumor model. We could demonstrate that NY-BR-1 expressing tumors could elicit an immune response against already published HLA-DR4- restricted $CD4^+$ T cell epitopes and the newly identified H2-D^b-resctricted $CD8^+$ T cells epitopes (Figure 25). Thus, this model would allow the investigation of NY-BR-1 as a candidate for therapeutic vaccination approaches like DC vaccination, peptide vaccination or adenovirus immunization. We already demonstrated that immunization with Ad.NY-BR-1 successfully induced anti-tumor immunity and was able to suppress tumor growth when immunization was performed before tumor inoculation (Figure 29). Our model can also be used to ascertain the efficacy of adenovirus immunization against NY-BR-1 in mice with pre-existing tumors. The success of such therapeutic immunization has clinical implications as recombinant adenoviral vectors have been safely

used as vaccines against prostate cancer (270, 271) and tuberculosis (272) and this would pave the way for the trial of adenoviral vaccines against breast cancer.

We also established EONY MHC I KO cells which could act as parental lines for transfection of human MHC I molecules. For example, these cells transfected to express the HLA-A2 molecule could be used to transplant HLA-transgenic mice which co-express HLA-A2 and HLA-DR4 (273) and the effect of peptide vaccination using previously identified HLA-A2 restricted $CD8^+$ T cell epitopes (101) and HLA-DR4 restricted $CD4^+$ T cell epitopes (102) could be investigated. This would not only allow us to evaluate the potential of peptide vaccination strategies in NY-BR-1 positive patients but also allow us to study the synergistic effect of NY-BR-1 specific $CD8^+$ and $CD4^+$ T cells in controlling NY-BR-1 expressing tumors. Peptide vaccination studies using synthetic long peptides which induce both $CD4^+$ and $CD8^+$ T cell response have been shown to perform better than short peptide vaccines which only induce CTL response (119) as $CD4^+$ T cell derived IL-2 might break tolerance against self-antigen, allowing enhanced anti-tumor effect of $CD8^+$ T cells (210). $CD4^+$ T cells not only support $CD8^+$ T cell function by facilitating secondary expansion and memory formation (103, 274), but also are capable of mediating tumor rejection by mechanisms independent of $CD8^+$ T cell function (275, 276). Besides T cells, NK cells also demonstrate cytotoxic effects on tumor cells as MHC I downregulation is a commonly observed phenomena in malignant cells of various tumor types including melanoma, colorectal carcinoma, cervical carcinoma and small cell lung carcinoma which allows them to evade T cell mediated destruction (277, 278) but make them susceptible to NK cells (226). The MHC I knockout cells we generated were also susceptible to NK cell recognition (Figure 16B, C) thereby allowing us to use this model for studying the role of NK cell mediated response in breast cancer. EO771 cells have been used for orthotopic transplantation of breast cancer (279, 280). However, we were unable to establish an orthotopic mouse model due to the development of necrosis. Thus, we adopted subcutaneous injection in the right flank as a lot of other tumor models including those for pancreatic cancer and colorectal cancer also rely on non-orthotopic tumor transplantation.

6.2 Modulation of macrophages by $CD4^+$ T cells

6.2.1 EONY tumors are highly infiltrated by TAMs

Breast cancer is known to be highly infiltrated with macrophages which generally correlated with poor prognosis (191, 193-195, 281). In our model we saw similar results and macrophages were the most abundant population among tumor-infiltrating leukocytes. We observed that more than 40% of all $CD45^+$ cells within the tumor were in fact $CD11b^+F4/80^+$ macrophages and in some cases the percentage was as high as 70% (Figure 26B). Similar infiltration levels have been reported in transplanted 4T1 tumor cells which are of BALB/c origin and $CD11b^+$ cells constituted up to 86% of tumor infiltrating leukocytes (282). This was in contrast to another study which showed that TAMs make about 33% of $CD45^+$ cells in EO771 tumors; although it is important to keep in mind they defined macrophages by another set of markers (283). Whereas the proportion of macrophages in the spontaneous model of breast cancer MMTV PYMT was reported to be 80% of $CD45^+$ cells (283) which again is in contrast to the reported proportion of TAMs in large PyMT tumors which are infiltrated with approximately 40% TAMs (284) which is again using another set of markers.

It appears interesting that the EONY tumors had a higher frequency of infiltrating macrophages compared to EO771 tumors (Figure 26B). The percentage of infiltrating TAMs have been shown to increase with increasing tumor size in the MMTV-PyMT tumor model

(284); however, we saw the reverse trend as smaller EONY tumors had larger proportions of infiltrating TAMs (Figure 26B), even though we could not find a significant correlation between tumor size and percentage of TAMs. EONY tumors were not only immunogenic and induced antigen specific $CD8^+$ T cell response (Figure 25) but also recruited more macrophages into the tumor (Figure 26B). Interestingly, successful vaccination using SLP against HPV 16 derived E7 induced regression of TC-1 tumors and was accompanied by enhanced infiltration of antigen specific CTLs and macrophages (285). The increased macrophage recruitment into the shrinking tumors was dependent on $CD8^+$ T cells and could be abrogated by depleting the $CD8^+$ T cells with antibody (285). Another vaccination approach in the same tumor model showed increased macrophage infiltration following vaccination and demonstrated that T cell infiltration follows myeloid cells (286). Both studies highlighted the importance of the recruited macrophages in mediating tumor regression as disruption of CSF-1R signaling abolished the efficacy of the vaccine (285, 286). In our model as well, immunization with adenovirus not only suppressed tumor growth but also induced an M1-like phenotype among TAMs and resulted in upregulation of HLA-DR4 expression levels on intratumoral macrophages (Figure 30A). Antigen specific $CD4^+$ T cells were also induced in NY-BR-1 expressing tumor bearing mice and they have been reported to activate TAMs in the tumor microenvironment to upregulate MHC II (209, 215) which might explain why the TAMs in the EONY tumors resembled a more M1-like phenotype compared to those from parental TAMs (Figure 30A, B).

6.2.2 Modulation of macrophages by NY-BR-1 specific CD4+ T cells

As mentioned earlier, intratumoral accumulation of TAMs is associated with bad prognosis; hence TAMs have emerged as a target for anti-cancer therapies (287). Therapeutic targeting of TAMs relies on blockage of their recruitment into the tumor as well as their elimination, or on their re-polarization towards a less immunosuppressive phenotype (287). It has been shown in a myeloma model that tumor infiltrating macrophages isolated from murine multiple myeloma cell line (MOPC) derived tumors could activate proliferation of $CD4^+$ T cells when co-cultured with tumor antigen specific $CD4^+$ T cells. These results indicate that the TAMs had taken up the tumor antigen *in vivo* and could present tumor antigen derived epitopes to the $CD4^+$ T cells in the context of MHC II (209, 214). The tumor antigen in this model was the idiotype specific (Id) peptide from the secreted immunoglobulin (Ig) L chain V region. The activated $CD4^+$ T cells secreted IFNγ which in turn activated the macrophages resulting in upregulation of MHC II on the TAMs (214) thereby enhancing their tumor-suppressive properties (209).

In our model we wanted to investigate if NY-BR-1 specific $CD4^+$ T cells would also recognize NY-BR-1 antigen derived epitopes presented in the context of MHC II molecules on the surface of TAMs isolated from NY-BR-1 expressing tumors. However, in our model, $CD11b^+$ cells isolated from NY-BR-1 expressing EONY #17 tumors did not stimulate NY-BR-1 specific $CD4^+$ T cells to a higher extent compared to those derived from parental tumors devoid of NY-BR-1 expression (Figure 31). This was not due to the lack of sufficient HLA-DR4 expression on cell surface, as the addition of the peptide to the co-culture effectively stimulated the $CD4^+$ T cells to secrete IFNγ (Figure 31). This does not necessarily mean that NY-BR-1 was not taken up by the TAMs, processed and presented on their cell surface. The half-life of peptide-MHC II complex can vary a lot and it has been reported that the half-life of HLA-DR*0401 binding to various HLA-DR4*0401- restricted epitopes varied between 1 hour to several days (288, 289). Importantly, immune-dominant peptide/HLA-DR4 complexes are

described to have a dissociation half-life varying between 1 hour to several days, whereas non-immunodominant ones showed a dissociation half-life of less than 30 minutes at 37°C (288, 289). The prediction algorithm NetMHCII (290, 291) generates predicted IC_{50} values (in nM) as a measure of binding affinities of peptides to different MHC molecules. IC_{50} is the concentration of the query peptide (in this case the epitope) which inhibits 50% of a reference peptide binding. Peptides with binding affinities of less than 50nM are considered to be strong binding peptides (292) since those peptides are more likely to remain bound to the MHC molecule. Using the NetMHCII algorithm, the binding affinities of the $CD4^+$ T cell epitopes for peptides #8862 and #9251 to the HLA-DR*0401 molecule were predicted to be 1200 nM and 340 nM, respectively (290, 291) indicating that the half-lives of these peptide-MHC complexes were likely to be short as well. In our model the sample preparation included enzymatic digestion of 1 hour followed by mechanical disruption, Ficoll gradient density centrifugation and MACS isolation which summed up to approximately 3-4 hours. Thus, the TAMs were not in contact with the dying tumor cells during the final 2-3 hours of sample preparation and there were no peptides to replace the ones exiting the pMHC complex. Since empty MHC molecules (MHC molecules not bound to peptides) are known to be internalized quickly (293), one possible explanation might be that the empty MHC II molecule was internalized during sample preparation.

Another reason for lack of TAM recognition by NY-BR-1 specific $CD4^+$ T cells could be that the density of HLA-DR4 molecules presenting the antigenic epitope was too low. Furthermore, the affinity of the $CD4^+$ T cell lines employed might have been insufficient. We showed for both $CD4^+$ T cell lines tested, that peptide concentration below 50 ng/ml was insufficient to induce an IFNγ response (Figure 23B). It has been shown that secreted antigen is better than non-secreted antigen for antigen uptake by TAMs resulting in activation of $CD4^+$ T cells (215) as high concentration of the tumor specific antigen facilitates its uptake. If NY-BR-1 expression was indeed lost *in vivo* and antigen negative breast cancer cells dominated the tumor, the local concentration of NY-BR-1 would not have been enough for TAMs to take it up.

To circumvent the aforementioned issues, we used *in vitro* polarized PECs loaded with synthetic peptide or tumor cell lysates as a surrogate for tumor infiltrating TAMs to study the effect of antigen specific interaction with $CD4^+$ T cells. We demonstrated that interaction of M2-polarized macrophages co-cultured with NY-BR-1 specific $CD4^+$ T cells could re-polarize these macrophages towards an M1 like phenotype *in vitro* (Figure 32). This is in agreement with published reports which show that human M2 polarized macrophages loaded with synthetic peptide *in vitro* (213) or murine tumor infiltrating macrophages which have taken up antigen *in vivo* (214, 215) can be instructed by antigen specific $CD4^+$ T cells to become less immunosuppressive as a result of IFNγ secretion by $CD4^+$ T cells. It is important to keep in mind that only when soluble peptide was loaded onto the PECs, detectible levels of IFNγ were secreted by our $CD4^+$ T cell lines resulting in upregulation HLA-DR4 expression and enhanced iNOS production, as detected by FACS (Figure 32 A,C). However, when tumor lysates were used; neither IFNγ secretion nor any increase in surface expression of HLA-DR4 or iNOS production could be detected (Figure32 A, C). Changes in macrophage polarization upon incubation with tumor lysates could only be seen at the transcriptional level. Tumor lysates comprise of other cellular proteins and the effective concentration of NY-BR-1-specific $CD4^+$ T cell epitopes within the lysates might have been below the detection limit of 50 ng/ml required for recognition by the NY-BR-1 specific $CD4^+$ T cell lines (Figure 23B).

Insufficient tumor uptake by macrophages can be overcome by the use of CD47 blocking antibody since CD47 which is also known as the 'don't eat me signal' allows tumors to evade phagocytosis (294). The downside of using this antibody is that, in spite of enhanced phagocytosis of tumor cells, macrophages did not prime $CD4^+$ T cells in the colon cancer model which was tested (294). Thus their capacity to present NY-BR-1 derived epitopes to $CD4^+$ T cells would need to be established in our model. However, switch in polarization of TAMs loaded with EONY#17 lysates following interaction with $CD4^+$ T cell lines #8862 and #9251 highlights two aspects, first the two epitopes are naturally processed in the EONY tumor cells or in the PECs after they had taken up the NY-BR-1 protein contained within the tumor lysates. Second, effective tumor lysis *in vivo* resulting in passive release of tumor antigen, might allow TAMs to take up and process NY-BR-1 protein and present epitopes to $CD4^+$ T cells stimulating them to secrete IFNγ which in turn could start their repolarization process towards an M1-like phenotype. Thus, it might be necessary to increase local levels of antigen within the tumor for TAMs to take it up. For example, chemotherapy and radiation therapy has been shown to result in immunogenic cell death (295) which augments uptake of dying cells by antigen presenting cells (296). It has been demonstrated that low dose irradiation can also induce CTL against tumor antigens and when combined with Th1 therapy it had synergistic effects in controlling tumor growth (297). Hence it would be interesting to combine low dose irradiation and antigen specific $CD4^+$ T cell therapy and study changes in TAM polarization. However, it should be kept in mind that low dose irradiation can reprogram TAMs towards an M1-like phenotype (150); thus, it would be necessary to delineate the contribution of irradiation and the antigen specific $CD4^+$ T cells on the polarization of TAMs.

Repolarization of TAMs using antigen specific $CD4^+$ T cells might be interesting to study in a clinical setting as it might be superior to other approaches used for therapeutic targeting of TAMs. For example, blocking macrophage recruitment into the tumors using a CCL2 blocking antibody was beneficial in the beginning and delayed tumor progression but resulted in aggressive metastasis following cessation of therapy (298) and did not show clinical benefit (201). Also, CSF1R antibody is known to deplete macrophages and was shown to be effective (199, 299). However, it has some undesirable side-effects like accumulation of pro-tumorigenic neutrophils (300, 301). Thus, it is better to re-program the macrophages than to just block their recruitment or deplete them completely and antigen specific $CD4^+$ T cells might be able to do so.

6.2.3 Depletion of $CD4^+$ T cells

We could show that peptide/tumor lysate loaded M2-polarized PECs could be re-polarized *in vitro* upon interaction with NY-BR-1 specific $CD4^+$ T cells and there are published reports documenting the role of antigen specific $CD4^+$ T cells in repolarizing TAMs (209, 214). Thus we hypothesized that antigen specific $CD4^+$ T cells induced by immunization were responsible for the shift in polarization towards M1 like TAMs and that depleting them should counteract the positive effect of adenovirus immunization (Figure 30). However, we observed that depletion of $CD4^+$ T cells in mice immunized with Ad.NY-BR-1 prior to tumor cell injection, resulted in an even less immunosuppressive TAM phenotype. This was unexpected because in our model we saw that immunization with adenovirus resulted in antigen specific response including NY-BR-1 specific $CD4^+$ effector T cells (Figure 20F), which was accompanied by upregulation of M1-associated markers (Figure 33 D,E). However tumor derived factors like VEGFA, IL-10 and PGE2 can induce the expression of FasL on tumor endothelium which results in the selective killing of T effector cells but not of Tregs (302).

This prevents infiltration of effector T cells in the tumor while Tregs preferentially accumulate in the tumor (302). The strong tumor-suppressive effects of $CD4^+$ T cell depletion in our study suggests that majority of the $CD4^+$ T cells in our model might have had tumor-promoting properties. Thus, failure of immunization induced $CD4^+$ T cells to infiltrate the tumor might explain why $CD4^+$ T cell depletion inhibited tumor progression irrespective of successful immunization. Besides Tregs, Th2 cells have been described to have tumor promoting activity as well. For example, the mammary tumors of MMTV-PyMT mice were shown to be infiltrated with IL-4 producing Th2 cells which can induce M2-like phenotype in the TAMs thereby promoting metastasis (303). Antibody mediated elimination of $CD4^+$ T cells in a melanoma model resulted in abolishment of Th2 cytokines but not Th1 cytokines in the tumor and was accompanied by enhanced anti-tumor immunity (304). Additionally, anti-CD4 antibody can also deplete immunosuppressive CD4 expressing regulatory T cells which can be recruited by CCL22 and result in poor prognosis (305). Antibody mediated depletion of $CD4^+CD25^+Foxp3^+$ Tregs and a subset of pDCs which is known to have immunosuppressive phenotype has been reported to result in delayed tumor growth (306). In this case however, the anti-tumor effect was mediated by $CD8^+$ T cells (306). Depletion of intratumoral $CD4^+CD25^+$ T cells during effector phase can cause tumor regression possibly via depletion of IL-10 and TGF-β in the tumor (307). Another study underscoring the immunosuppressive role $CD4^+$ T cells in breast cancer showed that inhibiting the recruitment of naïve $CD4^+$ T cells which eventually differentiate into Tregs resulted in delayed tumor growth (308).Taken together, it can be concluded that $CD4^+$ T cells infiltrating EONY tumors have immunosuppressive properties.

The impact of $CD4^+$ T cell infiltration on breast cancer prognosis depends on their phenotype. Th1 cells which can produce Th1 cytokines like IFNγ are normally associated with successful anti-tumor immunity by enhancing the performance of $CD8^+$ T cells (309) or by directly suppressing tumor cell growth (310). In breast cancer, high Treg infiltration usually correlates with poor prognosis (83, 305, 311, 312) due to their immunosuppressive phenotype. There are exceptions where high infiltration of $Foxp3^+$ Tregs in breast cancer specimen was accompanied by elevated number of $CD8^+$ TILs and correlated with good prognosis (84). Th2 cells have an immunosuppressive phenotype and promote tumor metastasis by inducing M2-like TAMs (303). However, a recent study showed that adoptively transferred Th2 cells can lead to tumor regression (313). Thus, detailed characterization of $CD4^+$ T cell phenotype and their function in tumor progression needs to be done before targeting $CD4^+$ T cells for depletion as a strategy for cancer therapy. In our model, the endogenous T cells seemed to have tumor promoting Th2 like phenotype as their abrogation resulted in less aggressive tumor growth and the infiltrating macrophages resembled M1-like macrophages.

6.3 Summary and outlook

To summarize, we could successfully generate the first NY-BR-1 expressing transplantable tumor model in which we could validate the newly identified $CD8^+$ T cell epitopes and the already known $CD4^+$ T cells. We also generated MHC I knockout cell lines which would allow us to study NK cells mediated immune responses and the synergism between $CD4^+$ and $CD8^+$ T cells following peptide vaccination. We showed the efficacy of adenovirus immunization in generating a $CD8^+$ and $CD4^+$ T cell response, in controlling tumor growth and in repolarizing TAMs. *In vitro* studies with PECs showed that $CD4^+$ T cells can re-polarize M2-like macrophages loaded with the cognate peptide but we could not demonstrate the same effect *in vivo*.

7 References

1. Weinberg RA. The Biology of Cancer. 2nd ed: Garland Science; 2013 May 15, 2013. 960 p.
2. Aguilera A, García-Muse T. Causes of Genome Instability. Annual Review of Genetics. 2013;47(1):1-32.
3. Ferlay J, Soerjomataram I, Dikshit R, Eser S, Mathers C, Rebelo M, et al. Cancer incidence and mortality worldwide: Sources, methods and major patterns in GLOBOCAN 2012. International Journal of Cancer. 2015;136(5):E359-E86.
4. Bray F, McCarron P, Parkin DM. The changing global patterns of female breast cancer incidence and mortality. Breast Cancer Research. 2004;6(6):229.
5. Society AC. Global Cancer Facts & Figures 3rd Edition. 2015.
6. Cuzick J, Powles T, Veronesi U, Forbes J, Edwards R, Ashley S, et al. Overview of the main outcomes in breast-cancer prevention trials. The Lancet. 2003;361(9354):296-300.
7. Cuzick J. Aromatase Inhibitors in Prevention — Data from the ATAC (Arimidex, Tamoxifen Alone or in Combination) Trial and the Design of IBIS-II (the Second International Breast Cancer Intervention Study). In: Senn H-J, Morant R, editors. Tumor Prevention and Genetics. Berlin, Heidelberg: Springer Berlin Heidelberg; 2003. p. 96-103.
8. Munsell MF, Sprague BL, Berry DA, Chisholm G, Trentham-Dietz A. Body Mass Index and Breast Cancer Risk According to Postmenopausal Estrogen-Progestin Use and Hormone Receptor Status. Epidemiologic Reviews. 2014;36(1):114-36.
9. Friedenreich CM. Physical Activity and Breast Cancer: Review of the Epidemiologic Evidence and Biologic Mechanisms. In: Senn H-J, Otto F, editors. Clinical Cancer Prevention. Berlin, Heidelberg: Springer Berlin Heidelberg; 2011. p. 125-39.
10. Key J, Hodgson S, Omar RZ, Jensen TK, Thompson SG, Boobis AR, et al. Meta-analysis of Studies of Alcohol and Breast Cancer with Consideration of the Methodological Issues. Cancer Causes & Control. 2006;17(6):759-70.
11. Singletary SE, Connolly JL. Breast Cancer Staging: Working With the Sixth Edition of the AJCC Cancer Staging Manual. CA: A Cancer Journal for Clinicians. 2006;56(1):37-47.
12. Society AC. Stages of Breast Cancer. 2016.
13. Perou CM, Sørlie T, Eisen MB, van de Rijn M, Jeffrey SS, Rees CA, et al. Molecular portraits of human breast tumours. Nature. 2000;406.
14. Herschkowitz JI, Simin K, Weigman VJ, Mikaelian I, Usary J, Hu Z, et al. Identification of conserved gene expression features between murine mammary carcinoma models and human breast tumors. Genome Biology. 2007;8(5):R76.
15. Prat A, Parker JS, Karginova O, Fan C, Livasy C, Herschkowitz JI, et al. Phenotypic and molecular characterization of the claudin-low intrinsic subtype of breast cancer. Breast Cancer Research. 2010;12(5):R68.
16. Sørlie T, Perou CM, Tibshirani R, Aas T, Geisler S, Johnsen H, et al. Gene expression patterns of breast carcinomas distinguish tumor subclasses with clinical implications. Proceedings of the National Academy of Sciences. 2001;98(19):10869-74.
17. Sørlie T, Tibshirani R, Parker J, Hastie T, Marron JS, Nobel A, et al. Repeated observation of breast tumor subtypes in independent gene expression data sets. Proceedings of the National Academy of Sciences. 2003;100(14):8418-23.
18. Malhotra GK, Zhao X, Band H, Band V. Histological, molecular and functional subtypes of breast cancers. Cancer Biology & Therapy. 2010;10(10):955-60.
19. Parker JS, Mullins M, Cheang MCU, Leung S, Voduc D, Vickery T, et al. Supervised Risk Predictor of Breast Cancer Based on Intrinsic Subtypes. Journal of Clinical Oncology. 2009;27(8):1160-7.
20. Cheang MCU, Chia SK, Voduc D, Gao D, Leung S, Snider J, et al. Ki67 Index, HER2 Status, and Prognosis of Patients With Luminal B Breast Cancer. JNCI Journal of the National Cancer Institute. 2009;101(10):736-50.
21. Nielsen TO, Hsu FD, Jensen K, Cheang M, Karaca G, Hu Z, et al. Immunohistochemical and Clinical Characterization of the Basal-Like Subtype of Invasive Breast Carcinoma. Clinical Cancer Research. 2004;10(16):5367.

22. Rostas JW, Dyess DL. Current Operative Management of Breast Cancer: An Age of Smaller Resections and Bigger Cures. International Journal of Breast Cancer. 2012;2012.
23. Society AC. Surgery for Breast Cancer 2016.
24. Carey LA, Dees EC, Sawyer L, Gatti L, Moore DT, Collichio F, et al. The Triple Negative Paradox: Primary Tumor Chemosensitivity of Breast Cancer Subtypes. Clinical Cancer Research. 2007;13(8):2329.
25. Goldhirsch A, Wood WC, Coates AS, Gelber RD, Thürlimann B, Senn HJ, et al. Strategies for subtypes—dealing with the diversity of breast cancer: highlights of the St Gallen International Expert Consensus on the Primary Therapy of Early Breast Cancer 2011. Annals of Oncology. 2011;22(8):1736-47.
26. Smith IE, Dowsett M. Aromatase Inhibitors in Breast Cancer. New England Journal of Medicine. 2003;348(24):2431-42.
27. Francis PA, Regan MM, Fleming GF, Láng I, Ciruelos E, Bellet M, et al. Adjuvant Ovarian Suppression in Premenopausal Breast Cancer. New England Journal of Medicine. 2015;372(5):436-46.
28. Mauri D, Pavlidis N, Polyzos NP, Ioannidis JPA. Survival With Aromatase Inhibitors and Inactivators Versus Standard Hormonal Therapy in Advanced Breast Cancer: Meta-analysis. Journal of the National Cancer Institute. 2006;98(18):1285-91.
29. Ellis MJ, Llombart-Cussac A, Feltl D, Dewar JA, Jasiówka M, Hewson N, et al. Fulvestrant 500 mg Versus Anastrozole 1 mg for the First-Line Treatment of Advanced Breast Cancer: Overall Survival Analysis From the Phase II FIRST Study. Journal of Clinical Oncology. 2015;33(32):3781-7.
30. Mehta RS, Barlow WE, Albain KS, Vandenberg TA, Dakhil SR, Tirumali NR, et al. Combination Anastrozole and Fulvestrant in Metastatic Breast Cancer. New England Journal of Medicine. 2012;367(5):435-44.
31. Burstein HJ. Novel Agents and Future Directions for Refractory Breast Cancer. Seminars in Oncology. 2011;38, Supplement 2:S17-S24.
32. Baselga J, Campone M, Piccart M, Burris HAI, Rugo HS, Sahmoud T, et al. Everolimus in Postmenopausal Hormone-Receptor–Positive Advanced Breast Cancer. New England Journal of Medicine. 2012;366(6):520-9.
33. Krop IE, Mayer IA, Ganju V, Dickler M, Johnston S, Morales S, et al. Pictilisib for oestrogen receptor-positive, aromatase inhibitor-resistant, advanced or metastatic breast cancer (FERGI): a randomised, double-blind, placebo-controlled, phase 2 trial. The Lancet Oncology. 2016;17(6):811-21.
34. Finn RS, Crown JP, Lang I, Boer K, Bondarenko IM, Kulyk SO, et al. The cyclin-dependent kinase 4/6 inhibitor palbociclib in combination with letrozole versus letrozole alone as first-line treatment of oestrogen receptor-positive, HER2-negative, advanced breast cancer (PALOMA-1/TRIO-18): a randomised phase 2 study. The Lancet Oncology.16(1):25-35.
35. Slamon DJ, Clark GM, Wong SG, Levin WJ, Ullrich A, McGuire WL. Human breast cancer: correlation of relapse and survival with amplification of the HER-2/neu oncogene. Science. 1987;235(4785):177.
36. Slamon DJ, Godolphin W, Jones LA, Holt JA, Wong SG, Keith DE, et al. Studies of the HER-2/neu proto-oncogene in human breast and ovarian cancer. Science. 1989;244(4905):707.
37. Seshadri R, Firgaira FA, Horsfall DJ, McCaul K, Setlur V, Kitchen P. Clinical significance of HER-2/neu oncogene amplification in primary breast cancer. The South Australian Breast Cancer Study Group. Journal of Clinical Oncology. 1993;11(10):1936-42.
38. Claret F, Vu T. Trastuzumab: Updated Mechanisms of Action and Resistance in Breast Cancer. Frontiers in Oncology. 2012;2(62).
39. Slamon DJ, Leyland-Jones B, Shak S, Fuchs H, Paton V, Bajamonde A, et al. Use of Chemotherapy plus a Monoclonal Antibody against HER2 for Metastatic Breast Cancer That Overexpresses HER2. New England Journal of Medicine. 2001;344(11):783-92.
40. Pegram MD, Lipton A, Hayes DF, Weber BL, Baselga JM, Tripathy D, et al. Phase II study of receptor-enhanced chemosensitivity using recombinant humanized anti-

p185HER2/neu monoclonal antibody plus cisplatin in patients with HER2/neu-overexpressing metastatic breast cancer refractory to chemotherapy treatment. Journal of Clinical Oncology. 1998;16(8):2659-71.
41. Swain SM, Baselga J, Kim S-B, Ro J, Semiglazov V, Campone M, et al. Pertuzumab, Trastuzumab, and Docetaxel in HER2-Positive Metastatic Breast Cancer. New England Journal of Medicine. 2015;372(8):724-34.
42. Hurvitz SA, Dalenc F, Campone M, O'Regan RM, Tjan-Heijnen VC, Gligorov J, et al. A phase 2 study of everolimus combined with trastuzumab and paclitaxel in patients with HER2-overexpressing advanced breast cancer that progressed during prior trastuzumab and taxane therapy. Breast Cancer Research and Treatment. 2013;141(3):437-46.
43. Santa-Maria CA, Gradishar WJ. Changing treatment paradigms in metastatic breast cancer: Lessons learned. JAMA Oncology. 2015;1(4):528-34.
44. von Minckwitz G, Schneeweiss A, Loibl S, Salat C, Denkert C, Rezai M, et al. Neoadjuvant carboplatin in patients with triple-negative and HER2-positive early breast cancer (GeparSixto; GBG 66): a randomised phase 2 trial. The Lancet Oncology. 2014;15(7):747-56.
45. Hartman A-R, Kaldate RR, Sailer LM, Painter L, Grier CE, Endsley RR, et al. Prevalence of BRCA mutations in an unselected population of triple-negative breast cancer. Cancer. 2012;118(11):2787-95.
46. Fong PC, Boss DS, Yap TA, Tutt A, Wu P, Mergui-Roelvink M, et al. Inhibition of Poly(ADP-Ribose) Polymerase in Tumors from BRCA Mutation Carriers. New England Journal of Medicine. 2009;361(2):123-34.
47. Kaufman B, Shapira-Frommer R, Schmutzler RK, Audeh MW, Friedlander M, Balmaña J, et al. Olaparib Monotherapy in Patients With Advanced Cancer and a Germline BRCA1/2 Mutation. Journal of Clinical Oncology. 2015;33(3):244-50.
48. O'Shaughnessy J, Schwartzberg L, Danso MA, Miller KD, Rugo HS, Neubauer M, et al. Phase III Study of Iniparib Plus Gemcitabine and Carboplatin Versus Gemcitabine and Carboplatin in Patients With Metastatic Triple-Negative Breast Cancer. Journal of Clinical Oncology. 2014;32(34):3840-7.
49. Miller K, Wang M, Gralow J, Dickler M, Cobleigh M, Perez EA, et al. Paclitaxel plus Bevacizumab versus Paclitaxel Alone for Metastatic Breast Cancer. New England Journal of Medicine. 2007;357(26):2666-76.
50. Janeway CAJ, Travers P, Walport M, Shlomchik MJ. Immunobiology, 5th edition. 2001.
51. Parkin J, Cohen B. An overview of the immune system. The Lancet. 2001;357(9270):1777-89.
52. Arstila TP, Casrouge A, Baron V, Even J, Kanellopoulos J, Kourilsky P. A Direct Estimate of the Human αβ T Cell Receptor Diversity. Science. 1999;286(5441):958-61.
53. Andersen MH, Schrama D, thor Straten P, Becker JC. Cytotoxic T Cells. Journal of Investigative Dermatology. 2006;126(1):32-41.
54. Zhu J, Paul WE. CD4 T cells: fates, functions, and faults. Blood. 2008;112(5):1557-69.
55. Neefjes J, Jongsma MLM, Paul P, Bakke O. Towards a systems understanding of MHC class I and MHC class II antigen presentation. Nat Rev Immunol. 2011;11(12):823-36.
56. Joffre OP, Segura E, Savina A, Amigorena S. Cross-presentation by dendritic cells. Nat Rev Immunol. 2012;12(8):557-69.
57. Schmid D, Pypaert M, Münz C. MHC class II antigen loading compartments continuously receive input from autophagosomes. Immunity. 2007;26(1):79-92.
58. Crotzer VL, Blum JS. Autophagy and its role in MHC-mediated antigen presentation. Journal of immunology (Baltimore, Md : 1950). 2009;182(6):3335-41.
59. Rammensee H-G. Chemistry of peptides associated with MHC class I and class II molecules. Current Opinion in Immunology. 1995;7(1):85-96.
60. Lundegaard C, Lamberth K, Harndahl M, Buus S, Lund O, Nielsen M. NetMHC-3.0: accurate web accessible predictions of human, mouse and monkey MHC class I affinities for peptides of length 8–11. Nucleic Acids Research. 2008;36(Web Server issue):W509-W12.

61. Rammensee H-G, Bachmann J, Emmerich NPN, Bachor OA, Stevanović S. SYFPEITHI: database for MHC ligands and peptide motifs. Immunogenetics. 1999;50(3):213-9.
62. Rammensee H-G, Friede T, Stevanović S. MHC ligands and peptide motifs: first listing. Immunogenetics. 1995;41(4):178-228.
63. Schreiber RD, Old LJ, Smyth MJ. Cancer immunoediting: integrating immunity's roles in cancer suppression and promotion. Science. 2011;331.
64. Swann JB, Smyth MJ. Immune surveillance of tumors. Journal of Clinical Investigation. 2007;117(5):1137-46.
65. Koebel CM, Vermi W, Swann JB, Zerafa N, Rodig SJ, Old LJ, et al. Adaptive immunity maintains occult cancer in an equilibrium state. Nature. 2007;450(7171):903-7.
66. Ramsdell F, Fowlkes BJ. Maintenance of in Vivo Tolerance by Persistence of Antigen. Science. 1992;257(5073):1130-4.
67. den Boer AT, van Mierlo GJD, Fransen MF, Melief CJM, Offringa R, Toes REM. The Tumoricidal Activity of Memory CD8⁺ T Cells Is Hampered by Persistent Systemic Antigen, but Full Functional Capacity Is Regained in an Antigen-Free Environment. The Journal of Immunology. 2004;172(10):6074-9.
68. Jiang Y, Li Y, Zhu B. T-cell exhaustion in the tumor microenvironment. Cell death & disease. 2015;6:e1792.
69. Jochems C, Schlom J. Tumor-infiltrating immune cells and prognosis: the potential link between conventional cancer therapy and immunity. Experimental biology and medicine (Maywood, NJ). 2011;236(5):567-79.
70. Galon J, Costes A, Sanchez-Cabo F, Kirilovsky A, Mlecnik B, Lagorce-Pagès C, et al. Type, Density, and Location of Immune Cells Within Human Colorectal Tumors Predict Clinical Outcome. Science. 2006;313(5795):1960-4.
71. Galon J, Mlecnik B, Bindea G, Angell HK, Berger A, Lagorce C, et al. Towards the introduction of the 'Immunoscore' in the classification of malignant tumours. The Journal of Pathology. 2014;232(2):199-209.
72. Dushyanthen S, Beavis PA, Savas P, Teo ZL, Zhou C, Mansour M, et al. Relevance of tumor-infiltrating lymphocytes in breast cancer. BMC Medicine. 2015;13(1):202.
73. Mahmoud S, Paish E, Powe D, Macmillan R, Grainge M, Lee A. Tumor-infiltrating CD8+ lymphocytes predict clinical outcome in breast cancer. J Clin Oncol. 2011;29.
74. Liu S, Lachapelle J, Leung S, Gao D, Foulkes WD, Nielsen TO. CD8+ lymphocyte infiltration is an independent favorable prognostic indicator in basal-like breast cancer. Breast Cancer Res. 2012;14.
75. Denkert C, Minckwitz G, Brase JC, Sinn BV, Gade S, Kronenwett R. Tumor-infiltrating lymphocytes and response to neoadjuvant chemotherapy with or without carboplatin in human epidermal growth factor receptor 2-positive and triple-negative primary breast cancers. J Clin Oncol. 2015;33.
76. Denkert C, Loibl S, Noske A, Roller M, Muller BM, Komor M. Tumor-associated lymphocytes as an independent predictor of response to neoadjuvant chemotherapy in breast cancer. J Clin Oncol. 2010;28.
77. Seo AN, Lee HJ, Kim EJ, Kim HJ, Jang MH, Lee HE. Tumour-infiltrating CD8+ lymphocytes as an independent predictive factor for pathological complete response to primary systemic therapy in breast cancer. Br J Cancer. 2013;109.
78. Loi S, Michiels S, Salgado R, Sirtaine N, Jose V, Fumagalli D. Tumor infiltrating lymphocytes are prognostic in triple negative breast cancer and predictive for trastuzumab benefit in early breast cancer: results from the FinHER trial. Ann Oncol. 2014;25.
79. Yu H, Yang J, Jiao S, Li Y, Zhang W, Wang J. T-box transcription factor 21 expression in breast cancer and its relationship with prognosis. Int J Clin Exp Pathol. 2014;7.
80. Teschendorff AE, Gomez S, Arenas A, El-Ashry D, Schmidt M, Gehrmann M, et al. Improved prognostic classification of breast cancer defined by antagonistic activation patterns of immune response pathway modules. BMC Cancer. 2010;10(1):604.
81. Gu-Trantien C, Loi S, Garaud S, Equeter C, Libin M, Wind A. CD4(+) follicular helper T cell infiltration predicts breast cancer survival. J Clin Invest. 2013;123.

82. Qi W, Huang X, Wang J. Correlation between Th17 cells and tumor microenvironment. Cellular Immunology. 2013;285(1–2):18-22.
83. Bates GJ, Fox SB, Han C, Leek RD, Garcia JF, Harris AL, et al. Quantification of Regulatory T Cells Enables the Identification of High-Risk Breast Cancer Patients and Those at Risk of Late Relapse. Journal of Clinical Oncology. 2006;24(34):5373-80.
84. West NR, Kost SE, Martin SD, Milne K, Deleeuw RJ, Nelson BH. Tumour-infiltrating FOXP3(+) lymphocytes are associated with cytotoxic immune responses and good clinical outcome in oestrogen receptor-negative breast cancer. Br J Cancer. 2013;108.
85. Martínez-Lostao L, Anel A, Pardo J. How Do Cytotoxic Lymphocytes Kill Cancer Cells? Clinical Cancer Research. 2015;21(22):5047-56.
86. Matsuzaki J, Tsuji T, Luescher IF, Shiku H, Mineno J, Okamoto S, et al. Direct tumor recognition by a human CD4+ T-cell subset potently mediates tumor growth inhibition and orchestrates anti-tumor immune responses. Scientific Reports. 2015;5:14896.
87. Haabeth OAW, Tveita AA, Fauskanger M, Schjesvold F, Lorvik KB, Hofgaard PO, et al. How Do CD4(+) T Cells Detect and Eliminate Tumor Cells That Either Lack or Express MHC Class II Molecules? Frontiers in Immunology. 2014;5:174.
88. Andersen RS, Thrue CA, Junker N, Lyngaa R, Donia M, Ellebæk E, et al. Dissection of T-cell Antigen Specificity in Human Melanoma. Cancer Research. 2012;72(7):1642-50.
89. Kvistborg P, Shu CJ, Heemskerk B, Fankhauser M, Thrue CA, Toebes M, et al. TIL therapy broadens the tumor-reactive CD8(+) T cell compartment in melanoma patients. Oncoimmunology. 2012;1(4):409-18.
90. Gubin MM, Zhang X, Schuster H, Caron E, Ward JP, Noguchi T, et al. Checkpoint blockade cancer immunotherapy targets tumour-specific mutant antigens. Nature. 2014;515(7528):577-81.
91. Srinivasan R, Wolchok JD. Tumor antigens for cancer immunotherapy: therapeutic potential of xenogeneic DNA vaccines. Journal of Translational Medicine. 2004;2:12-.
92. Kufe DW, Holland JF, Frei E, American Cancer S. Holland - Frei Cancer medicine 6. Hamilton, Ont.; Lewiston, NY: BC Decker [distributor]; 2003.
93. Van den Eynde BJ, van der Bruggen P. T cell defined tumor antigens. Current Opinion in Immunology. 1997;9(5):684-93.
94. Jäger D, Stockert E, Güre AO, Scanlan MJ, Karbach J, Jäger E, et al. Identification of a Tissue-specific Putative Transcription Factor in Breast Tissue by Serological Screening of a Breast Cancer Library. Cancer Research. 2001;61(5):2055-61.
95. Jäger D, Karbach J, Pauligk C, Seil I, Frei C, Chen Y-T, et al. Humoral and cellular immune responses against the breast cancer antigen NY-BR-1: Definition of two HLA-A2 restricted peptide epitopes. Cancer Immunity Archive. 2005;5(1).
96. Varga Z, Theurillat J-P, Filonenko V, Sasse B, Odermatt B, Jungbluth AA, et al. Preferential Nuclear and Cytoplasmic NY-BR-1 Protein Expression in Primary Breast Cancer and Lymph Node Metastases. Clinical Cancer Research. 2006;12(9):2745-51.
97. Jiang Y, Harlocker SL, Molesh DA, Dillon DC, Stolk JA, Houghton RL, et al. Discovery of differentially expressed genes in human breast cancer using subtracted cDNA libraries and cDNA microarrays. Oncogene. 2002;21(14):2270-81.
98. Seil I, Frei C, Sültmann H, Knauer SK, Engels K, Jäger E, et al. The differentiation antigen NY-BR-1 is a potential target for antibody-based therapies in breast cancer. International Journal of Cancer. 2007;120(12):2635-42.
99. Theurillat J-P, Zürrer-Härdi U, Varga Z, Barghorn A, Saller E, Frei C, et al. Distinct expression patterns of the immunogenic differentiation antigen NY-BR-1 in normal breast, testis and their malignant counterparts. International Journal of Cancer. 2008;122(7):1585-91.
100. Theurillat J-P, Zürrer-Härdi U, Varga Z, Storz M, Probst-Hensch NM, Seifert B, et al. NY-BR-1 protein expression in breast carcinoma: a mammary gland differentiation antigen as target for cancer immunotherapy. Cancer Immunology, Immunotherapy. 2007;56(11):1723-31.
101. Wang W, Epler J, Salazar LG, Riddell SR. Recognition of Breast Cancer Cells by $CD8^+$ Cytotoxic T-Cell Clones Specific for NY-BR-1. Cancer Research. 2006;66(13):6826-33.

102. Gardyan A, Osen W, Zörnig I, Podola L, Agarwal M, Aulmann S, et al. Identification of NY-BR-1-specific CD4+ T cell epitopes using HLA-transgenic mice. International Journal of Cancer. 2015;136(11):2588-97.
103. Janssen EM, Lemmens EE, Wolfe T, Christen U, von Herrath MG, Schoenberger SP. CD4+ T cells are required for secondary expansion and memory in CD8+ T lymphocytes. Nature. 2003;421(6925):852-6.
104. Okada H, Kalinski P, Ueda R, Hoji A, Kohanbash G, Donegan TE, et al. Induction of CD8+ T-Cell Responses Against Novel Glioma–Associated Antigen Peptides and Clinical Activity by Vaccinations With α-Type 1 Polarized Dendritic Cells and Polyinosinic-Polycytidylic Acid Stabilized by Lysine and Carboxymethylcellulose in Patients With Recurrent Malignant Glioma. Journal of Clinical Oncology. 2011;29(3):330-6.
105. Zeis M, Siegel S, Wagner A, Schmitz M, Marget M, Kühl-Burmeister R, et al. Generation of Cytotoxic Responses in Mice and Human Individuals Against Hematological Malignancies Using Survivin-RNA-Transfected Dendritic Cells. The Journal of Immunology. 2003;170(11):5391-7.
106. Van Tendeloo VF, Van de Velde A, Van Driessche A, Cools N, Anguille S, Ladell K, et al. Induction of complete and molecular remissions in acute myeloid leukemia by Wilms' tumor 1 antigen-targeted dendritic cell vaccination. Proceedings of the National Academy of Sciences. 2010;107(31):13824-9.
107. Antonia SJ, Mirza N, Fricke I, Chiappori A, Thompson P, Williams N, et al. Combination of p53 Cancer Vaccine with Chemotherapy in Patients with Extensive Stage Small Cell Lung Cancer. Clinical Cancer Research. 2006;12(3):878-87.
108. Kantoff PW, Higano CS, Shore ND, Berger ER, Small EJ, Penson DF, et al. Sipuleucel-T Immunotherapy for Castration-Resistant Prostate Cancer. New England Journal of Medicine. 2010;363(5):411-22.
109. Rosenberg SA, Restifo NP. Adoptive cell transfer as personalized immunotherapy for human cancer. Science. 2015;348(6230):62-8.
110. Rosenberg SA, Packard BS, Aebersold PM, Solomon D, Topalian SL, Toy ST, et al. Use of Tumor-Infiltrating Lymphocytes and Interleukin-2 in the Immunotherapy of Patients with Metastatic Melanoma. New England Journal of Medicine. 1988;319(25):1676-80.
111. Dudley ME, Wunderlich JR, Robbins PF, Yang JC, Hwu P, Schwartzentruber DJ, et al. Cancer Regression and Autoimmunity in Patients After Clonal Repopulation with Antitumor Lymphocytes. Science. 2002;298(5594):850-4.
112. Rosenberg SA, Yang JC, Sherry RM, Kammula US, Hughes MS, Phan GQ, et al. Durable Complete Responses in Heavily Pretreated Patients with Metastatic Melanoma Using T-Cell Transfer Immunotherapy. Clinical Cancer Research. 2011;17(13):4550-7.
113. Gill S, June CH. Going viral: chimeric antigen receptor T-cell therapy for hematological malignancies. Immunological Reviews. 2015;263(1):68-89.
114. Kochenderfer JN, Wilson WH, Janik JE, Dudley ME, Stetler-Stevenson M, Feldman SA, et al. Eradication of B-lineage cells and regression of lymphoma in a patient treated with autologous T cells genetically engineered to recognize CD19. Blood. 2010;116(20):4099-102.
115. Morgan RA, Dudley ME, Wunderlich JR, Hughes MS, Yang JC, Sherry RM, et al. Cancer Regression in Patients After Transfer of Genetically Engineered Lymphocytes. Science. 2006;314(5796):126-9.
116. Parkhurst MR, Yang JC, Langan RC, Dudley ME, Nathan D-AN, Feldman SA, et al. T Cells Targeting Carcinoembryonic Antigen Can Mediate Regression of Metastatic Colorectal Cancer but Induce Severe Transient Colitis. Molecular Therapy. 2011;19(3):620-6.
117. Kenter GG, Welters MJP, Valentijn ARPM, Lowik MJG, Berends-van der Meer DMA, Vloon APG, et al. Vaccination against HPV-16 Oncoproteins for Vulvar Intraepithelial Neoplasia. New England Journal of Medicine. 2009;361(19):1838-47.
118. Daayana S, Elkord E, Winters U, Pawlita M, Roden R, Stern PL, et al. Phase II trial of imiquimod and HPV therapeutic vaccination in patients with vulval intraepithelial neoplasia. Br J Cancer. 2010;102(7):1129-36.

119. Melief CJM, van Hall T, Arens R, Ossendorp F, van der Burg SH. Therapeutic cancer vaccines. The Journal of Clinical Investigation. 2015;125(9):3401-12.
120. Bagarazzi ML, Yan J, Morrow MP, Shen X, Parker RL, Lee JC, et al. Immunotherapy Against HPV16/18 Generates Potent T_H1 and Cytotoxic Cellular Immune Responses. Science Translational Medicine. 2012;4(155):155ra38.
121. Kim TJ, Jin H-T, Hur S-Y, Yang HG, Seo YB, Hong SR, et al. Clearance of persistent HPV infection and cervical lesion by therapeutic DNA vaccine in CIN3 patients. Nature Communications. 2014;5:5317.
122. Weide B, Pascolo S, Scheel B, Derhovanessian E, Pflugfelder A, Eigentler TK, et al. Direct Injection of Protamine-protected mRNA: Results of a Phase 1/2 Vaccination Trial in Metastatic Melanoma Patients. Journal of Immunotherapy. 2009;32(5):498-507.
123. Rittig SM, Haentschel M, Weimer KJ, Heine A, Muller MR, Brugger W, et al. Intradermal Vaccinations With RNA Coding for TAA Generate CD8+ and CD4+ Immune Responses and Induce Clinical Benefit in Vaccinated Patients. Molecular Therapy. 2011;19(5):990-9.
124. Kreiter S, Vormehr M, van de Roemer N, Diken M, Lower M, Diekmann J, et al. Mutant MHC class II epitopes drive therapeutic immune responses to cancer. Nature. 2015;520(7549):692-6.
125. Kranz LM, Diken M, Haas H, Kreiter S, Loquai C, Reuter KC, et al. Systemic RNA delivery to dendritic cells exploits antiviral defence for cancer immunotherapy. Nature. 2016;534(7607):396-401.
126. Kaufman HL, Kohlhapp FJ, Zloza A. Oncolytic viruses: a new class of immunotherapy drugs. Nat Rev Drug Discov. 2015;14(9):642-62.
127. Cawood R, Hills T, Wong SL, Alamoudi AA, Beadle S, Fisher KD, et al. Recombinant viral vaccines for cancer. Trends in Molecular Medicine. 2012;18(9):564-74.
128. Kantoff PW, Schuetz TJ, Blumenstein BA, Glode LM, Bilhartz DL, Wyand M, et al. Overall Survival Analysis of a Phase II Randomized Controlled Trial of a Poxviral-Based PSA-Targeted Immunotherapy in Metastatic Castration-Resistant Prostate Cancer. Journal of Clinical Oncology. 2010;28(7):1099-105.
129. Andtbacka RHI, Kaufman HL, Collichio F, Amatruda T, Senzer N, Chesney J, et al. Talimogene Laherparepvec Improves Durable Response Rate in Patients With Advanced Melanoma. Journal of Clinical Oncology. 2015;33(25):2780-8.
130. Lu W, Zheng S, Li X-F, Huang J-J, Zheng X, Li Z. Intra-tumor injection of H101, a recombinant adenovirus, in combination with chemotherapy in patients with advanced cancers: A pilot phase II clinical trial. World Journal of Gastroenterology : WJG. 2004;10(24):3634-8.
131. Rosenberg SA. IL-2: The First Effective Immunotherapy for Human Cancer. The Journal of Immunology. 2014;192(12):5451-8.
132. Rosenberg SA, Yang JC, Topalian SL, et al. Treatment of 283 consecutive patients with metastatic melanoma or renal cell cancer using high-dose bolus interleukin 2. JAMA. 1994;271(12):907-13.
133. Smith FO, Downey SG, Klapper JA, Yang JC, Sherry RM, Royal RE, et al. Treatment of Metastatic Melanoma Using Interleukin-2 Alone or in Conjunction with Vaccines. Clinical Cancer Research. 2008;14(17):5610-8.
134. Rosenberg SA, Yannelli JR, Yang JC, Topalian SL, Schwartzentruber DJ, Weber JS, et al. Treatment of Patients With Metastatic Melanoma With Autologous Tumor-Infiltrating Lymphocytes and Interleukin 2. JNCI: Journal of the National Cancer Institute. 1994;86(15):1159-66.
135. Belardelli F, Ferrantini M, Proietti E, Kirkwood JM. Interferon-alpha in tumor immunity and immunotherapy. Cytokine & Growth Factor Reviews. 2002;13(2):119-34.
136. OHNO S, OKUYAMA R, ARUGA A, SUGIYAMA H, YAMAMOTO M. Phase I Trial of Wilms' Tumor 1 (WT1) Peptide Vaccine with GM-CSF or CpG in Patients with Solid Malignancy. Anticancer Research. 2012;32(6):2263-9.
137. Le DT, Wang-Gillam A, Picozzi V, Greten TF, Crocenzi T, Springett G, et al. Safety and Survival With GVAX Pancreas Prime and Listeria Monocytogenes–Expressing

Mesothelin (CRS-207) Boost Vaccines for Metastatic Pancreatic Cancer. Journal of Clinical Oncology. 2015;33(12):1325-33.
138. Sabbatini P, Tsuji T, Ferran L, Ritter E, Sedrak C, Tuballes K, et al. Phase I Trial of Overlapping Long Peptides from a Tumor Self-Antigen and Poly-ICLC Shows Rapid Induction of Integrated Immune Response in Ovarian Cancer Patients. Clinical Cancer Research. 2012;18(23):6497-508.
139. Speiser DE, Li, xE, nard D, Rufer N, Rubio-Godoy V, et al. Rapid and strong human CD8+ T cell responses to vaccination with peptide, IFA, and CpG oligodeoxynucleotide 7909. The Journal of Clinical Investigation. 2005;115(3):739-46.
140. Cunningham D, Humblet Y, Siena S, Khayat D, Bleiberg H, Santoro A, et al. Cetuximab Monotherapy and Cetuximab plus Irinotecan in Irinotecan-Refractory Metastatic Colorectal Cancer. New England Journal of Medicine. 2004;351(4):337-45.
141. Verma S, Miles D, Gianni L, Krop IE, Welslau M, Baselga J, et al. Trastuzumab Emtansine for HER2-Positive Advanced Breast Cancer. New England Journal of Medicine. 2012;367(19):1783-91.
142. Witzig TE, Gordon LI, Cabanillas F, Czuczman MS, Emmanouilides C, Joyce R, et al. Randomized Controlled Trial of Yttrium-90–Labeled Ibritumomab Tiuxetan Radioimmunotherapy Versus Rituximab Immunotherapy for Patients With Relapsed or Refractory Low-Grade, Follicular, or Transformed B-Cell Non-Hodgkin's Lymphoma. Journal of Clinical Oncology. 2002;20(10):2453-63.
143. van Meerten T, van Rijn RS, Hol S, Hagenbeek A, Ebeling SB. Complement-Induced Cell Death by Rituximab Depends on CD20 Expression Level and Acts Complementary to Antibody-Dependent Cellular Cytotoxicity. Clinical Cancer Research. 2006;12(13):4027-35.
144. Topp MS, Gökbuget N, Zugmaier G, Klappers P, Stelljes M, Neumann S, et al. Phase II Trial of the Anti-CD19 Bispecific T Cell–Engager Blinatumomab Shows Hematologic and Molecular Remissions in Patients With Relapsed or Refractory B-Precursor Acute Lymphoblastic Leukemia. Journal of Clinical Oncology. 2014;32(36):4134-40.
145. Beatty GL, Chiorean EG, Fishman MP, Saboury B, Teitelbaum UR, Sun W, et al. CD40 Agonists Alter Tumor Stroma and Show Efficacy Against Pancreatic Carcinoma in Mice and Humans. Science (New York, Ny). 2011;331(6024):1612-6.
146. Hodi FS, O'Day SJ, McDermott DF, Weber RW, Sosman JA, Haanen JB, et al. Improved Survival with Ipilimumab in Patients with Metastatic Melanoma. New England Journal of Medicine. 2010;363(8):711-23.
147. Brahmer J, Reckamp KL, Baas P, Crinò L, Eberhardt WEE, Poddubskaya E, et al. Nivolumab versus Docetaxel in Advanced Squamous-Cell Non–Small-Cell Lung Cancer. New England Journal of Medicine. 2015;373(2):123-35.
148. Garon EB, Rizvi NA, Hui R, Leighl N, Balmanoukian AS, Eder JP, et al. Pembrolizumab for the Treatment of Non–Small-Cell Lung Cancer. New England Journal of Medicine. 2015;372(21):2018-28.
149. Sheng Sow H, Mattarollo SR. Combining low-dose or metronomic chemotherapy with anticancer vaccines: A therapeutic opportunity for lymphomas. Oncoimmunology. 2013;2(12):e27058.
150. Klug F, Prakash H, Huber Peter E, Seibel T, Bender N, Halama N, et al. Low-Dose Irradiation Programs Macrophage Differentiation to an iNOS+/M1 Phenotype that Orchestrates Effective T Cell Immunotherapy. Cancer Cell. 2013;24(5):589-602.
151. Vanneman M, Dranoff G. Combining Immunotherapy and Targeted Therapies in Cancer Treatment. Nature reviews Cancer. 2012;12(4):237-51.
152. Krop IE, Kim S-B, González-Martín A, LoRusso PM, Ferrero J-M, Smitt M, et al. Trastuzumab emtansine versus treatment of physician's choice for pretreated HER2-positive advanced breast cancer (TH3RESA): a randomised, open-label, phase 3 trial. The Lancet Oncology. 2014;15(7):689-99.
153. Junttila TT, Li J, Johnston J, Hristopoulos M, Clark R, Ellerman D, et al. Antitumor Efficacy of a Bispecific Antibody That Targets HER2 and Activates T Cells. Cancer Research. 2014;74(19):5561-71.

154. Haense N, Atmaca A, Pauligk C, Steinmetz K, Marmé F, Haag GM, et al. A phase I trial of the trifunctional anti Her2 × anti CD3 antibody ertumaxomab in patients with advanced solid tumors. BMC Cancer. 2016;16(1):420.
155. Peoples GE, Holmes JP, Hueman MT, Mittendorf EA, Amin A, Khoo S, et al. Combined Clinical Trial Results of a HER2/neu (E75) Vaccine for the Prevention of Recurrence in High-Risk Breast Cancer Patients: U.S. Military Cancer Institute Clinical Trials Group Study I-01 and I-02. Clinical Cancer Research. 2008;14(3):797-803.
156. Mittendorf EA, Clifton GT, Holmes JP, Schneble E, van Echo D, Ponniah S, et al. Final report of the phase I/II clinical trial of the E75 (nelipepimut-S) vaccine with booster inoculations to prevent disease recurrence in high-risk breast cancer patients. Annals of Oncology. 2014;25(9):1735-42.
157. Czerniecki BJ, Koski GK, Koldovsky U, Xu S, Cohen PA, Mick R, et al. Targeting HER-2/neu in Early Breast Cancer Development Using Dendritic Cells with Staged Interleukin-12 Burst Secretion. Cancer Research. 2007;67(4):1842-52.
158. Heery CR, Ibrahim NK, Arlen PM, et al. Docetaxel alone or in combination with a therapeutic cancer vaccine (panvac) in patients with metastatic breast cancer: A randomized clinical trial. JAMA Oncology. 2015;1(8):1087-95.
159. Vonderheide RH, LoRusso PM, Khalil M, Gartner EM, Khaira D, Soulieres D, et al. Tremelimumab in Combination with Exemestane in Patients with Advanced Breast Cancer and Treatment-Associated Modulation of Inducible Costimulator Expression on Patient T Cells. Clinical Cancer Research. 2010;16(13):3485-94.
160. Nanda R, Chow LQM, Dees EC, Berger R, Gupta S, Geva R, et al. Pembrolizumab in Patients With Advanced Triple-Negative Breast Cancer: Phase Ib KEYNOTE-012 Study. Journal of Clinical Oncology. 2016;34(21):2460-7.
161. Emens LA, Braiteh FS, Cassier P, Delord J-P, Eder JP, Fasso M, et al. Abstract 2859: Inhibition of PD-L1 by MPDL3280A leads to clinical activity in patients with metastatic triple-negative breast cancer (TNBC). Cancer Research. 2015;75(15 Supplement):2859-.
162. Lawrence MS, Stojanov P, Polak P, Kryukov GV, Cibulskis K, Sivachenko A, et al. Mutational heterogeneity in cancer and the search for new cancer-associated genes. Nature. 2013;499(7457):214-8.
163. Ali HR, Provenzano E, Dawson SJ, Blows FM, Liu B, Shah M. Association between CD8+ T-cell infiltration and breast cancer survival in 12,439 patients. Ann Oncol. 2014;25.
164. Mittendorf EA, Peoples GE. Injecting Hope--A Review of Breast Cancer Vaccines. Oncology. 2016;30(5):475-81.
165. McArthur HL, Diab A, Page DB, Yuan J, Solomon SB, Sacchini V, et al. A Pilot Study of Preoperative Single-Dose Ipilimumab and/or Cryoablation in Women with Early-Stage Breast Cancer with Comprehensive Immune Profiling. Clinical Cancer Research. 2016;22(23):5729-37.
166. Hanahan D, Weinberg Robert A. Hallmarks of Cancer: The Next Generation. Cell. 2011;144(5):646-74.
167. Hicklin DJ, Marincola FM, Ferrone S. HLA class I antigen downregulation in human cancers: T-cell immunotherapy revives an old story. Molecular Medicine Today. 1999;5(4):178-86.
168. Yee C, Thompson JA, Byrd D, Riddell SR, Roche P, Celis E, et al. Adoptive T cell therapy using antigen-specific CD8(+) T cell clones for the treatment of patients with metastatic melanoma: In vivo persistence, migration, and antitumor effect of transferred T cells. Proceedings of the National Academy of Sciences of the United States of America. 2002;99(25):16168-73.
169. Jäger E, Ringhoffer M, Karbach J, Arand M, Oesch F, Knuth A. Inverse relationship of melanocyte differentiation antigen expression in melanoma tissues and CD8+ cytotoxic-T-cell responses: Evidence for immunoselection of antigen-loss variants in vivo. International journal of cancer. 1996;66(4):470-6.
170. Zitvogel L, Kroemer G. Targeting PD-1/PD-L1 interactions for cancer immunotherapy. Oncoimmunology. 2012;1(8):1223-5.

171. Fantini MC, Becker C, Monteleone G, Pallone F, Galle PR, Neurath MF. Cutting Edge: TGF-β Induces a Regulatory Phenotype in $CD4^{+}CD25^{-}$ T Cells through Foxp3 Induction and Down-Regulation of Smad7. The Journal of Immunology. 2004;172(9):5149-53.
172. Hsu P, Santner-Nanan B, Hu M, Skarratt K, Lee CH, Stormon M, et al. IL-10 Potentiates Differentiation of Human Induced Regulatory T Cells via STAT3 and Foxo1. The Journal of Immunology. 2015.
173. Quatromoni JG, Eruslanov E. Tumor-associated macrophages: function, phenotype, and link to prognosis in human lung cancer. American Journal of Translational Research. 2012;4(4):376-89.
174. Sousa S, Brion R, Lintunen M, Kronqvist P, Sandholm J, Mönkkönen J, et al. Human breast cancer cells educate macrophages toward the M2 activation status. Breast Cancer Research. 2015;17(1):101.
175. Sharma S, Stolina M, Lin Y, Gardner B, Miller PW, Kronenberg M, et al. T Cell-Derived IL-10 Promotes Lung Cancer Growth by Suppressing Both T Cell and APC Function. The Journal of Immunology. 1999;163(9):5020-8.
176. Holmgaard Rikke B, Zamarin D, Li Y, Gasmi B, Munn David H, Allison James P, et al. Tumor-Expressed IDO Recruits and Activates MDSCs in a Treg-Dependent Manner. Cell Reports. 2015;13(2):412-24.
177. Curiel TJ, Coukos G, Zou L, Alvarez X, Cheng P, Mottram P, et al. Specific recruitment of regulatory T cells in ovarian carcinoma fosters immune privilege and predicts reduced survival. Nature medicine. 2004;10(9):942-9.
178. Sica A, Mantovani A. Macrophage plasticity and polarization: in vivo veritas. The Journal of Clinical Investigation. 2012;122(3):787-95.
179. Allavena P, Mantovani A. Immunology in the clinic review series; focus on cancer: tumour-associated macrophages: undisputed stars of the inflammatory tumour microenvironment. Clinical & Experimental Immunology. 2012;167(2):195-205.
180. Movahedi K, Laoui D, Gysemans C, Baeten M, Stangé G, Van den Bossche J, et al. Different Tumor Microenvironments Contain Functionally Distinct Subsets of Macrophages Derived from Ly6C(high) Monocytes. Cancer Research. 2010;70(14):5728.
181. Zaynagetdinov R, Sherrill TP, Polosukhin VV, Han W, Ausborn JA, McLoed AG, et al. A Critical Role for Macrophages in Promotion of Urethane-Induced Lung Carcinogenesis. The Journal of Immunology. 2011;187(11):5703-11.
182. Sica A, Schioppa T, Mantovani A, Allavena P. Tumour-associated macrophages are a distinct M2 polarised population promoting tumour progression: Potential targets of anti-cancer therapy. European Journal of Cancer. 2006;42(6):717-27.
183. Pollard JW. Tumour-educated macrophages promote tumour progression and metastasis. Nat Rev Cancer. 2004;4(1):71-8.
184. Lefebvre M-L, Krause SW, Salcedo M, Nardin A. Ex Vivo-activated Human Macrophages Kill Chronic Lymphocytic Leukemia Cells in the Presence of Rituximab: Mechanism of Antibody-dependent Cellular Cytotoxicity and Impact of Human Serum. Journal of Immunotherapy. 2006;29(4)(July/August 2006):388-97.
185. Ruttimann J. Macrophages and nitric oxide: A deadly combination. The Journal of Experimental Medicine. 2007;204(13):3057.
186. Forssell J, Öberg Å, Henriksson ML, Stenling R, Jung A, Palmqvist R. High Macrophage Infiltration along the Tumor Front Correlates with Improved Survival in Colon Cancer. Clinical Cancer Research. 2007;13(5):1472-9.
187. Welsh TJ, Green RH, Richardson D, Waller DA, O'Byrne KJ, Bradding P. Macrophage and Mast-Cell Invasion of Tumor Cell Islets Confers a Marked Survival Advantage in Non–Small-Cell Lung Cancer. Journal of Clinical Oncology. 2005;23(35):8959-67.
188. Bingle L, Brown NJ, Lewis CE. The role of tumour-associated macrophages in tumour progression: implications for new anticancer therapies. The Journal of Pathology. 2002;196(3):254-65.

189. Leek RD, Lewis CE, Whitehouse R, Greenall M, Clarke J, Harris AL. Association of Macrophage Infiltration with Angiogenesis and Prognosis in Invasive Breast Carcinoma. Cancer Research. 1996;56(20):4625.
190. Zhang Q-w, Liu L, Gong C-y, Shi H-s, Zeng Y-h, Wang X-z, et al. Prognostic Significance of Tumor-Associated Macrophages in Solid Tumor: A Meta-Analysis of the Literature. PLoS ONE. 2012;7(12):e50946.
191. Zhang Y, Cheng S, Zhang M, Zhen L, Pang D, Zhang Q, et al. High-Infiltration of Tumor-Associated Macrophages Predicts Unfavorable Clinical Outcome for Node-Negative Breast Cancer. PLoS ONE. 2013;8(9):e76147.
192. Ward R, Sims AH, Lee A, Lo C, Wynne L, Yusuf H, et al. Monocytes and macrophages, implications for breast cancer migration and stem cell-like activity and treatment. Oncotarget. 2015;6(16).
193. Medrek C, Pontén F, Jirström K, Leandersson K. The presence of tumor associated macrophages in tumor stroma as a prognostic marker for breast cancer patients. BMC Cancer. 2012;12(1):306.
194. Tsutsui S, Yasuda K, Suzuki K, Tahara K, Higashi H, Era S. Macrophage infiltration and its prognostic implications in breast cancer: The relationship with VEGF expression and microvessel density. Oncology Reports. 2005;14(2):425-31.
195. Mahmoud SMA, Lee AHS, Paish EC, Macmillan RD, Ellis IO, Green AR. Tumour-infiltrating macrophages and clinical outcome in breast cancer. Journal of Clinical Pathology. 2012;65(2):159-63.
196. Williams CB, Yeh ES, Soloff AC. Tumor-associated macrophages: unwitting accomplices in breast cancer malignancy. Npj Breast Cancer. 2016;2:15025.
197. Laoui D, Movahedi K, Van Overmeire E, Van den Bossche J, Schouppe E, Mommer C, et al. Tumor-associated macrophages in breast cancer: distinct subsets, distinct functions. Int J Dev Biol. 2011;55(7-9):861 - 7.
198. Zeisberger SM, Odermatt B, Marty C, Zehnder-Fjällman AHM, Ballmer-Hofer K, Schwendener RA. Clodronate-liposome-mediated depletion of tumour-associated macrophages: a new and highly effective antiangiogenic therapy approach. British Journal of Cancer. 2006;95(3):272-81.
199. Ries Carola H, Cannarile Michael A, Hoves S, Benz J, Wartha K, Runza V, et al. Targeting Tumor-Associated Macrophages with Anti-CSF-1R Antibody Reveals a Strategy for Cancer Therapy. Cancer Cell. 2014;25(6):846-59.
200. Qian B-Z, Li J, Zhang H, Kitamura T, Zhang J, Campion LR, et al. CCL2 recruits inflammatory monocytes to facilitate breast-tumour metastasis. Nature. 2011;475(7355):222-5.
201. Pienta KJ, Machiels J-P, Schrijvers D, Alekseev B, Shkolnik M, Crabb SJ, et al. Phase 2 study of carlumab (CNTO 888), a human monoclonal antibody against CC-chemokine ligand 2 (CCL2), in metastatic castration-resistant prostate cancer. Investigational New Drugs. 2013;31(3):760-8.
202. Paulus P, Stanley ER, Schäfer R, Abraham D, Aharinejad S. Colony-Stimulating Factor-1 Antibody Reverses Chemoresistance in Human MCF-7 Breast Cancer Xenografts. Cancer Research. 2006;66(8):4349-56.
203. Van Overmeire E, Stijlemans B, Heymann F, Keirsse J, Morias Y, Elkrim Y, et al. M-CSF and GM-CSF Receptor Signaling Differentially Regulate Monocyte Maturation and Macrophage Polarization in the Tumor Microenvironment. Cancer Research. 2016;76(1):35-42.
204. Roland CL, Dineen SP, Lynn KD, Sullivan LA, Dellinger MT, Sadegh L, et al. Inhibition of vascular endothelial growth factor reduces angiogenesis and modulates immune cell infiltration of orthotopic breast cancer xenografts. Molecular Cancer Therapeutics. 2009;8(7):1761-71.
205. Guiducci C, Vicari AP, Sangaletti S, Trinchieri G, Colombo MP. Redirecting *In vivo* Elicited Tumor Infiltrating Macrophages and Dendritic Cells towards Tumor Rejection. Cancer Research. 2005;65(8):3437-46.

206. Banerjee S, Halder K, Ghosh S, Bose A, Majumdar S. The combination of a novel immunomodulator with a regulatory T cell suppressing antibody (DTA-1) regress advanced stage B16F10 solid tumor by repolarizing tumor associated macrophages in situ. Oncoimmunology. 2015;4(3):e995559.
207. Buhtoiarov IN, Sondel PM, Wigginton JM, Buhtoiarova TN, Yanke EM, Mahvi DA, et al. Anti-tumour synergy of cytotoxic chemotherapy and anti-CD40 plus CpG-ODN immunotherapy through repolarization of tumour-associated macrophages. Immunology. 2011;132(2):226-39.
208. Rolny C, Mazzone M, Tugues S, Laoui D, Johansson I, Coulon C, et al. HRG Inhibits Tumor Growth and Metastasis by Inducing Macrophage Polarization and Vessel Normalization through Downregulation of PlGF. Cancer Cell. 2011;19(1):31-44.
209. Haabeth OAW, Lorvik KB, Hammarström C, Donaldson IM, Haraldsen G, Bogen B, et al. Inflammation driven by tumour-specific Th1 cells protects against B-cell cancer. Nature Communications. 2011;2:240.
210. Antony PA, Piccirillo CA, Akpinarli A, Finkelstein SE, Speiss PJ, Surman DR, et al. $CD8^+$ T Cell Immunity Against a Tumor/Self-Antigen Is Augmented by $CD4^+$ T Helper Cells and Hindered by Naturally Occurring T Regulatory Cells. The Journal of Immunology. 2005;174(5):2591-601.
211. Le Saout C, Mennechet S, Taylor N, Hernandez J. Memory-like CD8+ and CD4+ T cells cooperate to break peripheral tolerance under lymphopenic conditions. Proceedings of the National Academy of Sciences. 2008;105(49):19414-9.
212. Gao FG, Khammanivong V, Liu WJ, Leggatt GR, Frazer IH, Fernando GJP. Antigen-specific $CD4^+$ T-Cell Help Is Required to Activate a Memory $CD8^+$ T Cell to a Fully Functional Tumor Killer Cell. Cancer Research. 2002;62(22):6438-41.
213. Heusinkveld M, de Vos van Steenwijk PJ, Goedemans R, Ramwadhdoebe TH, Gorter A, Welters MJP, et al. M2 Macrophages Induced by Prostaglandin E_2 and IL-6 from Cervical Carcinoma Are Switched to Activated M1 Macrophages by $CD4^+$ Th1 Cells. The Journal of Immunology. 2011;187(3):1157-65.
214. Corthay A, Skovseth DK, Lundin KU, Røsjø E, Omholt H, Hofgaard PO, et al. Primary Antitumor Immune Response Mediated by CD4+ T Cells. Immunity. 2005;22(3):371-83.
215. Corthay A, Lundin KU, Lorvik KB, Hofgaard PO, Bogen B. Secretion of Tumor-Specific Antigen by Myeloma Cells Is Required for Cancer Immunosurveillance by CD4⁺ T Cells. Cancer Research. 2009;69(14):5901-7.
216. Tatano Y, Shimizu T, Tomioka H. Unique Macrophages Different from M1/M2 Macrophages Inhibit T Cell Mitogenesis while Upregulating Th17 Polarization. Scientific Reports. 2014;4:4146.
217. Zhu L, Yang T, Li L, Sun L, Hou Y, Hu X, et al. TSC1 controls macrophage polarization to prevent inflammatory disease. Nature Communications. 2014;5:4696.
218. Davis MJ, Tsang TM, Qiu Y, Dayrit JK, Freij JB, Huffnagle GB, et al. Macrophage M1/M2 Polarization Dynamically Adapts to Changes in Cytokine Microenvironments in Cryptococcus neoformans Infection. mBio. 2013;4(3):e00264-13.
219. Shaul ME, Bennett G, Strissel KJ, Greenberg AS, Obin MS. Dynamic, M2-Like Remodeling Phenotypes of CD11c+ Adipose Tissue Macrophages During High-Fat Diet–Induced Obesity in Mice. Diabetes. 2010;59(5):1171-81.
220. Gorer PA. Studies in Antibody Response of Mice to Tumour Inoculation. British Journal of Cancer. 1950;4(4):372-9.
221. Sugiura K, Stock CC. Studies in a tumor spectrum. I. Comparison of the action of methylbis(2-chloroethyl)amine and 3-bis(2-chloroethyl)aminomethyl-4-methoxymethyl-5-hydroxy-6-methylpyridine on the growth of a variety of mouse and rat tumors. Cancer. 1952;5(2):382-402.
222. Das K, Eisel D, Lenkl C, Goyal A, Diederichs S, Dickes E, et al. Generation of murine tumor cell lines deficient in MHC molecule surface expression using the CRISPR/Cas9 system. PLoS ONE. 2017;12(3):e0174077.
223. Salter RD, Howell DN, Cresswell P. Genes regulating HLA class I antigen expression in T-B lymphoblast hybrids. Immunogenetics. 1985;21(3):235-46.

224. Rosa FM, Fellous M. Regulation of HLA-DR gene by IFN-gamma. Transcriptional and post-transcriptional control. The Journal of Immunology. 1988;140(5):1660-4.
225. D'Urso CM, Wang ZG, Cao Y, Tatake R, Zeff RA, Ferrone S. Lack of HLA class I antigen expression by cultured melanoma cells FO-1 due to a defect in B2m gene expression. The Journal of Clinical Investigation. 1991;87(1):284-92.
226. Karre K, Ljunggren HG, Piontek G, Kiessling R. Selective rejection of H-2-deficient lymphoma variants suggests alternative immune defence strategy. Nature. 1986;319(6055):675-8.
227. Alter G, Malenfant JM, Altfeld M. CD107a as a functional marker for the identification of natural killer cell activity. Journal of Immunological Methods. 2004;294(1–2):15-22.
228. Lakshmikanth T, Burke S, Ali TH, Kimpfler S, Ursini F, Ruggeri L, et al. NCRs and DNAM-1 mediate NK cell recognition and lysis of human and mouse melanoma cell lines in vitro and in vivo. The Journal of Clinical Investigation. 2009;119(5):1251-63.
229. Tatsis N, Ertl HCJ. Adenoviruses as vaccine vectors. Molecular Therapy. 2004;10(4):616-29.
230. Altman JD, Moss PAH, Goulder PJR, Barouch DH, McHeyzer-Williams MG, Bell JI, et al. Phenotypic Analysis of Antigen-Specific T Lymphocytes. Science. 1996;274(5284):94-6.
231. Feltkamp MCW, Smits HL, Vierboom MPM, Minnaar RP, De Jongh BM, Drijfhout JW, et al. Vaccination with cytotoxic T lymphocyte epitope-containing peptide protects against a tumor induced by human papillomavirus type 16-transformed cells. European Journal of Immunology. 1993;23(9):2242-9.
232. Helms T, Boehm BO, Asaad RJ, Trezza RP, Lehmann PV, Tary-Lehmann M. Direct Visualization of Cytokine-Producing Recall Antigen-Specific CD4 Memory T Cells in Healthy Individuals and HIV Patients. The Journal of Immunology. 2000;164(7):3723-32.
233. Asemissen AM, Nagorsen D, Keilholz U, Letsch A, Schmittel A, Thiel E, et al. Flow cytometric determination of intracellular or secreted IFNγ for the quantification of antigen reactive T cells. Journal of Immunological Methods. 2001;251(1–2):101-8.
234. Gibbings DJ, Marcet-Palacios M, Sekar Y, Ng MCY, Befus AD. CD8α is expressed by human monocytes and enhances FcγR-dependent responses. BMC Immunology. 2007;8:12-.
235. Wooldridge L, Lissina A, Cole DK, van den Berg HA, Price DA, Sewell AK. Tricks with tetramers: how to get the most from multimeric peptide–MHC. Immunology. 2009;126(2):147-64.
236. Zhang X, Goncalves R, Mosser DM. The Isolation and Characterization of Murine Macrophages. Current protocols in immunology / edited by John E Coligan [et al]. 2008;CHAPTER:Unit-14.1.
237. Dobrzanski MJ, Reome JB, Dutton RW. Therapeutic Effects of Tumor-Reactive Type 1 and Type 2 CD8⁺ T Cell Subpopulations in Established Pulmonary Metastases. The Journal of Immunology. 1999;162(11):6671-80.
238. Moore MW, Carbone FR, Bevan MJ. Introduction of soluble protein into the class I pathway of antigen processing and presentation. Cell. 1988;54(6):777-85.
239. Engelhardt JJ, Boldajipour B, Beemiller P, Pandurangi P, Sorensen C, Werb Z, et al. Marginating Dendritic Cells of the Tumor Microenvironment Cross-present Tumor Antigens and Stably Engage Tumor-Specific T cells. Cancer Cell. 2012;21(3):402-17.
240. Rötzschke O, Falk K, Stevanovic S, Jung G, Walden P, Rammensee H-G. Exact prediction of a natural T cell epitope. European Journal of Immunology. 1991;21(11):2891-4.
241. Murphy K, Heimberger A, Loh D. Induction by antigen of intrathymic apoptosis of CD4+CD8+TCRlo thymocytes in vivo. Science. 1990;250(4988):1720-3.
242. Hogquist KA, Jameson SC, Heath WR, Howard JL, Bevan MJ, Carbone FR. T cell receptor antagonist peptides induce positive selection. Cell. 1994;76(1):17-27.
243. Barnden MJ, Allison J, Heath WR, Carbone FR. Defective TCR expression in transgenic mice constructed using cDNA-based α- and β-chain genes under the control of heterologous regulatory elements. Immunol Cell Biol. 1998;76(1):34-40.

244. Schüler T, Blankenstein T. Cutting Edge: CD8$^+$ Effector T Cells Reject Tumors by Direct Antigen Recognition but Indirect Action on Host Cells. The Journal of Immunology. 2003;170(9):4427-31.
245. Shrikant P, Khoruts A, Mescher MF. CTLA-4 Blockade Reverses CD8+ T Cell Tolerance to Tumor by a CD4+ T Cell– and IL-2-Dependent Mechanism. Immunity. 1999;11(4):483-93.
246. Curran MA, Montalvo W, Yagita H, Allison JP. PD-1 and CTLA-4 combination blockade expands infiltrating T cells and reduces regulatory T and myeloid cells within B16 melanoma tumors. Proceedings of the National Academy of Sciences. 2010;107(9):4275-80.
247. Gottschalk S, Yu F, Ji M, Kakarla S, Song X-T. A Vaccine That Co-Targets Tumor Cells and Cancer Associated Fibroblasts Results in Enhanced Antitumor Activity by Inducing Antigen Spreading. PLoS ONE. 2013;8(12):e82658.
248. Ramsbottom KM, Sacirbegovic F, Hawkins ED, Kallies A, Belz GT, Van Ham V, et al. Lethal giant larvae-1 deficiency enhances the CD8+ effector T-cell response to antigen challenge in vivo. Immunol Cell Biol. 2016;94(3):306-11.
249. Gilfillan S, Chan CJ, Cella M, Haynes NM, Rapaport AS, Boles KS, et al. DNAM-1 promotes activation of cytotoxic lymphocytes by nonprofessional antigen-presenting cells and tumors. The Journal of Experimental Medicine. 2008;205(13):2965-73.
250. Nelson DJ, Mukherjee S, Bundell C, Fisher S, van Hagen D, Robinson B. Tumor Progression Despite Efficient Tumor Antigen Cross-Presentation and Effective “Arming” of Tumor Antigen-Specific CTL. The Journal of Immunology. 2001;166(9):5557-66.
251. Samorski R, Gissmann L, Osen W. Codon optimized expression of HPV 16 E6 renders target cells susceptible to E6-specific CTL recognition. Immunology Letters. 2006;107(1):41-9.
252. Kalluri R. The biology and function of fibroblasts in cancer. Nat Rev Cancer. 2016;16(9):582-98.
253. Bussard KM, Mutkus L, Stumpf K, Gomez-Manzano C, Marini FC. Tumor-associated stromal cells as key contributors to the tumor microenvironment. Breast Cancer Research : BCR. 2016;18:84.
254. Ohnuki H, Jiang K, Wang D, Salvucci O, Kwak H, Sánchez-Martín D, et al. Tumor-infiltrating myeloid cells activate Dll4/Notch/TGF-β signaling to drive malignant progression. Cancer research. 2014;74(7):2038-49.
255. Khong HT, Restifo NP. Natural selection of tumor variants in the generation of “tumor escape” phenotypes. Nature immunology. 2002;3(11):999-1005.
256. Monjazeb AM, Zamora AE, Grossenbacher SK, Mirsoian A, Sckisel GD, Murphy WJ. Immunoediting and antigen loss: overcoming the Achilles heel of immunotherapy with antigen non-specific therapies. Front Oncol. 2013;3.
257. Jensen SM, Twitty CG, Maston LD, Antony PA, Lim M, Hu H-M, et al. Increased Frequency of Suppressive Regulatory T Cells and T-cell Mediated Antigen Loss Results in Murine Melanoma Recurrence. Journal of immunology (Baltimore, Md : 1950). 2012;189(2):767-76.
258. Tveita AA, Schjesvold FH, Sundnes O, Haabeth OAW, Haraldsen G, Bogen B. Indirect CD4+ T-cell-mediated elimination of MHC IINEG tumor cells is spatially restricted and fails to prevent escape of antigen-negative cells. European Journal of Immunology. 2014;44(9):2625-37.
259. Landsberg J, Kohlmeyer J, Renn M, Bald T, Rogava M, Cron M, et al. Melanomas resist T-cell therapy through inflammation-induced reversible dedifferentiation. Nature. 2012;490(7420):412-6.
260. Kaufman WL, Kocman I, Agrawal V, Rahn H-P, Besser D, Gossen M. Homogeneity and persistence of transgene expression by omitting antibiotic selection in cell line isolation. Nucleic Acids Research. 2008;36(17):e111-e.
261. Artelt P, Grannemann R, Stocking C, Friel J, Bartsch J, Hauser H. The prokaryotic neomycin-resistance-encoding gene acts as a transcriptional silencer in eukaryotic cells. Gene. 1991;99(2):249-54.

262. Robins DM, Ripley S, Henderson AS, Axel R. Transforming DNA integrates into the host chromosome. Cell. 1981;23(1):29-39.
263. Parkhurst MR, Fitzgerald EB, Southwood S, Sette A, Rosenberg SA, Kawakami Y. Identification of a Shared HLA-A*0201-restricted T-Cell Epitope from the Melanoma Antigen Tyrosinase-related Protein 2 (TRP2). Cancer Research. 1998;58(21):4895-901.
264. Kobayashi H, Wood M, Song Y, Appella E, Celis E. Defining Promiscuous MHC Class II Helper T-Cell Epitopes for the HER2/*neu* Tumor Antigen. Cancer Research. 2000;60(18):5228-36.
265. Gnjatic S, Atanackovic D, Jäger E, Matsuo M, Selvakumar A, Altorki NK, et al. Survey of naturally occurring CD4+ T cell responses against NY-ESO-1 in cancer patients: Correlation with antibody responses. Proceedings of the National Academy of Sciences. 2003;100(15):8862-7.
266. Sinigaglia F, Guttinger M, Kilgus J, Doran DM, Matile H, Etlinger H, et al. A malaria T-cell epitope recognized in association with most mouse and human MHC class II molecules. Nature. 1988;336(6201):778-80.
267. Bian H, Hammer J. Discovery of promiscuous HLA-II-restricted T cell epitopes with TEPITOPE. Methods. 2004;34(4):468-75.
268. Shi Y, Sahai BM, Green DR. Cyclosporin A inhibits activation-induced cell death in T-cell hybridomas and thymocytes. Nature. 1989;339(6226):625-6.
269. Smith CA, Williams GT, Kingston R, Jenkinson EJ, Owen JJT. Antibodies to CD3/T-cell receptor complex induce death by apoptosis in immature T cells in thymic cultures. Nature. 1989;337(6203):181-4.
270. Lubaroff DM, Konety BR, Link B, Gerstbrein J, Madsen T, Shannon M, et al. Phase I Clinical Trial of an Adenovirus/PSA Vaccine for Prostate Cancer: Safety and Immunologic Results. Clinical cancer research : an official journal of the American Association for Cancer Research. 2009;15(23):7375-80.
271. Lubaroff DM, Williams RD, Vaena D, Joudi F, Brown J, Smith M, et al. Abstract 2692: An ongoing Phase II trial of an adenovirus/PSA vaccine for prostate cancer. Cancer Research. 2012;72(8 Supplement):2692-.
272. Smaill F, Jeyanathan M, Smieja M, Medina MF, Thanthrige-Don N, Zganiacz A, et al. A Human Type 5 Adenovirus–Based Tuberculosis Vaccine Induces Robust T Cell Responses in Humans Despite Preexisting Anti-Adenovirus Immunity. Science Translational Medicine. 2013;5(205):205ra134-205ra134.
273. Majji S, Wijayalath W, Shashikumar S, Pow-Sang L, Villasante E, Brumeanu TD, et al. Differential effect of HLA class-I versus class-II transgenes on human T and B cell reconstitution and function in NRG mice. Scientific Reports. 2016;6:28093.
274. Williams MA, Tyznik AJ, Bevan MJ. Interleukin-2 signals during priming are required for secondary expansion of CD8+ memory T cells. Nature. 2006;441(7095):890-3.
275. Quezada SA, Simpson TR, Peggs KS, Merghoub T, Vider J, Fan X, et al. Tumor-reactive $CD4^+$ T cells develop cytotoxic activity and eradicate large established melanoma after transfer into lymphopenic hosts. The Journal of Experimental Medicine. 2010;207(3):637-50.
276. Xie Y, Akpinarli A, Maris C, Hipkiss EL, Lane M, Kwon E-KM, et al. Naive tumor-specific $CD4^+$ T cells differentiated in vivo eradicate established melanoma. The Journal of Experimental Medicine. 2010;207(3):651-67.
277. Seliger B, Cabrera T, Garrido F, Ferrone S. HLA class I antigen abnormalities and immune escape by malignant cells. Seminars in Cancer Biology. 2002;12(1):3-13.
278. Garrido F, Cabrera T, Aptsiauri N. “Hard” and “soft” lesions underlying the HLA class I alterations in cancer cells: Implications for immunotherapy. International Journal of Cancer. 2010;127(2):249-56.
279. EWENS A, MIHICH E, EHRKE MJ. Distant Metastasis from Subcutaneously Grown E0771 Medullary Breast Adenocarcinoma. Anticancer Research. 2005;25(6B):3905-15.
280. Hoover R, Gullickson G, Kornbluth J. Natural killer lytic-associated molecule plays a role in controlling tumor dissemination and metastasis. Frontiers in Immunology. 2012;3(393).

281. Ruffell B, Au A, Rugo HS, Esserman LJ, Hwang ES, Coussens LM. Leukocyte composition of human breast cancer. Proc Natl Acad Sci U S A. 2012;109.
282. DuPré SA, Redelman D, Hunter KW. The mouse mammary carcinoma 4T1: characterization of the cellular landscape of primary tumours and metastatic tumour foci. International Journal of Experimental Pathology. 2007;88(5):351-60.
283. Yu Y-RA, O'Koren EG, Hotten DF, Kan MJ, Kopin D, Nelson ER, et al. A Protocol for the Comprehensive Flow Cytometric Analysis of Immune Cells in Normal and Inflamed Murine Non-Lymphoid Tissues. PLoS ONE. 2016;11(3):e0150606.
284. Franklin RA, Liao W, Sarkar A, Kim MV, Bivona MR, Liu K, et al. The Cellular and Molecular Origin of Tumor-associated Macrophages. Science (New York, NY). 2014;344(6186):921-5.
285. van der Sluis TC, Sluijter M, van Duikeren S, West BL, Melief CJM, Arens R, et al. Therapeutic Peptide Vaccine-Induced CD8 T Cells Strongly Modulate Intratumoral Macrophages Required for Tumor Regression. Cancer Immunology Research. 2015;3(9):1042-51.
286. Thoreau M, Penny HL, Tan K, Regnier F, Weiss JM, Lee B, et al. Vaccine-induced tumor regression requires a dynamic cooperation between T cells and myeloid cells at the tumor site. Oncotarget. 2015;6(29):27832-46.
287. Tang X, Mo C, Wang Y, Wei D, Xiao H. Anti-tumour strategies aiming to target tumour-associated macrophages. Immunology. 2013;138(2):93-104.
288. Belmares MP, Busch R, Wucherpfennig KW, McConnell HM, Mellins ED. Structural Factors Contributing to DM Susceptibility of MHC Class II/Peptide Complexes. The Journal of Immunology. 2002;169(9):5109-17.
289. Hall FC, Rabinowitz JD, Busch R, Visconti KC, Belmares M, Patil NS, et al. Relationship between kinetic stability and immunogenicity of HLA-DR4/peptide complexes. European Journal of Immunology. 2002;32(3):662-70.
290. Nielsen M, Lund O. NN-align. An artificial neural network-based alignment algorithm for MHC class II peptide binding prediction. BMC Bioinformatics. 2009;10:296-.
291. Nielsen M, Lundegaard C, Lund O. Prediction of MHC class II binding affinity using SMM-align, a novel stabilization matrix alignment method. BMC Bioinformatics. 2007;8(1):238.
292. Nielsen M, Lundegaard C, Worning P, Lauemøller SL, Lamberth K, Buus S, et al. Reliable prediction of T-cell epitopes using neural networks with novel sequence representations. Protein Science : A Publication of the Protein Society. 2003;12(5):1007-17.
293. Reid PA, Watts C. Constitutive endocytosis and recycling of major histocompatibility complex class II glycoproteins in human B-lymphoblastoid cells. Immunology. 1992;77(4):539-42.
294. Tseng D, Volkmer J-P, Willingham SB, Contreras-Trujillo H, Fathman JW, Fernhoff NB, et al. Anti-CD47 antibody–mediated phagocytosis of cancer by macrophages primes an effective antitumor T-cell response. Proceedings of the National Academy of Sciences. 2013;110(27):11103-8.
295. Panaretakis T, Kepp O, Brockmeier U, Tesniere A, Bjorklund AC, Chapman DC, et al. Mechanisms of pre-apoptotic calreticulin exposure in immunogenic cell death. The EMBO Journal. 2009;28(5):578-90.
296. Obeid M, Tesniere A, Ghiringhelli F, Fimia GM, Apetoh L, Perfettini J-L, et al. Calreticulin exposure dictates the immunogenicity of cancer cell death. Nat Med. 2007;13(1):54-61.
297. Takeshima T, Chamoto K, Wakita D, Ohkuri T, Togashi Y, Shirato H, et al. Local Radiation Therapy Inhibits Tumor Growth through the Generation of Tumor-Specific CTL: Its Potentiation by Combination with Th1 Cell Therapy. Cancer Research. 2010;70(7):2697-706.
298. Bonapace L, Coissieux M-M, Wyckoff J, Mertz KD, Varga Z, Junt T, et al. Cessation of CCL2 inhibition accelerates breast cancer metastasis by promoting angiogenesis. Nature. 2014;515(7525):130-3.

299. DeNardo DG, Brennan DJ, Rexhepaj E, Ruffell B, Shiao SL, Madden SF. Leukocyte complexity predicts breast cancer survival and functionally regulates response to chemotherapy. Cancer Discov. 2011;1.
300. Pahler JC, Tazzyman S, Erez N, Chen Y-Y, Murdoch C, Nozawa H, et al. Plasticity in Tumor-Promoting Inflammation: Impairment of Macrophage Recruitment Evokes a Compensatory Neutrophil Response. Neoplasia (New York, NY). 2008;10(4):329-39.
301. Swierczak A, Cook AD, Lenzo JC, Restall CM, Doherty JP, Anderson RL, et al. The Promotion of Breast Cancer Metastasis Caused by Inhibition of CSF-1R/CSF-1 Signaling Is Blocked by Targeting the G-CSF Receptor. Cancer Immunology Research. 2014;2(8):765-76.
302. Motz GT, Santoro SP, Wang L-P, Garrabrant T, Lastra RR, Hagemann IS, et al. Tumor endothelium FasL establishes a selective immune barrier promoting tolerance in tumors. Nat Med. 2014;20(6):607-15.
303. DeNardo DG, Barreto JB, Andreu P, Vasquez L, Tawfik D, Kolhatkar N, et al. CD4+ T Cells Regulate Pulmonary Metastasis of Mammary Carcinomas by Enhancing Protumor Properties of Macrophages. Cancer Cell. 2009;16(2):91-102.
304. Nagai H, Horikawa T, Oka M, Ichihashi M, Hara I, Kamidono S. Elimination of CD4+ T Cells Enhances Anti-Tumor Effect of Locally Secreted Interleukin-12 on B16 Mouse Melanoma and Induces Vitiligo-Like Coat Color Alteration. Journal of Investigative Dermatology. 2000;115(6):1059-64.
305. Gobert M, Treilleux I, Bendriss-Vermare N, Bachelot T, Goddard-Leon S, Arfi V, et al. Regulatory T Cells Recruited through CCL22/CCR4 Are Selectively Activated in Lymphoid Infiltrates Surrounding Primary Breast Tumors and Lead to an Adverse Clinical Outcome. Cancer Research. 2009;69(5):2000-9.
306. Ueha S, Yokochi S, Ishiwata Y, Ogiwara H, Chand K, Nakajima T, et al. Robust Antitumor Effects of Combined Anti–CD4-Depleting Antibody and Anti–PD-1/PD-L1 Immune Checkpoint Antibody Treatment in Mice. Cancer Immunology Research. 2015;3(6):631-40.
307. Yu P, Lee Y, Liu W, Krausz T, Chong A, Schreiber H, et al. Intratumor depletion of CD4(+) cells unmasks tumor immunogenicity leading to the rejection of late-stage tumors. The Journal of Experimental Medicine. 2005;201(5):779-91.
308. Su S, Liao J, Liu J, Huang D, He C, Chen F, et al. Blocking the recruitment of naive CD4+ T cells reverses immunosuppression in breast cancer. Cell Res. 2017;27(4):461-82.
309. Kmieciak M, Worschech A, Nikizad H, Gowda M, Habibi M, Depcrynski A, et al. CD4+ T cells inhibit the neu-specific CD8+ T-cell exhaustion during the priming phase of immune responses against breast cancer. Breast cancer research and treatment. 2011;126(2):385-94.
310. Braumuller H, Wieder T, Brenner E, Aszmann S, Hahn M, Alkhaled M, et al. T-helper-1-cell cytokines drive cancer into senescence. Nature. 2013;494(7437):361-5.
311. Xu L, Xu W, Qiu S, Xiong S. Enrichment of CCR6+Foxp3+ regulatory T cells in the tumor mass correlates with impaired CD8+ T cell function and poor prognosis of breast cancer. Clinical Immunology. 2010;135(3):466-75.
312. Schmidt H-H, Ge Y, Hartmann FJ, Conrad H, Klug F, Nittel S, et al. HLA Class II tetramers reveal tissue-specific regulatory T cells that suppress T-cell responses in breast carcinoma patients. Oncoimmunology. 2013;2(6):e24962.
313. Lorvik KB, Hammarström C, Fauskanger M, Haabeth OAW, Zangani M, Haraldsen G, et al. Adoptive Transfer of Tumor-Specific Th2 Cells Eradicates Tumors by Triggering an *In Situ* Inflammatory Immune Response. Cancer Research. 2016;76(23):6864-76.

8 Publications and Presentations

8.1 Publications

Das K, Eisel D, Lenkl C, Goyal A, Diederichs S, Dickes E, Osen W, Eichmüller SB (2017). Generation of murine tumor cell lines deficient in MHC molecule surface expression using the CRISPR/Cas9 system. PLoS ONE 12(3): e0174077.

8.2 Presentations

Das K, Eisel D, Nicolaus C, Goyal A, Diederichs S, Dickes E, Osen W, Eichmüller SB. Generation of MHC class I and class II deficient tumor cell lines using the CRISPR/Cas9 system. Cancer Immunotherapy Meeting 2016, Mainz, Germany.

Das K, Gardyan A, Vormehr M, Müller-Decker K, Zörnig I, Jäger D, Osen W, Eichmüller SB. Establishment of a transplantable, NY-BR-1 expressing breast cancer model in HLA-transgenic mice. Cancer Immunotherapy Meeting 2015, Mainz, Germany.

Das K, Gardyan A, Vormehr M, Müller-Decker K, Zörnig I, Jäger D, Osen W, Eichmüller SB. Establishment of a transplantable, NY-BR-1 expressing breast cancer tumor model for *in vivo* analysis in HLA-transgenic mice. AACR Annual Meeting 2015, Philadelphia, USA.

Nicolaus C, Das K, Goyal A, Diederichs S, Dickes E, Osen W, Eichmüller SB (2015). Generation of murine β_2-microglobulin deficient tumor cell lines using the CRISPR/Cas9 system. Cancer Immunotherapy Meeting 2015, Mainz, Germany.

Das K, Gardyan A, Vormehr M, Müller-Decker K, Zörnig I, Jäger D, Osen W, Eichmüller SB. Establishment of a transplantable, NY-BR-1 expressing breast cancer tumor model for *in vivo* analysis in HLA-transgenic mice. Annual Meeting of the German Society for Immunology 2014, Bonn, Germany.

Das K, Gardyan A, Vormehr M, Müller-Decker K, Zörnig I, Jäger D, Osen W, Eichmüller SB. Establishment of a NY-BR-1 expressing breast cancer tumor model in HLA- transgenic mice. Cancer Immunotherapy Meeting 2014, Mainz, Germany.

9 Acknowledgements

At this point I would like to thank all the people who supported me to make this Dissertation possible.

First, I would like to give my special thanks to my supervisor, Prof. Dr. Stefan Eichmüller for giving me the opportunity to work on this project. I am very thankful for his continuous support, help, scientific guidance and patience. I am especially grateful to him for promoting independent thinking and for cultivating a wonderful atmosphere in the lab.

I am extremely thankful to Dr. Wolfram Osen for his constant supervision, feedback, guidance and scientific input not only during my doctoral studies but also in writing my thesis. I have deep gratitude for him for all his support and patience throughout my PhD time.

I am very obliged to my Thesis Advisory Committee Members: PD Dr. Karin Müller-Decker and Prof. Dr. Michael Kirschfink for their positive feedback and valuable advice regarding my project.

I am very grateful to my PhD Committee Members for their willingness to support me at this important final step of my PhD: PD Dr. Suat Özbek, Prof. Dr. Martin Müller and PD Dr. Karin Müller-Decker.

I would like to thank Dr. Inka Zörnig for kindly providing the anti-NY-BR-1 monoclonal antibody.

I would like to thank all the members of the FACS core facility: Dr. Steffen Schmitt, Klaus Hexel and Claudia Felbinger for their generous support.

I would like to acknowledge all the members of the central animal laboratory for their continued support.

I would like to thank Dr. Rafael Carreterro, Dr. Ulrike Träger and Dr. Ana Stojanovic for sharing their valuable knowledge on macrophages and NK cells.

I would like to thank all my wonderful colleagues as this thesis would not have been possible without their support. My special thanks to Dr. Chonglin Luo and Dr. Claudia Weber for sharing their valuable knowledge and expertise. I am very thankful to Dr. Adriane Gardyan for her valuable guidance, for her positive attitude and for her willingness to help with everything. I am very happy to have had colleagues like Mathias, Danuta, Clarissa, Edurne, Miriam, Alina, Claudia and Rainer who were always helpful and made my time in the lab pleasant.

Elke, I am extremely grateful to you for your incredible support throughout my PhD. Thank you for helping me with all my mouse experiments and also for your emotional support. I would not have been able to perform my ‘monster’ experiments without your help.

Julia, thank you for the support, for cheering me up and all the fun we had together.

Toni, I had a great time working with you. Thank you for always being so helpful and forgiving about all the jokes we made.

David, it was a great pleasure to work with you and to learn from you. Thank you for helping with everything from FACS to mouse work. I am very thankful for all the stimulating discussions we had even though I questioned everything you said by asking, “What it is the source of your information?”

Theresa, you are so much more than a colleague. Thank you for always being there for me and for everything you have done for me, in the lab and outside it. I can proudly say that one of the biggest personal achievements during my time in Heidelberg is earning a friend like you.

I would like to thank my dearest friends and family for their unwavering support. Priyanka, I have deep respect for the kindness of your heart. Thank you for being my pillar of support and for being a constant source of joy. Rajdeep and Ambika, thank you for being there for me during the most trying times and for being able to bring a smile to my face no matter what. Gautham, thank you for introducing me to this exciting world of cancer biology and for always inspiring me. Munu Ba, thank you for being a wonderful role model and for everything you have done for me.

Finally, I would like to thank my parents for their unconditional love and endless support. Deuta, thank you for fueling my curiosity and for encouraging me to pursue science. Ma, thank you for always being there for me. Thank you for teaching me to be independent and for letting me chase my dreams. I would not be here without you.